2-D Analysis Of The Performance Of Connections With Unprotected Steel Structural Members Exposed To Parametric Fire

JEREMY CHANG

Fire Engineering Research Report 03/7

2003

2-D Analysis Of The Performance Of Connections With Unprotected Steel Structural Members Exposed To Parametric Fire

By

JEREMY CHANG

Supervised by

Professor Andrew H. Buchanan

Assoc. Professor Peter J. Moss

Fire Engineering Research Report 03/7

June 2003

A research project report presented as partial fulfilment of the requirements
for the degree of Master of Engineering in Fire Engineering
School of Engineering
University of Canterbury
Private Bag 4800
Christchurch, New Zealand
Phone +64-3 364-2250, Fax +64-3 364-2758

Abstract

This report examines the performance of steel and composite steel beams, frames, and steel trusses subjected to realistic fires. High axial tensile forces at the beam connections are induced while cooling and could cause failure at the beam connections.

Two-dimensional structural analysis and the thermal analysis were carried out using the SAFIR finite element program. An unprotected 610UB101 steel section was used for the steel beams; and the composite beams were formed by the unprotected steel beams acting compositely with the reinforced concrete slab and spanning between steel columns which were assumed to be fire protected. The results show that the induced tensile axial forces are larger in the frames without composite action. They also show that the maximum compressive force is larger when the connections have rotation fixation, but the maximum tensile force is independent of the connection type.

The report also investigated the effect of changing the stiffness and strength of the columns. The results show that stronger columns induce larger tensile forces while cooling, and the resulting behaviour of the beam is very similar to the single span pin-pin connected beam.

When comparing fast fire growth and slow fire growth, the axial forces in the steel and composite beams were strongly dependent on the maximum steel temperature reached during the fire, and largely independent of the fire duration.

The last section discusses the structural fire behaviour of steel trusses with the same dimensions as in the World Trade Center tower, with and without insulation. The results show excellent behaviour if the insulation remains in place, but rapid failure due to high axial forces if the insulation is removed.

Acknowledgements

I would like to thank the following people who have helped me a lot with my project:

- Professor Andrew Buchanan for supervising my project, and offering invaluable assistance and guidance.
- Associate Professor Peter Moss for supervising my project and providing invaluable assistance in structural theory as well as methodically proof reading this report. I would also like to thank him for supplying the programs for extracting data from the SAFIR results.
- Dr. Linus Lim for the ideas and the assistances in the finite element modelling, and always being available to help with the SAFIR model.
- Dr. Jean-Marc Franssen, for the use of the finite element software, SAFIR. This research would not be possible without this program.
- Jenny Seputro, Clayton Wastney and Richard Welsh. Without their previous brilliant studies, this research would be much more difficult to carry out than it is.
- The New Zealand Fire Service for their financial assistance in providing me with a scholarship.
- The lecturers in Fire Engineering and my classmates, for making the study enjoyable.
- And finally, to my family for their unwavering support.

Table of contents

List of figures

List of tables

1 Introduction

1.1 Overview

The performance of structural steel under fire has been studied intensively in the past years, and it is understood that the loss of strength and stiffness of the steel members in a structure under the elevated temperatures contributes much to the structural failure.

According to the New Zealand Standard for steel structures, NZS 3404: Part 1 (1997), it is not necessary to protect all the structure members except the ones which require a fire resistance rating (FRR). Based on the explanation in Buchanan (2001), to design a structure with certain FRR is to ensure that the fire resistance of the structure or its members is greater than the severity of the fire. Most multi-story steel structures have all steel members protected.

The steel industry is very interested in using protected columns, but removing the protection from beams in order to reduce cost of construction. It was observed in the full-scale fire testing of a typical steel framed office building at the Cardington Research facility that high tensile axial forces would be induced in slabs after the structural members cool down (Martin & Moore, 1997). Hence, neglecting the induced tensile forces but only designing for sustaining a high temperature may still cause a structural failure. This report will examine the structural behaviour of composite and steel beams and their interaction with the end connections; and then some recommendations for the connection design will be made.

Because in normal practice the bolted connections are designed as rotationally unrestrained, pinned beam-column connections in frames are considered in this report. However, the connections generally have a significant rotational stiffness (El-Rimawi et al., 1997), therefore the actual behaviour of bolted beam-column connections lies somewhere between a fully pinned and a fully fixed connection. Hence, this report will also look at the fixed connections in frames as comparison. In reality, welded connections have full fixation in rotation and are generally used in seismic frames.

Therefore, the simulation results of frames with fixed beam-column connections can represent the behaviour of a seismic frame.

Tests carried out at Cardington have already proved the presence of high tensile forces during and after the cooling period in steel beams. However, after the events of September 2001 at the World Trade Center 1 and 2, one would question whether large tensile forces would be induced in the floor trusses of those two buildings, and whether that could have been factor for the failure of the floors. In order to shed light on this, a floor truss exposed to elevated temperatures was modelled to assess the magnitude of the induced tensile force.

1.2 Impetus for the research

Steel structures are popular among industry for their strength and ease of construction. Studies have been carried out using different computer packages modelling the fire behaviour of steel structural members and the effect on the connections (Liu, 1999). Studies using the SAFIR program in the University of Canterbury during the last few years (Seputro 2001, Wastney 2002, Welsh 2001) had no decay phase in the fire temperatures. This study attempts to understand the behaviour of steel structures during the decay phase in order to improve connection design in the future.

1.3 Objective of this research

- The first objective is to investigate the behaviour of composite and steel beams with different supporting conditions exposed to fires with a decay phase.
- The second objective is to provide some recommendations for the design of connections to overcome the forces generated during and after fires.

1.4 Scope of this research

The scope of this research covers the structural behaviour with:

Beams

- Effect of support conditions; a 610UB101 beam with pin-pin, pin-roller, fix-fix, fix-slide and column supporting conditions including or excluding composite action with a 120mm thick concrete slab is exposed to the ISO fire with a decay phase.
- Durability under the ISO fire; various durations of the ISO fire before the decay phase are used in the simulation to observe the influence of the fire temperatures during the heating phase to the induced tensile force as the temperature returns to ambient.

Frames

- Effect of stiffness and strengths of columns in frames; four levels of column stiffness and strengths are used in the simulations: two are stronger than the beam, and two are weaker. This investigates the relationship between the axial force in the beam and the column stiffness and strength during and after heating.

Trusses

- Steel truss with insulation; a steel truss with insulation is analysed to investigate the structural behaviour if the insulation is intact during fire. The structural behaviour will also be compared with a single span composite or steel beam.
- Steel truss without insulation; a steel truss without insulation is analysed to compare its structural behaviour with a steel truss with insulation.
- Axial spring; this investigates the influence of a limited amount of axial restraint upon the steel truss structure without rotational restraints at the ends. A comparison will be drawn between this scenario and the pin-pin or pin-roller supported truss.

Parametric fire

- Parametric fire; the structure is exposed to fires which do not follow the growth curve of the ISO834 standard fire. This investigates whether the rate of growth of the fire temperature affects the structural behaviour.

The thermal and structural analysis of this report is conducted with the use of the two dimensional non-linear finite element computer program, SAFIR. (Franssen et al, 2001)

1.5 Organisation of this report

This report consists of thirteen chapters. Chapter 2 describes the dimensions and materials of the structural members used in this report. Chapter 3 explains the analysis method used in SAFIR, and the finite element program used to model the structural behaviour under elevated temperatures. Chapter 4 reviews the steel and concrete material properties under elevated temperatures, which is used by the SAFIR program.

Regarding the composite steel/concrete sections, Chapter 5 describes the simulation results of single span composite steel beam exposed to various durations of the ISO834 standard fire with a decay phase, and Chapter 6 discusses the simulation results of the composite beam in frames. It also reports the observed results of the influence of variation in column strength and stiffness.

Chapters 7 and 8 discuss the simulation results of single span steel beams or steel frames exposed to various durations of the ISO fire before the decay phase. Chapter 8 also discusses the influence of changing column strength and stiffness on the structural behaviour of steel frames under fire.

Chapter 9 provides a review of the effect of changing the growth rate of the fire temperatures on the composite frame, and discusses the suitability of only using the ISO fire with a decay phase in this scenario while design.

Chapters 10 and 11 show the simulation results for a steel truss exposed to elevated temperatures with and without insulation, respectively. They also discuss the effect of introducing an axial spring into the model. Chapter 11 further describes the structural behaviour of exposing a truss without insulation to fires with a growth period as rapid as under an explosion.

Chapter 12 summarises the findings in this report and makes recommendations for future research.

2 Structural members used in the analysis

This section describes the structural members used in the input models for SAFIR, including the dimensions, layout and loading of the beams and column.

This report investigated three types of steel structure exposed to elevated temperatures: simply supported beams, frames and trusses. The first two types of structure are similar, where frames were formed by replacing the end supports of simply supported beams with beam-column connections and columns. The models of the truss structures were based on the description in FEMA (2002) of World Trade Center One's main floor truss.

Two types of beams were used in the analysis: steel beam and composite beam. The dimensions and loading of beams were the same as in Welsh (2001), Seputro (2001) and Wastney (2002). This allowed a comparison of the results. In frame structures, only one type of column was used. The layout and section properties of the beams, column, and the truss are described separately below.

2.1 Composite beam layout and section properties

2.1.1 Section properties

A composite 610UB101 steel beam supporting a profiled 120mm concrete slab was used in composite beam scenarios. The concrete profile followed the size of the Diamond Hi-Bond proprietary profile decking. It was assumed that there was a full composite action between the steel beam and the concrete slab. Figure 1 and Table 2-1, both duplicated from Welsh (2001), show the cross section and the dimensions of the composite beam used in models.

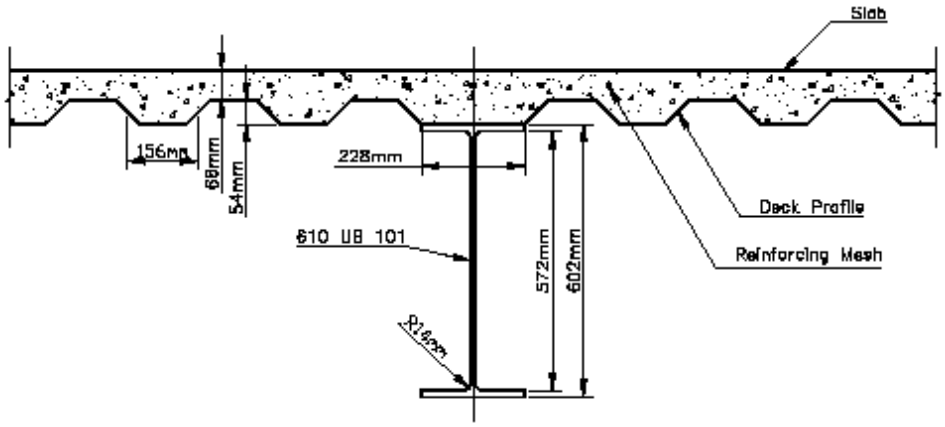

Figure 2-1 Cross section of the composite beam in the model (Welsh 2001)

Table 2-1 Dimensions of composite beam

Steel beam size	610UB101 steel beam
Effective width of slab	1000 mm
Gross cross-sectional area of concrete	13000 mm^2
Second moment of area of composite beam	1.893 x 109 mm^4
Depth to neutral axis of composite beam	242 mm
Depth of concrete slab (through deck profile)	120 mm
Depth of concrete slab (between deck profiles)	65 mm
Mesh size	665 (Diamond Industries, 1997)
Concrete cover above mesh	25mm (Diamond Industries, 1997)

2.1.2 Layout of the beam and applied load

The layout of the beam and the applied load on the beam were the same as in Welsh (2001) and Wastney (2002). In all scenarios, the composite beam spanned 8.0m between the supports.

Based on the New Zealand loading code NZS 4203:1992:

> *For the period of time during a fire emergency when the structure is subjected to elevated temperatures and designated members are required to remain stable, the affected members shall be designed for the following combination of factored load.*

$$G + Q_u$$

Where: G = *Dead Load.*

$Q_u = \Psi_u Q$

Q = *Live load.*

Ψ_u = *0.4 for office buildings.*

The loadings considered in the models are listed in Table 2-2. The load was assumed distributed uniformly along the beam.

Table 2-2 Calculation of composite beam loads from Welsh (2001)

Component of load	**Value**	**Unit**	**kN/m**
Slab + Deck	2.5	kPa	22.25
610UB101	0.99	kN/m	0.99
Self imposed dead load (SDL)	2.00	kPa	17.08
Live load	2.5	kPa	
Adjustment for $Q_u = \Psi Q$	0.4 x 2.5	kPa	8.9
Total	5.62	kPa	50.00

2.2 Steel beam layout and section properties

2.2.1 Section properties

610UB101 steel beam was used in the steel beam only scenarios, which assumes no composite action with the concrete slab above. The dimensions of the beam are shown in Table 2-3.

Table 2-3 Dimensions of the steel beam

Beam size	610UB101 steel beam
Depth of section	602 mm
Flange width	228 mm
Flange thickness	14.8 mm
Root radius	14.0 mm
Gross cross-sectional area	13000 mm^2
Second moment of area	761 x 10^6 mm^4
Depth to neutral axis	301 mm
Plastic section modulus	2900 x 10^3 mm^3

2.2.2 Layout of the beam and applied loads

In all steel beam only scenarios, the 610UB101 steel beam spanned 8.0m between the supports. Since no composite action was considered in these scenarios, the concrete slab only acted as a source of dead load and had no physical presence in the model. The load on the steel beam was 37.5kNm^{-1}, which was the loading in the composite beam reduced proportionally in accordance with its strength.

2.3 Column layout and section properties

In all scenarios with frames, the columns were assumed to have the same properties as a 610UB101 steel beam, of which the dimensions were shown in Table 2-3. The columns were 8.0 metres long, and the beam-column connections were situated at the mid-height of the columns. Figure 2-2 shows the layout of the frame model used in the simulation.

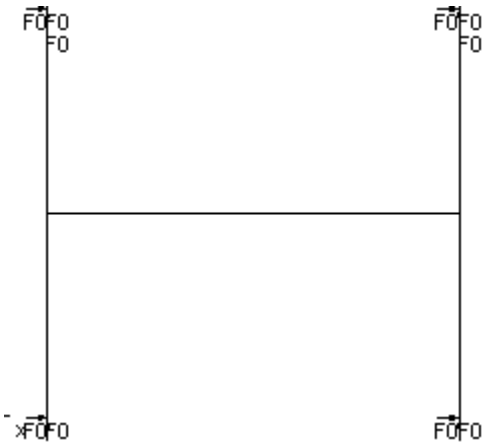

Figure 2-2 Layout of the frame model

2.4 Truss structure layout and section properties

The dimensions of the truss structure were based on the description of the main floor truss of World Trade Center 1 in the official investigation report of building performance (FEMA, 2002). Figure 2-3 shows the floor truss layout from the report.

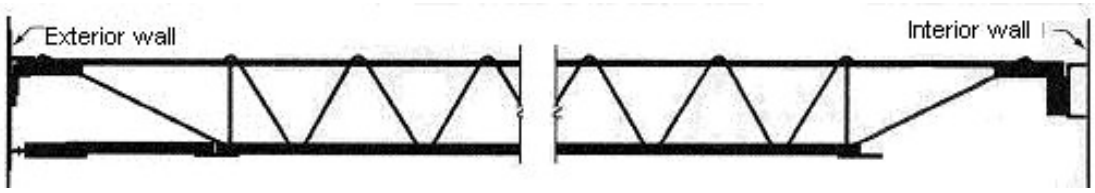

Figure 2-3 Floor truss member of WTC 1 & 2 (FEMA, 2002)

2.4.1 Section properties

The floor trusses were in pairs and spanned between the central core and the exterior wall as shown in Figure 2-4.

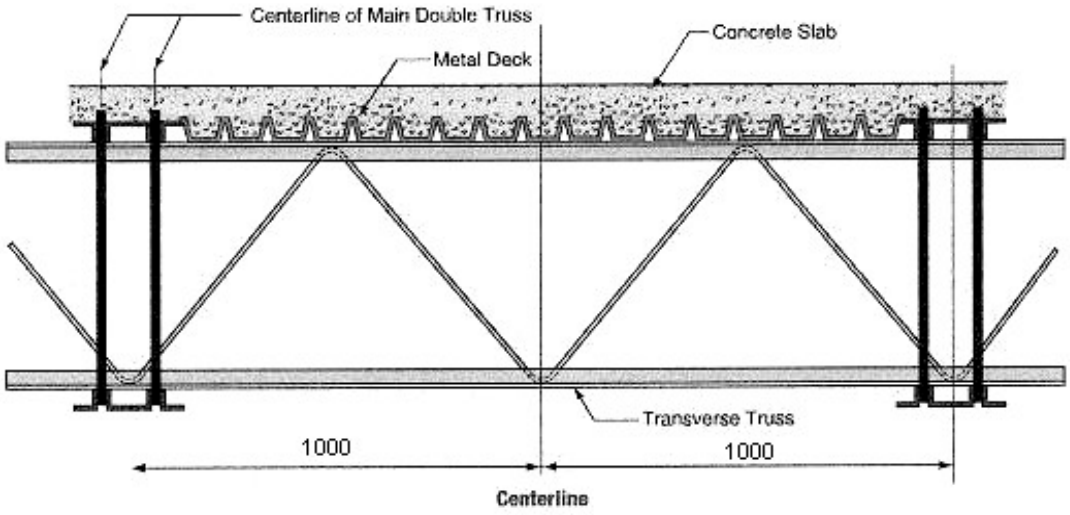

Figure 2-4 Cross-section through main double trusses, showing transverse truss (FEMA, 2002)

The structure was divided up to three parts for the thermal analysis: top chord with covering concrete, bottom chord, and truss web. Based on the diagrams given in FEMA (2002), it was determined that the top chord was formed by two 51 x 64 x 8mm angles, and the bottom chord was formed by two 76 x 51 x 9mm angles. From the description in FEMA (2002), the diameter of the web metal rod was 28mm. The cross-section of the rod was modelled as a square with the same cross-sectional area to simplify the simulation effort. The main floor trusses were covered by a 64mm thick concrete slab, and the composite action between the main floor trusses and the concrete section was achieved by extending the truss diagonals above the top chord into the concrete as shown in Figure 2-5. This composite behaviour was embraced by having the presence of the covering concrete slab in the model.

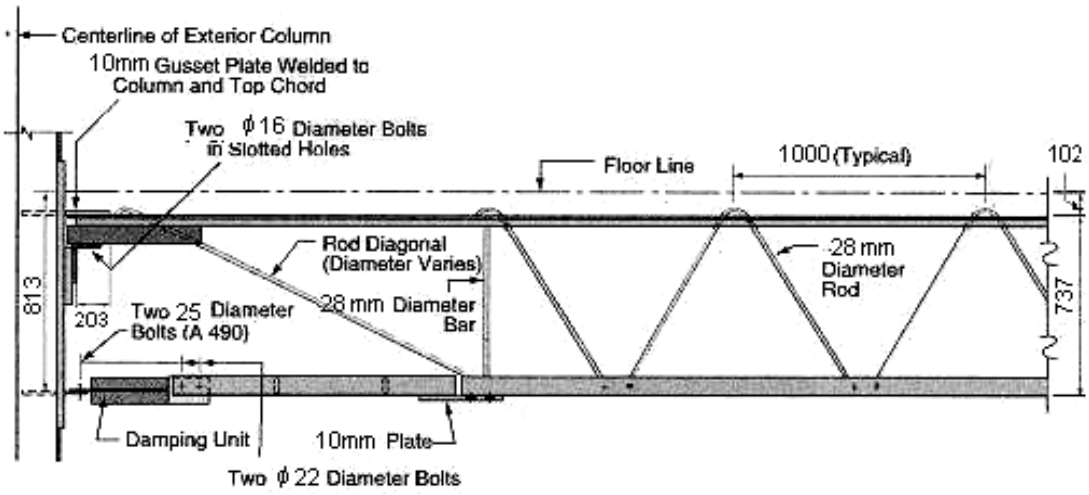

Figure 2-5 Truss - Exterior wall end detail (FEMA, 2002)

Two types of structures were used in the truss model: one coated with insulation, and one without. FEMA (2002) described the coating material as "a spray-applied, asbestos-free mineral fibre material", and the average thickness of the spray-applied insulation was approximately 20mm (3/4 inches) before an upgrade took place in the 1990s. The upgraded fire protection has fireproofing thickness of approximately 40mm (1-1/2 inches). However, by September 11, 2001, only one floor in the impact zone in WTC2 had been upgraded. In the insulated model for this report, a 20mm thick insulation coat was used to simulate a worse case scenario. The thermal properties of the spray-applied insulating material are shown in Table 2-4, referenced from ECCS (1995).

Table 2-4 thermal properties of sprayed mineral fibre (ECCS, 1995)

Material	Density	Thermal conductivity	Specific heat	Equilibrium, moisture content
	ρ_i	k_i	c_i	%
	(kg/m^3)	(W/mK)	(J/kgK)	
Sprayed mineral fibre	300	0.12	1200	1

In the simulation, it was assumed that all the steel members were covered by 20mm of sprayed insulation in the protected truss. Figure 2-6 and Figure 2-7 show the profiles of the three structure members used for thermal analysis in protected and unprotected structures respectively.

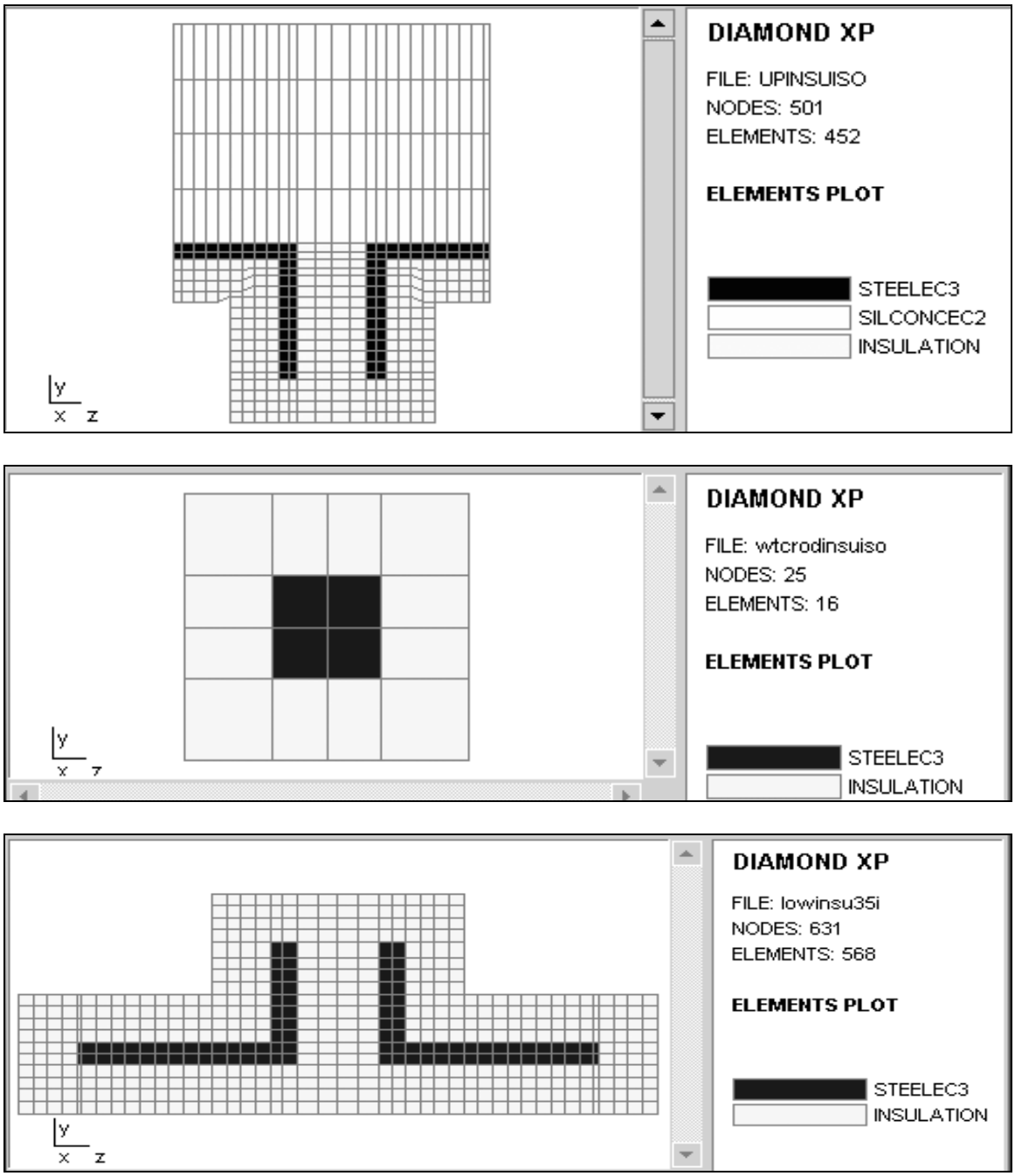

Figure 2-6 Cross-section of the protected truss members for thermal analysis: (from the top) upper chord with the concrete cover; truss rod; bottom chord

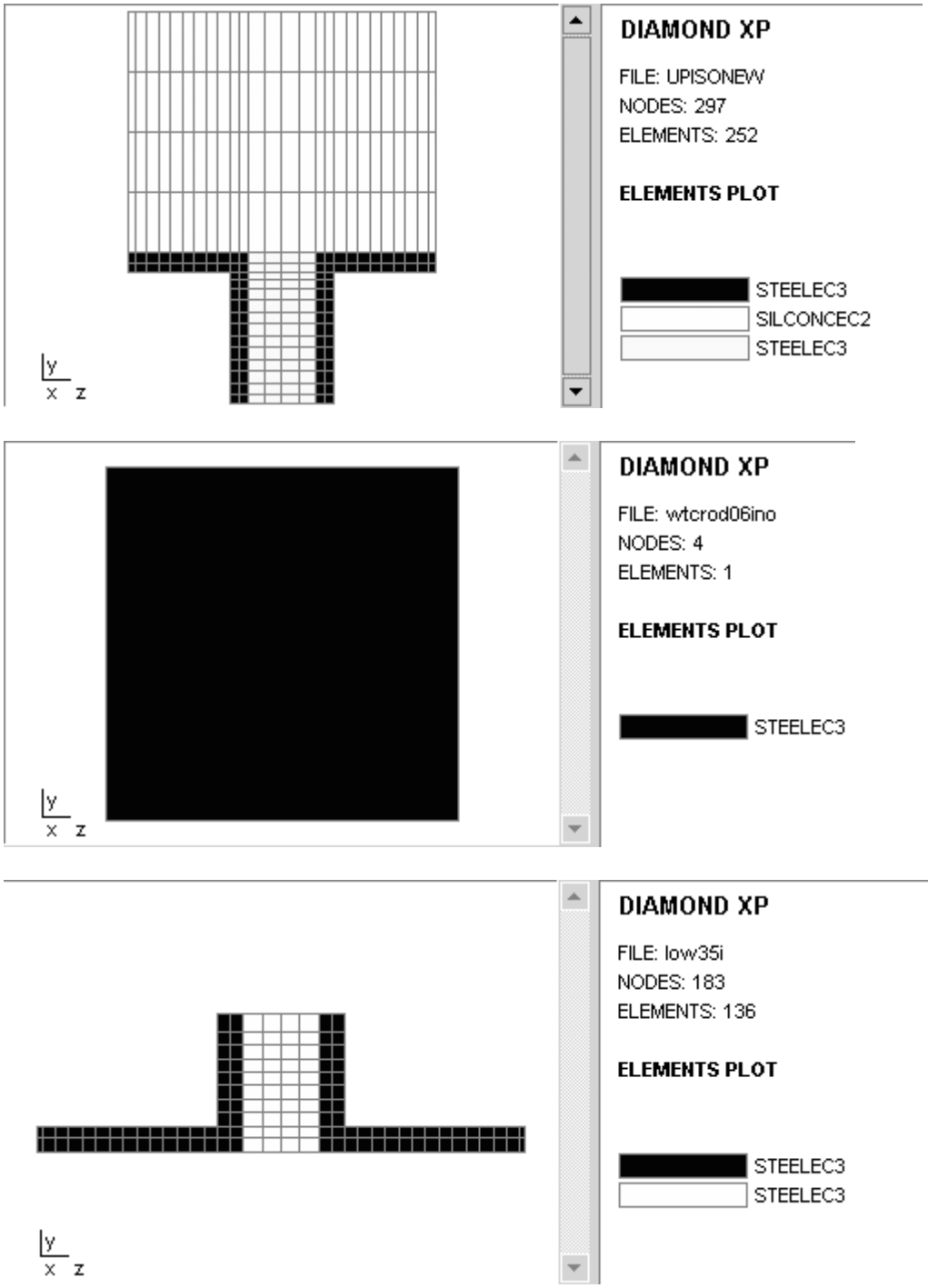

Figure 2-7 Cross-section of the unprotected truss members for thermal analysis: (from the top) upper chord with the concrete cover; truss rod; bottom chord

2.4.2 Layout of the truss

The main truss shown in Figure 2-4 had a spacing of 2m and length of 18.3m to the sides and 10.7m to the ends of the central core. Figure 2-8 shows the truss model used in the simulation. The length and depth of the truss was 18.3m and 0.74m respectively based on the description in FEMA (2002). The other dimensions of the truss can be found in Figure 2-4 and Figure 2-5.

Figure 2-8 Truss model simulated using SAFIR (unit in metres)

2.4.3 Applied load on the truss

FEMA (2002) states that the transverse bridging trusses were used to support the 102mm thick concrete and the 38mm thick, 22-gauge non-composite steel deck. The transverse trusses spaced at 4.0m and intermediate deck support angles spaced at 2.0m from the transverse trusses. The main trusses, transverse trusses, and deck support in the floor system acted as a grillage to transfer loads into the central or the exterior core, which is shown in Figure 2-9.

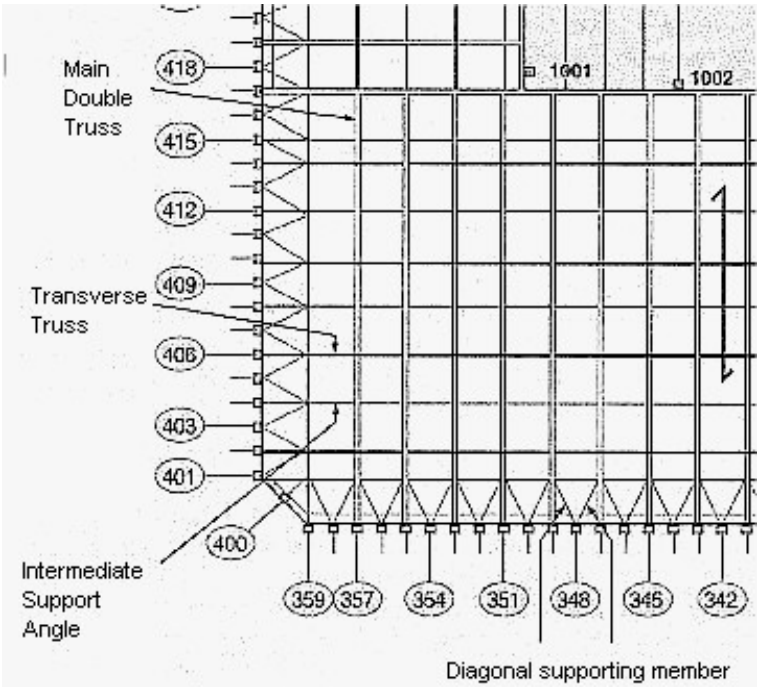

Figure 2-9 Representative structural framing plan, upper floor (FEMA, 2002)

Based on the description of the building as well as Figure 2-4 and Figure 2-9, the loads applied to the truss were assumed to be point loads to represent the transverse truss transferring load onto the main truss. The location of the point loads are shown in Figure 2-10. The calculation of the point loads is shown in Table 2-5.

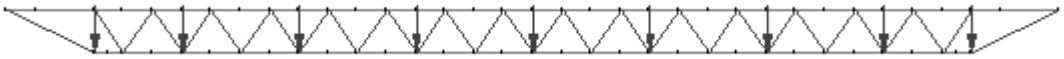

Figure 2-10 Locations of the point loads in the main truss

Table 2-5Calculation of point loads on the truss

Item		**Value**	**Unit**
Area of span	2.03 x 1.02	2.07	m^2
Concrete load (G)			
Depth	0.102		m
Concrete density	23		kN/m^3
Concrete load (near connections)	23 x 0.102	**2.3**	**kPa**
Live load (Q)		4.8	kPa
Fire load (G + 0.4 Q)	2.3 + 0.4 x 4.8	**4.3**	**kPa**
Point load	4.2 x 2.07	**9**	**kN**

3 Analysis method used in the SAFIR program

All the structural and thermal analyses used in this report were conducted using SAFIR, a non-linear finite element computer program developed at University of Liège. The explanation and description in this section about the program and its features are interpreted from the User's Manual (Franssen et al, 2000).

SAFIR is based on the Finite Element Method (FEM), and it can be used to study the behaviour of one, two or three-dimensional structures, where in this report only two-dimensional analysis was used. There are two steps in the SAFIR analysis procedure: the first step is to obtain the temperature distribution across the structural members, this step is named "thermal analysis"; the second step determines the response of the structure from its static and thermal loading, this is called "structural analysis". Each step is illustrated in details in the following sections.

3.1 Thermal Analysis

SAFIR calculates the temperature distribution throughout the cross-section of the structure. For a complex structure, such as the truss and the frame structure analysed in the report, the whole structure is divided into several substructures and the thermal analysis is performed individually for each substructure. Each cross-section is discretised into a finite element mesh to allow temperature calculation at different locations.

It is assumed that heat can only transfer through the cross-section but not along the axis of the beams. In the models analysed for this report, the temperature of the fire was defined before conducting the thermal analysis, and the fire temperature was consistent on the sides and bottom perimeter of the beam, while the top side of the beam was not heated. Figure 3-1 and Figure 3-2 show the discretised steel and composite beam used in the report respectively, and the cross sections used for the truss structure were shown in Figure 2-6 and Figure 2-7. Figure 3-2, Figure 2-6 and Figure 2-7 all demonstrate that the SAFIR thermal analysis allows for different materials in the cross-section.

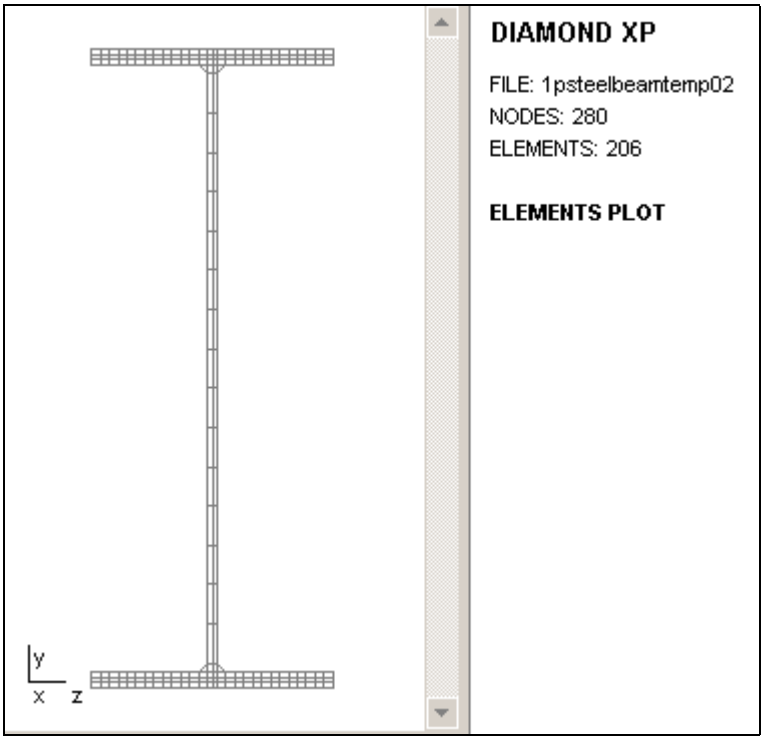

Figure 3-1 Discretised steel beam used in the models

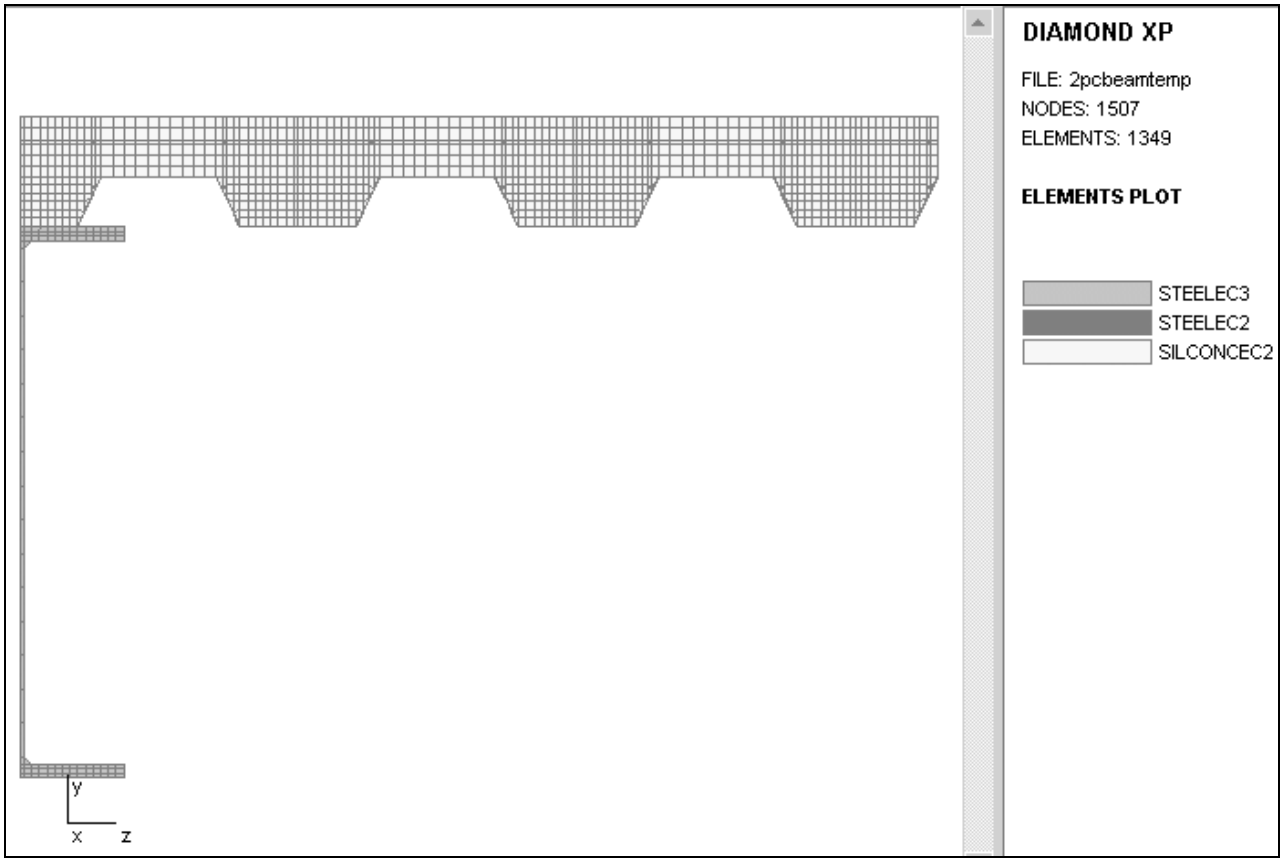

Figure 3-2 Discretised composite beam used in the models

3.2 Structural Analysis

The SAFIR structural analysis incorporates the outputs from the thermal analysis to calculate the structural behaviour under the static and thermal loads, with the thermal characteristics of the materials following the Eurocode as described in the following chapter. In the beam and frame structures, the BEAM elements in the program were used, where the ends of each element have three degrees of freedom in a two-dimensional model. In the truss structures, the top and bottom chords were defined as BEAM elements, but the rod was defined as a TRUSS element. Each TRUSS element only allows a single material with one temperature and one strain, and it can only resist axial forces.

The User's Manual (Franssen et al., 2000) states the assumptions made for the BEAM elements are as follows:

- the Bernoulli Hypothesis is adopted, that the cross-section of the beam remains plane under the bending moment
- plastifications are only considered in the longitudinal direction of the member.

4 Material properties at elevated temperatures

This chapter describes the material properties of steel and siliceous concrete used by SAFIR. These material properties are as a function of the temperature, and SAFIR uses the relationships suggested by the Eurocode to simulate the non-linear temperature dependent properties of the material.

4.1 Steel mechanical properties

This section describes the temperature dependent mechanical properties of the structural steel used in the SAFIR analysis. The non-linear temperature dependent relationships of the material used in SAFIR are based on the Eurocode (EC3: 1995).

4.1.1 Ambient Properties

Table 4-1 shows the ambient properties of all the steel sections used for this report. These values were parts of the input data for the SAFIR simulations. The properties in the truss structure are different to the frame structure, as the angles and rods of World Trade Center floor truss were fabricated using ASTM-A36 steel.

Table 4-1 Ambient steel properties

Property	**Notation**	**Value**	**Unit**
Truss angles/rods yield strength	f_y	248	MPa
Poisson's Ratio (for beam & frame cases)	ν	0.3	-
Poisson's Ratio (for truss angles)	ν	0.26	-
Elastic Modulus (for beam & frame cases)	E_{steel}	210	GPa
Elastic Modulus (for truss angles)	E_{steel}	200	GPa
Density	ρ	7850	Kg/m3

4.1.2 Steel properties at elevated temperatures

The yield strength of steel at elevated temperatures is not as well defined as at ambient temperatures. However, one needs the value of the yield strength and the proportional limit, which define when steel would yield and when the strain no longer has a linear relationship with the stress, to study the steel behaviour at elevated temperatures. SAFIR adopts the relationships from the Eurocode to calculate the yield strength. The Eurocode (EC3:1995) states that for heating rates between 2 and 50°C/min, the strength and deformation properties of steel at elevated temperatures shall be obtained from the stress-strain relationship as shown in Figure 14-1 in Appendix 1. Table 14-1 Appendix 1 gives the reduction factors to the appropriate values at the ambient temperature. These reduction factors, as shown in Figure 4-1, are used to determine the resistance to tension, compression, moment or shear.

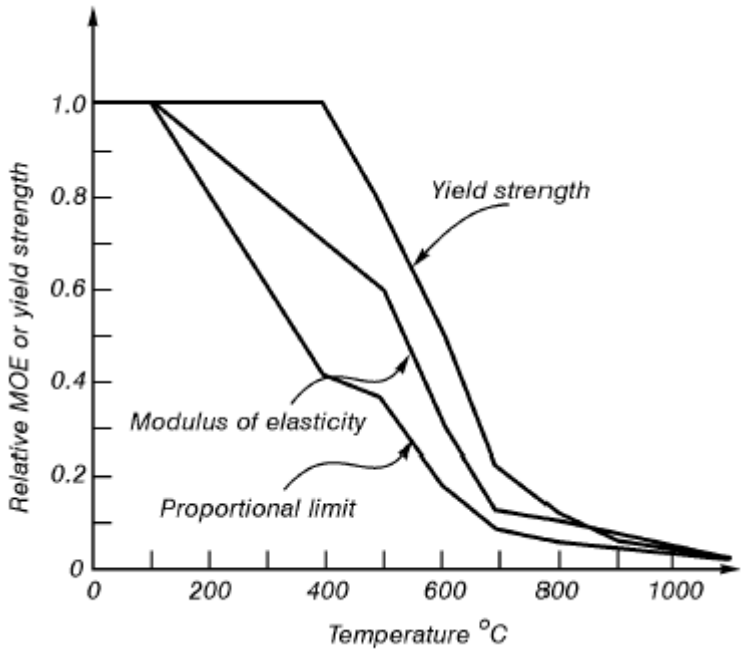

Figure 4-1 Reduction factors for the yield strength and modulus of elasticity of steel at elevated temperatures(EC3:1995)

The reduction factors can be described as follows:

- effective yield strength, relative to yield strength at 20°C: $k_{y,\theta} = f_{y,\theta} / f_y$
- proportional limit, relative to yield strength at 20°C: $k_{p,\theta} = f_{p,\theta} / f_y$
- modulus of elasticity, relative to the elastic modulus at 20°C: $k_{E,\theta} = E_{a,\theta} / E_a$

These factors have been used for the steel sections in the model.

4.2 Steel thermal properties

This section describes the thermal properties of the structural steel from the Eurocode (EC3:1995) used by SAFIR.

4.2.1 Thermal Conductivity – λ

The thermal conductivity defines how rapidly the material can conduct heat, and it is dependent on the composition and temperature of steel. Figure 4-2 shows that the EC3 steel model has a linear reduction in thermal conductivity from 20 to 80°C and is taken as constant thereafter. The equations for thermal conductivity, λ, from the Eurocode (EC3: 1995) are shown below.

λ = 54 – (0.0333 x T)	**(W/mK)**	**for 20°C≤ T<800°C**	**Equation 4-1**
λ = 27.3	**(W/mK)**	**for 800°C≤ T≤1200°C**	**Equation 4-2**

where T is the steel temperature.

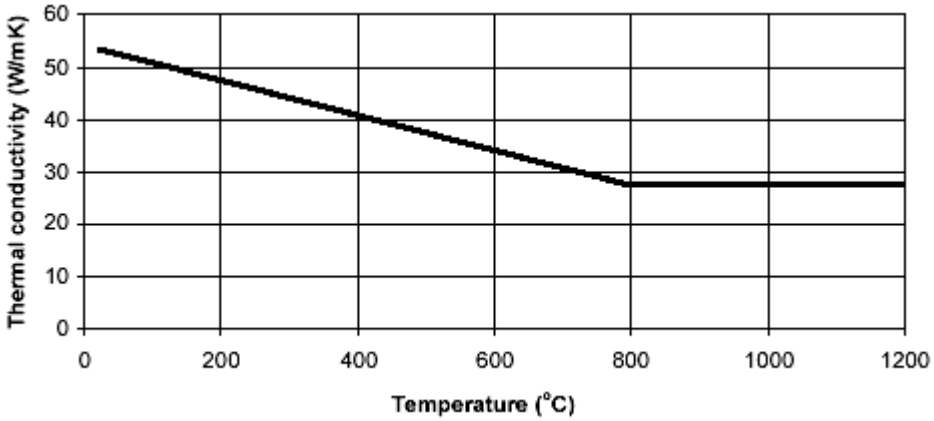

Figure 4-2 EC3 (1995) thermal conductivity of steel as a function of temperature

4.2.2 Specific heat – c_p

Specific heat is the ability of the material to absorb heat. This value is independent of the steel composition but varies with the temperature. The Eurocode (EC3:1995) suggests that the relationship of specific heat and temperature of steel are as shown in the following equations.

$c_p = 425 + 0.773\,T - 1.69\times10^{-3}T^2 + 2.22\times10^{-6}T^3$	for $20^oC \leq T < 600^oC$	Equation 4-3
$c_p = 666 + 13002/(738 - T)$	for $600^oC \leq T < 735^oC$	Equation 4-4
$c_p = 545 + 17820/(T - 731)$	for $735^oC \leq T < 900^oC$	Equation 4-5
$c_p = 650$	for $900^oC \leq T$	Equation 4-6

Figure 4-3 shows that the specific heat varies with the steel temperature. The sharp peak of specific heat at 730°C is caused by a metallurgical change in the steel crystal structure.

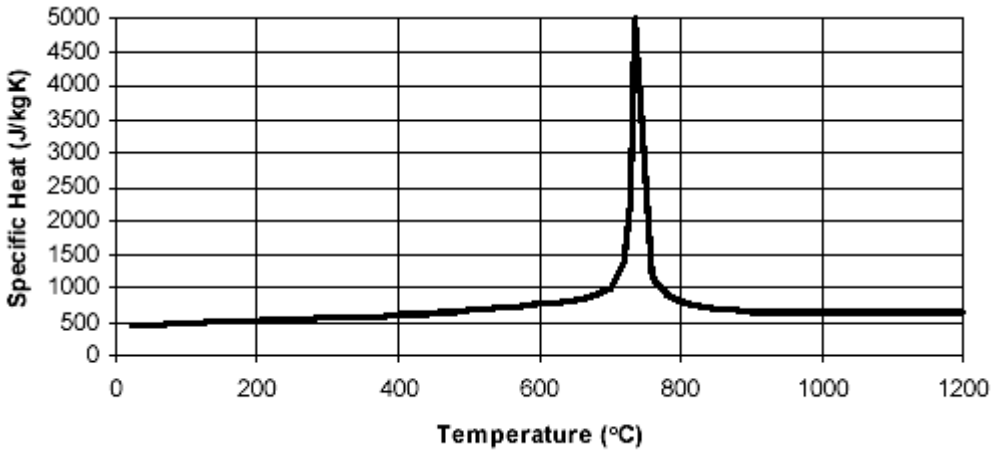

Figure 4-3 EC3 (1995) specific heat of steel as a function of temperature

4.2.3 Thermal elongation – Δl/l

The thermal elongation of steel, Δl/l, is the increase in the length of the member caused by heating divided by the initial length. Figure 4-4 shows the relationship between the elongation and the temperature of the steel from the Eurocode (EC3:1995). The discontinuity in the thermal elongation occurring at 750°C to 860°C is due to a phase transformation in the steel.

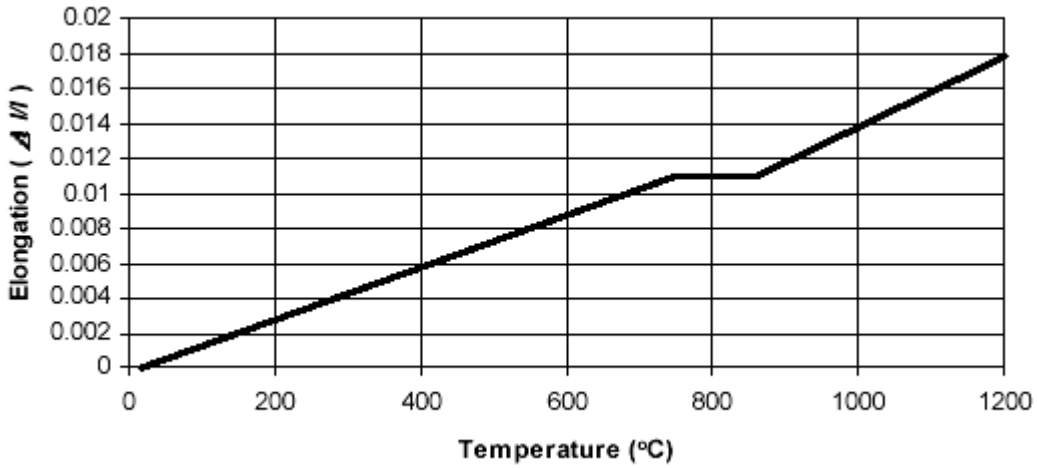

Figure 4-4 EC3 thermal elongation of steel as a function of temperature

The following equations also describe the relationship between the thermal elongation and the temperature of steel according to the Eurocode (EC3:1995).

$\Delta l/l = 1.2\times10^{-5}\,T + 0.4\times10^{-8}\,T^2 - 2.416\times10^{-4}$	for $20^oC \leq T < 750^oC$	Equation 4-7
$\Delta l/l = 1.1\times10^{-2}$	for $750^oC \leq T < 860^oC$	Equation 4-8
$Dl/l = 2\times10^{-5}T - 6.2\times10^{-3}$	for $860^oC \leq T < 1200^oC$	Equation 4-9

4.3 Concrete mechanical properties

This section describes the thermal properties of siliceous aggregate concrete used in the SAFIR analysis. The mechanical properties of concrete at elevated temperatures in SAFIR are based on the Eurocode (EC2:1993) relationships.

4.3.1 Ambient properties

The properties were used for the concrete section at the ambient temperature as part of the input data in the SAFIR simulation models.

Table 4-2 Ambient concrete properties

Property	Notation	Value	Unit
Concrete			
Concrete compressive strength	f'_c	30	MPa
Concrete tensile strength	f_r	0	MPa
Elastic modulus	E_{conc}	23.5	GPa
Poisson's ratio	ν	0.02	--
Density	ρ	2300	Kg/m^3

The concrete section is assumed to crack at zero stress under tension to avoid computational errors from SAFIR. In reality, the concrete has some tensile strength which is not great; and one can make this assumption and not expect a significant difference between the simulation results and the real situation.

In World Trade Centers 1 and 2, the floor framing at the non-mechanical floors (floors other than level 7, 41, 75 and 108) consists of 102mm of normal weight concrete slab with a compressive strength of 27.5MPa. It was assumed that the concrete section gained strength over the years and the compressive strength was increased to 30MPa which is the same value as used in the frame models.

4.3.2 Properties at elevated temperatures

The stress-strain relationship for siliceous aggregate concrete at elevated temperatures is shown in Figure 14-4 and Table 14-3 in Appendix 1. The reduction of the characteristic compressive strength of concrete, $f_{ck}(T)$, as a function of the temperature, T, is allowed for by the coefficient $k_c(T)$, for which:

	$f_{ck}(T)=k_c(T)f'_c(20^oC)$	Equation 4-10
where k_c :	$k_c(T)=1.0$	for $20^oC \leq T \leq 100^oC$
	$k_c(T)=(1600-T)/1500$	for $100^oC \leq T \leq 400^oC$
	$k_c(T)=(900-T)/625$	for $400^oC \leq T \leq 900^oC$
	$k_c(T)=0$	for $900^oC \leq T \leq 1200^oC$

The relationship between the coefficient $K_c(T)$ and the concrete temperature can be plotted as shown in Figure 4-5.

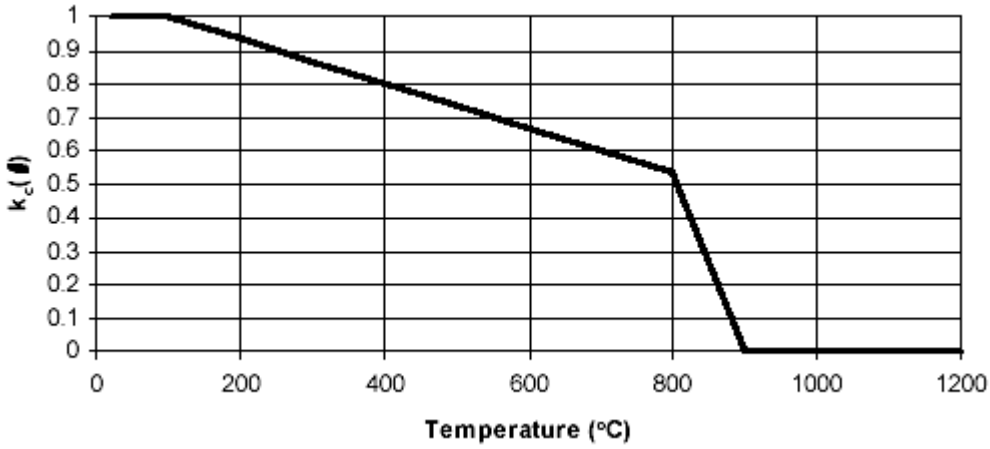

Figure 4-5 Coefficient $k_c(T)$ allowing for decrease of compressive strength f_{ck} (EC2:1993)

4.4 Concrete thermal properties

This section describes the thermal properties of the siliceous aggregate concrete used by SAFIR based on the Eurocode (EC2:1993).

4.4.1 Thermal conductivity – λ_c

The thermal conductivity of concrete depends on the temperature as well as the type of aggregate. Figure 4-6 and the equation below show the relationship between the thermal conductivity, λ_c, and the concrete temperature for concrete with siliceous aggregates.

$$\lambda_c = 2 - 0.24T/120 + 0.012(T/120)^2 \text{ (W/mK)} \quad \text{for } 20^oC \leq T \leq 1200^oC \qquad \text{Equation 4-11}$$

where T is the temperature of the concrete.

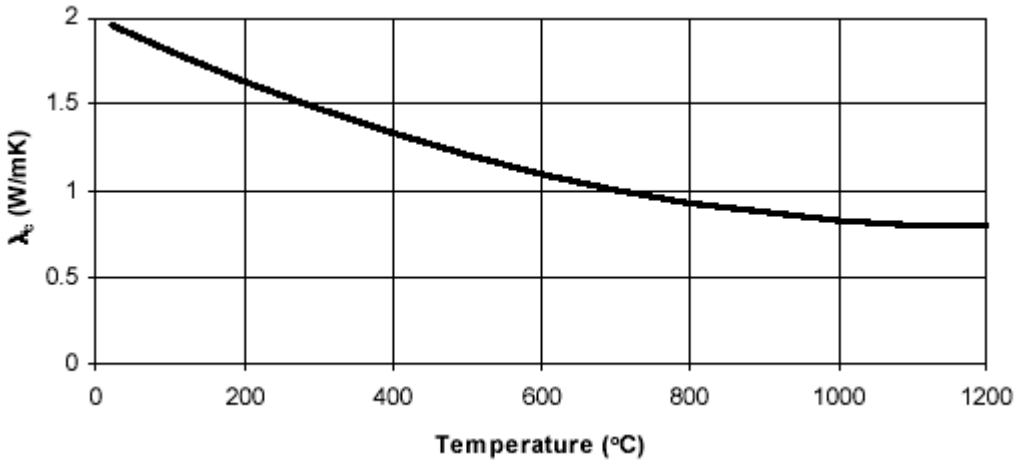

Figure 4-6 EC2 thermal conductivity of concrete as a function of temperature

4.4.2 Concrete specific heat – c_c

The value of the specific heat of concrete is dominated by the moisture content which for EC2 concrete has a maximum of 2%. Figure 4-7 shows the relationship between the specific heat and the concrete temperature as suggested by the Eurocode (EC2:1993). There is a peak in the specific heat between 100°C and 200°C due to water being driven off.

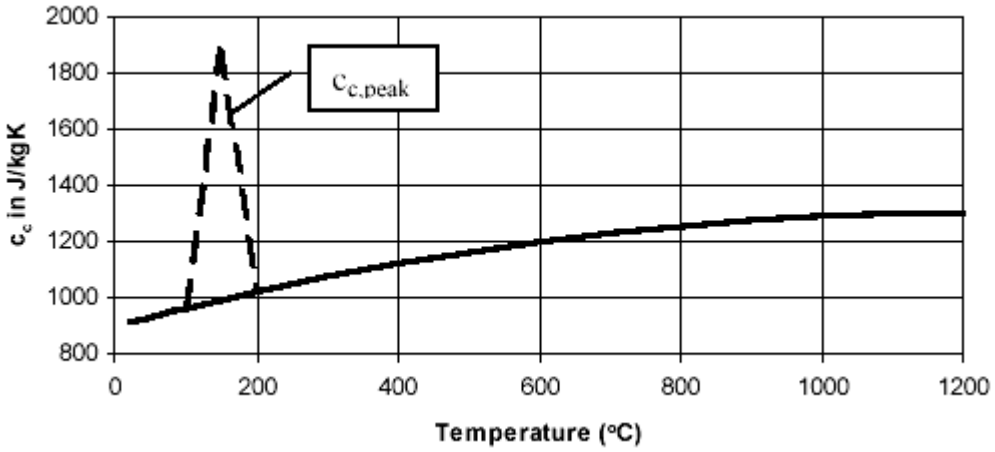

Figure 4-7 EC2 Specific heat of concrete as a function of temperature

The Eurocode suggests the following relationship for the calculation of the specific heat of concrete, C_c.

$$C_c=900+80T/120-4(T/120)^2 \quad \text{(JkgK) for } 20^oC \le T \le 100^oC$$

$$\text{and for } 200^oC \le T \le 1200^oC \qquad \text{Equation 4-12}$$

where T is the temperature of the concrete.

Between 100°C and 200°C there is a peak in the specific heat due to water being driven off from the concrete, which has a value as shown below:

$c_{c,peak}$= **1875J/kgK** **for 2% moisture**

$c_{c,peak}$= **2750J/kgK** **for 4% moisture**

4.4.3 Concrete thermal elongation – $(\Delta l/l)_c$.

Figure 4-8 shows the relationship between the thermal elongation and the concrete temperature suggested by the Eurocode (EC2:1993). This relationship is non-linear until 700°C and then becomes constant. The following equations represent this relationship:

$$(Dl/l) = -1.8\times10^{-4} + (9.0\times10^{-6})T + (2.3\times10^{-11})T^3 \quad \text{for } 20^oC \leq T \leq 700^oC \qquad \text{Equation 4-13}$$

$$(Dl/l) = 14\times10^{-3} \quad \text{for } 700^oC \leq T \leq 1200^oC \qquad \text{Equation 4-14}$$

where T is the temperature of the concrete.

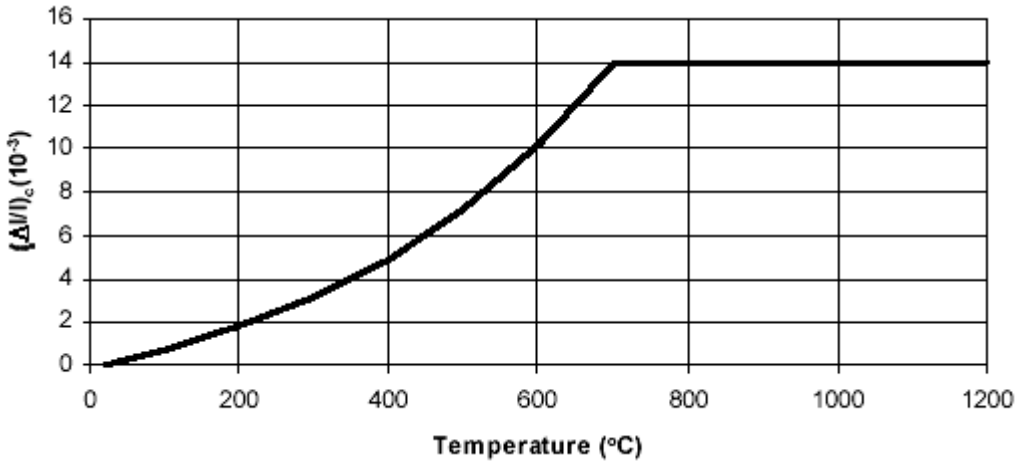

Figure 4-8 Thermal elongation of concrete as a function of temperature (EC2:1993)

5 Simulation results of composite steel beams exposed to the ISO fire with a decay phase

This chapter discusses the simulation results of modelling single span composite beams exposed to different durations of the ISO834 standard fire with a decay phase. Four end connection conditions are considered here: pin-pin, pin-roller, fix-fix and fix-slide, of which the pin-roller and fix-slide beams are axially unrestrained, and the other two are axially restrained. Parts of these analyses were studied previously by Welsh (2001) and Wastney (2002), However, the simulations for these analyses were conducted again to corroborate their previous findings.

The growth period of the fire temperature was following the ISO834 standard fire; and the decay rate was based on the ISO834 testing standard. The temperature decay rate during the decay phase was 625^{o}C per hour for fires with a burning period of less than half an hour, decreased to 250^{o}C per hour for fires with a burning period longer than 2 hours. Figure 5-1 shows the relationship between the decay rate and the duration of fire.

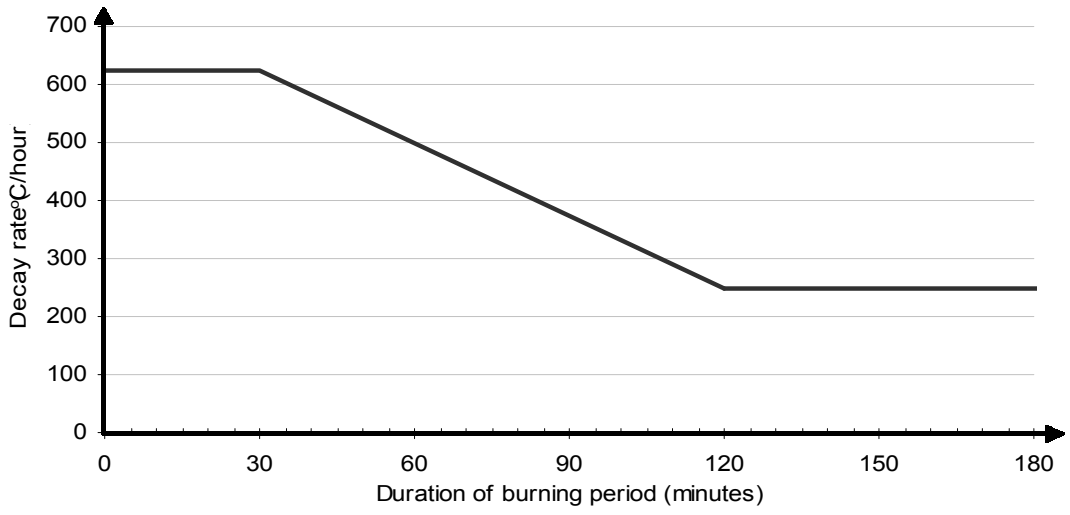

Figure 5-1 Rate of temperature decay in Eurocode parametric fires

The analysis was conducted by observing the axial force, displacement along the beam, and the stress distribution across the vertical centreline of the beam. The axial forces and displacements were extracted using Diamond XP, a computer program developed by University of Liège, which can reduce data from output files of SAFIR, and these values were plotted against time. The stresses along the beam centrelines were reduced directly from the output files using Excel, and were plotted against the height of the cross section to compare with the thermally reduced EC3 Proportional and Yield Limit stresses at desired times. Using the temperature files from the thermal analysis, one can obtain the temperatures distribution across the steel beam at different times, and consequently the steel strength distribution by using EC3 Table 3.1. *Reduction factors for stress-strain relationship of steel at elevated temperatures.*

5.1 Thermal analysis results for composite beam

The number of thermal analysis results needed in this research was based on the duration of the ISO834 standard fire the beams can sustain before reaching failure. The results in Wastney (2002) indicated that in an ISO834 standard fire, the pin-pin connected beam lasts longer before failure occurs compared with the other three connection types. Therefore, the number of thermal analyses in the single span studies was in accordance with the failure time of the pin-pin connected beam, which was 37 minutes. Eight parametric fire curves, comprising from 8 minutes fire to 34 minutes of the ISO834 standard fire before the decay phase, together with the one without decay phase, were used in the thermal analyses.

Figure 5-2 shows the temperatures of the top and bottom steel flange and at the top and bottom of the concrete slab. These figures show that the bottom steel flange had the most rapid temperature rise, but it also cooled down the fastest. Although the top of the concrete slab had the coolest temperature during the developing phase of fire, it had the highest temperature at 166minutes (10000 seconds), which was long after the air returns to room temperature.

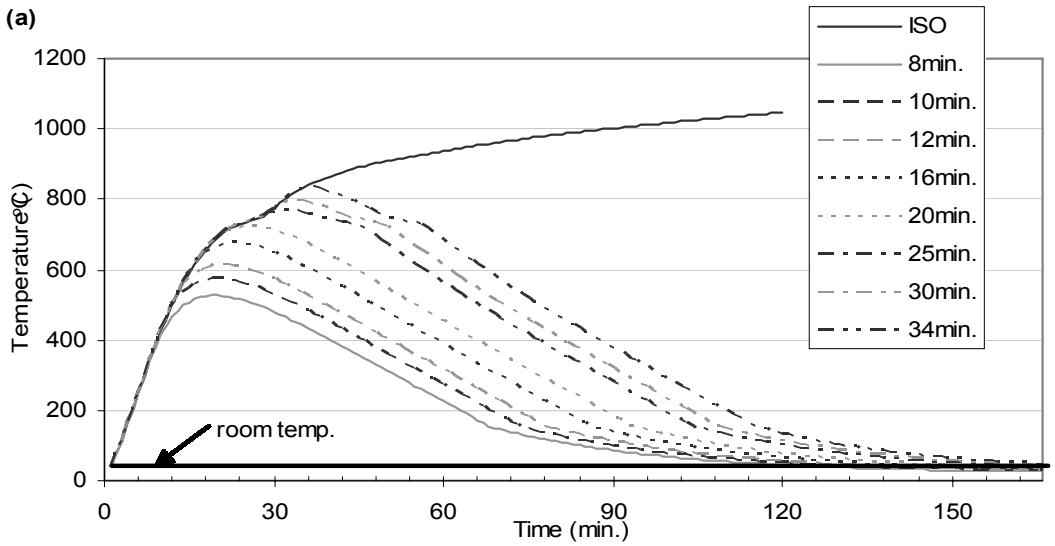
(a)
ISO
8min.
10min.
12min.
16min.
20min.
25min.
30min.
34min.
1200
1000
800
600
400
200
0
Temperature(℃)
room temp.
0
30
60
90
120
150
Time (min.)

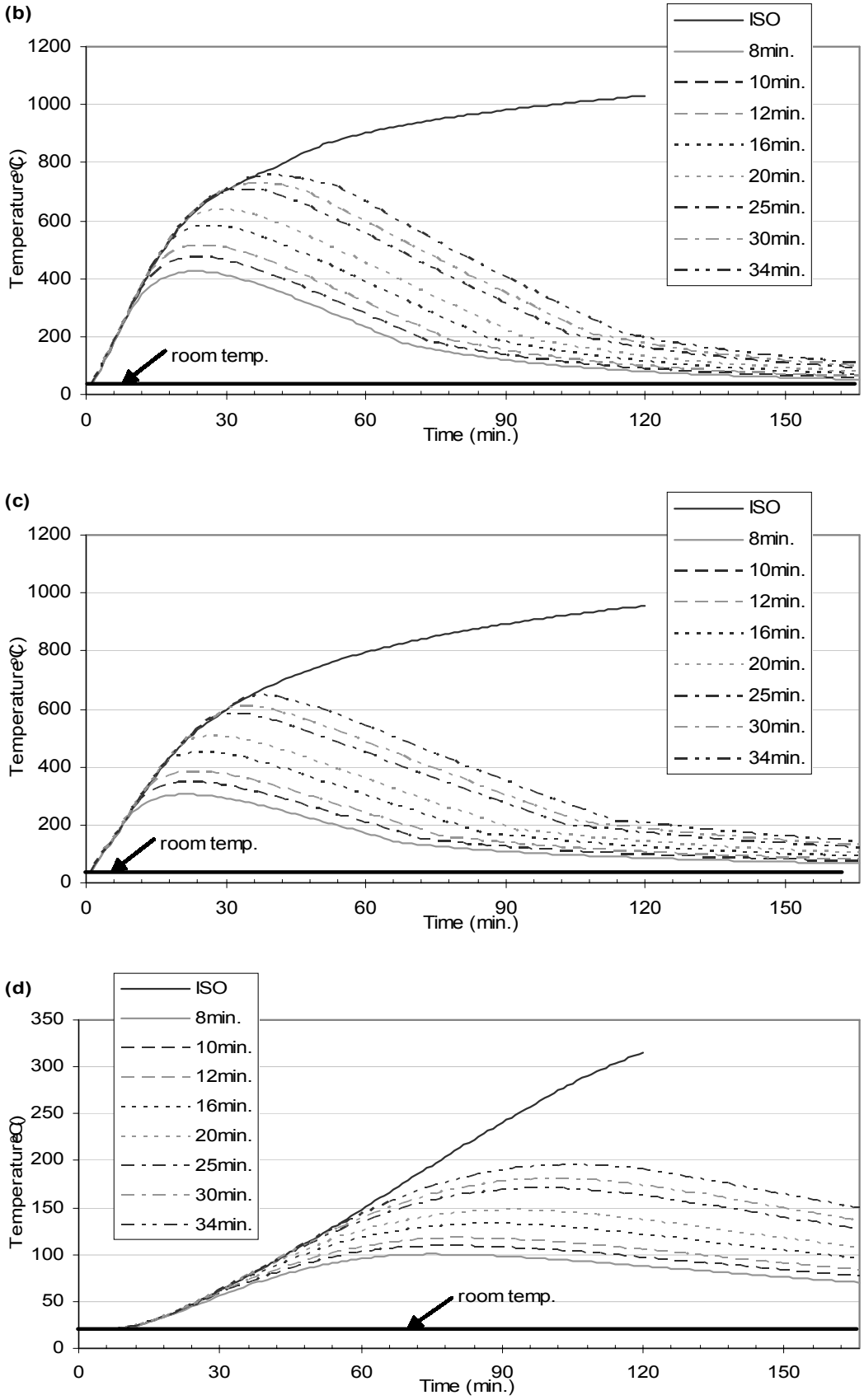

Figure 5-2 Temperature of composite steel beam exposed to various durations of the ISO fire with a decay phase: a) at the bottom steel flange; b) at the top steel flange; c) at the bottom of the concrete slab; d) at the top of the concrete slab

5.2 Structural analysis results of single span composite beams

5.2.1 Pin-pin composite beam

The first scenario discussed for the structural analysis results is the pin-pin connected composite beam. Figure 5-3 shows the support schematic.

Figure 5-3 Support schematic for Pin-pin case

In the case where the beam was exposed to the ISO834 standard fire without a decay phase, the beam failed after 37 minutes. Eight parametric fires, following from 8 to 34 minutes of the ISO fire, were used in the model for comparison. The beam did not fail under any of these fires before the end of the simulation at 166 minutes. Figure 5-4 shows the axial force and midspan displacement versus time of the beam exposed to various durations of the ISO fire with a decay phase or only the ISO834 standard fire.

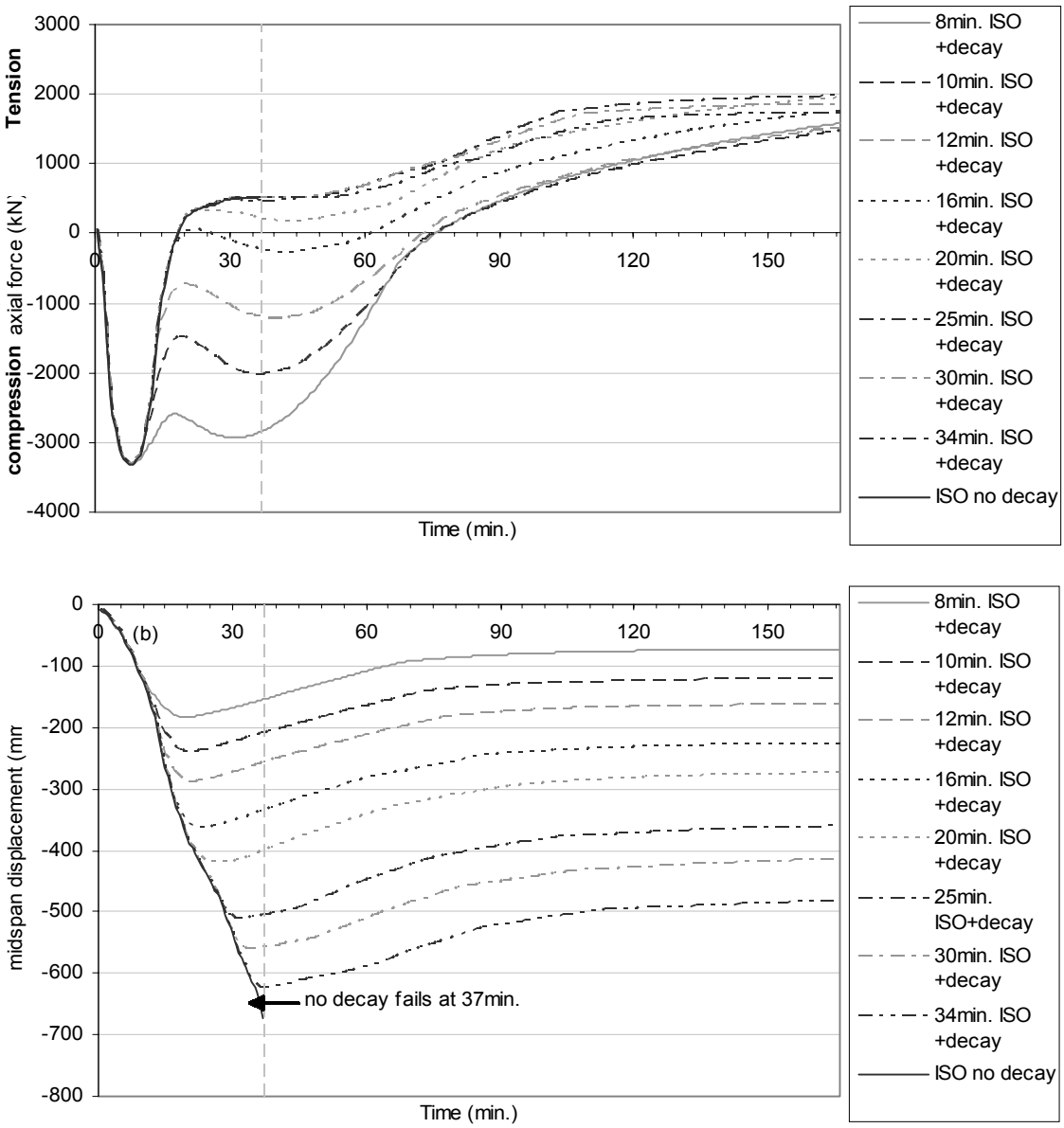

Figure 5-4 SAFIR outputs for pin-pin connected composite beam: (a) axial force; (b) vertical displacement at the midspan.

5.2.1.1 ISO834 standard fire (without decay phase)

The timeline for the ISO834 standard fire case is tabulated in Table 5-1.

Table 5-1 Event timeline of pin-pin connected composite beam under ISO834 standard fire (without decay)

Event	Time
Part of the bottom steel flange reaches the tensile proportional limit	5 minutes
Part of the top steel flange reaches the compressive proportional limit	6 minutes
The maximum compressive axial force occurs; the whole top steel flange reaches proportional limit	8 minutes
The bottom steel flange reaches the tensile yield limit; the stress in the top steel flange shifting rapidly to tension; axial force reduces because the steel section is losing stiffness	13 minutes
Top steel flange reaches the tensile proportional limit	23 minutes
Top steel flange is close to the tensile yield limit and a plastic hinge forms at midspan (the failure mechanism achieved)	37 minutes

The midspan bottom flange stress was plotted against time as shown in Figure 5-5. The bottom flange initially experienced a tensile stress from its loading under the ambient temperature. During the first 5 minutes of fire, the bottom flange became hot and expanded as the fire temperature increased rapidly. However, the temperature of the concrete slab increased much less than in the steel flange as suggested in Figure 5-2, which caused thermal bowing and further built up the tensile stress in the bottom flange. At a time of 5 minutes, the tensile stress reached the temperature-reduced proportional limit; this was when the bottom flange began to behave inelastically. Afterwards the tensile stress remained roughly constant as the increase in the midspan displacement relieved some axial stresses. As given by EC3, the yield limit continued to decrease as the temperature of the steel increased. The tensile stress eventually reached the yield limit at 13 minutes when the bottom flange yielded.

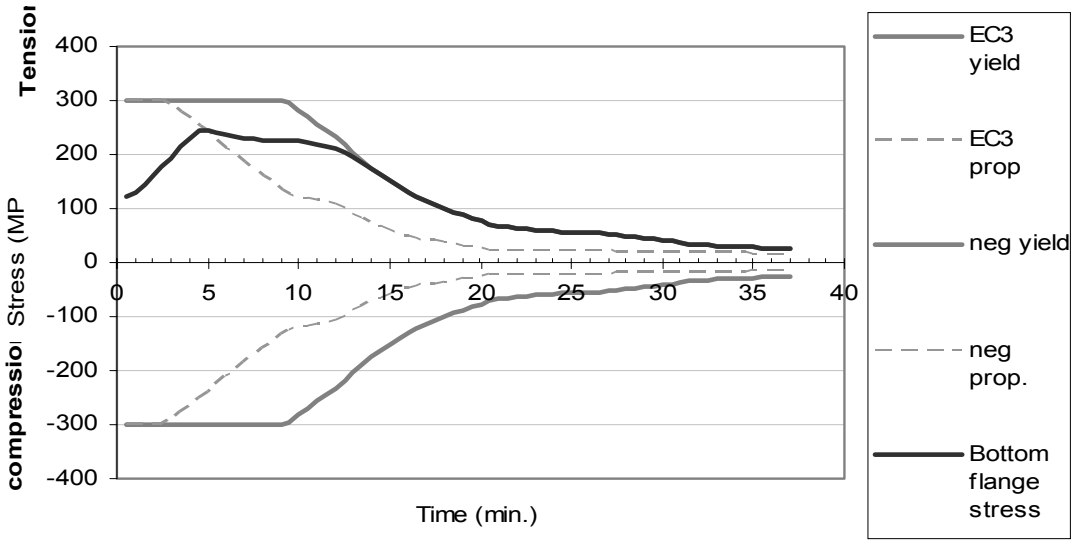

Figure 5-5 Bottom flange stress of pin-pin connected composite beam exposed to the ISO fire without decay

Figure 5-6 shows the centreline stress of this case at 8 minutes when the midspan displacement was at its maximum. At this time the entire bottom flange and the lower part of the web had reached the tensile proportional limit, while the top flange exceeded the compressive proportional limit.

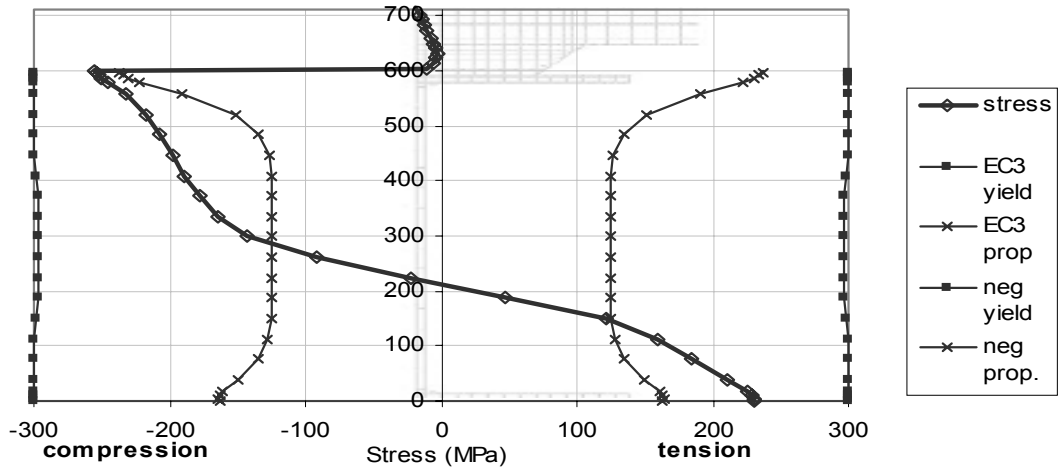

Figure 5-6 Centreline stress for pin-pin connected composite beam exposed to the ISO fire at 8 minutes

Figure 5-7 shows the changes of top flange stress over time. Because the temperature difference between the top and bottom flange caused thermal bowing, together with the axial restraint on the beam preventing thermal expansion, the compressive stress built up during the first 6 minutes. At a time of 6 minutes, the compressive stress in the top flange reached the proportional limit and decreased a little bit as non-linear elastic behaviour took place. At 13 minutes, the compressive stress started to reduce rapidly; meanwhile, the bottom flange yielded, and then the top flange stress eventually became tensile. This was because a rapid displacement occurred at the centre of the beam when the bottom flange was yielding, which decreased the bending moment and produced a net tension across the entire steel section. The stress in the top flange reached the proportional limit at 23 minutes, and then it became constant until the beam failed. The program determined the structure failed at 37.5 minutes. The failure was caused by a plastic hinge forming at the midspan and allowing a very rapid increase in deflection.

The temperatures and stresses used in Figure 5-5 and Figure 5-7 were obtained by using the average values in the finite elements of the top and bottom flanges. Therefore, the time suggested in these two graphs is earlier than the time when the top or the bottom flanges yielded completely.

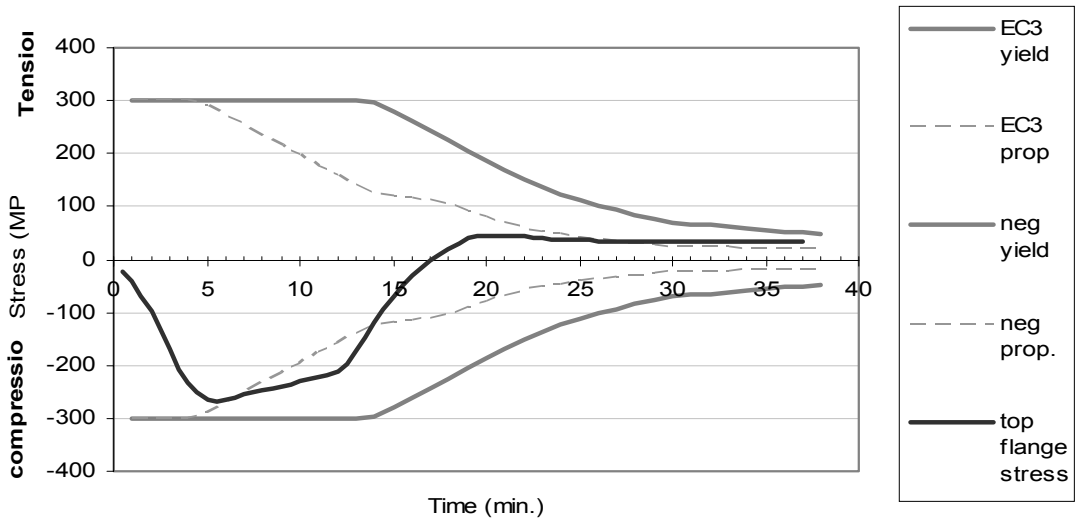

Figure 5-7 top flange stress for pin-pin connected composite beam exposed to the ISO fire without decay

5.2.1.2 Various durations of the ISO fire with a decay phase

The axial forces and midspan displacements in the pin-pin composite beam under different parametric fires are plotted in Figure 5-4. Figure 5-4(a) showed that the maximum compressive force approximated 3300kN in all cases and occurred at 8 minutes after fire started. The centreline stress distribution in Figure 5-6 showed that the stress of the entire top flange section exceeded the proportional limit at this time. The axial force decreased afterwards as the result of a loss of stiffness in the steel beam.

The axial force reached another turning point shortly after the rapid recovery from the maximum compressive force. The bottom flange was close to yield at this time. The neutral axis was almost at the bottom of the top flange, so the web and bottom flange were in tension.

Figure 5-4 (a) showed that if the duration of the ISO fire is longer, such as 30 or 34 minutes of the ISO fire before the decay phase, the difference in the axial force at any time is less obvious. In the case exposed to 34 minutes of the ISO fire with a decay phase, the beam did not fail before the end of the simulation. This was because the stress at the top flange never reached the yield limit, the plastic hinge could not be formed; therefore, the complete failure mechanism was not achieved. However, since most of the steel section of the case with 34 minutes of the ISO fire yielded in the same fashion as of the case without a decay phase, the axial force plots of these two cases appeared to be similar. On the contrary, the vertical displacement differed with the size of the fire, as a larger fire produces a greater thermal bowing in a composite beam.

Figure 5-4 (a) also showed that the axial forces for the cases exposed to small fires were similar while cooling. A small fire caused less of the steel section to yield, so the elastic neutral axis could be lower. In the results of these cases, most of the midspan displacement was recovered and less tensile force was created while cooling. This phenomenon was more significant in the cases exposed to fires following less than 12 minutes of the ISO fire.

The midspan vertical displacement of the pin-pin connected composite beam exposed to various durations of the ISO fire with a decay phase was shown in Figure 5-4(b). The figure showed that the shorter the fire, the less the vertical midspan displacement, and the more the displacement can recover when the beam cools down. Reading Figure 5-4(b) together with Figure 5-2 shows that the maximum midspan displacement occurred when the bottom flange reached its peak temperature, this displacement resulted from the thermal bowing as well as the yielding of the bottom flange.

5.2.1.3 20 minutes of the ISO834 standard fire with a decay phase

The events that happened in the first 20 minutes in this case were the same as in the scenario with ISO834 standard fire without a decay phase. Therefore, this section pays more attention to the behaviour of the beam while cooling.

Figure 5-8 shows the bottom flange stress in the pin-pin connected composite beam, and Figure 5-9 shows the top flange stress. After a time of 30 minutes, the tensile stress at the bottom flange started to reduce because the steel was recovering from its prior thermal expansion. Figure 5-10(a) shows the centreline stress at the time the bottom flange stress starts to reduce. The bottom flange and web carried the loads and were in tension after the bottom flange yielded. Figure 5-10(c) indicates that when the bottom flange was recovering from the thermal expansion and under compression, the web was still carrying the load and remained in tension. This tensile force in the web was so large that the centre of the web reached the tensile yield limit. Nevertheless, the plastic hinge did not form during any stage of the simulation.

Figure 5-4(b) showed the midspan vertical displacement. At the end of the simulation, because plastification had already taken place in both the top and bottom flanges, the vertical displacement at the midspan was not able to return to the initial height.

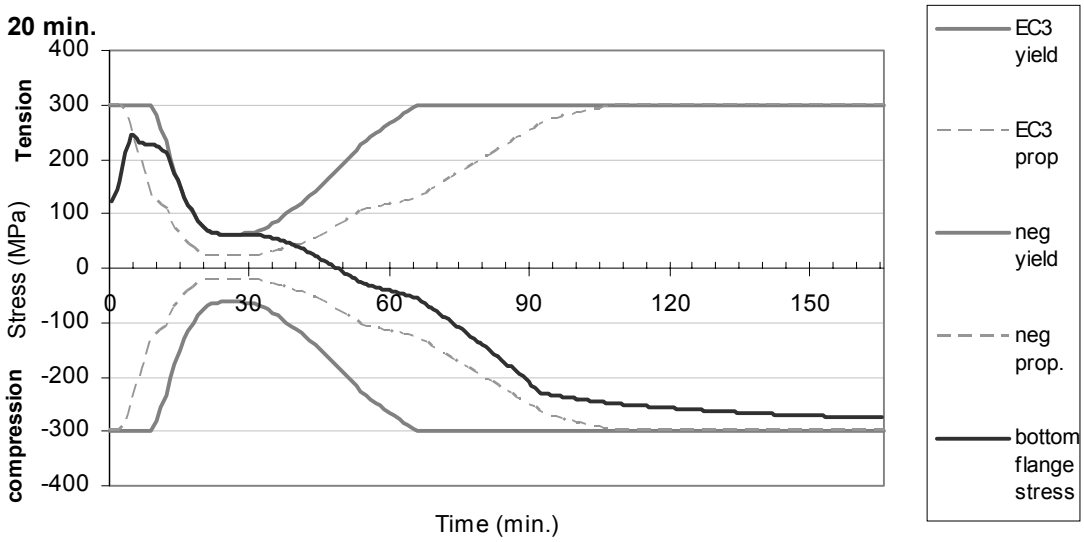

Figure 5-8 Bottom flange stress of pin-pin connected composite beam exposed to 20min. ISO fire with a decay phase

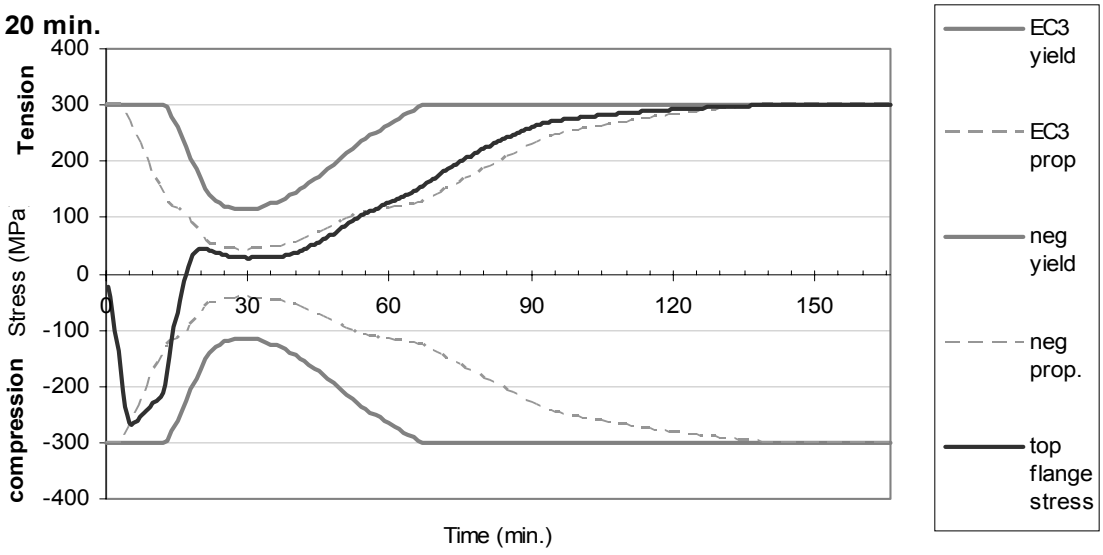

Figure 5-9 Top flange stress in pin-pin connected composite beam exposed to 20min. ISO fire with a decay phase

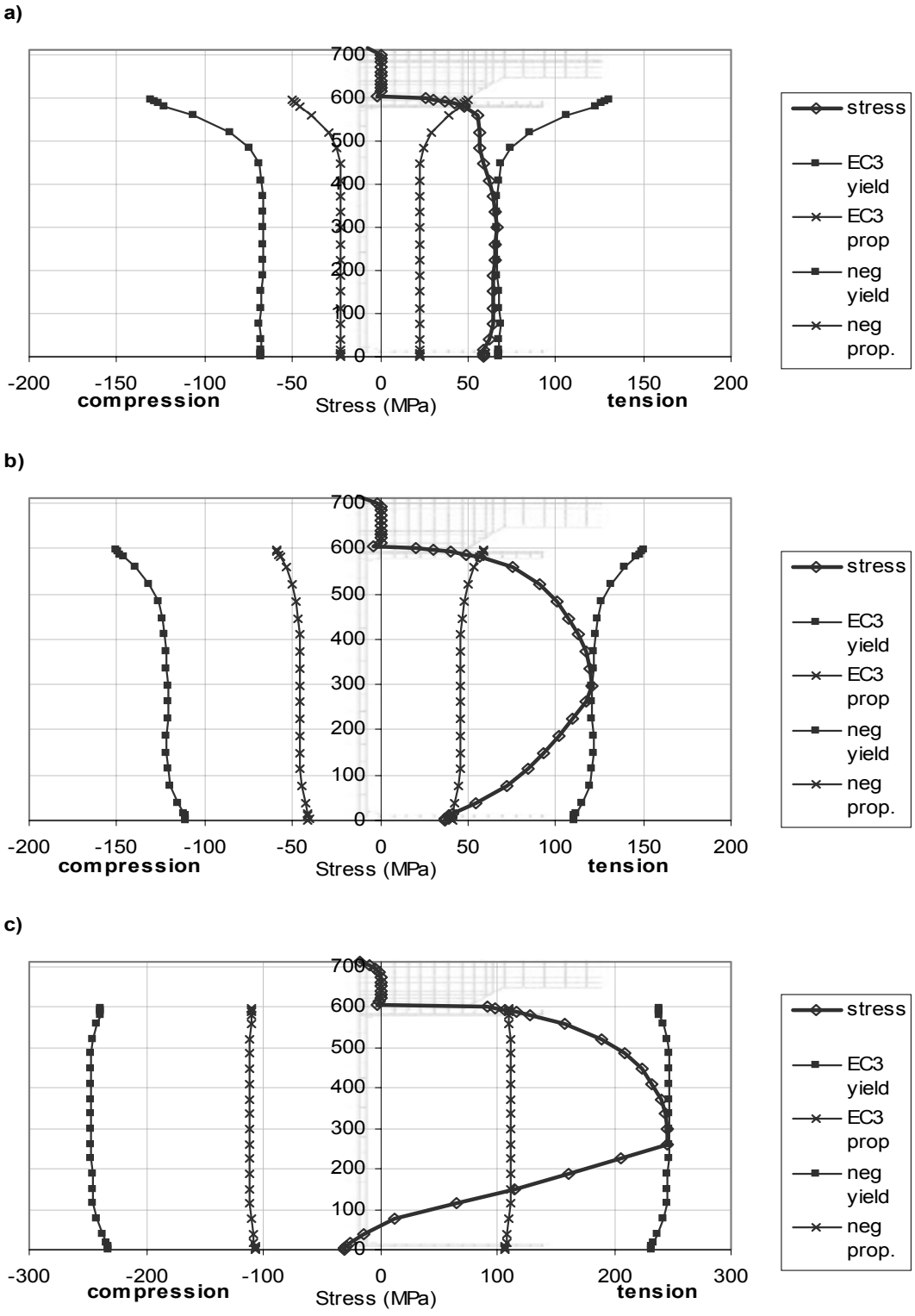

Figure 5-10 Centreline stress in pin-pin connected composite beam at 32 minutes, 40 minutes and 55 minutes exposed to 20 minutes of the ISO fire with a decay phase (from a to c, notice the horizontal scale is different)

5.2.1.4 10 minutes of the ISO834 standard fire with a decay phase

The structural behaviour in the cases with less than 10 minutes of the ISO fire and a decay phase was different to the cases discussed previously. Because the lower part of the steel beam did not reach the tensile yield limit by the end of the simulation, more midspan displacement was able to be recovered.

Figure 5-11 and Figure 5-12 show the bottom and top flange stress versus time respectively. Figure 5-11 indicates that the bottom flange remained at the temperature-reduced yield limit for a shorter time than in the case exposed to 20 minutes of the ISO fire.

Figure 5-13 shows the centreline stress distribution when the tensile stress at the bottom flange reached the yield limit as well as when the tensile stress started to reduce. This figure shows how the bottom flange stress progressed from the tensile yield limit to being in compression. It also shows the stress at the top flange developed from the compressive proportional limit to the tensile proportional limit. The graphs further indicate that there was no tensile yielding in the web until the bottom flange was in compression, but the web yielded in tension before the top flange did.

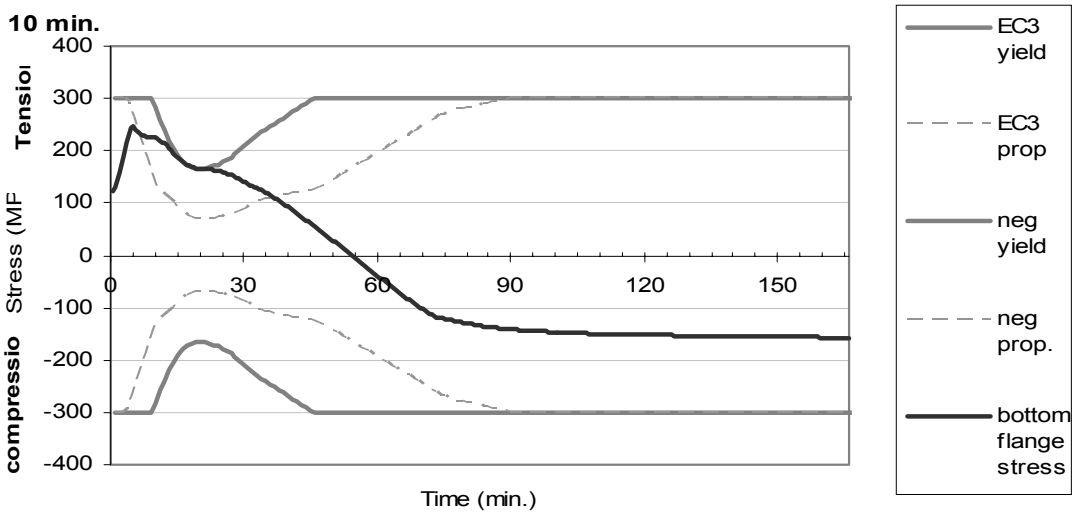

Figure 5-11 Bottom flange stress in pin-pin connected composite beam under 10 minutes of the ISO fire with a decay phase

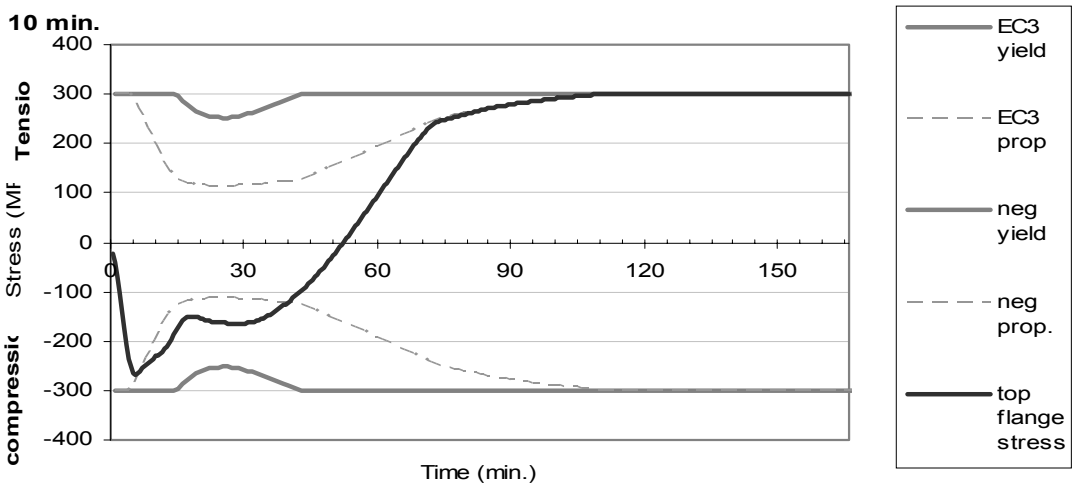

Figure 5-12 Top flange stress in pin-pin connected composite beam under 10minutes of the ISO fire with a decay phase

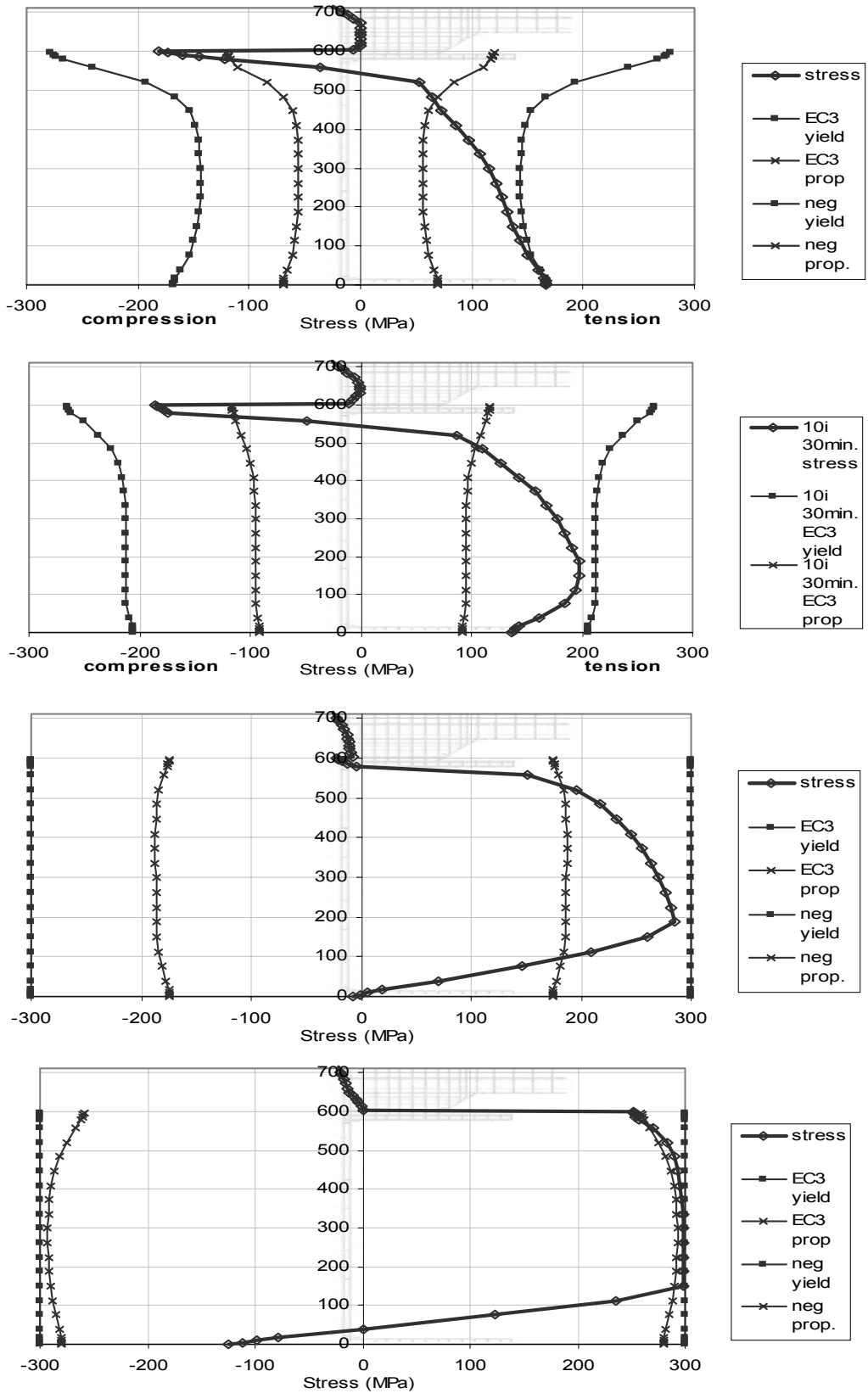

Figure 5-13 Centreline stress in pin-pin connected composite beam at 19 minutes, 30 minutes, 55 minutes and 78 minutes exposed to 10 minutes of the ISO fire with a decay phase (from top to bottom)

5.2.1.5 Summary for single span pin-pin composite beams

In the scenario where a single span pin-pin composite beam was exposed to the ISO834 standard fire, the structure failed after 37 minutes because a plastic hinge formed at midspan. In the cases where the beam was exposed to 8 parametric fire curves which followed 8 to 34 minutes of the ISO fire before the decay phase, the structure did not fail before the end of the simulation.

The graph of the axial forces in Figure 5-4 suggested that the maximum compressive axial force occurred when the top steel flange reached the temperature reduced compressive proportional limit. The magnitude of this compressive force did not vary with the fire temperature.

The time of occurrence of the maximum tensile force varied with the fire temperature, and the beam exposed to a less intensive fire reached the maximum tensile axial force much slowly. Nevertheless, in the scenarios modelled here, the maximum axial force approximated 2000kN and happened after the steel cooled. Unlike the maximum compressive axial force which lasted for a very brief time, the tensile force at the beam remained at its maximum after the beam was cooled.

The graph of the midspan vertical displacement in Figure 5-4 showed that the permanent displacement was in proportion to the fire temperature, and that all the fires used caused a permanent displacement at the midspan.

The centreline stress diagrams in Figure 5-10 and Figure 5-13 showed that the web at the midspan would reach the tensile yield limit while cooling. This occurred much earlier than the time at which the top flange reached the tensile yield limit in those cases where yield occurred. Meanwhile, the compressive stress at the bottom flange would increase with time.

5.2.2 Fix-fix composite beam

In the scenario of which a single span fix-fix composite beam was exposed to the ISO834 standard fire without a decay phase, the beam failed in 18 minutes; and the beam exposed to 16 minutes ISO834 standard fire with a decay phase failed at 18.5 minutes. Three other temperature curves, with 8 to 12 minutes of the ISO fire and a decay phase, were used in this model for comparison, and the beam did not fail under these three fires. Figure 5-14 shows the support schematic for the fix-fix connected composite beam; and Figure 5-15 shows the axial force and the midspan vertical displacement of the beam.

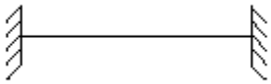

Figure 5-14 Support schematic for fix-fix case

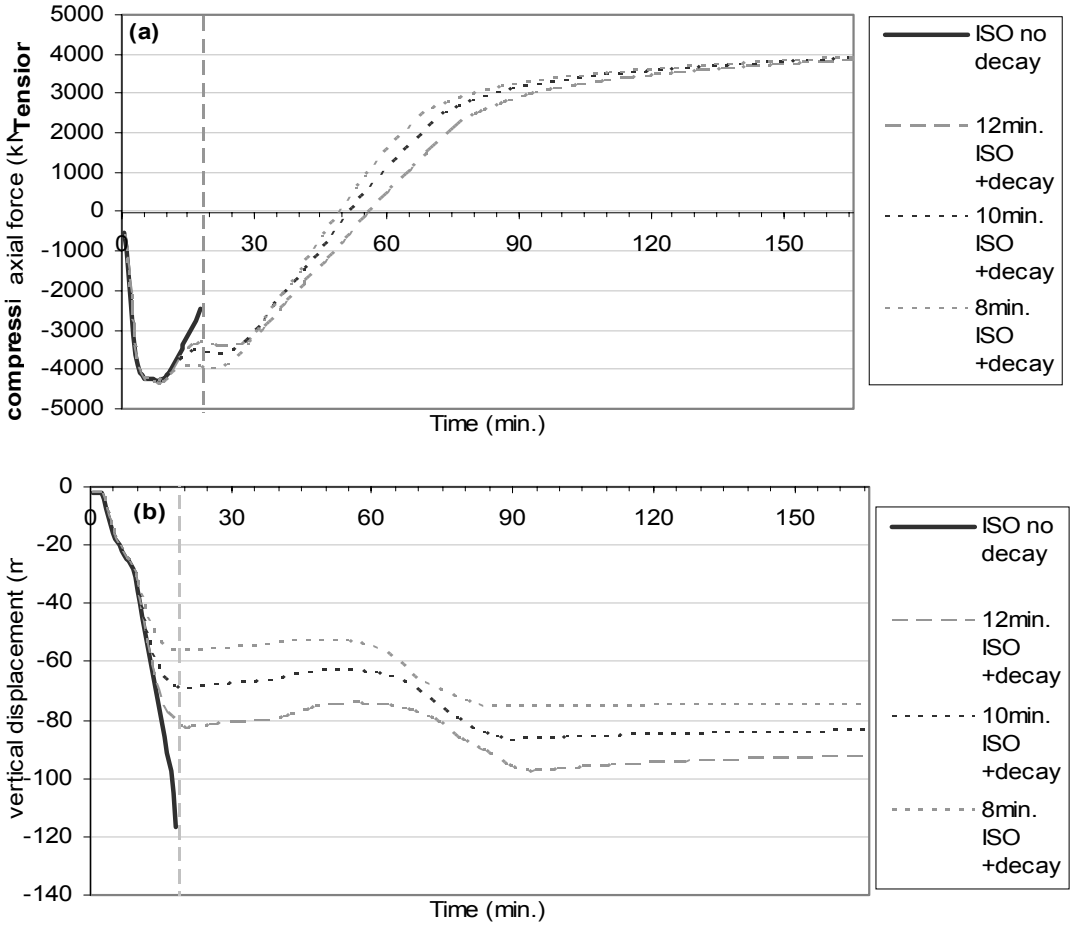

Figure 5-15 SAFIR outputs for fix-fix connected composite beam: (a) axial force; (b) midspan vertical displacement

5.2.2.1 ISO834 standard fire (without decay phase)

The case of a single span fix-fix connected composite beam exposed to the ISO834 standard fire has been discussed by Wastney (2002). The observed behaviour from the newly conducted simulation was similar except for a slight difference in the time each event occurred. This was due to using a different precision of the convergence in the SAFIR calculation. The timeline of the structural behaviour is shown in Table 5-2.

Table 5-2 Timeline of the structural behaviour in single span fix-fix connected composite beam exposed to the ISO834 standard fire (without a decay phase).

Event	Time
The bottom flange of the steel beam near the connection reaches the compressive yield limit. The midspan of the beam deflects suddenly. The rate of increase of the compressive axial force reduces.	3 minutes
The top flange of the steel beam near the connection reaches the temperature reduced compressive proportional limit	4 minutes
The top flange at the midspan reaches the compressive proportional limit.	5 minutes
The bottom flange at the midspan reaches the compressive proportional limit. The compressive axial force reaches the maximum value of 4.3MN.	8 minutes
The yield limit of steel in the bottom flange starts to reduce because of the elevated temperature. The compressive bottom flange stress at the midspan and near the connection starts to reduce. The increase rate of the compressive axial force becomes much greater.	9 minutes
The bottom flange at the midspan reaches the temperature reduced tensile proportional limit.	16 minutes
The top flange near the connection reaches the compressive yield limit. The maximum vertical displacement at the midspan is reached as 117mm. SAFIR determines structural failure occurs at this time.	18 minutes

Figure 5-16 and Figure 5-17 show the stresses in the top and bottom flange at the midspan of the beam and near the connection, they also show the thermal-reduced yield limit and proportional limit at different times. Before heating, the applied loads caused the bottom flange at the midspan to be in tension and the top flange to be in compression. When the beam was heated, the bottom flange stress at the midspan quickly shifted to compression because of the thermal expansion.

Figure 5-18 shows the centreline stress distribution at the midspan of the beam. At a time of 3 minutes, almost the entire beam section was under compression. This indicates the beam had a large compressive force but little displacement; otherwise, one would find a force couple in the beam.

The axial force curve is shown in Figure 5-15. Since the beam axial force was large, the horizontal reaction force at the connections needed to be large. Because of the P-Δ effect, the product of this large horizontal reaction force and the vertical displacement caused a large bending moment at the midspan. However, since the difference from the top and the bottom flange stresses caused by the bending moment was not large, one can assume that the vertical displacement at the midspan of the beam was small at this time. This was confirmed in the vertical displacement of the midspan curve in Figure 5-15.

Also at 3 minutes, the bottom flange stress near the connections reached the temperature-reduced proportional limit and the bottom flange started to soften. Because of this inelastic behaviour, the bottom flange stress in the midspan as well as near the connection became nearly constant, and a sudden increase in the midspan vertical displacement happened at this time.

At a time of 8 minutes, the bottom flange near the connection yielded and the stress remained at the level of the yield limit. The curves of the bottom flange stress at the midspan and near the connection were nearly parallel to each other. For the bottom flange, when the compressive stress near the connection began decreasing along with the yield stress, the stress at the midspan also reduced and became tensile, reaching the proportional limit at 16 minutes. Figure 5-18(c) shows the stress in the cross section at the midspan at 16 minutes.

In a fix-fix supported beam, the failure mechanism is one plastic hinge forming at each end of the span and one at the midspan of the beam. Figure 5-16 and Figure 5-17 show that at the time the beam failed, both the top and bottom flange near the connection were at the compressive yield limit; and at the centre of the beam, the bottom flange reached the tensile yield limit and the top flange reached the compressive yield limit allowing the three hinges to form.

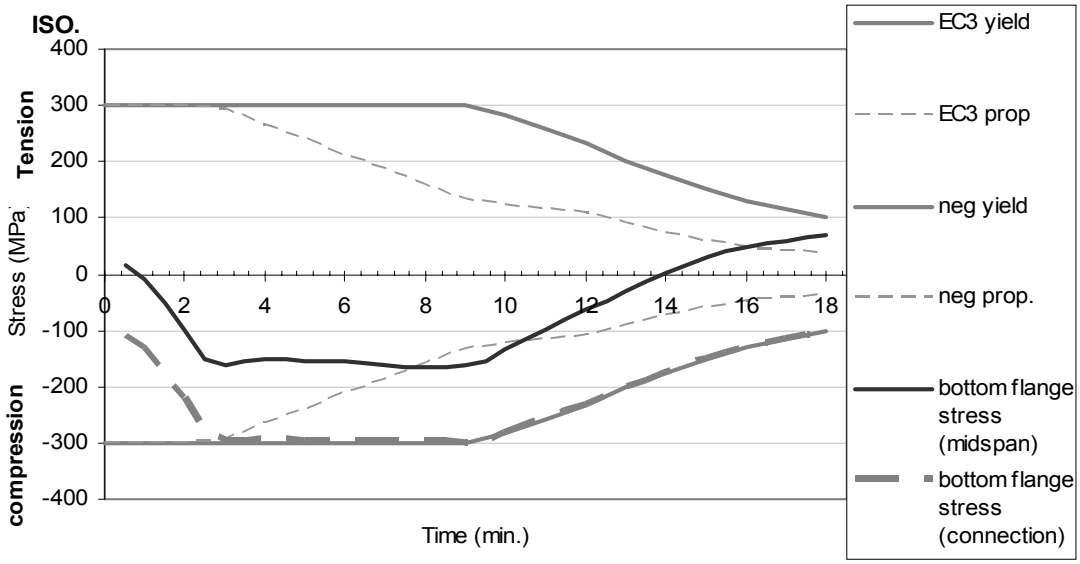

Figure 5-16 Bottom flange stress in single span fix-fix connected composite beam

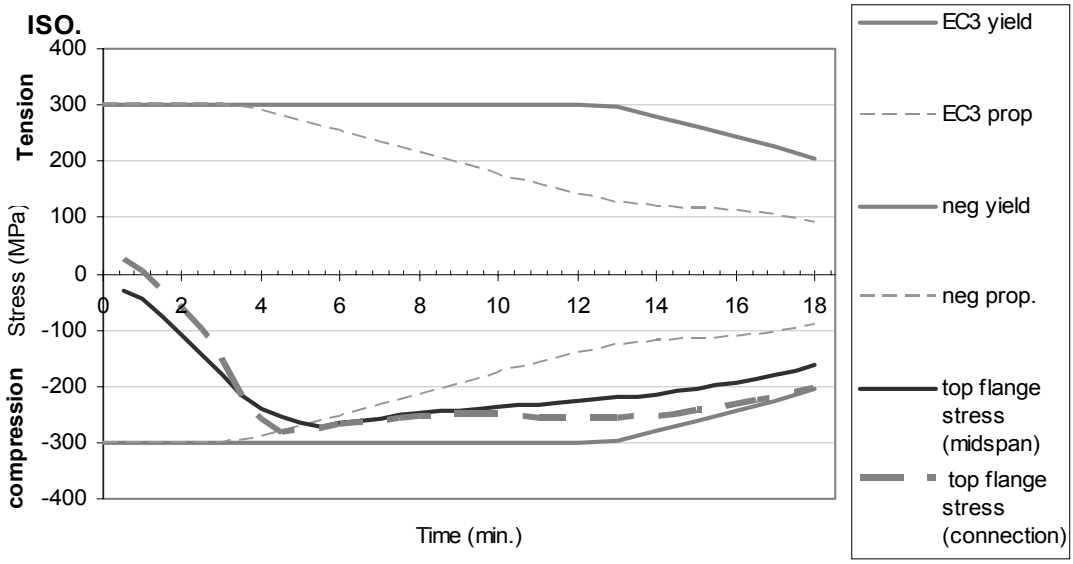

Figure 5-17 top flange stress in single span fix-fix connected composite beam

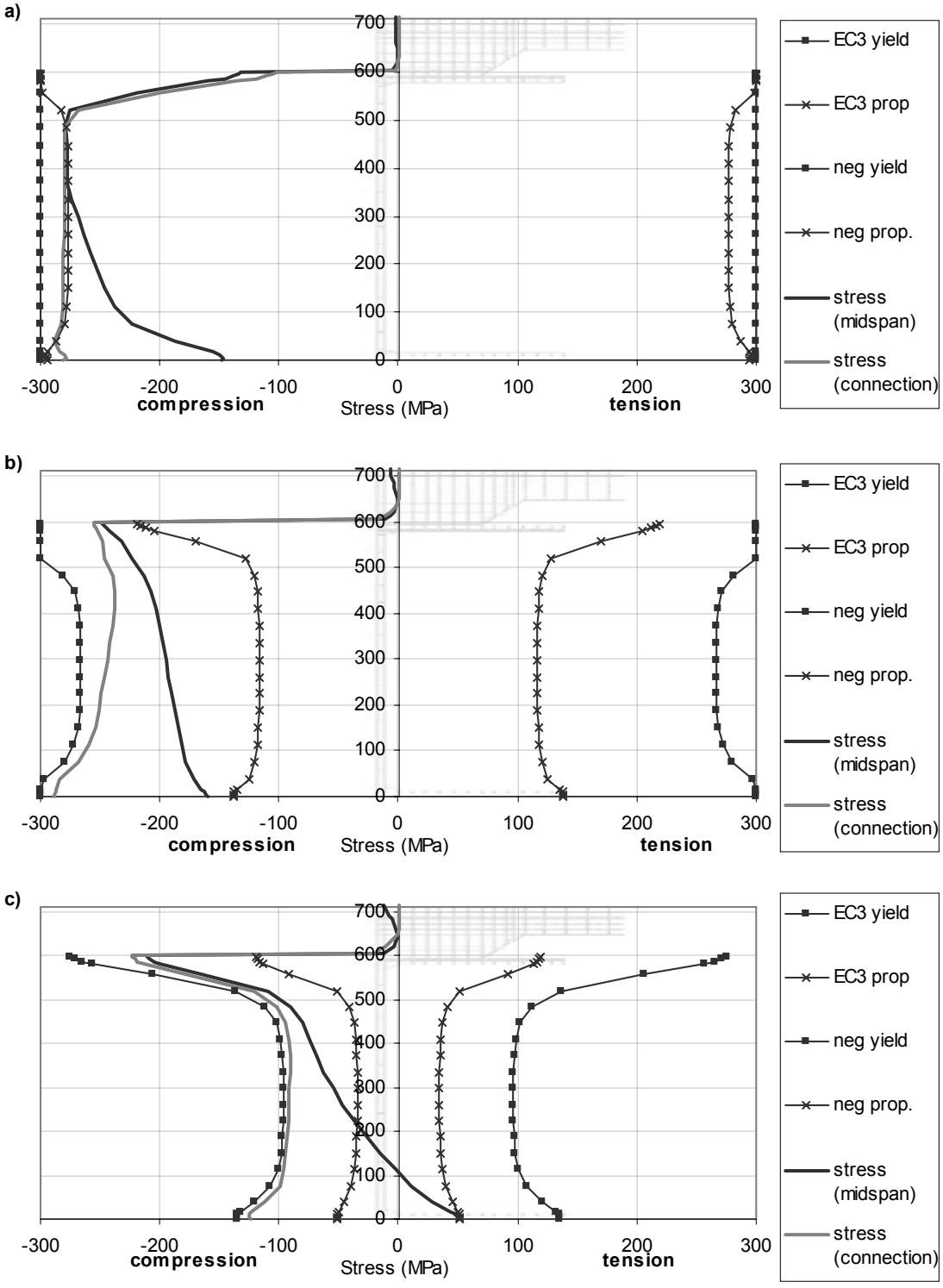

Figure 5-18 Centreline stress distribution in the single span fix-fix connected composite beam at (a) 3 minutes, (b) 9 minutes and (c) 16 minutes exposed to the ISO834 standard fire without a decay phase

5.2.2.2 10 minutes of the ISO834 standard fire with a decay phase

Figure 5-15 showed the axial force and the midspan vertical displacement of the beam. The tensile axial force increased while cooling as in the case with the pin-pin supports. However, one can compare Figure 5-15(a) with Figure 5-4(a) to observe that both the maximum tensile and compressive force were larger than in a pin-pin supported beam. For example, when the beam was exposed to 10 minutes of the ISO fire with a decay phase, the axial force at 166 minutes was 4000kN, which was twice the value of the case with pin-pin supports.

Figure 5-19 and Figure 5-20 show the bottom and top flange stresses in this case. The graphs show that the bottom flange stress at the midspan developed in a similar way to the stress near the connection. After the bottom flange near the connection reached the compressive yield limit, both the stresses at the top and bottom flanges started to shift to tension. Although the structure did not fail before the end of the simulation, the top and bottom flange stresses at the midspan and near the connection all reached the tensile yield limit. This indicates the beam was in catenary behaviour.

The behaviour of the beam at three particular times was chosen to be analysed using centreline stress distribution diagrams. Figure 5-21 shows the centreline stresses at 24, 60 and 166 minutes. At 24 minutes, the bottom flange stress near the connection started to increase from the temperature-reduced yield limit level, IN the mean time the midspan bottom flange stress became zero; at 60 minutes, the midspan vertical displacement had a sudden increase; and 166 minutes was the end of the simulation.

The centreline stresses show that at 24 minutes, the entire steel beam section near the connection was almost at the compressive yield limit, but at the midspan, only the upper portion of the beam exceeded the compressive proportional limit. Figure 5-2(a) and (b) showed that at this time, the temperature of the steel beam started to reduce, and the steel beam started to recover from its thermal expansion. Figure 5-15(a) showed that before 24 minutes, the axial stress in the beam was constant as the beam was softening, and after this time, the compressive axial force decreased. This agrees with the behaviour in Figure 5-19 which the bottom flange stress was moving towards tension after a time of 24 minutes.

The graph for the centreline stress distribution at 60 minutes shows that the stress at the lower portion of the beam at the midspan exceeded the tensile proportional limit, so the web and lower flange were inelastic. This would cause a sudden increase in the midspan vertical displacement as well as a mild increase in the tensile axial force as shown in Figure 5-15.

The centreline stress at 166 minutes was at the tensile yield limit, which indicates that the beam was experiencing a large tensile axial force and was in catenary behaviour as observed from Figure 5-19 and Figure 5-20.

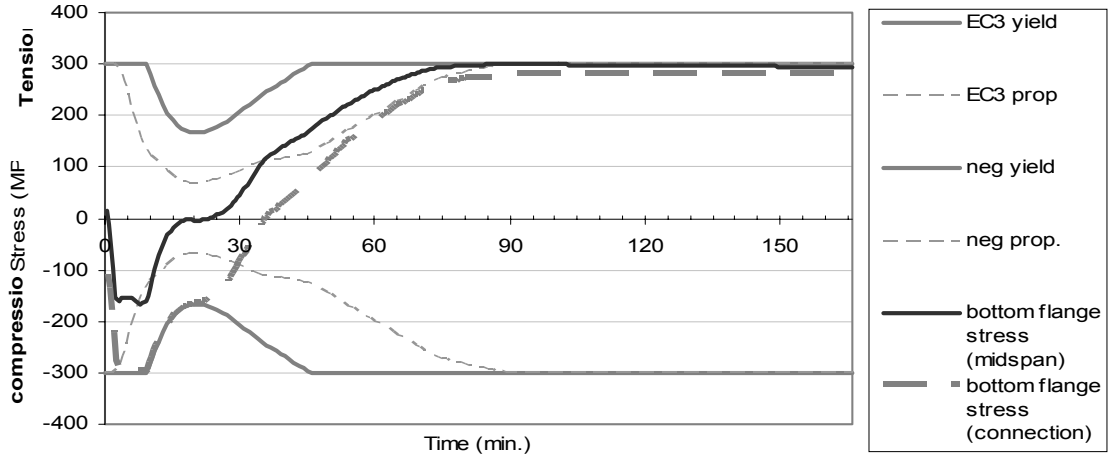

Figure 5-19 Bottom flange stress in single span fix-fix connected composite beam exposed to 10min. of the ISO fire with a decay phase

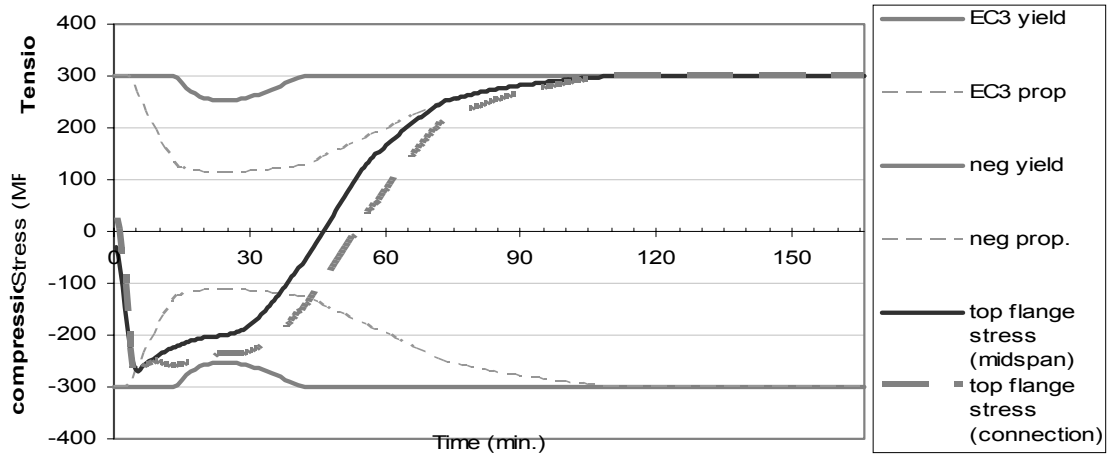

Figure 5-20 Top flange stress in single span fix-fix connected composite beam exposed to 10min. of the ISO fire with a decay phase

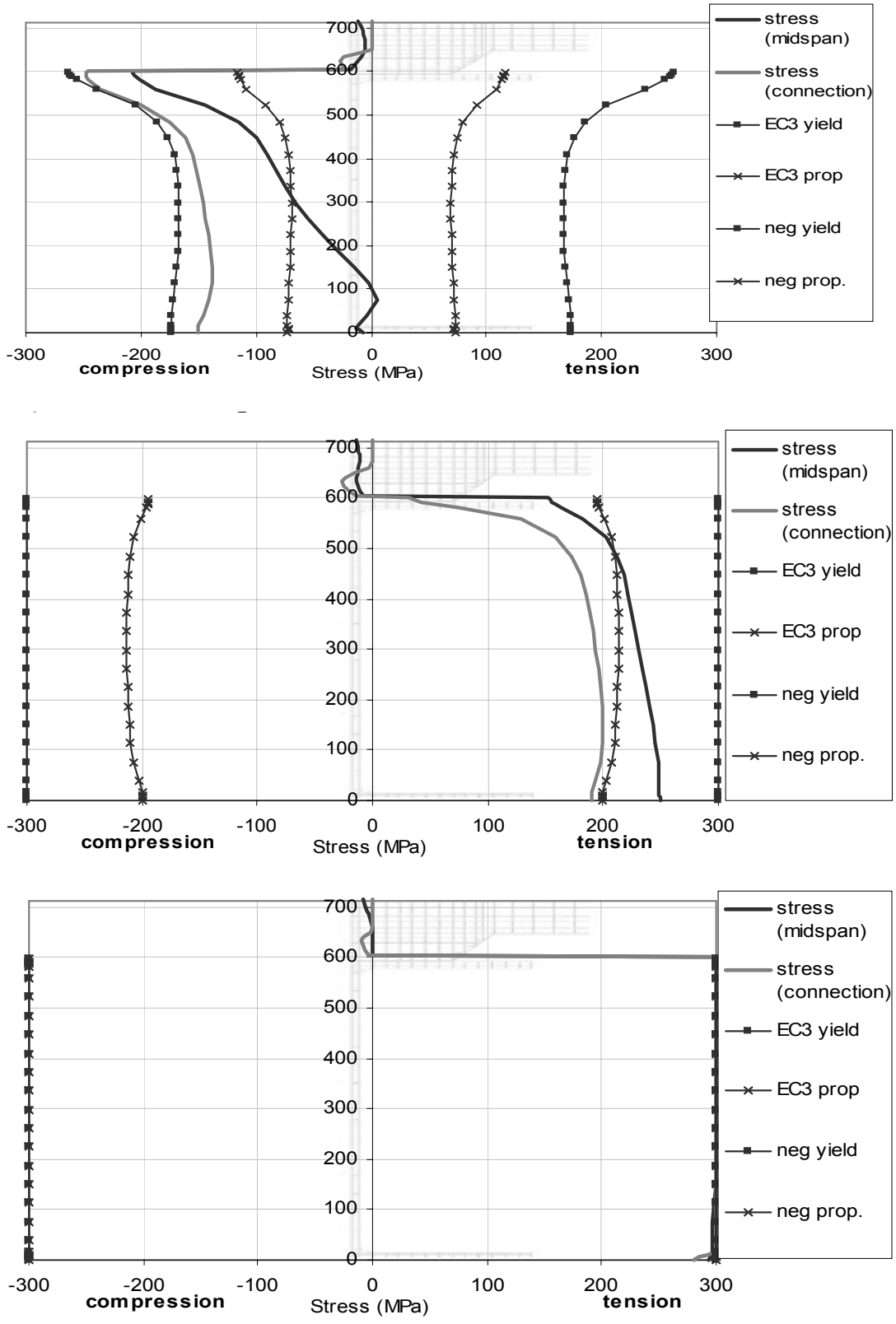

Figure 5-21 Centreline stresses at 24, 60 and 166 minutes in single span fix-fix connected composite beam exposed to 10 minutes of the ISO fire with a decay phase

5.2.2.3 Summary for single span fix-fix connected composite beam

For the case of a single span fixed-fixed composite beam exposed to the ISO834 standard fire, the beam failed after 18 minutes as one plastic hinge formed at the centre of the beam and two at the connections. Four parametric fire curves range from 8 to 16 minutes of the ISO fire and a decay phase were used for comparison. The beam exposed to 16 minutes of the ISO fire with a decay phase failed at 18.5 minutes, while the other fires did not cause the beam to fail.

The graph for axial force in Figure 5-15 showed the tensile force at the end of the simulation had a similar magnitude to the maximum compressive force caused during the heating phase. It is inconclusive whether the maximum tensile force had been reached at the end of the simulation. Both the maximum compressive and tensile axial forces were larger than those for the pin-pin case were, but in this case, the compressive axial force remained at its maximum level longer.

Because the fix-fix connected beam had moment restraints at both ends, both the rotation of the beam and the midspan vertical displacement were limited before a plastic hinge was formed near the connection. The graph for midspan vertical displacement showed the moment restraints reduced the displacement by half compared to the pin-pin case. It also showed that the rate of increase of the displacement after the decay phase was larger than during the heating period. The sudden deflection at the midspan while cooling suggests that more than one location along the beam started to behave inelastically. The graph further showed that the vertical displacement after the structure cooled was in proportion to the size of the fire.

Figure 5-18 and Figure 5-21, the centreline stress distribution diagrams, show that the entire steel section was under compression during the heating period; during the decay phase, the steel section started to experience tensile stress. The web and the bottom flange reached the yield limit at a similar time which was earlier than when the top flange yields in tension.

5.2.3 Pin-roller composite beam

The third scenario studied for the single span composite beams was with a pin-roller connection condition. Figure 5-22 shows the support schematic for the pin-roller case. In the scenario where the beam was exposed to the ISO834 standard fire without a decay phase, SAFIR determined that the beam failed at 21.5 minutes. When the beam was exposed to 20 minutes of the ISO fire with a decay phase, it failed after 22 minutes. Four fire curves, range from 12 minutes to 18 minutes of the ISO fire with a decay phase, were chosen for comparison, and the beam did not fail in any of these fires during the simulation.

Figure 5-22 support schematic for pin-roller case

Figure 5-23 shows the vertical displacement at midspan as well as the horizontal displacement at the roller end versus time of these cases. Further discussion about these two graphs are made in the following sections.

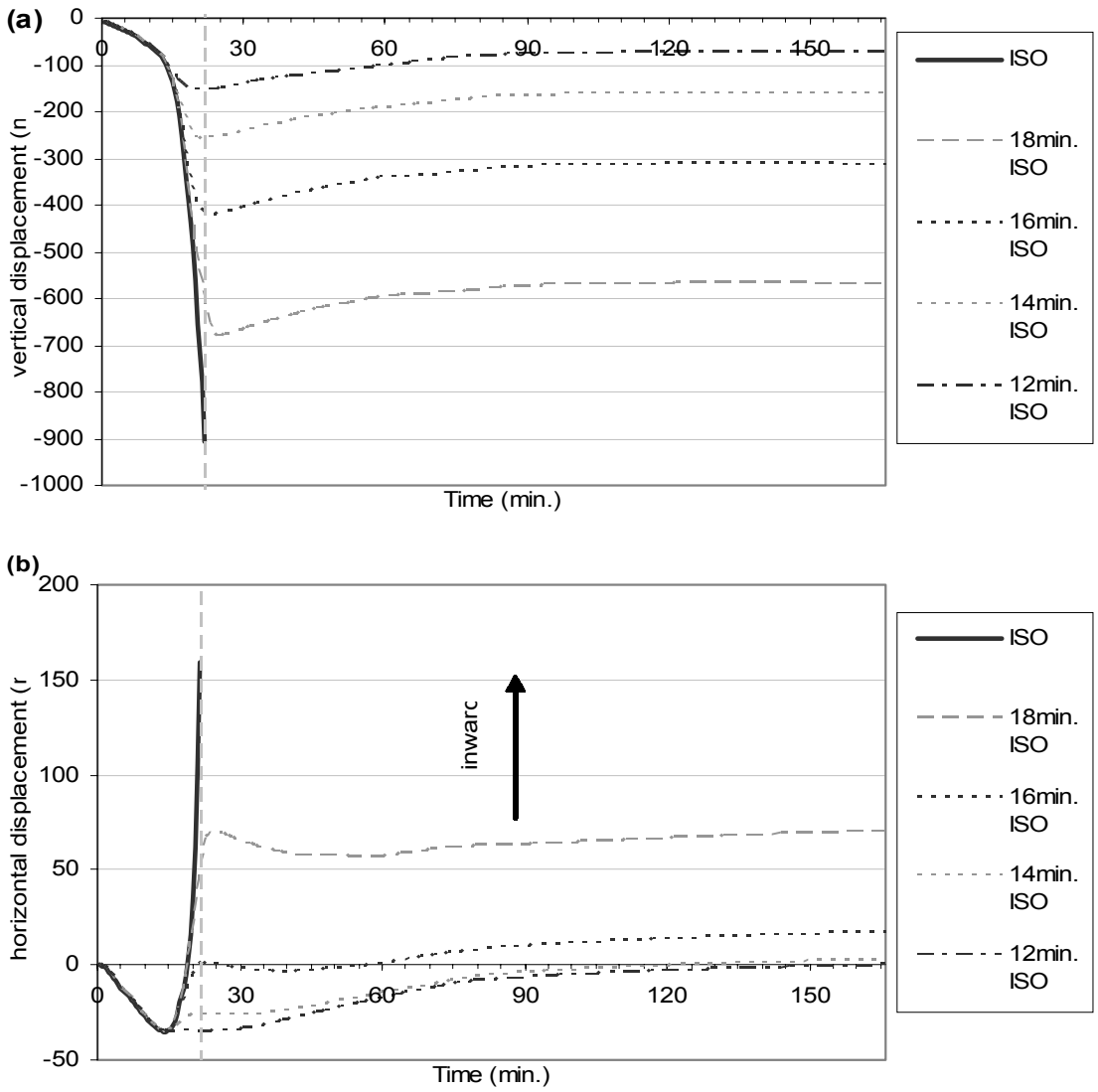

Figure 5-23 SAFIR simulation results for single span pin-roller connected composite beam exposed to various durations of the ISO fire: (a) vertical displacement at the midspan; (b) horizontal movement at the roller end.

5.2.3.1 ISO834 standard fire (without decay phase)

The behaviour of a pin-roller connected composite beam exposed to the ISO834 standard fire was also discussed by Wastney (2002) and Welsh (2001). The behaviour timeline for this case is shown in Table 5-3.

Table 5-3 timeline for structural behaviour of single span pin-roller connected composite beam exposed to the ISO834 standard fire

Event	Time
The bottom flange of the steel beam reaches the temperature reduced tensile proportional limit.	6 minutes
The top flange of the steel beam reaches the temperature reduced compressive proportional limit. The vertical displacement at the midspan starts to increase more rapidly. The horizontal displacement at the roller end reaches the maximum outward movement of 35mm.	13.5 minutes
The bottom flange reaches the tensile yield limit.	16 minutes
The top flange reaches the tensile proportional limit.	19 minutes
The top flange reaches the tensile yield limit forming one plastic hinge at the centre of the beam. The vertical displacement at the midspan is large at this time. SAFIR determines that the structure fails due to runaway deflections.	21 minutes

Wang (2002) summarised the test results on beams and concluded that the structural failure in a simply supported beam is dominated by the tensile yielding of the steel section. This finding was shown in this simulation result as well. The bottom and top flange stresses were plotted against time in Figure 5-24 and Figure 5-25 respectively. The bottom flange reached the temperature-reduced tensile proportional limit at 6 minutes. This was slightly slower than in the pin-pin case when it occurred at 5 minutes. The stresses shown in these figures were different to those for the pin-pin case. Because there was no horizontal restraint at the connection, less stress was built up, which made the top flange reach the compressive proportional limit at 13.5 minutes rather than at 6 minutes in the pin-pin case. The horizontal translation at the end allowed the bottom flange tensile stress to decrease after the beam reached the proportional limit.

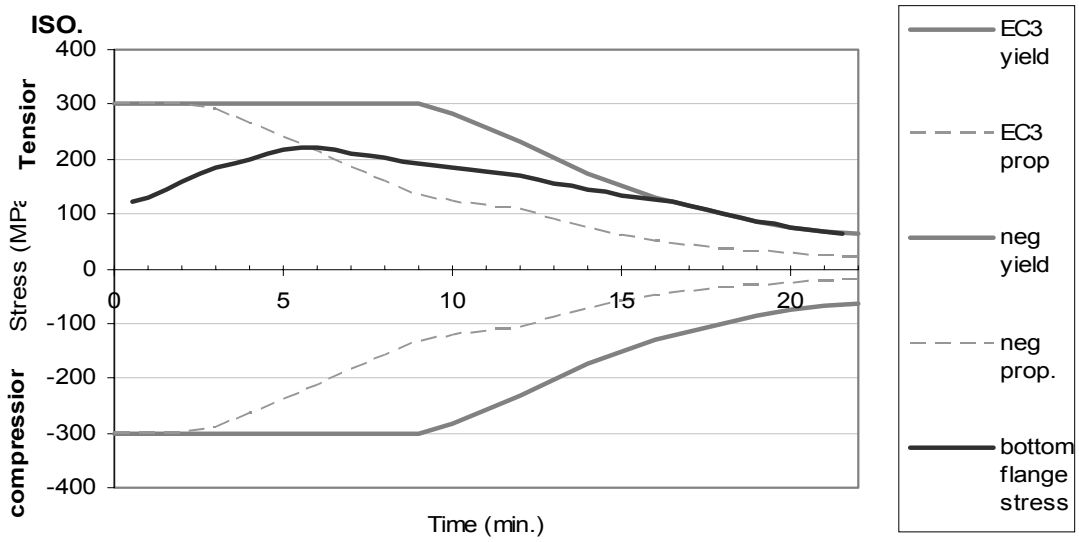

Figure 5-24 Bottom flange stress at the midspan in single span pin-roller connected composite beam exposed to the ISO fire

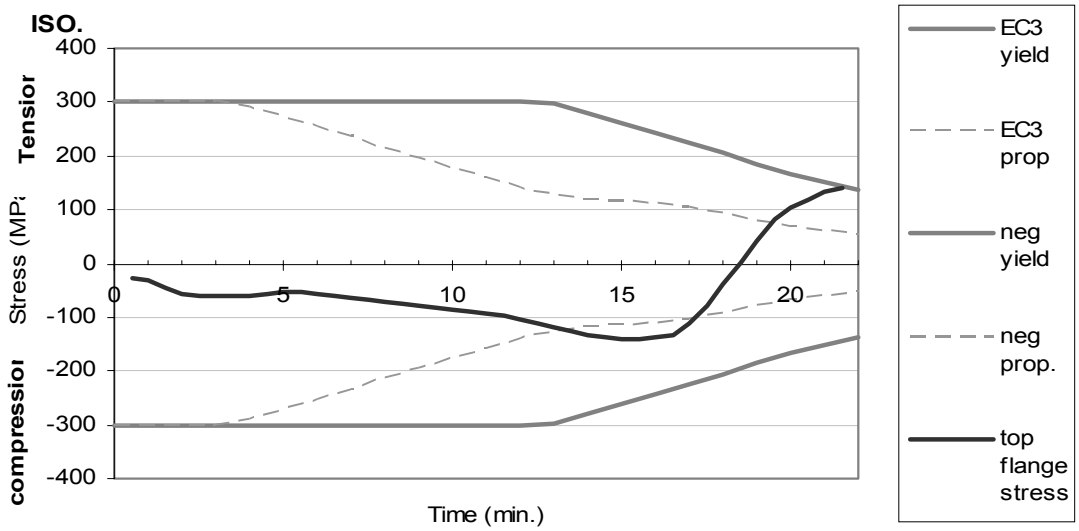

Figure 5-25 Top flange stress at the midspan in single span pin-roller connected composite beam exposed to the ISO fire

Figure 5-23(b) showed the horizontal displacement at the roller end of the beam. This can be compared with Figure 5-23(a), the midspan vertical displacement graph. When the midspan vertical displacement was small, the thermal expansion of the beam was reflected in the horizontal movement and made the roller end move outward. After a time of 16 minutes, the tensile bottom flange stress reached the temperature-reduced yield point, and the top flange stress exceeded the compressive proportional limit as shown in the centreline stress distribution in Figure 5-26. The vertical displacement at the midspan at this time increased rapidly, which pulled the whole structure towards

the centre of the beam. Figure 5-23(b) showed the roller end of the beam moved inwards until the program determined that the beam failed.

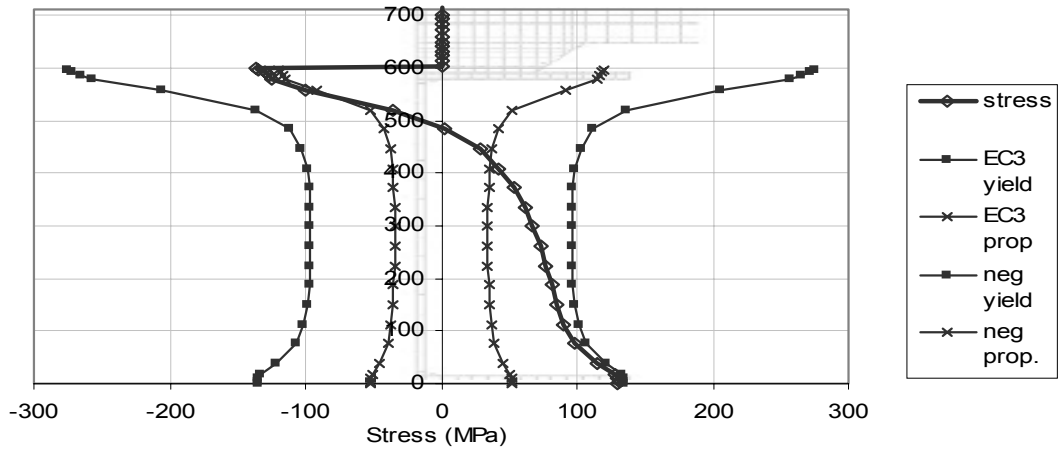

Figure 5-26 Centreline stress distribution of pin-roller supported composite beam exposed to the ISO fire at 16 minutes

5.2.3.2 16 minutes of the ISO834 standard fire with a decay phase

The results of a single span pin-roller connected composite beam exposed to various durations of the ISO fire with a decay phase are similar. The case discussed in this section can be used to represent all of the other cases. However, if the temperature of the fire is higher, the midspan vertical displacement is greater, and the roller end moves closer to the centre of the beam.

Before a time of 16 minutes, the beam behaved in the same fashion as in the case with the ISO834 standard fire. When the fire temperature started to decrease, the midspan vertical displacement increased slowly until it reached the maximum at 23 minutes; and then the midspan of the beam started to rise as shown in Figure 5-23(a). Figure 5-27 shows the centreline stress distribution at the midspan at this time. The entire steel beam was in tension, with the bottom flange and most of the web reaching the tensile yield limit. This tensile stress was introduced by the loading on the beam interacting with the deformation of the beam rather than by the thermal expansion of the beam section. The tensile force in the steel beam was balanced by the compressive stress in the concrete slab.

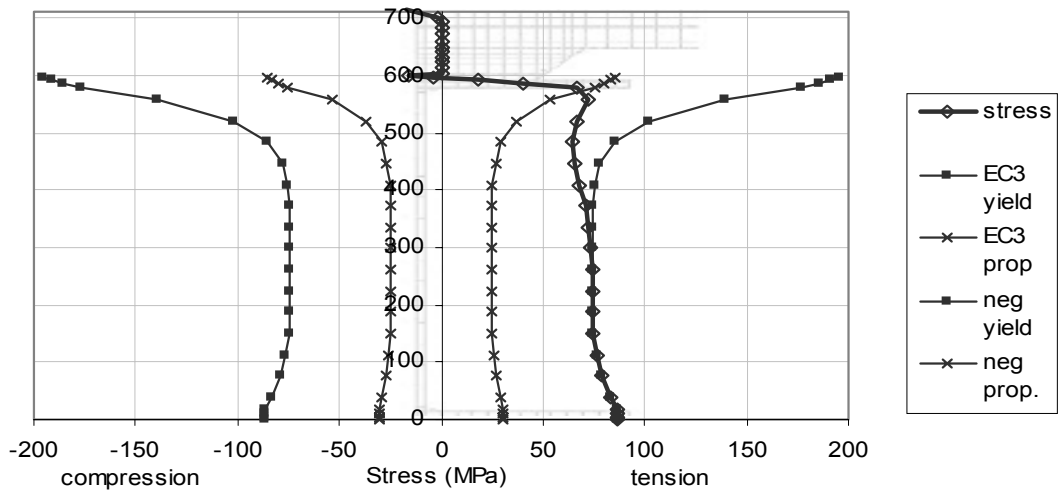

Figure 5-27 Centreline stress distribution at the midspan of the pin-roller connected composite beam at 23 minutes exposed to 16 minutes of the ISO fire with a decay phase

Figure 5-28 and Figure 5-29 show the bottom and top flange stresses in this case. The bottom flange reached the proportional limit at 7 minutes and yielded at 16 minutes in a similar manner to the case exposed to the ISO fire without a decay phase. While the bottom flange stress remained at the temperature-reduced yield limit, the compressive top flange stress decreased rapidly. After 23 minutes, the bottom flange stress started to shift towards compression. Before the bottom flange stress became smaller than the tensile proportional limit, the top flange stress showed little variation. However, after this time the top flange stress moved towards tension, reached the tensile proportional limit at 66.5 minutes and the yield limit at 128 minutes.

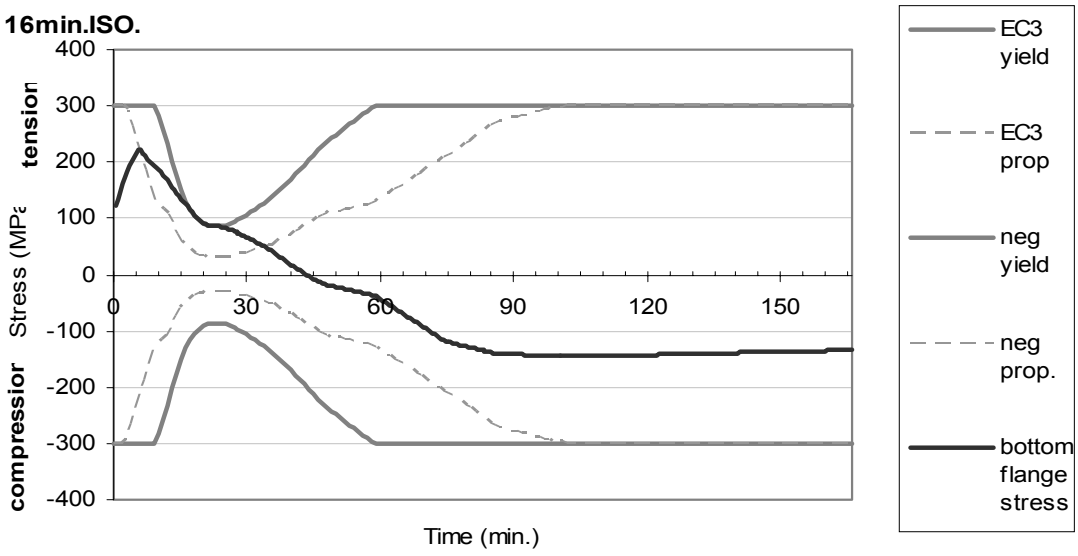

Figure 5-28 Bottom flange stress in single span pin-roller connected composite beam exposed to 16 minutes of the ISO fire with a decay phase

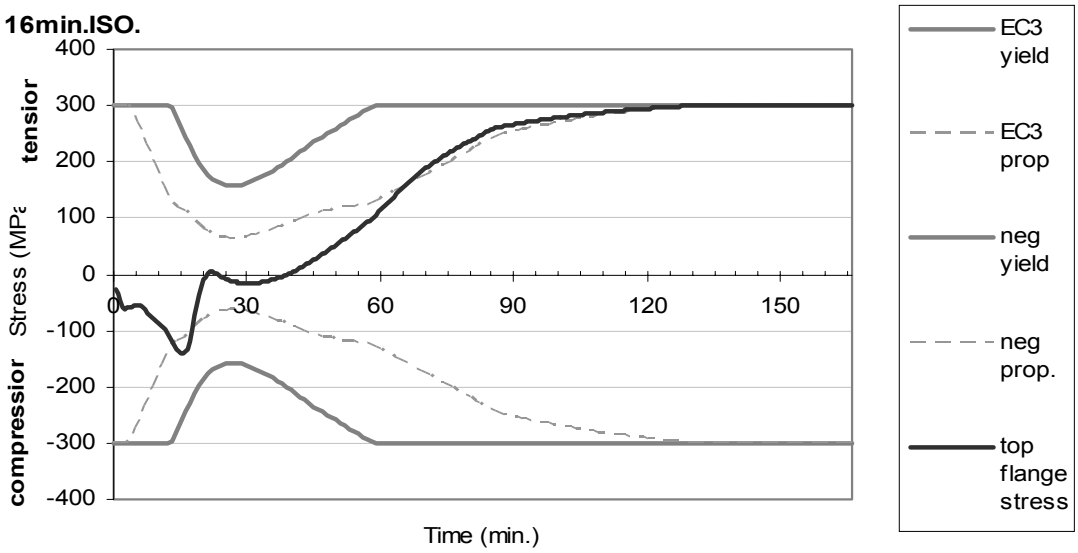

Figure 5-29 Top flange stress in single span pin-roller connected composite beam exposed to 16 minutes of the ISO fire with a decay phase

Comparing Figure 5-28 with Figure 5-8, and Figure 5-29 with Figure 5-9, one can see the similarity of the pin-pin supported case with the pin-roller supported case under a length of the ISO fire with a decay phase. The stress curves of these two supporting conditions had a similar trend. Because the pin-roller supported case does not have the horizontal restraints applying an axial force, the compressive stress was always lower than in the pin-pin connected beam during the simulation. For example, although in both cases the top flange eventually yielded in tension, the pin-roller case had a lower compressive stress in the bottom flange than the pin-pin case.

5.2.3.3 Summary for single span pin-roller connected composite beam

When the beam was exposed to the ISO834 standard fire, SAFIR determined the beam failed at 21.5 minutes possibly because a plastic hinge formed at the midspan as a run-away failure occurred; when the beam was exposed to 20 minutes of the ISO fire with a decay phase, it failed at 22 minutes. Four other fire curves range from 12 minutes to 20 minutes of the ISO fire with a decay phase were used for comparison, and none of these caused a structural failure during the simulation.

The graph for midspan vertical displacement in Figure 5-23 showed that a larger fire causes a larger displacement at the midspan. It also showed that when the temperature of the steel section was reducing, the horizontal displacement recovered slightly and remained constant until the end of the simulation. Comparing these curves with the ones for the pin-pin case, the midspan vertical displacement in this case was larger because the roller end was free to move in the horizontal direction, which consequently contributed to the deflection of the beam.

The graph for the horizontal displacement showed that when the fire followed shorter or equal to 14 minutes of the ISO fire, the horizontal displacement caused by the thermal expansion would recover to zero. However, in a larger fire, the horizontal displacement was affected by the midspan vertical displacement and pulled towards the centre of the beam at the late stage of the heating phase; therefore, when the beam was recovering from its thermal expansion, the inward horizontal displacement became even larger.

The curves for top and bottom flange stresses shown in Figure 5-29 indicate that before cooling the bottom flange at midspan was under tension and the top flange was under compression; this was due to the loads applied to the beam as well as to thermal bowing. While the structure was cooling, the recovery of the thermal expansion caused the midspan displacement to decrease, and consequently caused the bottom flange to be under compression and the top flange under tension. At the end of the simulation, the bottom flange remained in compression, and the top flange yielded in tension. It was expected that the concrete slab at the end of simulation was already cracked under tension. However, because the bottom flange and the lower part of the web had yet to yield, SAFIR determined that the structure had not failed at this stage.

5.2.4 Fix-slide composite beam

The last scenario to be discussed for the single span composite beams is with fix-slide supports. The support scheme is shown in Figure 5-30. The case exposed to the ISO834 standard fire without a decay phase failed in 27.5 minutes. Four other fire curves derived from the ISO fire were used for comparison, ranging from 12 minutes to 22minutes. None of these fire curves caused failure of the structure within the simulation time. Figure 5-31 shows the vertical displacement at the centre of the beam and the horizontal displacement at the slide end in these cases.

Figure 5-30 Support scheme for fix-slide case

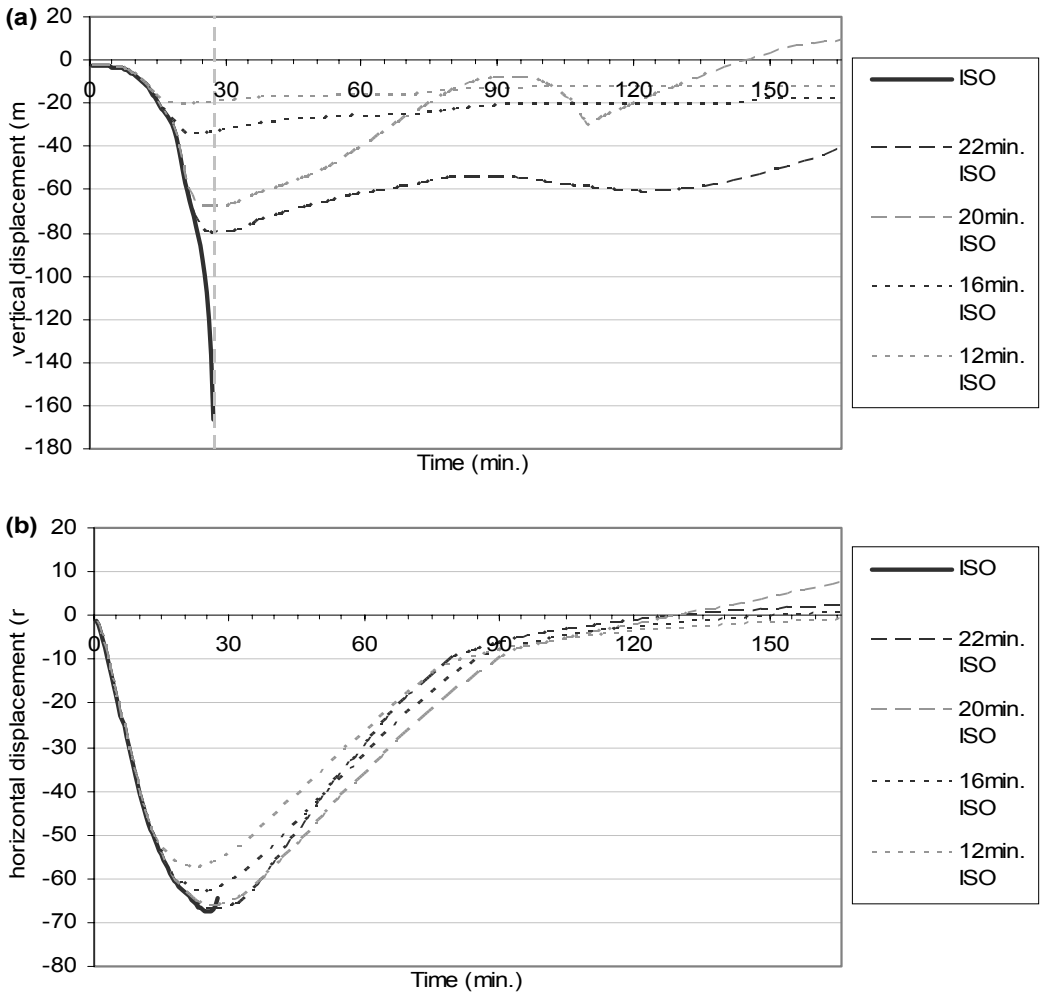

Figure 5-31 SAFIR outputs for single span fix-slide composite beam exposed to various durations of the ISO fire: (a) midspan vertical displacement; (b) horizontal displacement at the sliding end

5.2.4.1 ISO834 standard fire (without decay phase)

The timeline of the structural behaviour in this case is shown in Table 5-4.

Table 5-4 Timeline of the structural behaviour of a single span fix-slide supported composite beam exposed to the ISO834 standard fire

Event	Time
The top flange of the steel beam near the connection reaches the temperature reduced tensile proportional limit. The bottom flange near the connection reaches the temperature reduced compressive proportional limit. The vertical displacement at the midspan increases more rapidly.	7.5 minutes
The horizontal displacement at the slide ends moves outwards slower. The bending moment at the midspan and near the connection reach their maximum.	11 minutes
The bottom flange near the connection reaches the temperature reduced compressive yield limit.	17 minutes
The bottom flange at the midspan reaches the tensile proportional limit. The rate of the midspan vertical displacement increases.	17.5 minutes
The top flange at the midspan reaches the compressive proportional limit. The rate of increase of the midspan vertical displacement becomes greater. The bending moment at the midspan and near the connection change much slowly.	21 minutes
The bottom flange at the midspan reaches the tensile yield limit. The horizontal displacement at the slide end reaches the maximum of 68mm outwards.	26 minutes
Maximum vertical displacement occurs at this time, the top flange near the connection may have reached the tensile yield limit. SAFIR determines the structure fails at this time.	27.5 minutes

The bottom and top flange stresses at the midspan and near the connection in this case are shown in Figure 5-32 and Figure 5-33. At a time of 27.5 minutes, which was when SAFIR concluded that the structure failed, the bottom flange stress near the connection was at the compressive yield limit, and the bottom flange at the midspan had just reached the tensile yield limit. Meanwhile, the top flange stresses at the

midspan and near the connection exceeded the temperature-reduced proportional limit. Figure 5-34 shows the centreline stress distribution in the beam before the beam failed. Near the connection, the entire web section of the steel beam reached the compressive yield limit; at the midspan, the bottom flange had yielded, and then the web section became inelastic due to its tensile stress.

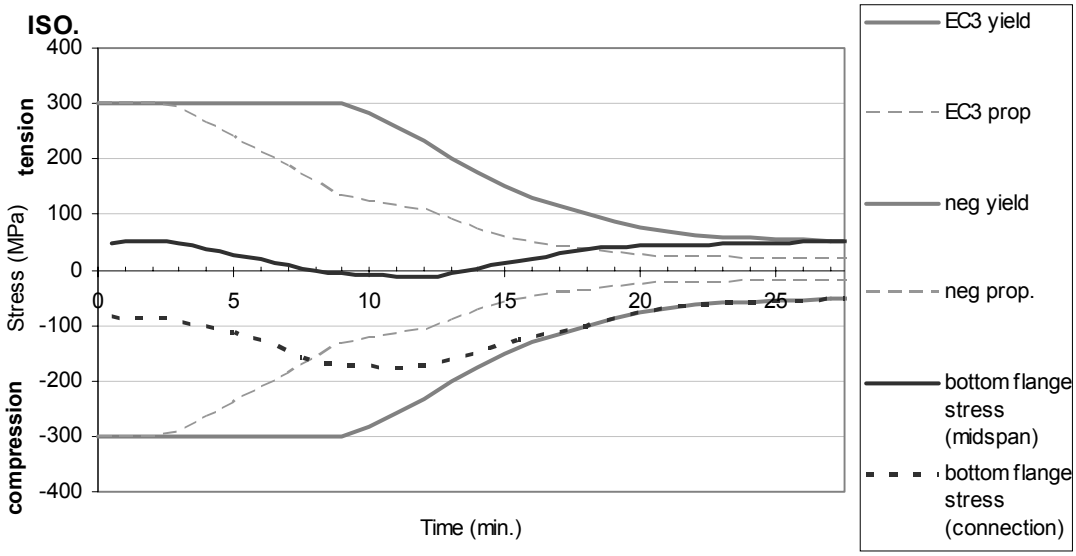

Figure 5-32 Bottom flange stress in single span fix-slide composite beam exposed to the ISO fire

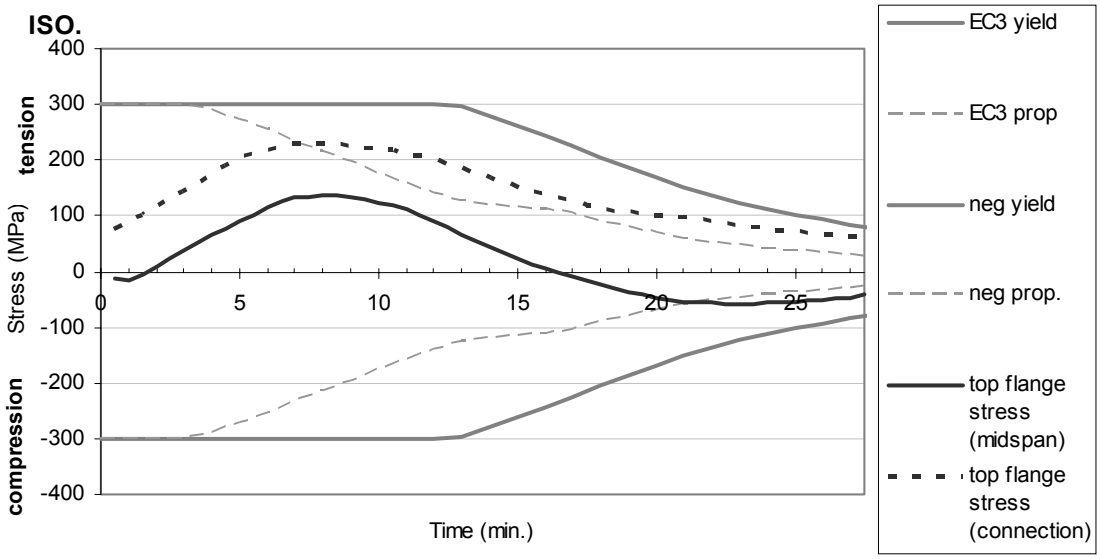

Figure 5-33 Top flange stress in single span fix-slide composite beam exposed to the ISO fire

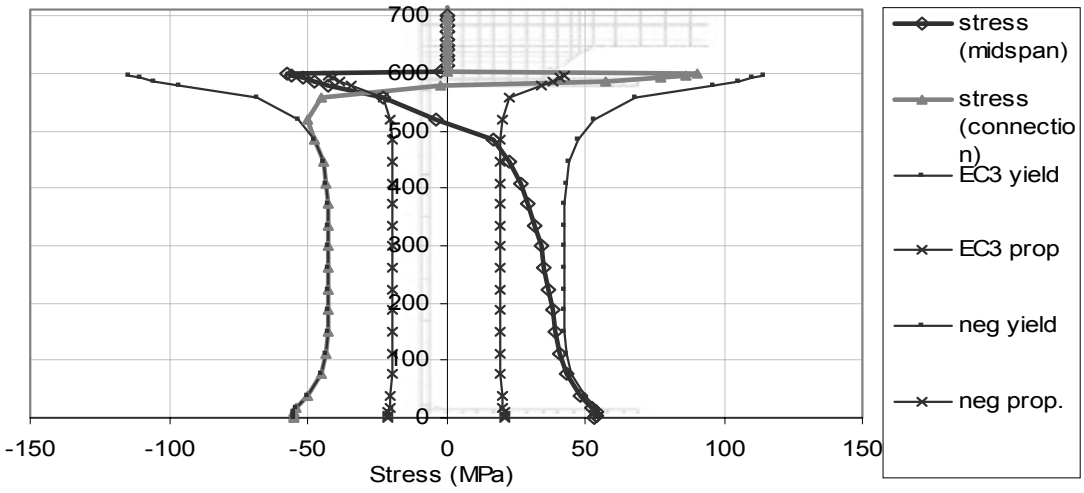

Figure 5-34 Centreline stress at the midspan and near the connection in single span fix-slide connected composite beam exposed to the ISO fire at 27 minutes.

Comparing Figure 5-31 with Figure 5-23, it shows that the vertical displacement was smaller than in the pin-roller supported case because of the rotation fixation at the ends; however, the vertical displacement was larger than in the fix-fix supported case because the horizontal translation allowed more deformation under the loads on the beam.

The horizontal displacement curve shows the slide end moved outwards and went beyond its original position minutes before the structure failed. This is different from the pin-roller case because there was no large vertical displacement at the midspan pulling the slide end closer towards the centre of the beam, hence the horizontal displacement was dominated by the thermal expansion of the beam.

5.2.4.2 16 minutes of the ISO834 standard fire with a decay phase

As Figure 5-31 shows, the results of the fix-slide supported beam exposed to various durations of the ISO fire were similar except the vertical displacement of the beam exposed to 20 minutes of the ISO fire behaved less regularly. The case discussed here represents the structural behaviour of the scenarios with similar setups. Figure 5-35 and Figure 5-36 show the bottom and top flange stresses at the midspan and near the connection. The behaviour during the first 16 minutes was the same as in the case exposed to the ISO fire, hence those events are omitted in this section.

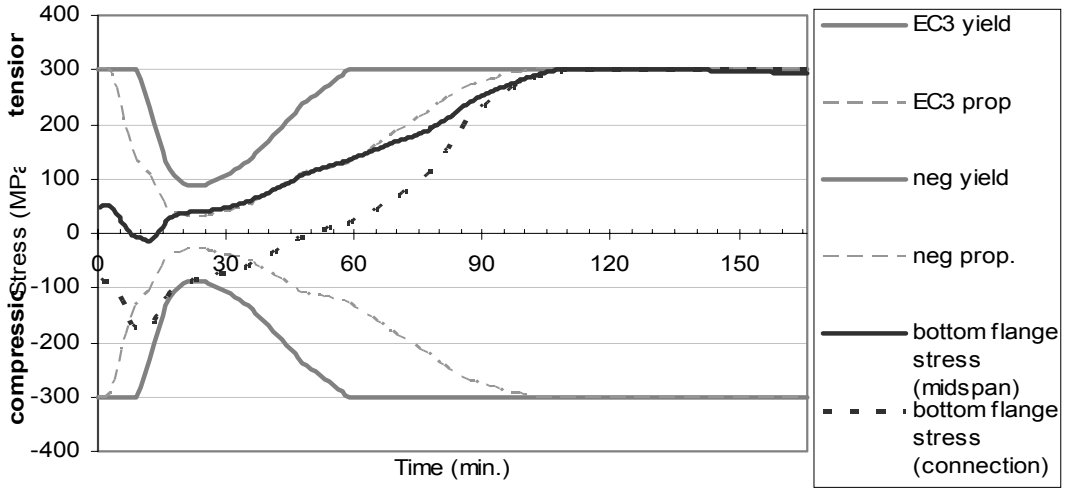

Figure 5-35 Bottom flange stresses in single span fix-slide supported composite beam exposed to 16 minutes of the ISO fire with a decay phase

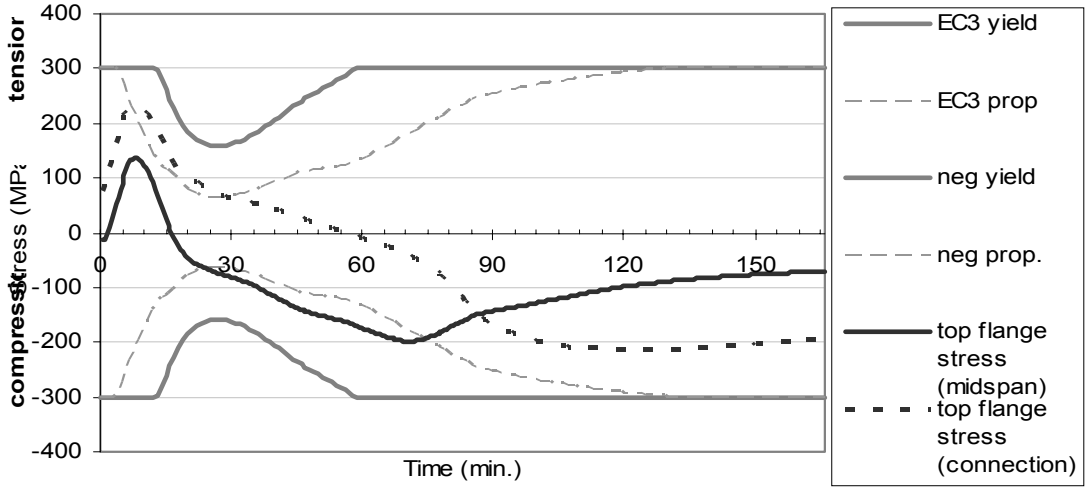

Figure 5-36 Top flange stresses in single span fix-slide supported composite beam exposed to 16 minutes of the ISO fire with a decay phase

The vertical displacement at the midspan reached a maximum at 24 minutes while the temperature of the steel beam was at its highest. Afterwards the bottom flange stress

near the connection recovered from the level of the compressive yield limit, and the top flange from the tensile proportional limit. While the steel section was cooling, the top flange stress went into compression, and the bottom flange stress into tension. However, the tensile stress at the bottom flange was larger than the compression stress at the top flange, and this resultant tension force pulled the slide end back towards its original location. One can observe that the midspan stopped rising when the horizontal displacement at the slide end was returning to its original position. This is more obvious under a smaller fire.

The bottom and top flange stress curves of this case was compared with the fix-fix supported case. The bottom flange stresses of these cases were similar, however, because of the horizontal translation at the support, no axial force was able to build up. This phenomenon reduced the tensile force in the beam, and was reflected in the top flange stress curves.

At the end of the simulation, the bottom flange stresses at the midspan or near the connection were both at the tensile yield limit; the top flange was in compression but did not reach the compressive proportional limit. Not much permanent horizontal displacement was observed, but the midspan of the beam sagged a little bit due to the inelastic behaviour in parts of the beam.

Figure 5-37 shows the centreline stress distribution at the midspan and near the connection at different times. These graphs show that at the midspan, the tensile stress at the lower part of the web was greater than at the bottom flange, and the lower part of the web yielded in tension at the end of the simulation. Throughout the simulation, the height of the neutral axis at the midspan did not vary much, but both the tensile and compressive stress increased with time while the beam was cooling. At the end of the simulation, the top flange almost yielded in compression while the bottom flange had yielded in tension near the connection. At the midspan, the bottom flange almost yielded in tension, while the top flange had a compression stress less than 100MPa.

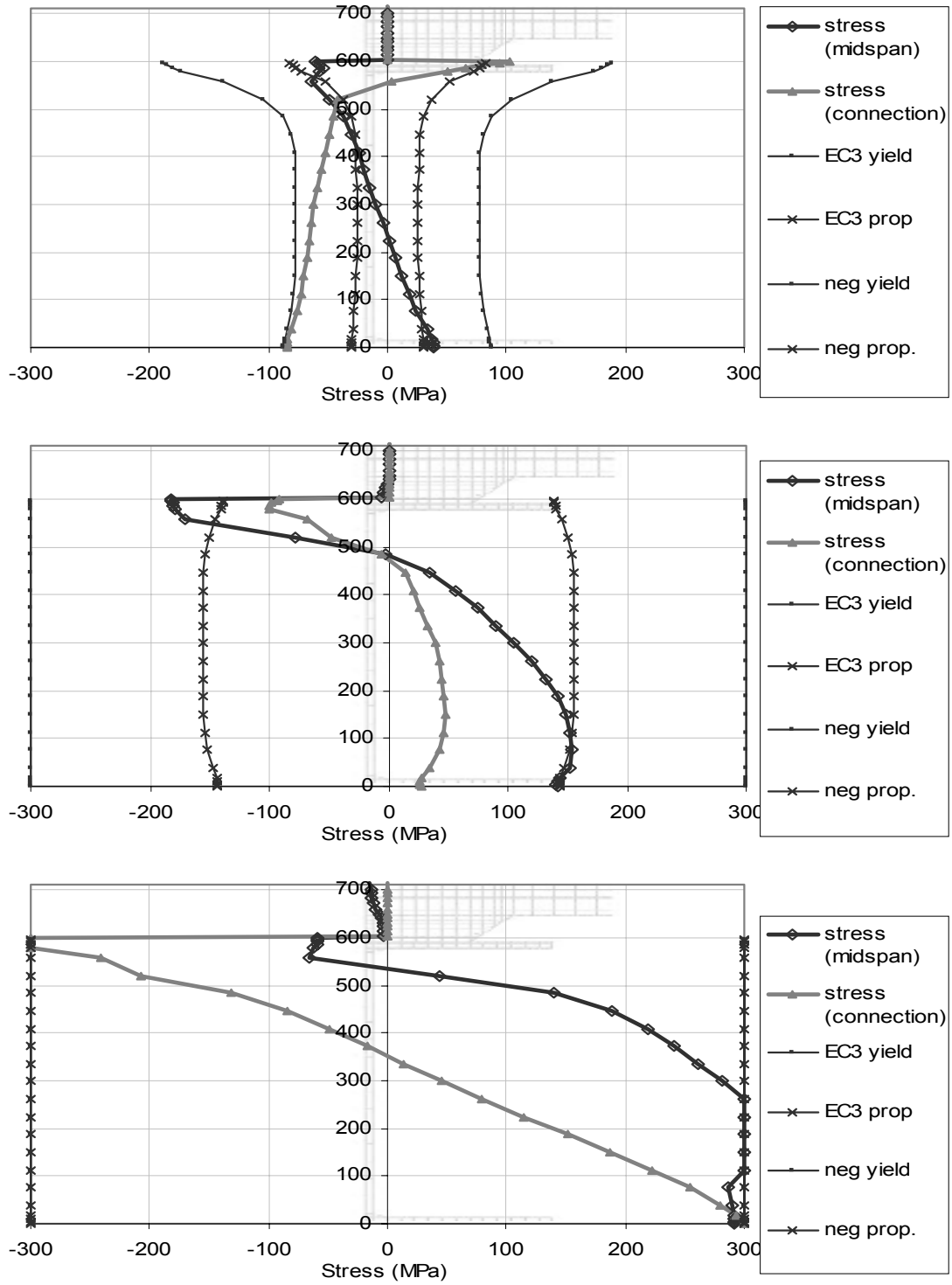

Figure 5-37 Centreline stress at the midspan and near the connection in single span fix-slide connected composite beam at 24 min, 62min, and 100min exposed to 16 minutes of the ISO fire (from top to bottom)

5.2.4.3 Summary of single span fix-slide connected composite beam

SAFIR determined that the beam exposed to the ISO834 standard fire failed after 27.5 minutes. Four other fire curves ranging from 12 minutes to 22 minutes of the ISO fire with a decay phase were used for comparison. None of these fire curves caused failure of the structure during the simulation.

The graph for the midspan vertical displacement in Figure 5-31 suggests that the higher fire temperature from a longer fire causes a larger permanent vertical displacement. The vertical displacement was significantly lower than in the pin-roller case simply because of the rotation fixation at the ends.

The graph for the horizontal displacement at the roller ends shows that the horizontal displacement was dominated by the thermal expansion of the beam, and had little 'pulling' effect from the midspan vertical displacement especially when the fire was less than or equal to 16 minutes of the ISO fire. By comparing this graph with the one for the pin-roller case, it shows that under a small fire the horizontal displacement at the end without horizontal restraint is similar. This is also related to the size of the midspan vertical displacement which can pull the unrestrained end inwards.

The trend of the midspan stresses at the bottom and top flange versus time here was different to the pin-roller case. The bottom flange stress in this case was rather similar to the fix-fix case. However, because no axial force was present in this case, the top flange stress balanced the lower flange stress. Although the bottom flange yielded at the end of the simulation, in the cases in which the beam did not fail before the end of the simulation, the upper part of the steel beam as well as the concrete slab had sufficient strength to resist the compressive stresses that occurred so that SAFIR determined the structure had not failed at this time.

5.3 Summary of the simulation results of single span composite beams

Table 5-5 shows the summary of the results for single span composite beams. The fix-fix connected beam had the shortest time to failure when exposed to the ISO834 standard fire due to the large bending moments induced at the connections and at the midspan. The pin-roller connected beam failed earlier than the fix-slide beam because SAFIR determined a rapid deflection had occurred at the midspan of the pin-roller beam. Besides, although the pin-roller connected beam failed earlier than the fix-slide one, the difference in the steel temperature at these two times was not large due to the rate of increase in the ISO fire temperature.

Table 5-5 Analysis results of the single span composite beams exposed to various durations of the ISO fire

Connection type		**Pin-pin**	**Fix-fix**	**Pin-Roller**	**Fix-Slide**
Time to fail in the ISO fire without a decay phase	Min.	37	18	21.5	27.5
Steel temperature at failure (at the bottom flange)	^{o}C	848	656	709	748
Maximum compressive axial force	kN	3250	4280	--	--
Maximum tensile axial force	kN	2000	3900	--	--

6 Simulation results of composite frames exposed to the ISO fire with a decay phase

6.1 Thermal analysis results of composite frames

The thermal analysis results used in the beams of composite frames were based on the thermal analysis outcomes in the single span beam scenarios. The columns of the composite frame were assumed to have full thermal protection against fire and the temperature remained at 20^{o}C.

6.2 Structural analysis results of composite frames

The setup of the initial model contained columns with the same dimensions, strength and stiffness as the steel beam. The composite beam connected to the columns at their mid-height. Two types of beam-column connections were considered: the pin-pin and the fix-fix connections. Each case is discussed separately below.

6.2.1 Frames with pin-pin connected composite beam

In the scenarios of frames with a pin-pin connected composite beam, the frame exposed to the ISO834 standard fire without a decay phase failed after 39 minutes. Based on this result, six fires following from 18 to 36 minutes of the ISO fire with a decay phase were used for comparison. The frame did not fail under any of these six fires. Figure 6-1 shows the axial force, the vertical displacement at the midspan and the horizontal displacement of one connection plotted against time. The graphs show that a larger fire induced a larger tensile axial force as well as a larger midspan vertical displacement at the end of the simulation.

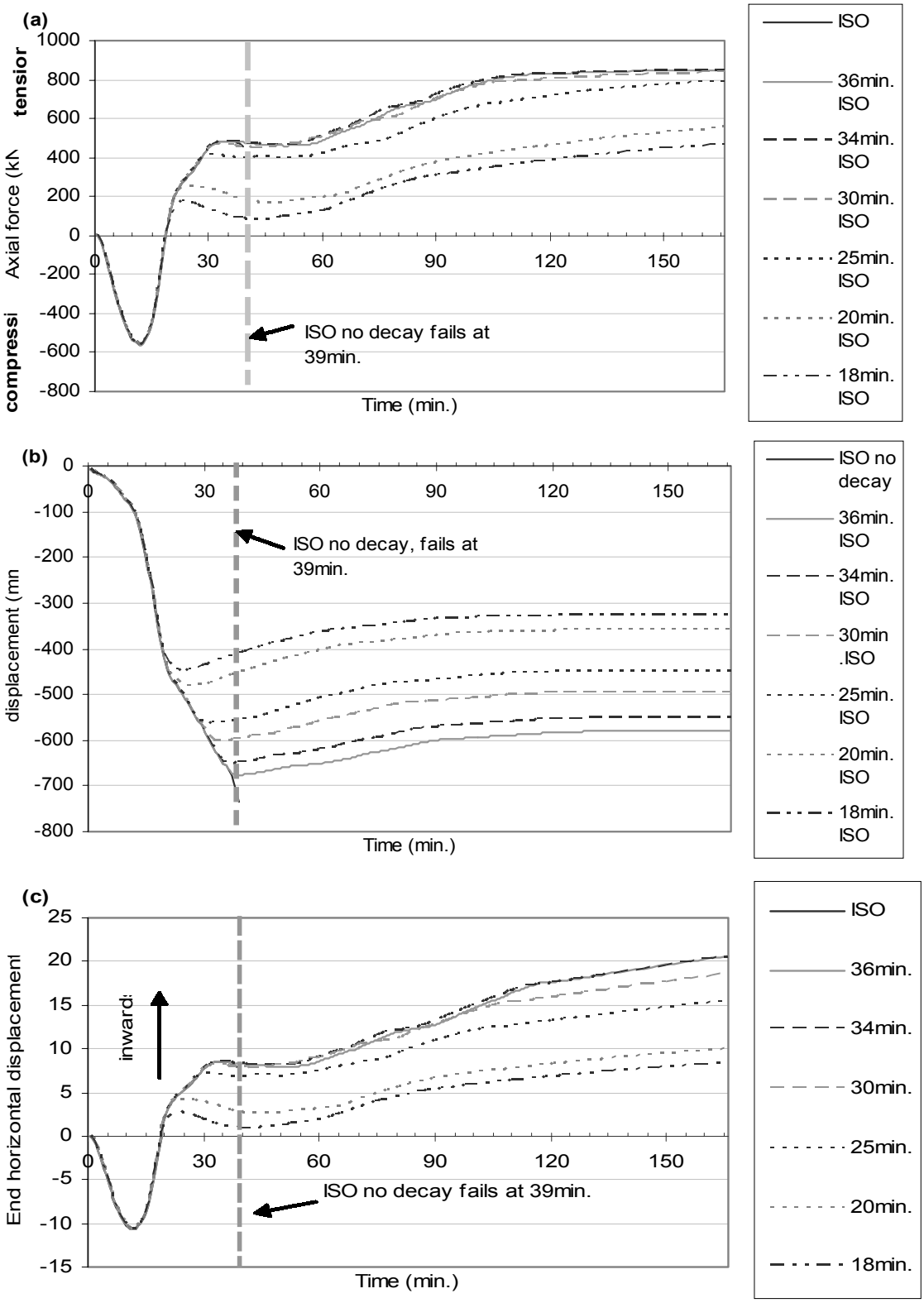

Figure 6-1 Results from pin-pin composite frame exposed to the ISO fire (a) axial force; (b) Vertical displacement at the midspan; (c) Horizontal displacement at one end.

Comparing Figure 6-1 with Figure 5-4, it shows that the frame case and the single span case with a pin-pin connected beam were quite similar. Before heating, there was no difference in the axial forces. When the structure was heated, because the composite frame allowed for a limited amount of horizontal movement at the beam-column connections, the beam axial force in the composite frame was significantly less than in the single span pin-pin connected beam.

Both Figure 5-4(b) and Figure 6-1(b) showed the midspan vertical displacement of the beam, and they indicated that the midspan displacement in the frame case was slightly larger while cooling than the single span pin-pin connected beam case. Since the thermal expansion and thermal bowing in both cases should be the same at any time as the temperatures of the beams in these scenarios were the same, this difference in midspan displacement would be contributed by the inward horizontal movement of the connections in the frame scenario.

Figure 6-1(c) showed the horizontal displacement at the beam-column connection. During the first 13 minutes, the connection moved outwards as the beam expanded, through this time the vertical movement at the midspan was less rapid. After 13 minutes, the yielding at the bottom flange caused a faster vertical displacement at the midspan and pulled the connection inwards. One should be aware that the horizontal movement in this case occurred at both connections, but previously in the single span cases the horizontal displacement only appeared at the end without the horizontal restraint.

Under a large fire, such as the ones following 36 or 34 minutes of the ISO fire, because the horizontal displacement was still increasing while both the axial force and midspan vertical displacement became constant, one can deduce that yielding occurred at the mid-height or at the ends of the columns.

6.2.1.1 ISO834 standard fire (without decay phase)

The timeline for the behaviour of the structure is shown in Table 6-1.

Table 6-1 Timeline of the behaviour of composite frame with pin-pin connected beam exposed to the ISO834 standard fire

Event	Time
Bottom flange of the steel beam reaches the tensile proportional limit;	6 min.
Top flange of the steel beam reaches the compressive proportional limit;	10min.
Maximum compressive axial force in the composite beam, 550kN; maximum outward horizontal displacement at the connection, 10mm;	13min.
Bottom steel flange reaches tensile yield point;	15 min.
Top flange of the steel beam reaches the tensile proportional limit	20 min.
Maximum tensile axial force in the composite beam; maximum inward horizontal displacement at the connection, 8.2mm	33 min.
Plastic hinge occurs at the midspan (failure of the structure); the midspan vertical displacement is 735mm	39 min.

This case can be compared with Table 5-1 and Table 5-3, the single span pin-pin connected and pin-roller connected beam cases. The time to failure in the composite frame was similar to the single span pin-pin connected beam, with the same failure mechanism.

Figure 6-2 and Figure 6-3 show the bottom and top flange stresses respectively of the pin-pin connected composite beam exposed to the ISO834 standard fire in a frame layout. These two graphs can be compared with the curves for the top and bottom flange stresses in the single span pin-roller case and pin-pin case. The behaviour of the beam in the frame lay between the behaviour of the pin-pin and the pin-roller single span beam. However, because the columns were not very stiff, the beam in this case behaved more like the single span pin-roller connected beam.

The top flange in this case experienced a larger stress when it reached the compressive proportional limit, which happened 5 minutes earlier than in the pin-roller single span beam. This was because the column stiffness still provided a limited amount of horizontal restraint to the beam. Wastney (2002) suggests that when the

column is stiffer, the behaviour of the beams in the frame would be more similar to the single span connected beams with axial restraints. The effect of changing column stiffness will be discussed in detail later.

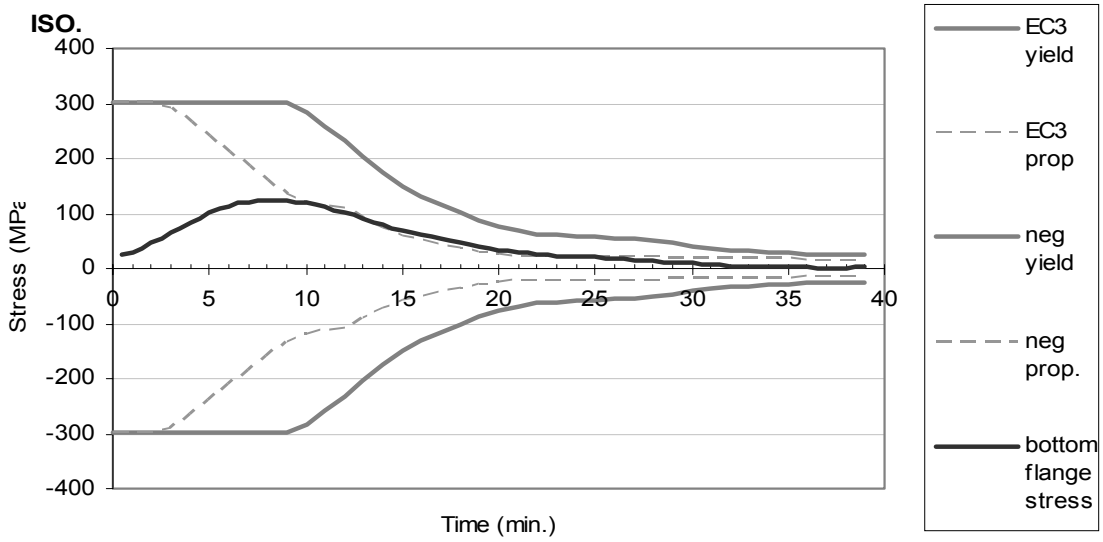

Figure 6-2 Bottom flange stress at the midspan in composite frame with pin-pin connected beam exposed to the ISO834 standard fire

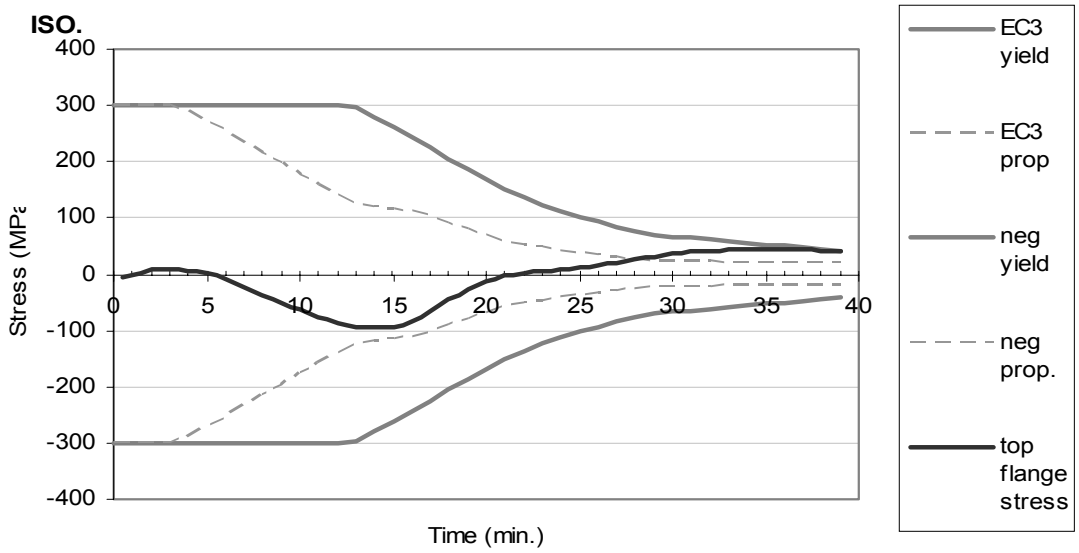

Figure 6-3 Top flange stress at the midspan in composite frame with pin-pin connected beam exposed to the ISO834 standard fire

6.2.1.2 16 minutes of the ISO834 standard fire with a decay phase

Figure 6-4 and Figure 6-5 compare the top and bottom flange stresses in the frame case with pin-pin connected beam to the stresses of the simply span pin-pin case and pin-roller case. They show that the stresses in this case were always in between the stresses of the pin-roller and pin-pin case. Before the bottom flange returned to the ambient temperature, its curve followed the curve of the single span pin-roller case very closely. Nevertheless, because the beam-column connection acted as horizontal restraint, the bottom stress in this case behaved more like the single span pin-pin case, this was more obvious at the end of the simulation.

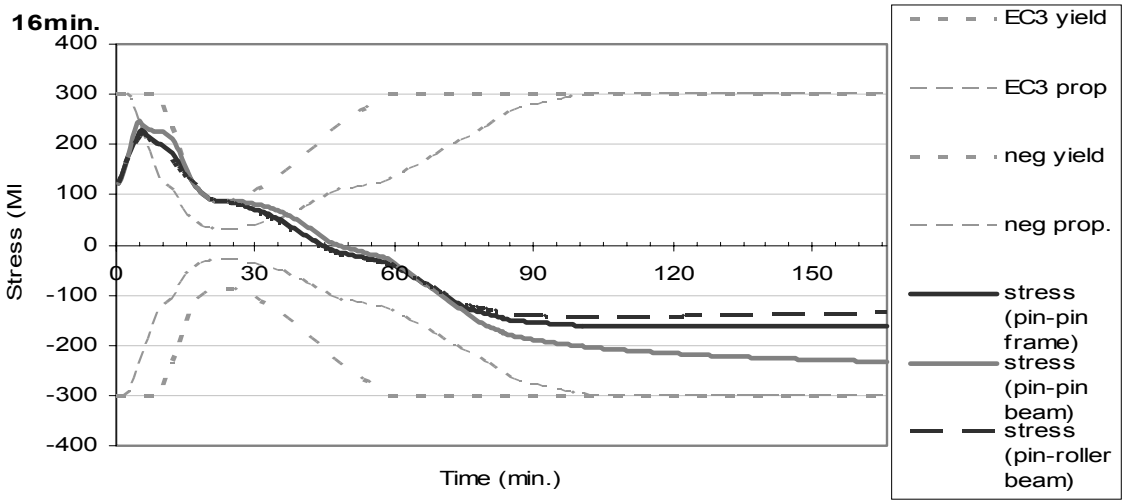

Figure 6-4 Midspan bottom flange stress in a frame with pin-pin connected beam and in the single span pin-pin and pin-roller case exposed to 16min. of the ISO834 standard fire

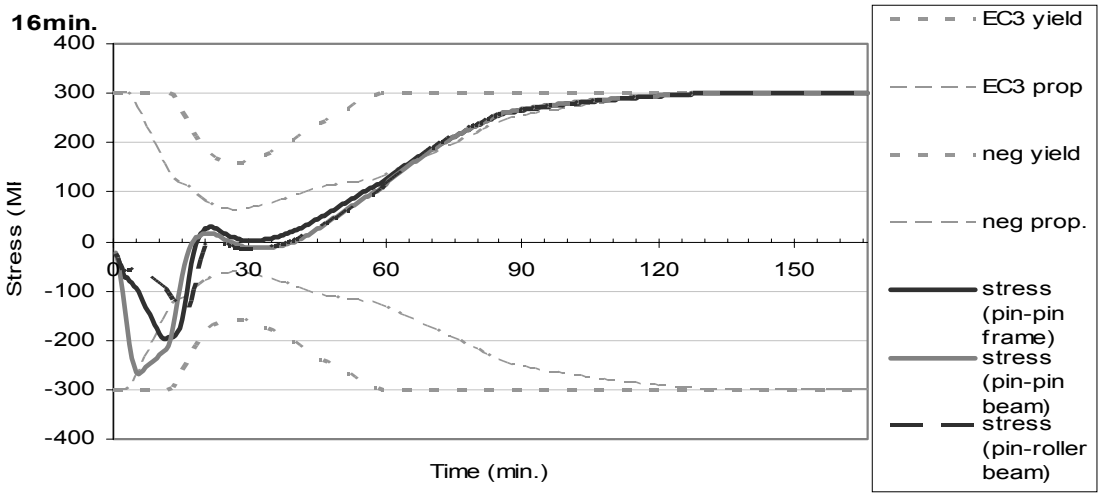

Figure 6-5 Midspan top flange stress in composite frame with pin-pin connected beam and in the single span pin-pin and pin-roller case exposed to 16min. of the ISO834 standard fire

6.2.1.3 Summary of frame with pin-pin connected composite beam

The simulation results indicate that the behaviour of the pin-pin connected composite beam in a steel frame had a mixture of behaviour of the single span pin-pin case and the single span pin-roller case. Figure 6-1 showed that the axial force and the midspan vertical displacement at the end of the simulation depend on the size of fire. The figure also indicated that the columns can yield when the fire is large. The yielding of columns will be discussed later in this chapter.

6.2.2 Frames with fix-fix connected composite beam

In the simulation which in the composite frame with a fix-fix connected beam was exposed to the ISO834 standard fire, the structure failed after 22.5 minutes. Six fires, from 12 minutes to 22 minutes of the ISO fire followed by a decay phase, were chosen to compare the structural behaviour. In these six cases, the structure exposed to 22 minutes of the ISO fire with a decay phase failed at 23 minutes, while the others were still intact at the end of the simulation time.

The axial force in the composite beam, vertical displacement at the midspan, and horizontal displacement at the connection are shown in Figure 6-6. The axial force had a similar trend to the force in the single span fix-fix beam but with less than one-fifth of the value. The reason that the beam axial force was small in this case was the same as in the pin-pin frame case, as the beam column connection provided a certain level of freedom for horizontal movement and released the beam axial force.

The curves of the midspan vertical movement show a mixture of behaviour of the single span fix-fix beam and fix-slide beam. In the frame scenario, the midspan of the beam rose when the steel beam was cooling. This behaviour in the single span fix-slide scenario was only found when the fire lasts longer than 12 minutes of the ISO fire, and it was not observed in any of the single span fix-fix beam cases.

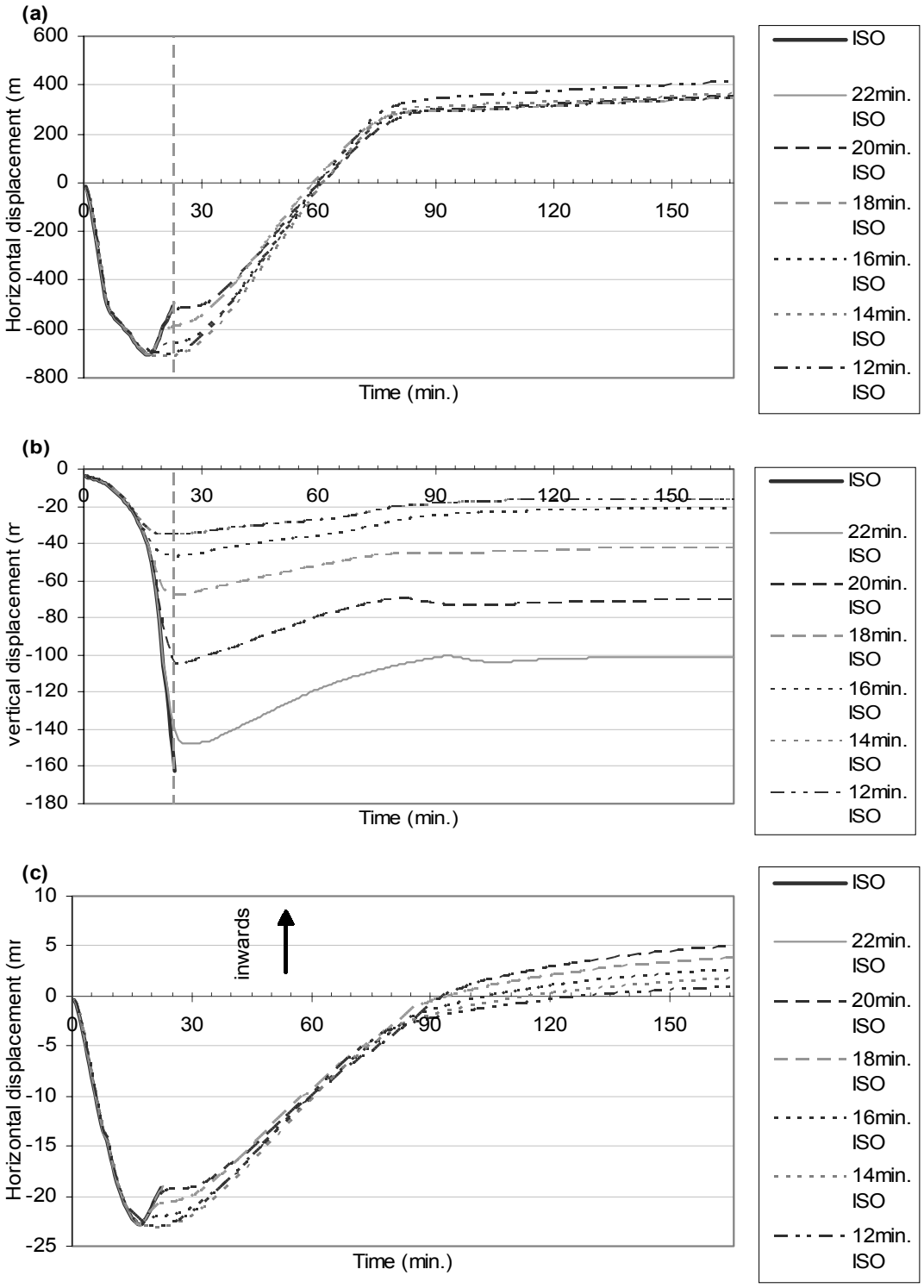

Figure 6-6 Simulation results for composite frame with fix-fix connected composite beam exposed to various length of the ISO834 standard fire: (a) axial force in the composite beam; (b) midspan vertical displacement; (c) horizontal displacement at beam-column connection.

6.2.2.1 ISO834 standard fire (without decay phase)

The structural behaviour in this case has also been discussed in Wastney (2002). The timeline of the structural behaviour is shown in Table 6-2.

Table 6-2 Timeline of structural behaviour of the frame with a fix-fix connected composite beam

Event	Time
The bottom flange near the connection reaches the temperature-reduced compressive proportional limit	7 min.
The top flange at the midspan reaches the compressive proportional limit	16 min.
The bottom flange at the midspan reaches the tensile proportional limit. The maximum outward horizontal displacement at the connection and the maximum axial force occurs at this time.	17min.
The bottom flange at the midspan reaches the tensile yield limit; the bottom flange near the connection reaches the compressive yield limit; the top flange near the connection reaches the compressive proportional limit.	22 min.
SAFIR determines the structure fails at this time.	22.5 min.

Figure 6-7 and Figure 6-8 show the bottom and top flange stresses in a composite frame with fix-fix connected beam exposed to the ISO834 standard fire. The bottom flange stress curves were very similar to the curves for the single span fix-slide beam, except the times for the stresses to reach the proportional limits or yield limits were different. The top flange stresses of these two cases were also similar but the variations in the top flange stresses were smaller. Conversely, these curves were quite different from the stress curves for the single span fix-fix beam.

Figure 6-9 shows the centreline stress distribution of the composite beam at 18 minutes and 22.5 minutes, which were when the midspan bottom flange reached the temperature reduced tensile proportional limit, and when SAFIR determined the structure failed. These graphs show that the entire steel section at the midspan was under compression, while at the connection, the bottom flange was under tension and the top flange was under compression. Although the beam did not yield at midspan or near the connection at 22.5 minutes according to the centreline stress distribution, a rapid increase of midspan vertical displacement occurred at this time and caused SAFIR to be unable to continue the simulation.

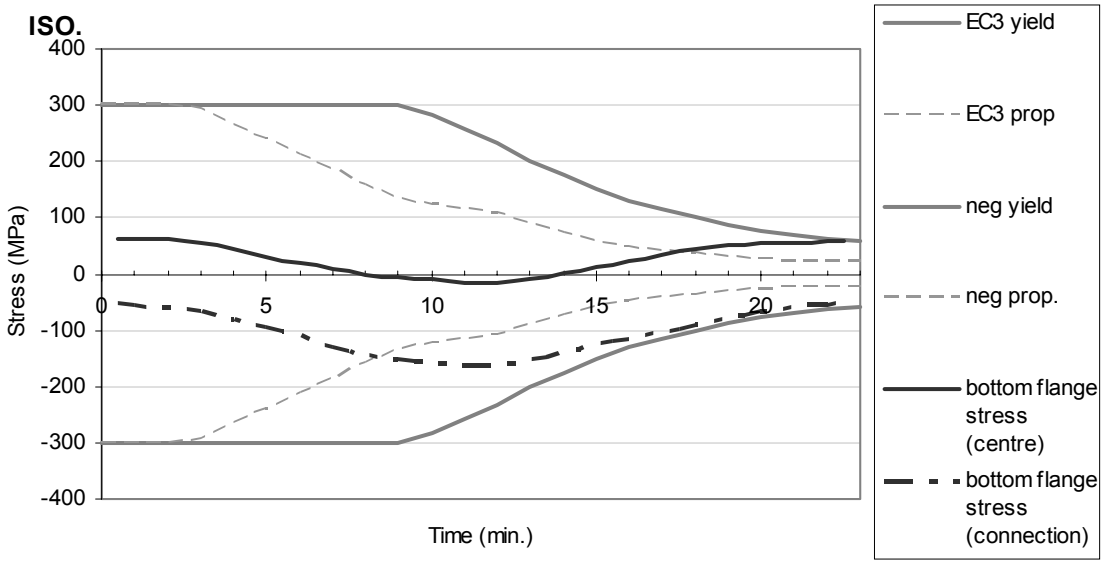

Figure 6-7 Bottom flange stress in composite frame with fix-fix connected beam exposed to the ISO834 standard fire

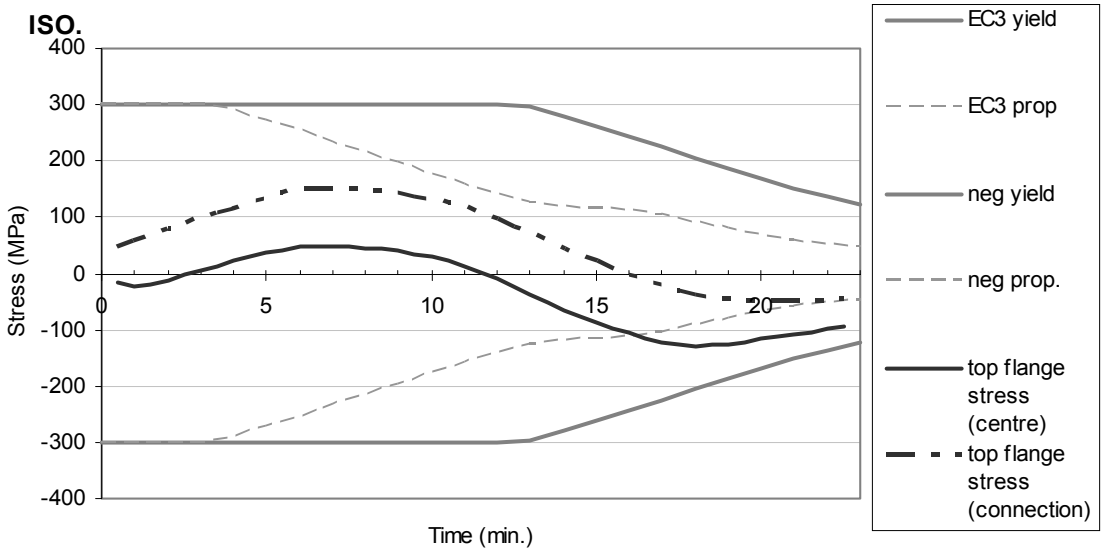

Figure 6-8 Top flange stress in composite frame with fix-fix connected beam exposed to the ISO834 standard fire

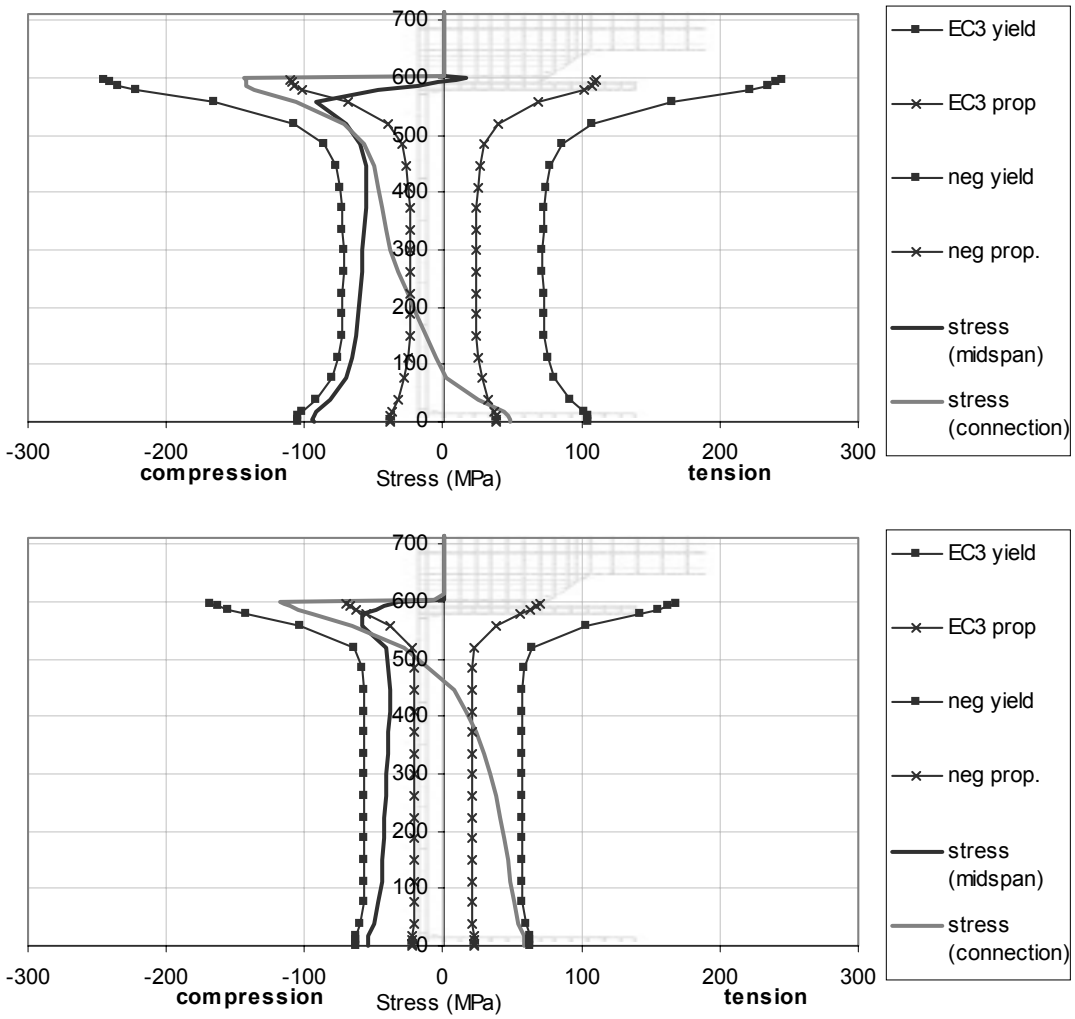

Figure 6-9 Centreline stress of the fix-fix connected composite beam at 18 and 22.5 min. in a frame exposed to the ISO fire

6.2.2.2 ISO834 standard fire with a decay phase

Figure 6-6 showed that the fire size had little effect on the tensile axial force at the end of the simulation; this was in contrast to the finding for the pin-pin connected frame. However, it showed that a larger fire caused a larger midspan vertical displacement. The graph also indicated that the horizontal displacement at the beam-column connection had a close relationship with the axial force.

6.2.2.3 Summary of frame with fix-fix connected composite beam

The simulation results showed that the beam had behaviour intermediate between the single span fix-fix beam and the single span fix-roller beam cases. They also showed that the fire size had little effect on the axial force after the beam cooled down, but it was able to influence the midspan vertical displacement.

6.3 Variation in column strength and stiffness

There were five column strengths and stiffnesses used for simulation: 50%, 100%, 250%, 500% and 1000% of the steel beam strength and stiffness. Different column strength and stiffness were achieved by varying the yield strength and Young's modulus of the column respectively while retaining the cross-sectional area and second moment of area of the column. The column strength and stiffness were expressed as a ratio to the values of the universal steel beam 610UB101.

Since the composite beam had a flexural stiffness ratio of 2.49 to the column due to the difference in the second moment of area (I_{xx} composite beam / I_{xx} steel column = 1.8930E+9mm^4 / 7.610E+6mm^4), when the columns were named as having 100% steel beam stiffness, the columns actually had 40% of the composite beam stiffness.

6.3.1 Changed strengths and stiffness in pin-pin composite frame

When the column strengths and stiffness was increased to 1000% of the original value, the frame with pin-pin connected composite beam exposed to the ISO834 standard fire reached failure after 37.5 minutes. Three fires following 32, 25 and 18 minutes of the ISO fire were used in simulation to see the effect of column strength and stiffness to the beam under different sizes of fire.

Figure 6-10 shows the axial force with changed strengths and stiffnesses in a pin-pin composite frame when the beam was exposed to 32, 25, or 18 minutes of the ISO fire with a decay phase. The graphs indicate that the time at which the maximum compressive force occurred was not influenced by the column strength. However, the stronger column triggered the beam to have a larger axial force in both tension and compression. Besides, in a frame with a strong column, the induced tensile force would eventually be larger than the maximum compressive force from the heating phase.

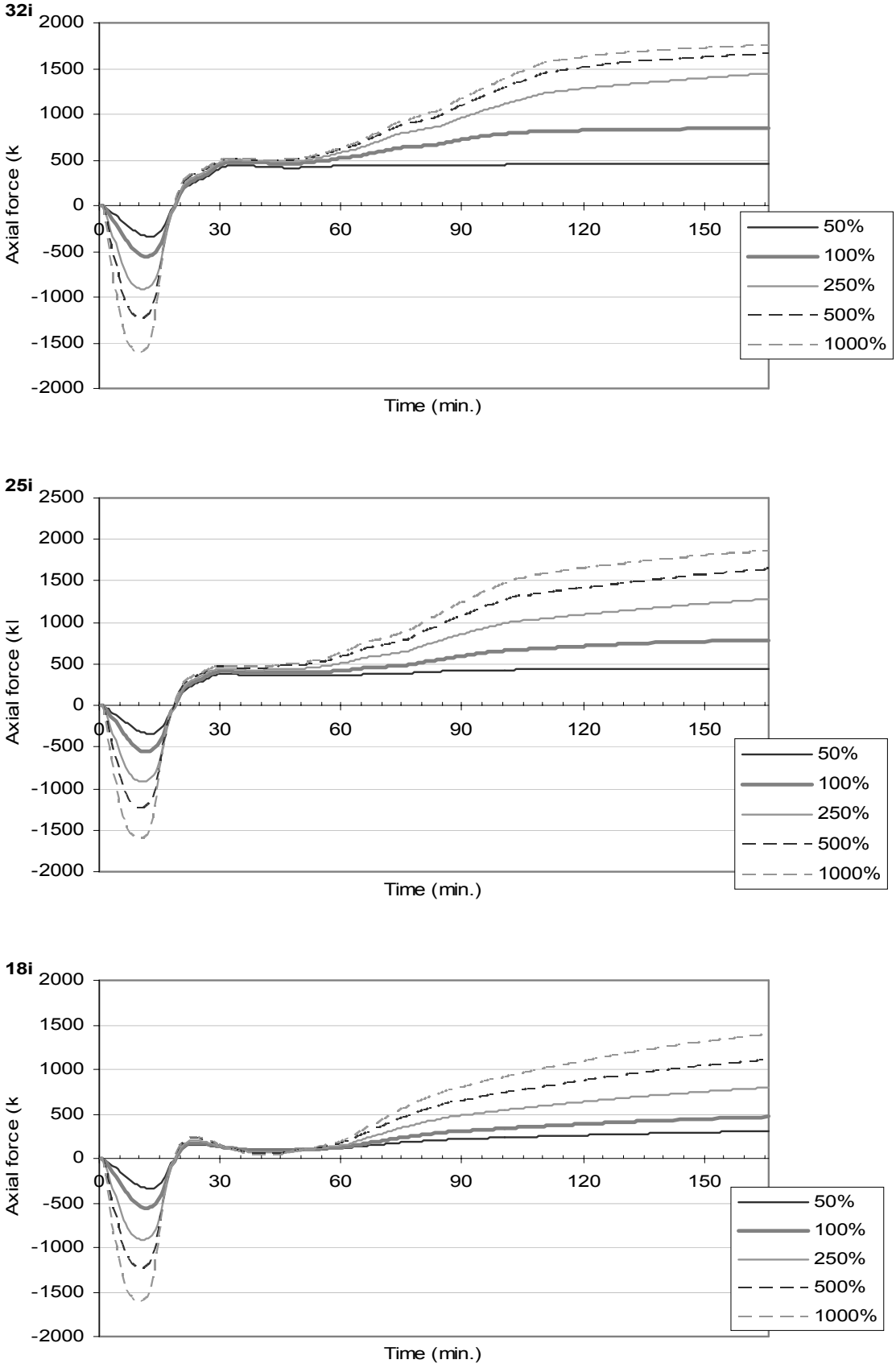

Figure 6-10 Axial force with changed strengths and stiffness in pin-pin composite frame exposed to 32, 25 and 18 minutes of the ISO fire with a decay phase

The graphs for the beam exposed to 32 and 25 minutes of the ISO fire in Figure 6-10 showed that when the fire temperature was high, the beam experienced a 500kN tensile axial force for around 10 minutes at the early stage when the structure cooled.

Figure 6-10 also showed that although the tensile axial force at the end of the simulation was smaller when the beam exposed to a smaller fire, the rate of increase of the tensile force at the end of the simulation was higher.

Figure 6-11 shows the midspan vertical displacement. The simulation result was as expected: larger fires caused a larger vertical displacement, and the stiffer columns caused a slightly smaller permanent displacement. It also shows that before the axial force returned to zero, the influence of the stiffness or strength of the columns to the midspan displacement was minimal.

Figure 6-12 shows the horizontal displacement at the connection. The graphs suggest that the stiffness of the column dominated the horizontal displacement, but the fire temperature also had some effect on the displacement. The effect of column stiffness is best observed in the beam exposed to 32 minutes of the ISO fire at the period between 30 to 40 minutes. The beam axial forces of the frames were the same with different column strengths and stiffness; but the magnitude of the horizontal displacement was in inverse proportion to the column stiffness.

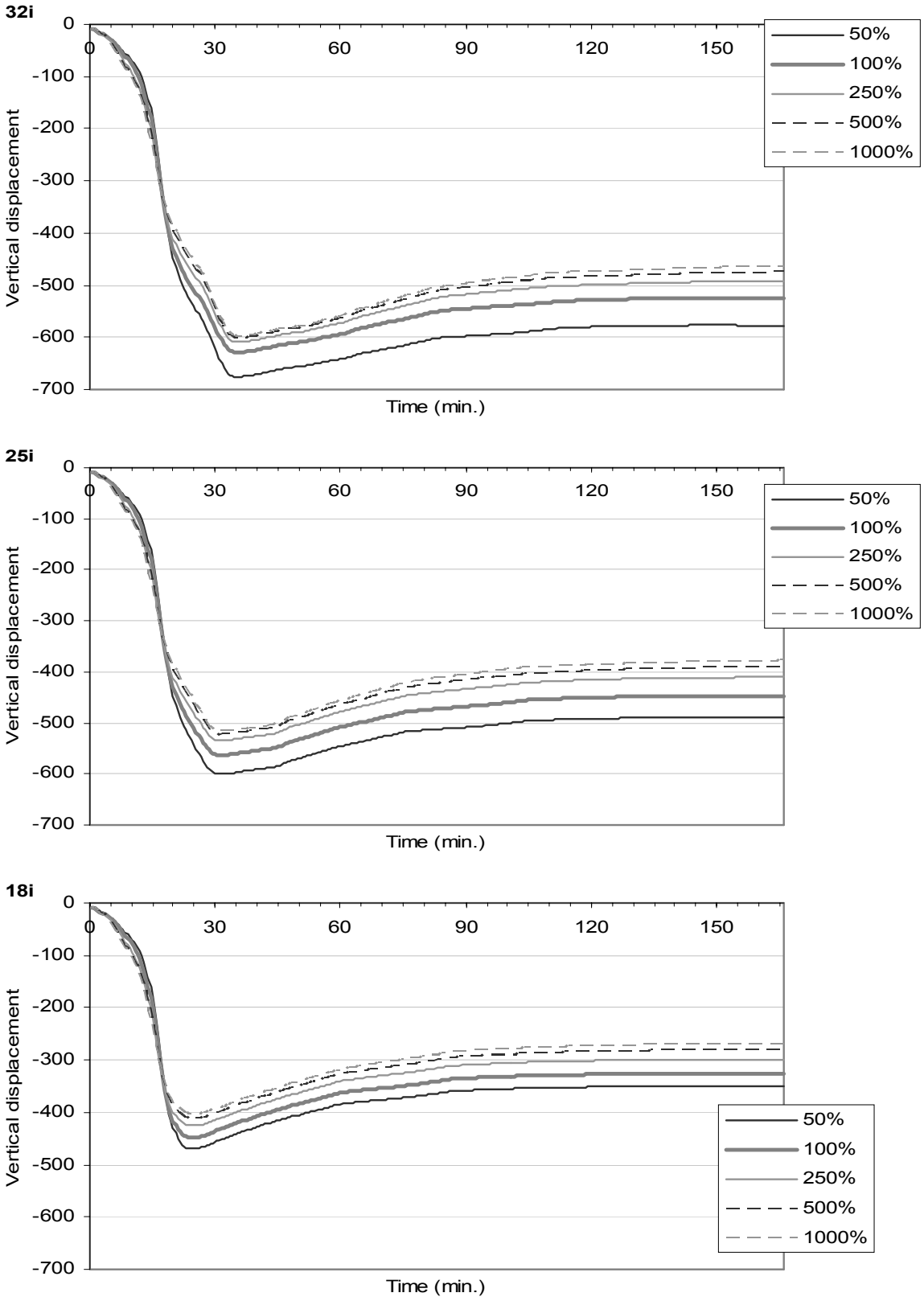

Figure 6-11 Midspan vertical displacement with changed strengths and stiffness in pin-pin composite frame exposed to 32, 25, and 18 minutes of the ISO fire with a decay phase

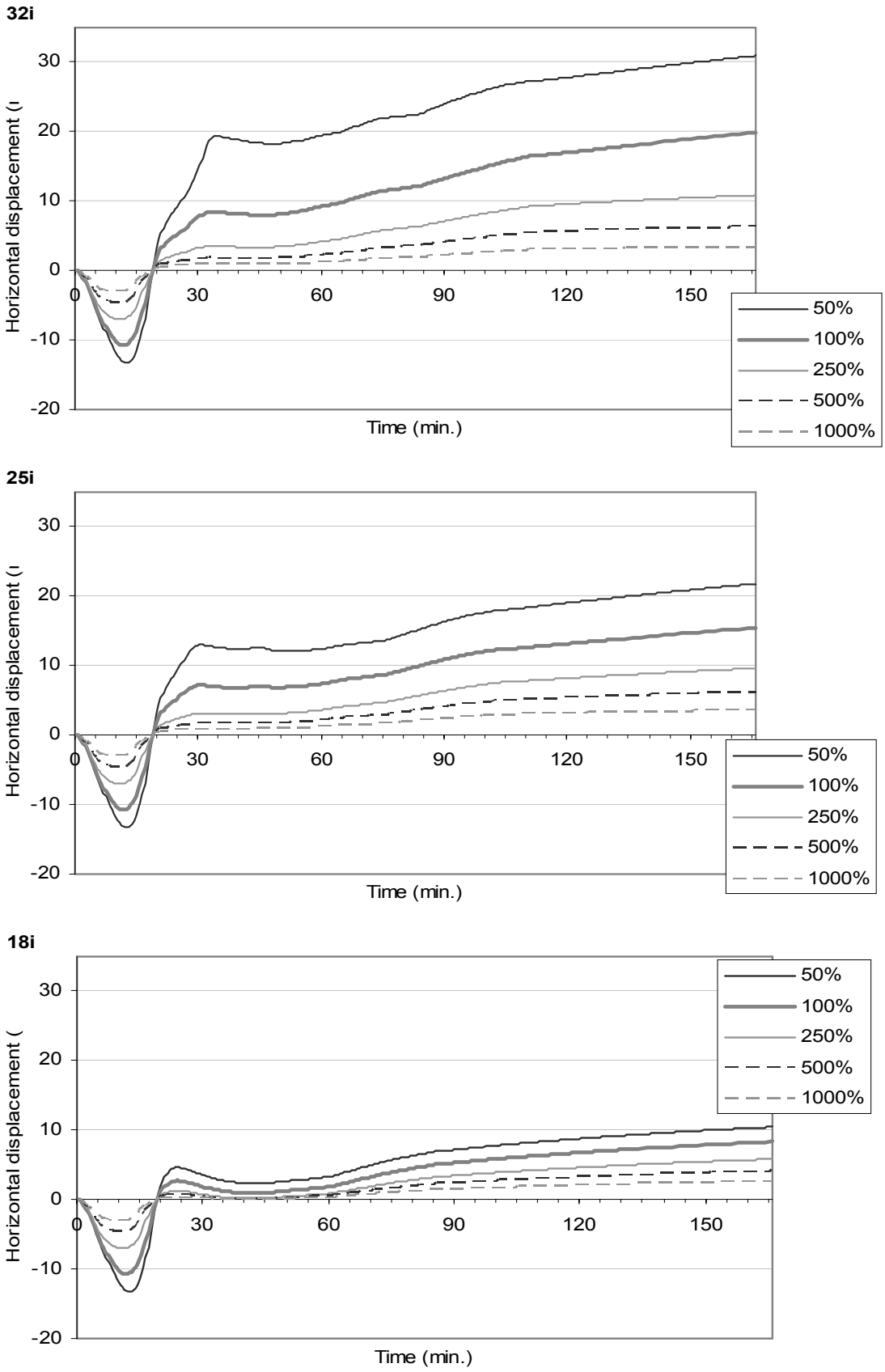

Figure 6-12 Horizontal displacement at one connection with changed strengths and stiffness in pin-pin composite beam exposed to 32, 25 and 18 minutes of the ISO fire with a decay phase

6.3.1.1 Changed stiffness only in pin-pin composite frame

The columns with changed stiffness only were also used for simulation, so that the strength of the columns remained at 100% to the original strength in this scenario. The four levels of column stiffness discussed here are 50%, 100%, 500% and 1000% of the steel beam stiffness.

Figure 6-13 shows the axial force in the frames with a pin-pin connected composite beam. Other than the behaviour observed before, an envelope of axial force at approximate ±850kN is observed in the graph. This indicates that the column started to yield after the axial force reaches this limit. The idea is confirmed in the horizontal displacement graphs in Figure 6-15. While the axial force remained constant at 850kN while cooling, and the midspan vertical displacement shown in Figure 6-14 also remained constant, the horizontal displacement was still increasing. This behaviour indicates that yielding occurred at the mid-height and/or the ends of the columns.

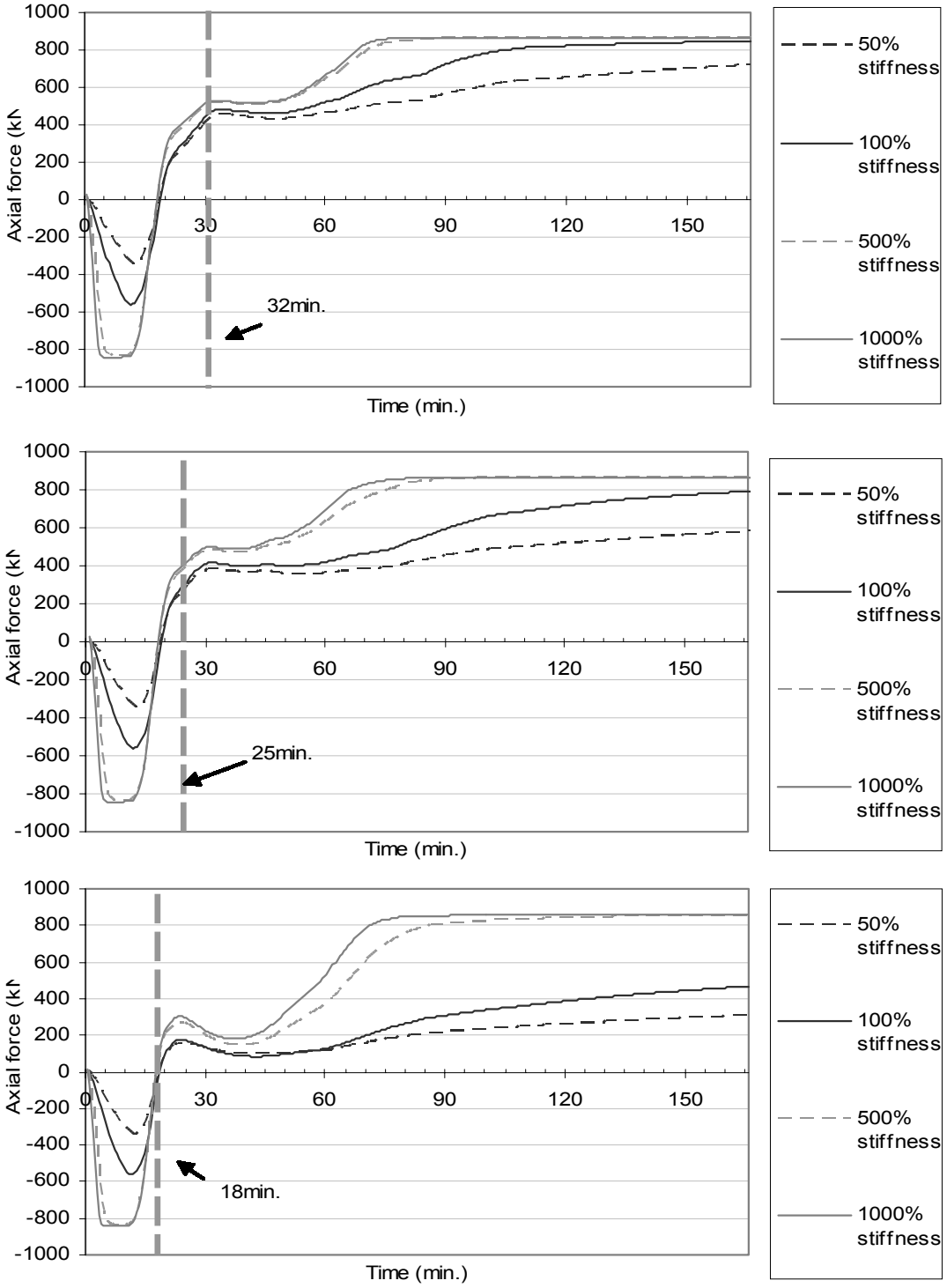

Figure 6-13 Axial force with variation in column strength in composite with pin-pin connected beam exposed to: 32min., 25min., and 18min. ISO834 standard fire with a decay phase

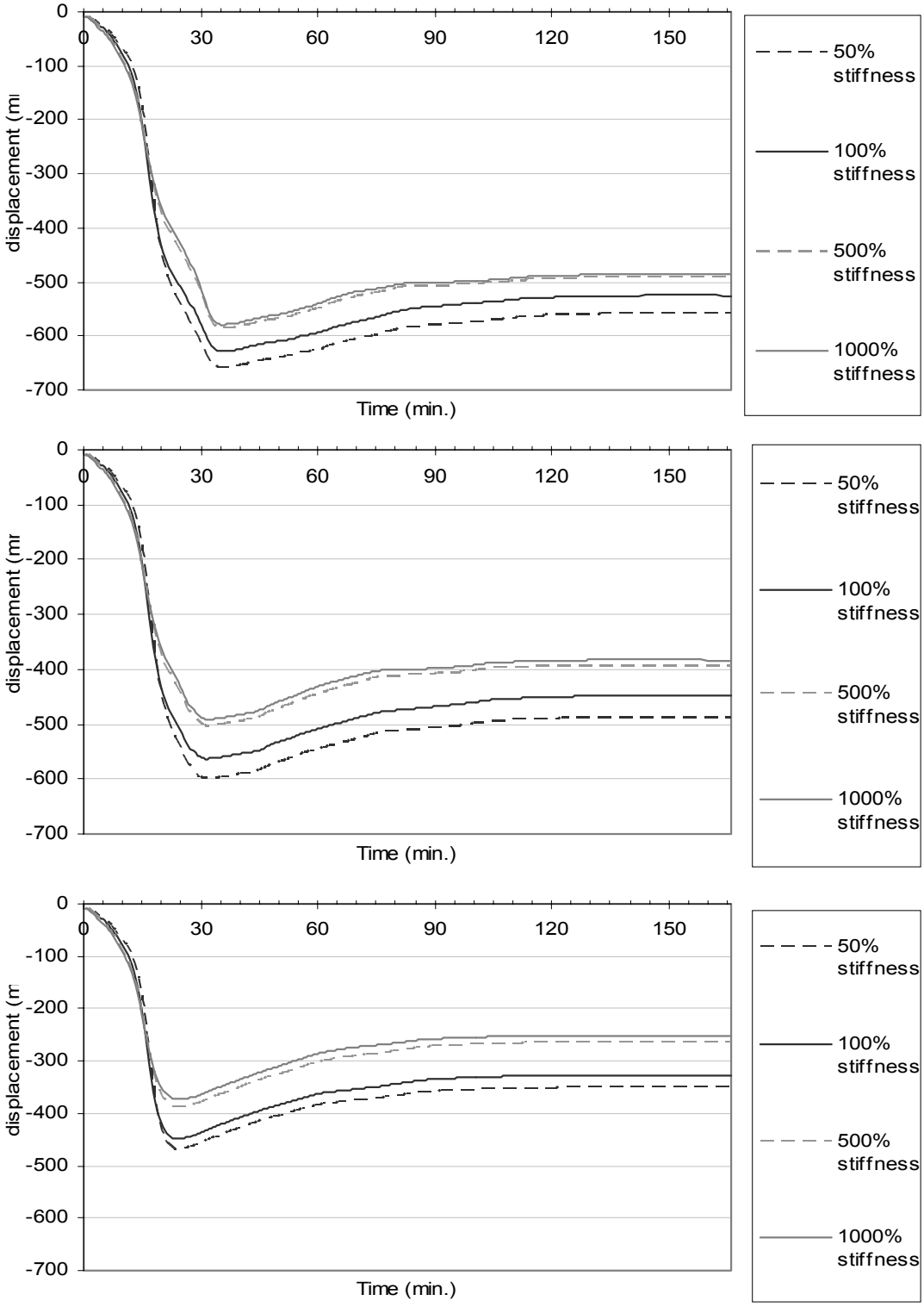

Figure 6-14 Vertical midspan displacements with variation in column strength in composite with pin-pin connected beam exposed to: 32min., 25min., and 18min. ISO834 standard fire with a decay phase

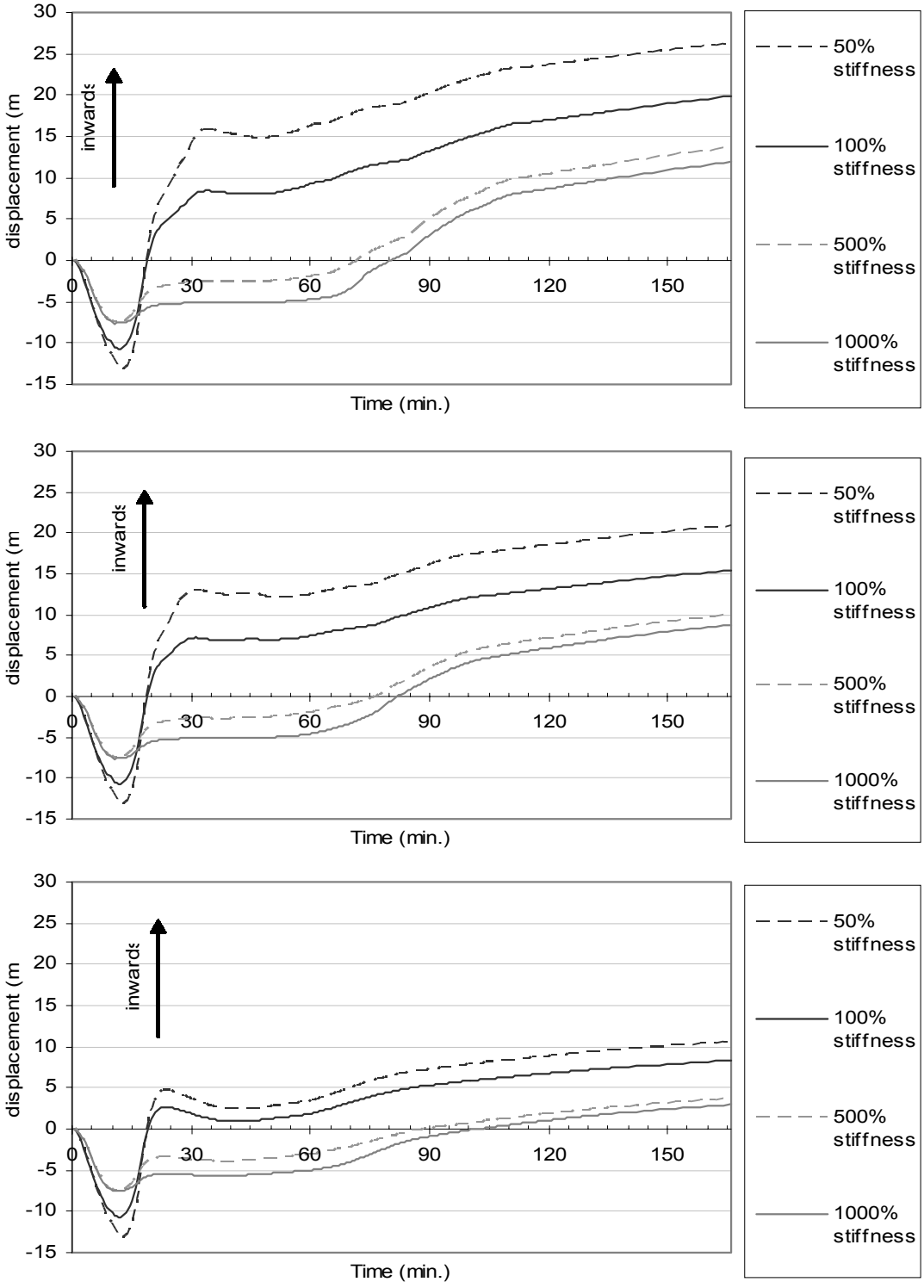

Figure 6-15 Horizontal displacements at one beam-column connection with variation in column strength in composite with pin-pin connected beam exposed to: 32min., 25min., and 18min. ISO834 standard fire with a decay phase

6.3.1.2 Summary of changed column strengths and stiffness in pin-pin composite frame

The scenario with changes in both strength and stiffness of the columns in a frame represents a change of column size. The results showed that the stronger columns give a slightly smaller permanent vertical displacement at the midspan of the beam and a much less horizontal displacement at the beam-column connections.

The beam axial force becomes larger when the columns are strong. The results showed that if the fire size was sufficient to cause a tensile beam axial force before the decay phase started, the axial force would stay at 500kN for around 10 minutes during the early stage when the structure cooled, after which this force would increase and eventually would become more than or equal to the maximum compressive force.

The cases where only the column stiffness was changed in the frame showed different behaviour to the cases with changes in both column strength and stiffness. After the axial force reached 850kN in tension or compression it stopped increasing, meanwhile the horizontal displacement increased more rapidly due to the yielding of the columns. This simulation also showed that only changing the column stiffness has little effect on the midspan vertical displacement of the beam.

The combination of axial force, horizontal displacement at the connection and vertical displacement at the midspan shows that yielding may occur at the mid-height or the ends of the columns. Although the SAFIR program does not allow for failure at the beam-column connections in the simulation, this result can represent the situation in which the bearing failure of the bolted connection occurs in a frame. Figure 6-16 shows one possible failure mode of the connection under large tensile axial force.

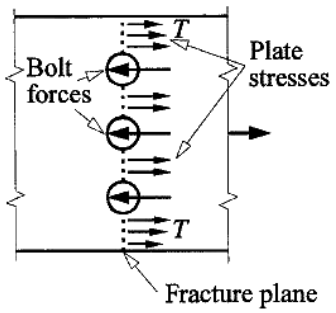

Figure 6-16 Possible failure mode of connection in the pin-pin case (Trahair & Bradford, 1998)

6.3.2 Changed strengths and stiffness in fix-fix composite frame

In the frame with fix-fix connected beam with both column strength and stiffness increased to 1000% of the original value, the structure failed after 17.5 minutes. Three fires, following 16, 12 and 8 minutes of the ISO fire with a decay phase, were used in the simulation. The frame with 1000% column strength and stiffness failed at 21.5 minutes under 16 minutes of the ISO fire due to the rapid vertical displacement at the midspan. All the other frames did not reach failure before the end of the simulation.

Figure 6-17 shows the axial force for frames with a fix-fix connected composite beam. The time the maximum compressive force occurred was independent of the fire size or the column stiffness or strength; but the stronger column induced a larger axial force in both tension and compression. These findings were similar to those from the pin-pin frame. However, comparing Figure 6-17 with the axial force for the pin-pin frame in Figure 6-10, the compressive axial force was significantly larger, especially when the columns were strong. Besides, the compressive force decreased much more slowly than in the pin-pin frame, and this happened after the structure started cooling. Nevertheless, the tensile forces at the end of the simulation in these two cases were about the same.

Figure 6-18 shows the vertical displacement at the midspan. A smaller fire caused a smaller vertical displacement. However, unlike the displacement in pin-pin frame shown in Figure 6-11, a stronger column induced a larger midspan vertical displacement of the beam. In the cases where the columns had 50% or 100% of its original strength and stiffness, the midspan displacement decreased while cooling, so the maximum vertical displacement occurred when the temperature of the steel beam is at its maximum. In the cases where the column strength and stiffness was increased to 500% or 1000%, the vertical displacement decreased only at the early stage when the structure cooled. When the axial force reduced to zero and started to become tensile, the midspan deflections of the beam increased rapidly and then remained constant as the temperature of the steel beam almost returned to the ambient temperature.

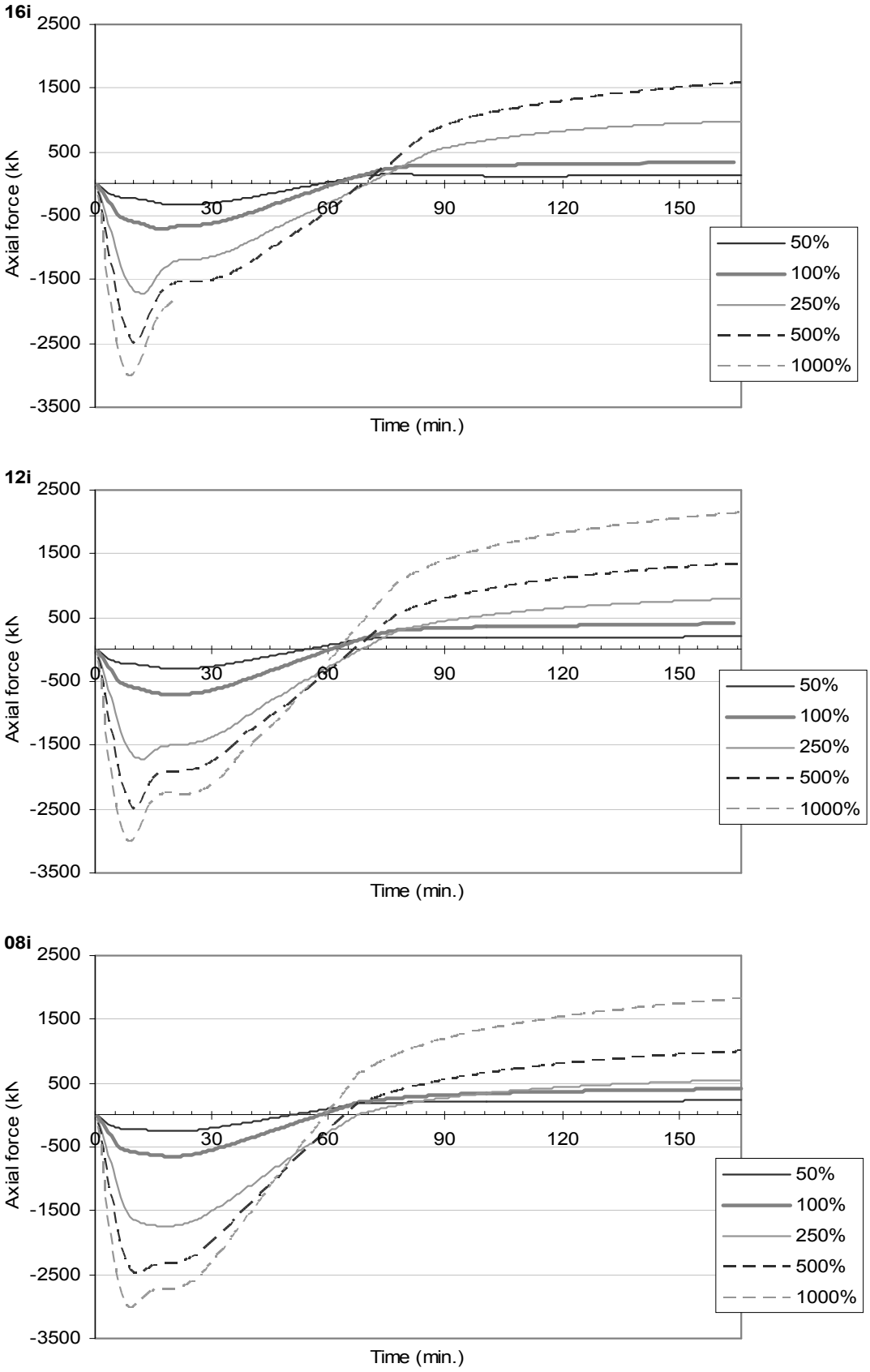

Figure 6-17 Axial force with changed strength and stiffness in fix-fix composite frame exposed to 16, 12, and 8 minutes of the ISO fire with a decay phase

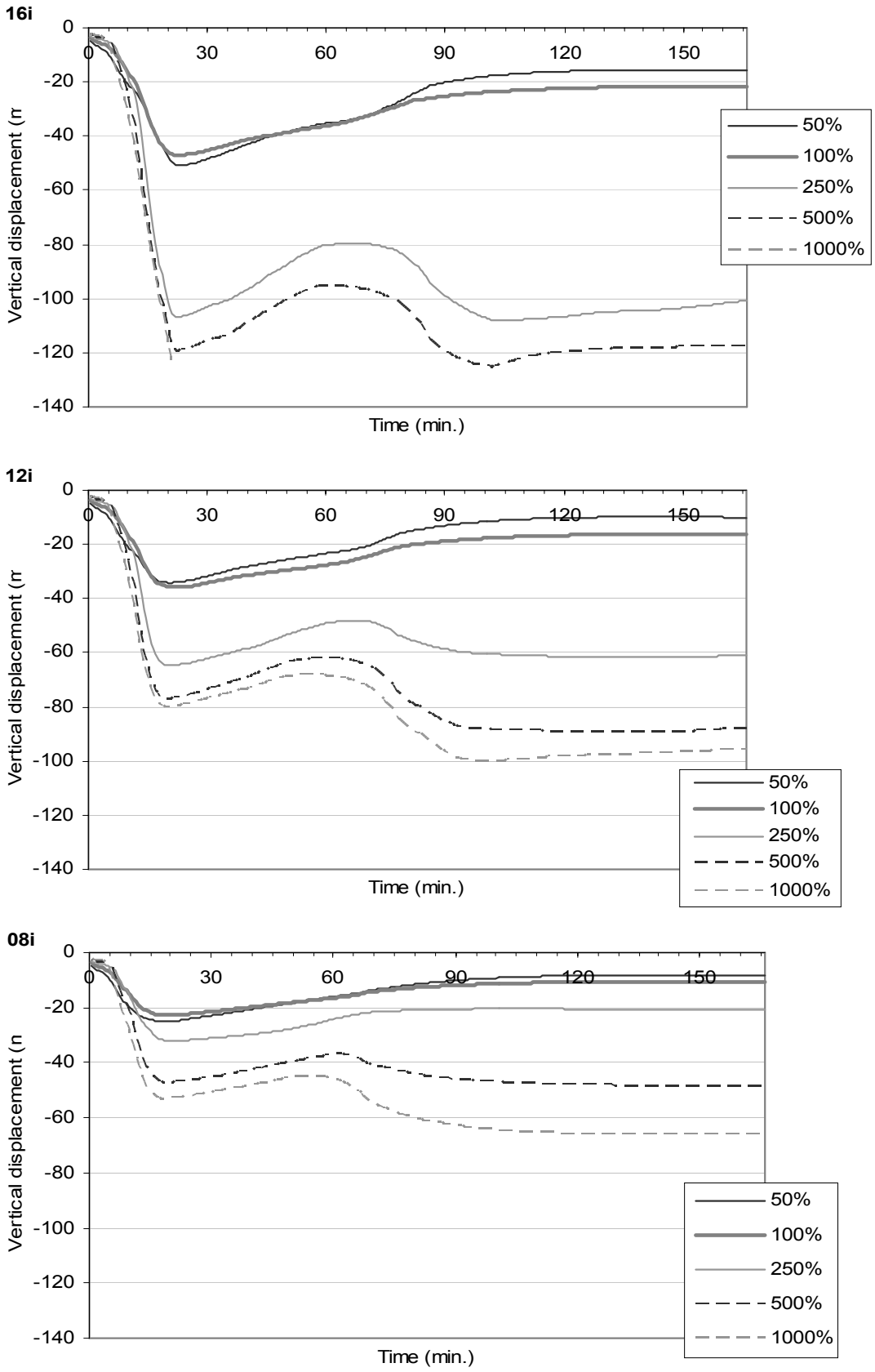

Figure 6-18 Midspan vertical displacement with changed strengths and stiffness in fix-fix composite frame exposed to 16, 12, and 8 minutes of the ISO fire with a decay phase

The vertical displacement graph also suggested that the behaviour of the frame with 250% column strength and stiffness depended on the size of the fire. When the frame was exposed to 16 minutes of fire, the behaviour of the frame was similar to the strong-columns scenario in which the vertical displacement increased while the steel beam temperature returned to ambient; but when the frame was exposed to 8 minutes of fire, the behaviour became closer to the weak-column scenario.

Figure 6-19 shows the horizontal displacement at the connection. Weaker columns allowed a larger horizontal displacement at the beam-column connections during the heating phase. With reference to Figure 6-18, the graph indicates that when the steel beam temperature returned to ambient, the extent of the inward movement at the beam-column connections was in proportion to the midspan vertical displacement.

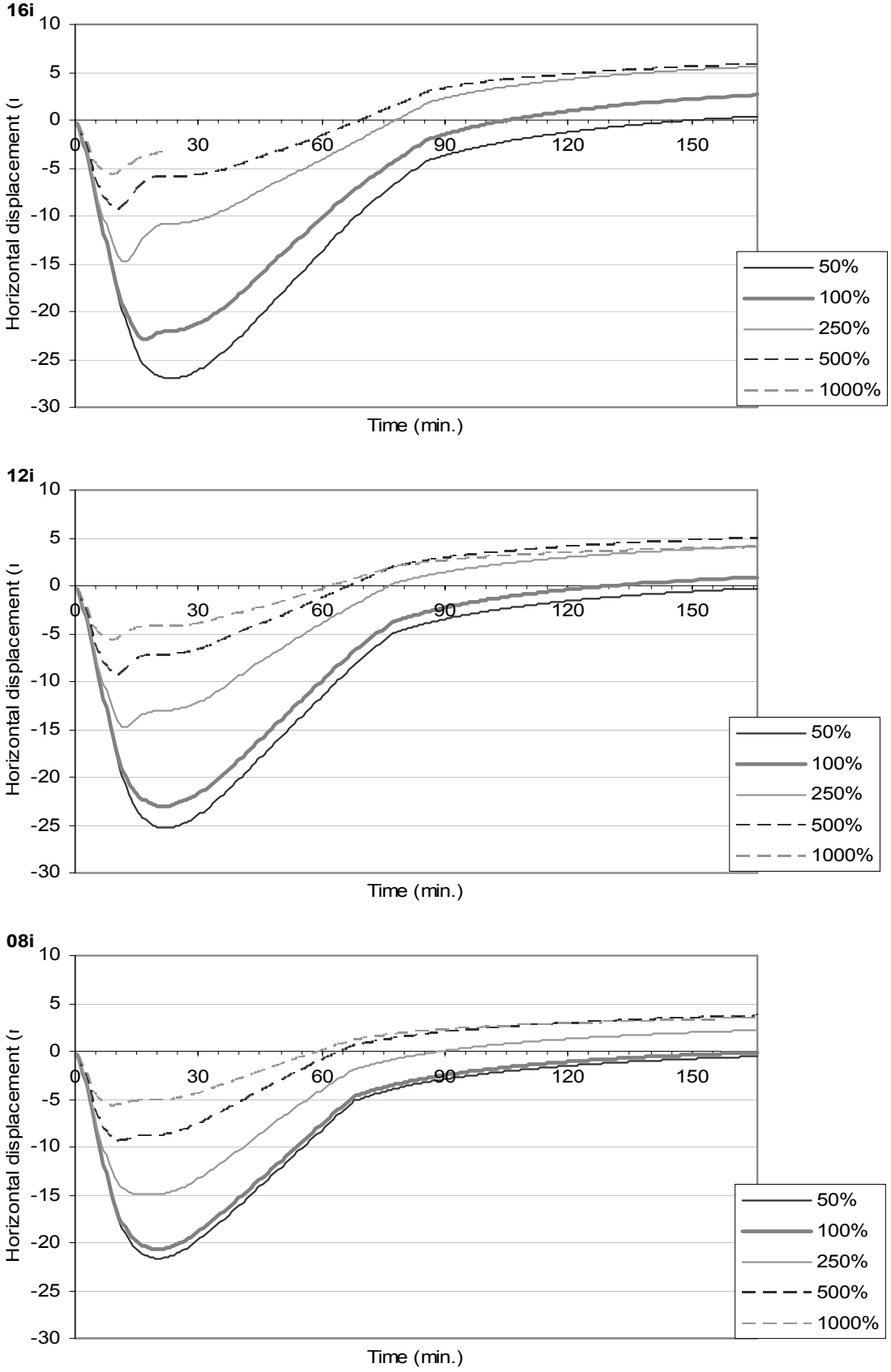

Figure 6-19 Horizontal displacement at one connection with changed strengths and stiffness in fix-fix composite frame exposed to 16, 12, and 8 minutes of the ISO fire with a decay phase

6.3.2.1 Changed stiffness only in fix-fix composite frame

The four levels of column stiffness, 50%, 100%, 500% and 1000% of the steel beam stiffness, were also used for the fix-fix models with changed column stiffness only. All the models could sustain exposure to more than 20 minutes of the ISO fire, which was longer than the cases with changed both the strength and stiffness of the column. Three fires, following 20, 16 and 12 minutes of the ISO fire before the decay phase, were used for comparison.

Figure 6-20 shows the effect of changing stiffness on the axial force under different fires. The axial force in the frame with high stiffness columns had a very rapid change from compression to tension at the early stage when the structure cooled. In the cases with stiff columns, the tensile force reached its peak at the early stage when the structure cooled, and then reduced when the temperature of the beam became steady. In the cases with soft columns, the largest tensile force was found at the end of the simulation and it was still increasing.

Figure 6-20 can be compared with Figure 6-17 to see the effect of changing only the column stiffness. The maximum compressive and tensile forces was significantly less than the cases with both the changed strength and stiffness. Also, in Figure 6-17, the axial forces in all cases returned to zero at almost the same time as the steel temperature equaled the temperature at the bottom of the concrete. This situation was not observed in the changed stiffness only scenarios.

Figure 6-21 shows the midspan vertical displacement of the beam, and Figure 6-22 shows the horizontal displacement at one beam-column connection. At the end of the simulation, the midspan vertical displacement was steady; but the beam-column connections were still moving inwards. This horizontal movement was scarcely affected by the change of stiffness. However, since the axial force in the structures with high column stiffness became stable before the end of the simulation, the behaviour of the midspan displacement and the horizontal translation at the ends indicates that the column yielded. The yielding was due to the beam shortening while cooling. Compared to the changed column stiffness only pin-pin frames, the axial forces that causes the column to yield were almost the same.

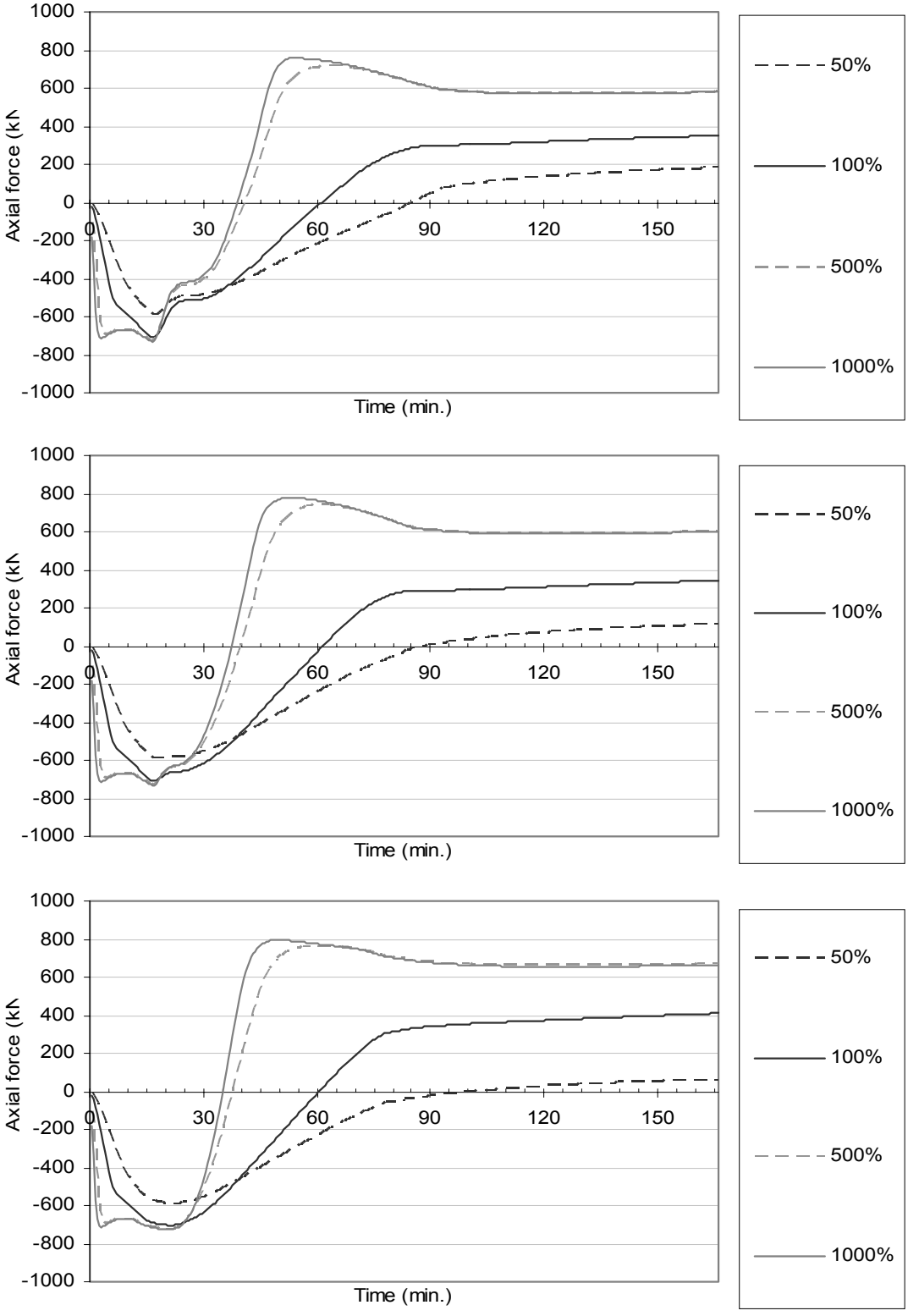

Figure 6-20 Axial force curves for frames with columns of various stiffness and a fix-fix composite beam exposed to 20, 16, and 12 minutes of the ISO fire with a decay phase

Figure 6-21 shows that the change in the column stiffness had little effect on the vertical displacement at the midspan, especially when the fire was small.

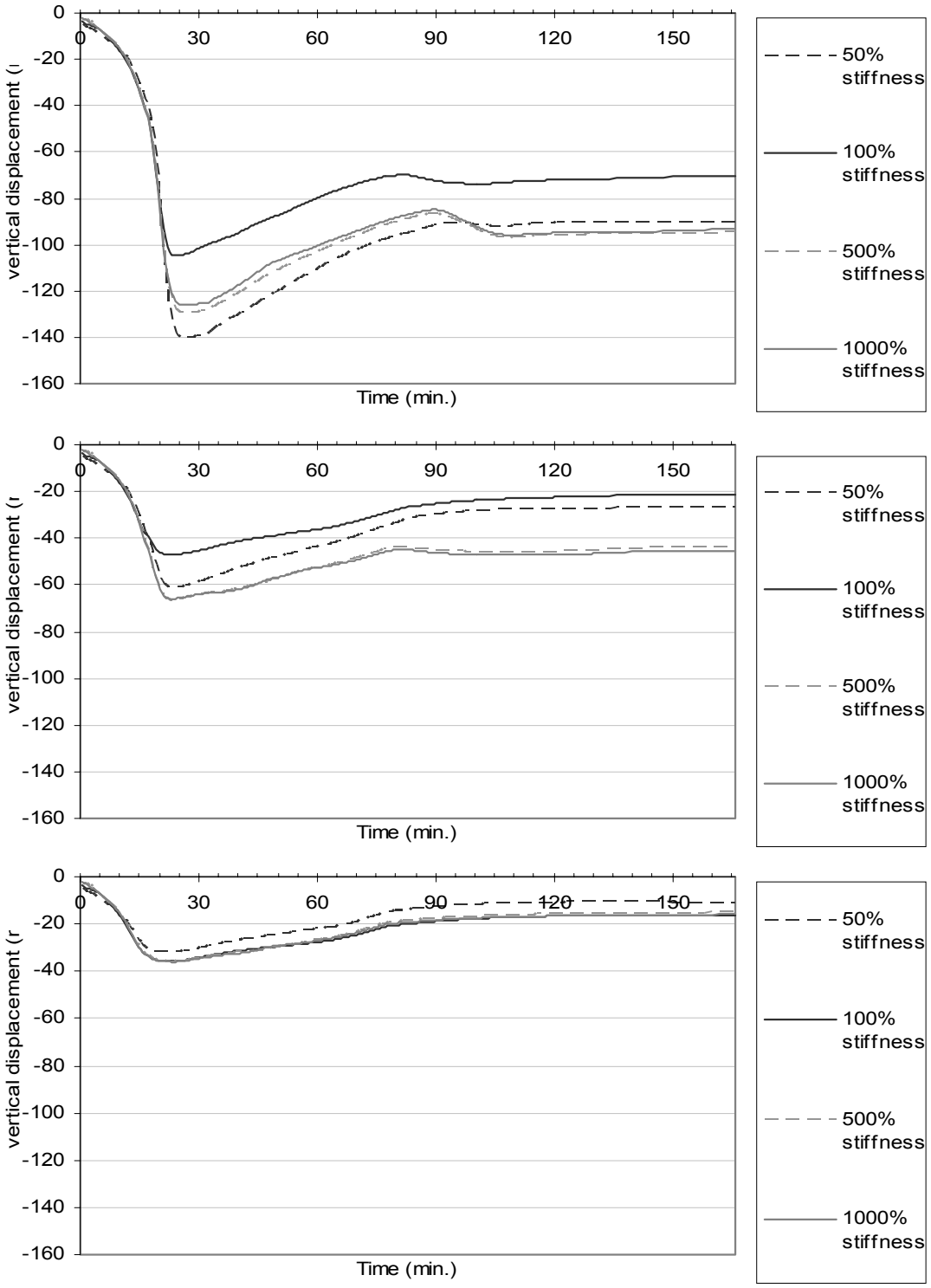

Figure 6-21 Midspan vertical displacement curves for frames with columns of various stiffness and a fix-fix composite beam exposed to 20, 16, and 12 minutes of the ISO fire.

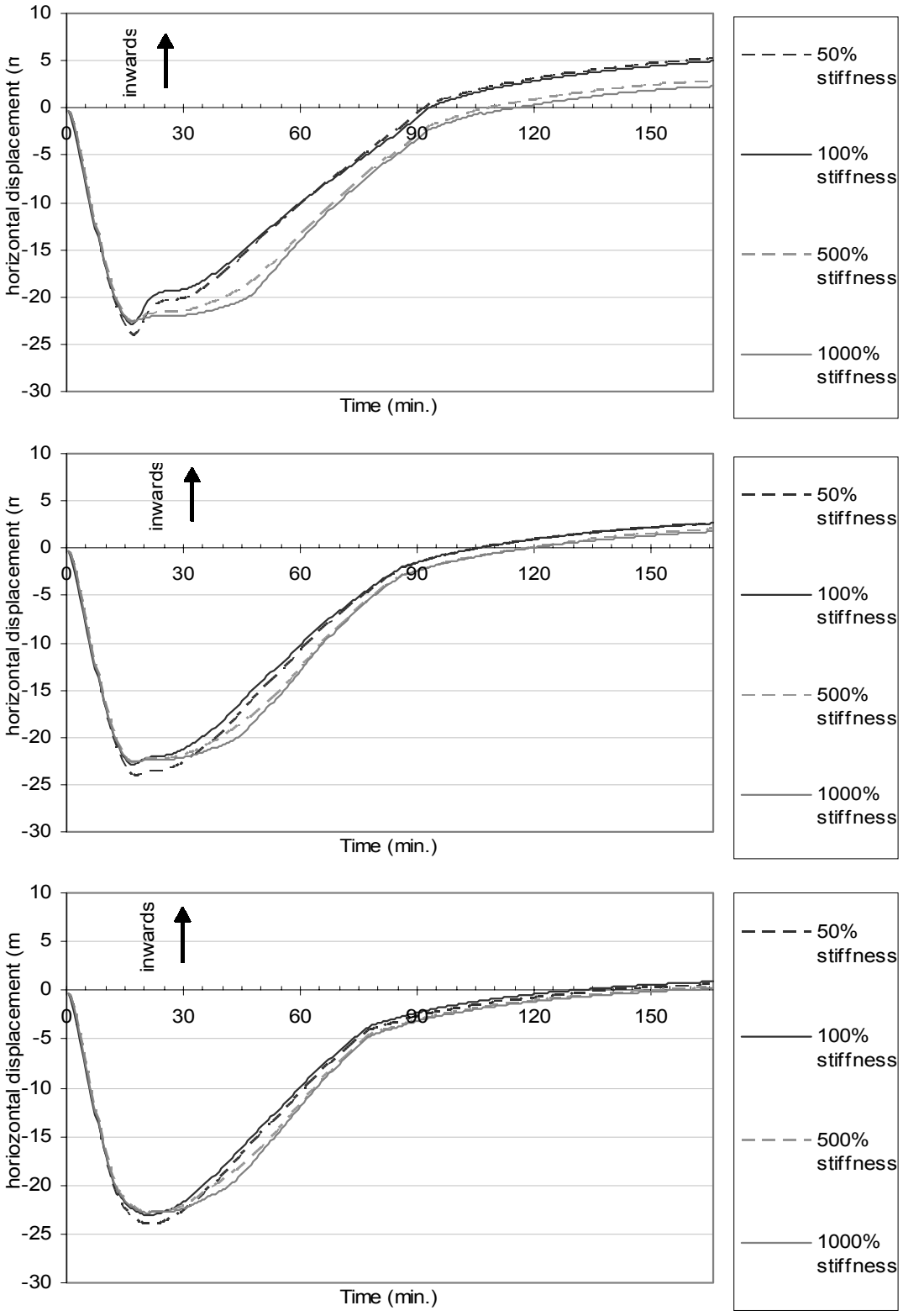

Figure 6-22 Horizontal displacement curves for frames with columns of various stiffness and a fix-fix connected composite beam exposed to 20, 16, and 12 minutes of the ISO fire.

6.3.2.2 Summary of changed column strengths and stiffness in fix-fix composite frame

In the scenario where both the column strength and stiffness were changed, the stronger columns allowed less outward movement at the connections while heating, but permitted more inward movement at the end of the simulation. This horizontal movement was much less than in the pin-pin frame. The midspan vertical displacement graph in Figure 6-21 showed that stronger columns caused a larger permanent vertical displacement. Besides, when the columns were strong, the midspan deflection increased suddenly when the temperature of the steel beam and the bottom of the concrete slab were the same. This behaviour had been observed in the simply supported fix-fix composite beam and was discussed in Section 5.2.2. If the columns have less stiffness, most of the midspan vertical displacement will be recovered while cooling. In terms of the beam axial force, the stronger columns induced a larger axial force. The maximum compressive force was almost twice as large as in the pin-pin frame case, but the maximum tensile forces in these two cases were the same.

In the scenario where only the column stiffness was changed, the results showed that the vertical displacement at the midspan and the horizontal displacement at the connection were not affected much by the stiffness of the columns. However, when the columns were stiff, the axial force changed more rapidly with the fire temperature, it would reach its maximum tensile force during the early stage when the structure cooled, and then it would reduce and remain constant by the end of the simulation. The axial force was less than in the pin-pin frame case and was not as large as in the frame with changed both column strength and stiffness. However, a comparison of the axial force with the horizontal displacement graph showed that the horizontal displacement was still increasing while the axial force remained constant, indicating that the stiff columns yielded in this scenario as well.

6.4 Summary of the simulation results of composite frames

This chapter reviewed the simulation results of frames with pin-pin or fix-fix connected composite beams; it also discussed the effect of changing the stiffness and strength of the columns. The behaviour of the beam in a frame lies between the behaviour of the single span beam with and without the horizontal restraints. The amount of freedom in the horizontal translation at the beam-column connection depends on the stiffness and the strength of the columns. In the 100% column strength and stiffness cases, the frames behaved quite similar to the single span beams without the horizontal restraints except for the presence of the beam axial force.

It is crucial in connection designs to know the maximum axial force in the frame. Table 6-3 shows the axial force in the frames with pin-pin connected composite beams. The maximum compressive axial force in the beam occurred when the bottom flange at the midspan was yielding. The fire size did not affect the magnitude of this compressive force as long as the steel temperature was high enough to reduce the tensile yield limit at the bottom of the beam so that the steel could yield. The stiffer column had a higher compressive force because it behaved more like a single span pin-pin supported beam.

Table 6-3 Analysis results of the frames with pin-pin connected composite beam

Frame with pin-pin composite beam						
Column strength & stiffness		50%	100%	250%	500%	1000%
Time to fail in the ISO fire without a decay phase	min.	40.5	39	39	38.5	37.5
Steel temperature at failure (at the bottom flange)	^{o}C	869	861	861	858	848
Maximum compressive axial force	kN	340	560	910	1240	1610
Maximum tensile axial force (in 32 minutes of the ISO fire and a decay phase)	kN	450	850	1450	1660	1750

Comparing Table 6-3 with Table 5-5, it shows that the column stiffness has to be very large to achieve a horizontal restraint similar to that in the single span pin-pin beam. Figure 6-23 shows the comparison between the single span pin-pin supported beam and the pin-pin connected beam in a frame with 1000% column strength and stiffness. The failure time and the midspan vertical displacements in these two cases were similar; however, the compressive force in the frame was half the value in the single span beam.

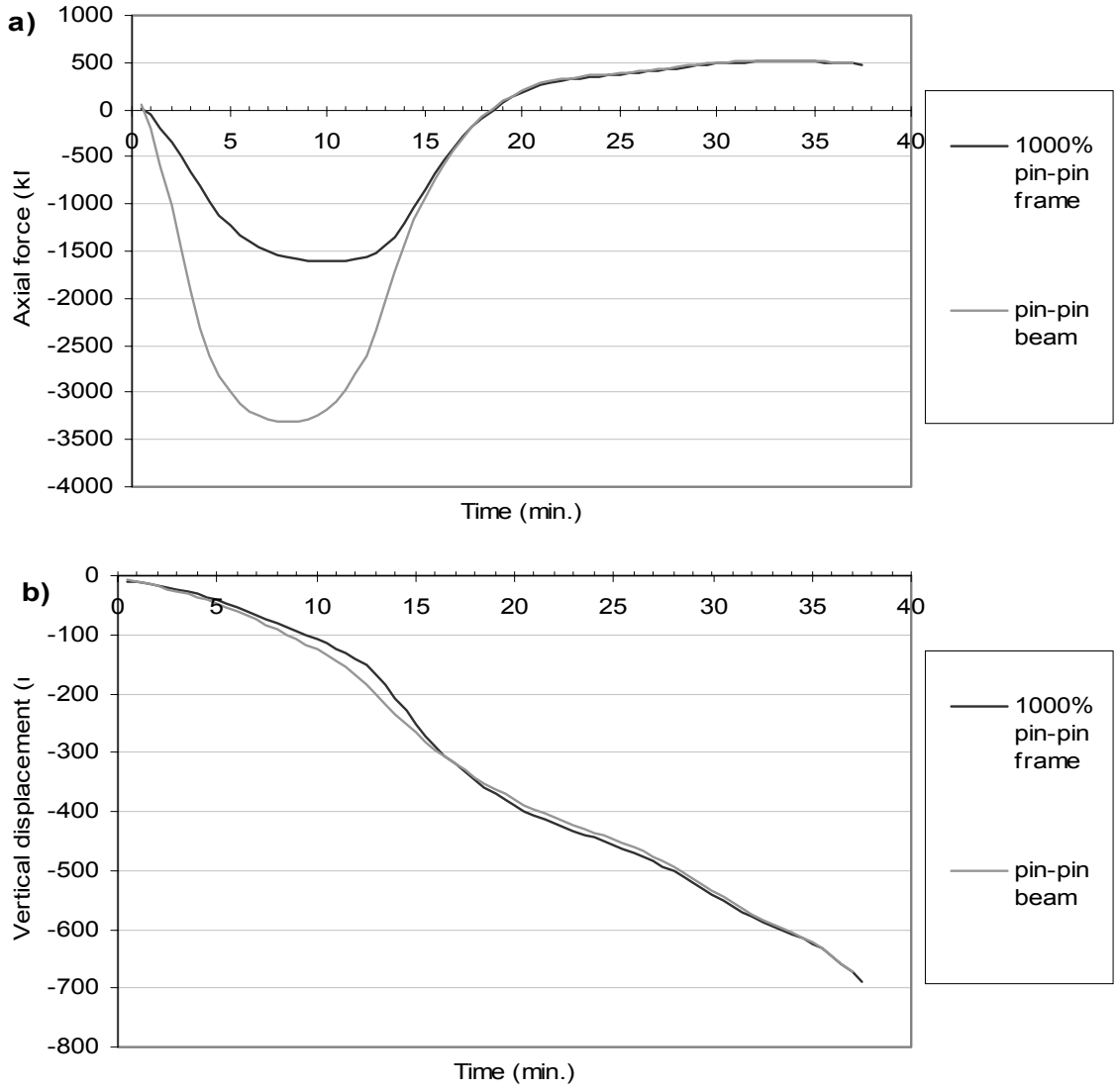

Figure 6-23 Comparison between the behaviour of frame with pin-pin connected composite beam (with 1000% column strength and stiffness) and of single span pin-pin beam: a) axial force; b) midspan displacement

Table 6-4 shows the axial forces in the frames with fix-fix connected beams. The maximum compressive axial force was independent of the fire size, but the tensile force became larger when the maximum fire temperature was high. Compared to the pin-pin frame, this structure could sustain less of the ISO fire; and both the compressive and tensile axial forces were larger. However, being similar to the pin-pin frame, the axial force was in proportion to the strengths of the columns.

Table 6-4 Analysis results for the frames with fix-fix connected beams

Frame with fix-fix composite beam						
Column stiffness		50%	100%	250%	500%	1000%
Time to fail in the ISO fire without a decay phase	min.	26	22.5	20	19	18.5
Steel temperature at failure (at the bottom flange)	^{o}C	739	719	690	674	665
Maximum compressive axial force	kN	325	700	1730	2500	3020
Maximum tensile axial force (in 12 minutes of the ISO fire with a decay phase)	kN	210	410	800	1340	2140

Comparing Table 6-4 with Table 5-5, it shows that the failure time of the frame with stiffer columns was closer to that of the single span fix-fix beam. Figure 6-23 shows the comparison between the single span fix-fix connected composite beam and the beam in a frame with column strength and stiffness increased to 1000%. The graphs show that the failure time and the midspan vertical displacement in these two cases were similar, but the maximum axial force in the frame was 25% less than for a single span beam.

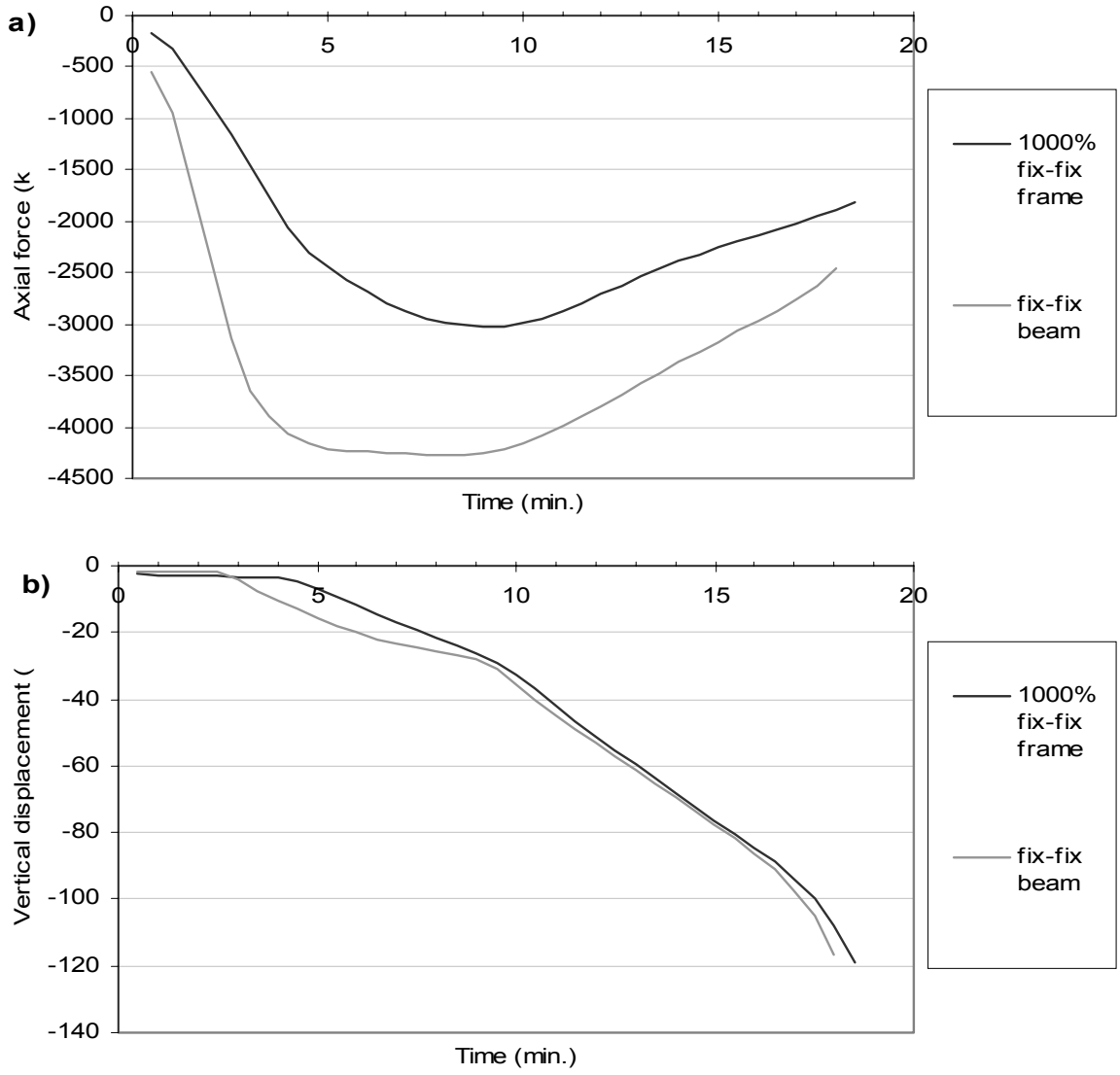

Figure 6-24 Comparison between the behaviour of frame with fix-fix connected composite beam (with 1000% column strength and stiffness) and of single span fix-fix beam: a) axial force; b) midspan displacement

From the design point of view, frames with stiff columns and a fix-fix connected beam require more attention because the beam has a larger tensile force induced during the decay phase than its maximum compressive force. Unlike the maximum compressive axial force which does not vary with the fire temperature as long as the bottom flange stress reaches the temperature-reduced yield limit, the maximum tensile axial force differs with the size of the fire. Hence, it is still possible for the induced force to exceed the designed capacity of the connections.

Rotation fixation in reality can be achieved by using welded connections; and fixed beam-column connections are often used in seismic frames. Different kinds of connections are shown in Figure 6-25. A bolted connection from the design point of view is assumed as not being able to transfer any bending moment from the connected beam or column. However, as the experimental data in Nethercot (1985) showed, a simple bolted connection often has a considerable amount of moment capacity. Therefore, most of the bolted connections have behaviour somewhere between a pinned and a fixed connection, and the result of a composite frame using bolted connections and the same setups as those used in the simulation model should lie between the values shown in Table 6-3 and Table 6-4.

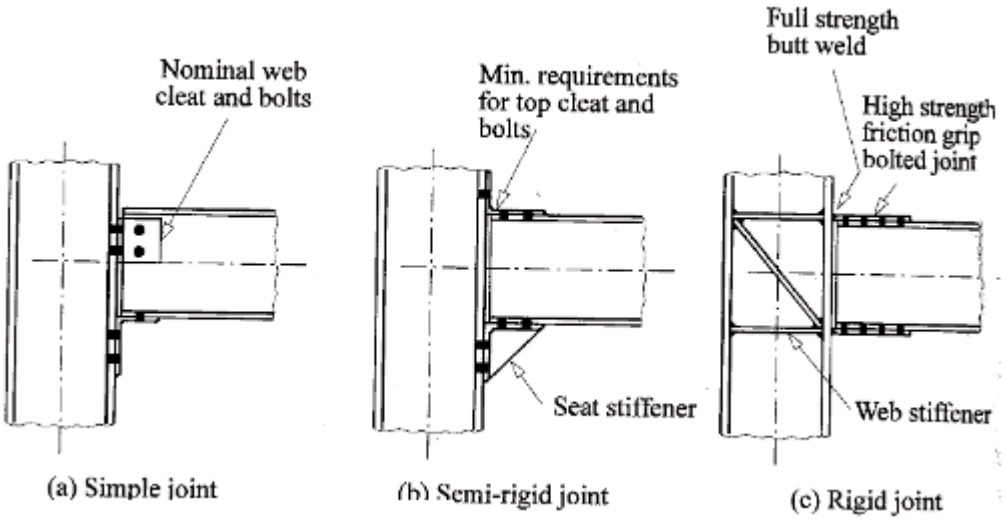

Figure 6-25 Sample connection types (Trahair & Bradford, 1998)

7 Simulation results of steel beams exposed to the ISO fire with a decay phase

This chapter discusses the simulation results of modelling single span steel beams exposed to various durations of the ISO834 standard fire with a decay phase. The layout and end conditions in the steel structures were the same as in the composite steel structures. The method of varying the fire temperature and the analysis method were the same as discussed in Chapter 5.

7.1 Thermal analysis results for the steel beams

After simulating the beams with different supporting conditions exposed to the ISO834 standard fire, the pin-pin connected beam, which was the most durable model, reached failure after 40 minutes under the fire. Six other fires, with from 8 minutes to 30 minutes of the ISO fire with a decay phase, were used for comparison of the steel structures. Figure 7-1 and Figure 7-2 show the temperatures at the bottom and top flange. These temperatures were quite similar to the temperatures of the steel section in the composite beam, except the temperature at the top flange in this arrangement was slightly higher.

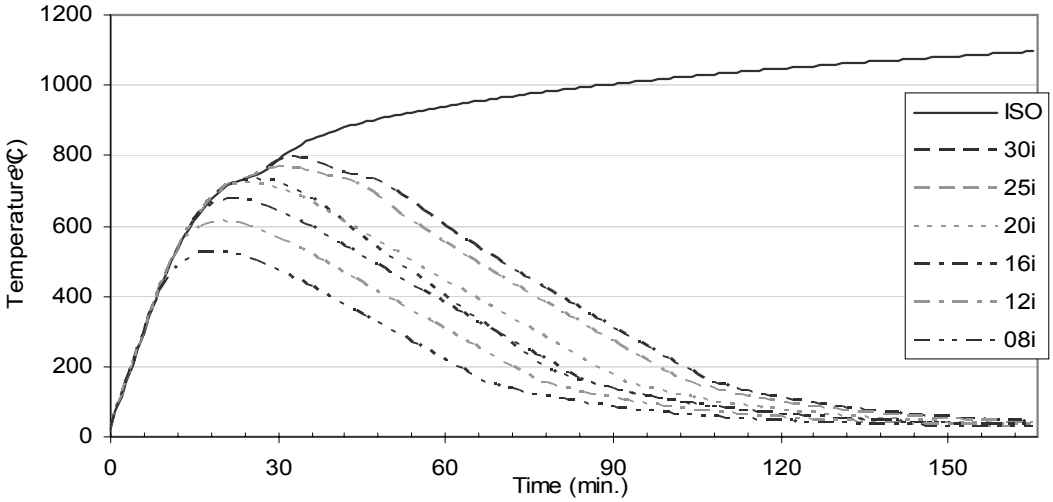

Figure 7-1 Thermal analysis output of various durations of the ISO fire at the bottom flange

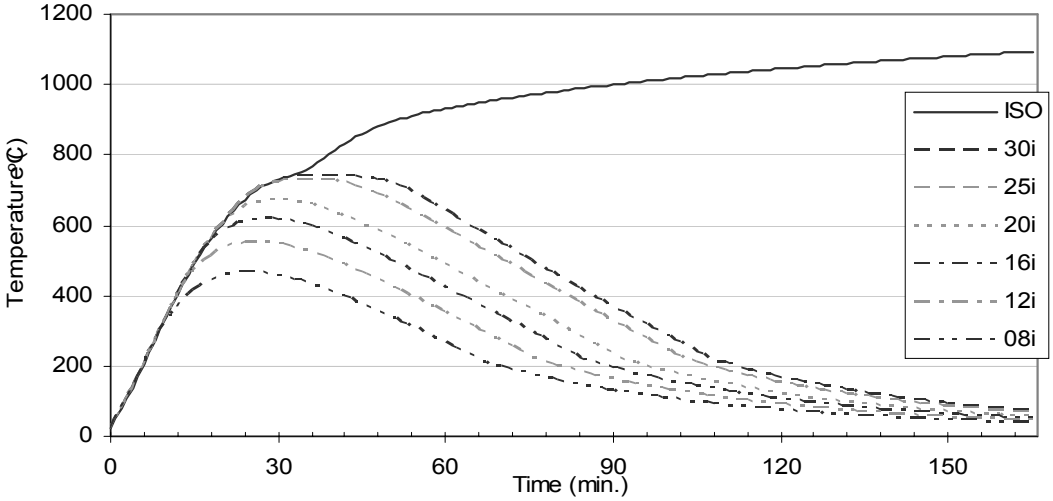

Figure 7-2 Thermal analysis output of the steel beam at the top flange

7.2 Structural analysis results for the steel beams

7.2.1 Pin-pin steel beam

The single span pin-pin connected steel beam reached failure after being exposed to 40 minutes of the ISO834 standard fire. Six other fires, ranging from 8 minutes to 30 minutes of the ISO fire with a decay phase, were used for comparison. The axial force and the midspan vertical displacement in these cases are shown in Figure 7-3.

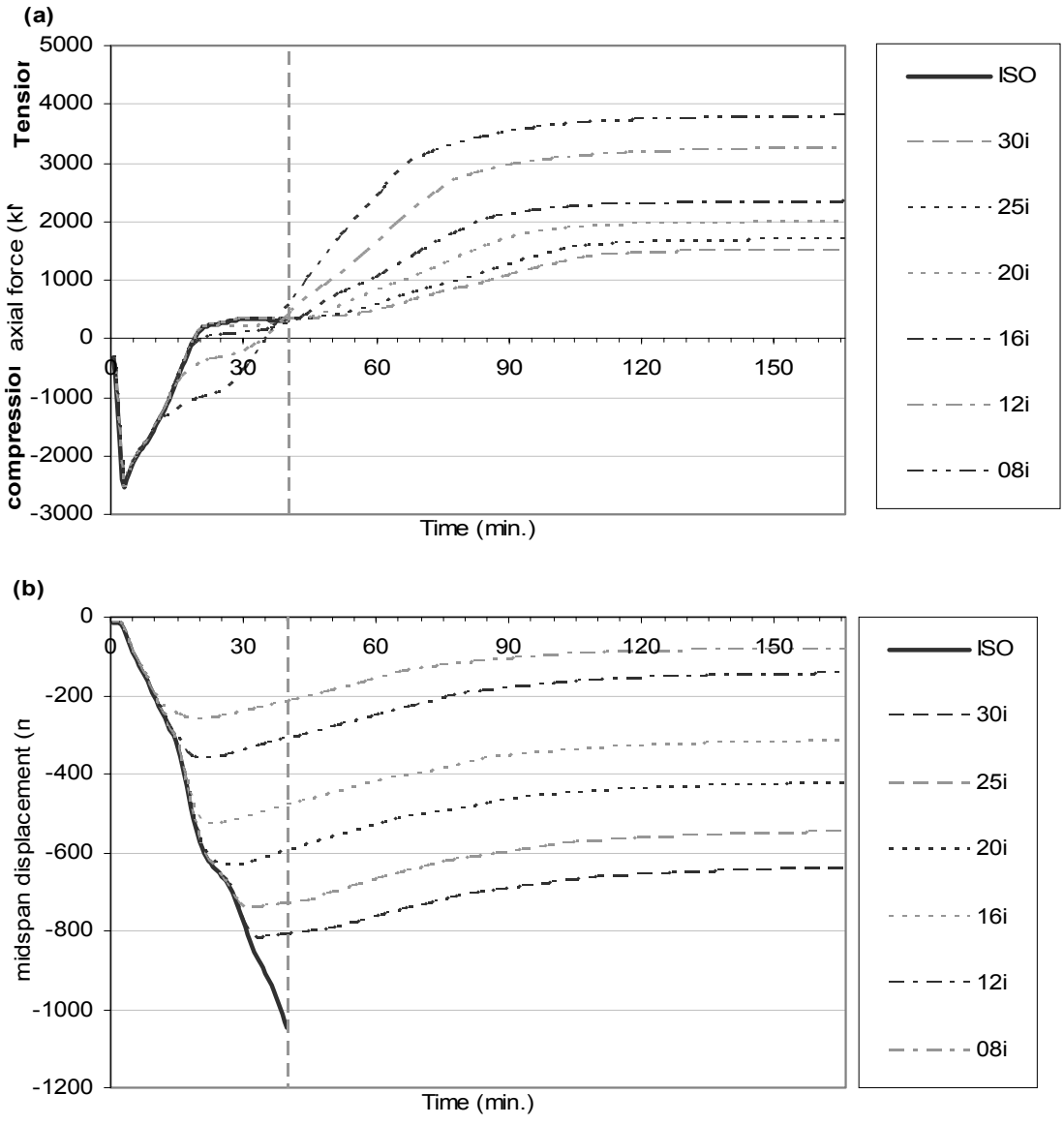

Figure 7-3 simulation results of single span pin-pin connected steel beam: (a) axial force (b) midspan displacement

7.2.1.1 Comparison with the pin-pin composite beam case

The results shown in Figure 7-3 are slightly different to the results for a single span pin-pin connected composite beam shown in Figure 5-4. The axial force diagrams show that the force increased linearly in compression and reached its maximum compressive force rapidly, afterwards this force decreased rather slowly but also linearly. This was different to the composite beam case. Besides, the compressive force decreased more linearly than of the composite beam case.

The beams exposed to shorter lengths of the ISO fire had larger tensile forces at the end of the simulation; this situation was in contrast to the finding in the composite beam case. Figure 7-4 shows the centreline stress distribution of the midspan at this time. Because the temperature of the beam was cooler than 400^{o}C at the end of the simulation, the yield limit had returned to its original value of 300MPa. The figure shows that if the fire was small, the entire cross-section of the beam would reach or approximate the tensile yield limit; if the fire was large, the top flange and most of the web was close to the tensile yield limit, and the bottom flange was almost at the compressive yield limit. Although the centreline stress diagram suggests that a plastic hinge formed at the midspan in all cases, which achieved the failure mechanism of a pin-pin connected beam, SAFIR determined that failure did not occur before the end of the simulation in all these cases.

The magnitude of the axial force in this case was compared with the composite beam case. One needs to be aware that the loads on the steel beam were reduced to reflect the stiffness difference of the steel beam to the composite beam. The maximum compressive force in the steel beam was smaller, but the maximum tensile force could be twice as big as the force in the composite beam.

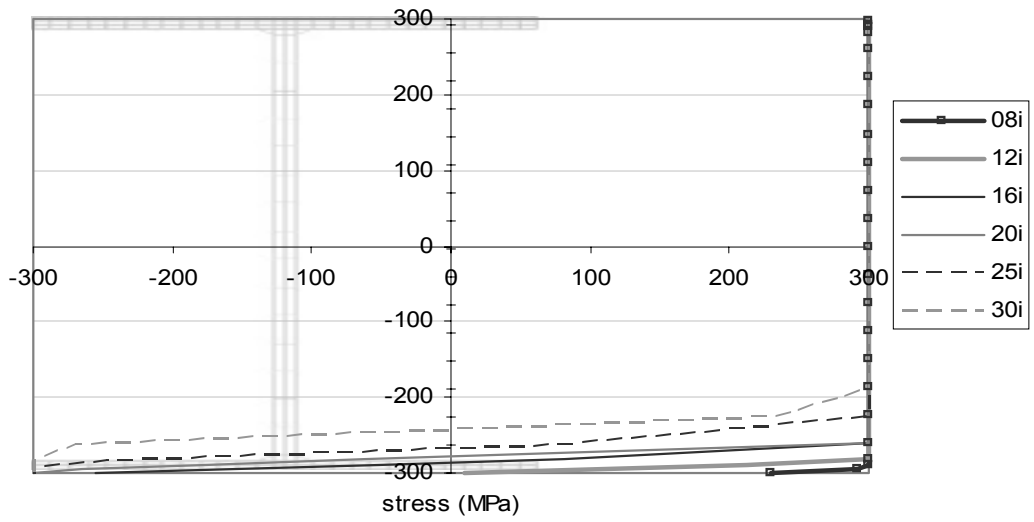

Figure 7-4 Centreline stress distribution of single span pin-pin connected steel beam at 166 min. exposed to various durations of fire

The midspan displacement diagram in Figure 7-3(b) shows the same characteristic as in the single span pin-pin connected composite beam case. A larger fire induced a larger permanent vertical displacement at the midspan, and even the least severe fire simulated caused a permanent displacement. The midspan vertical displacement in the steel beam case was approximately 100mm larger than in the composite beam case. This was due to the lack of the concrete slab to contribute to the bending stiffness.

Figure 7-5 and Figure 7-6 show the bottom and top flange stresses at the midspan of the steel beam exposed to 8 minutes of the ISO fire and a decay phase. These two figures can be compared with the ones of the composite beam, Figure 5-5 and Figure 5-7. The top flange stresses of these two cases were similar, but without the presence of the concrete slab to resist the compressive force, the top flange of the beam yielded in compression during the heating phase. This caused a permanent vertical displacement, and consequently allowed the bottom flange to be under tension instead of compression during and after cooling.

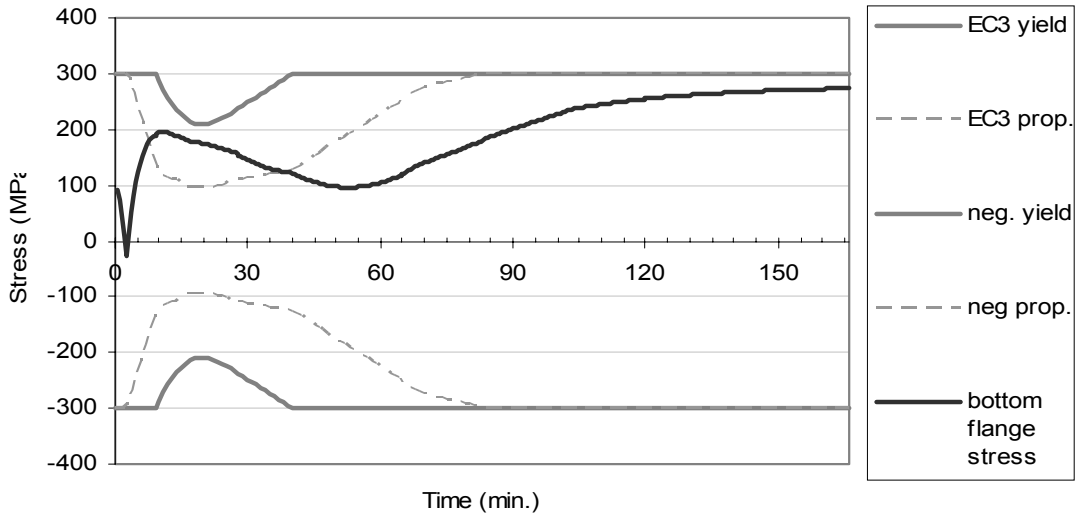

Figure 7-5 Bottom flange stress in pin-pin connected steel beam under 8 minutes of the ISO fire with a decay phase

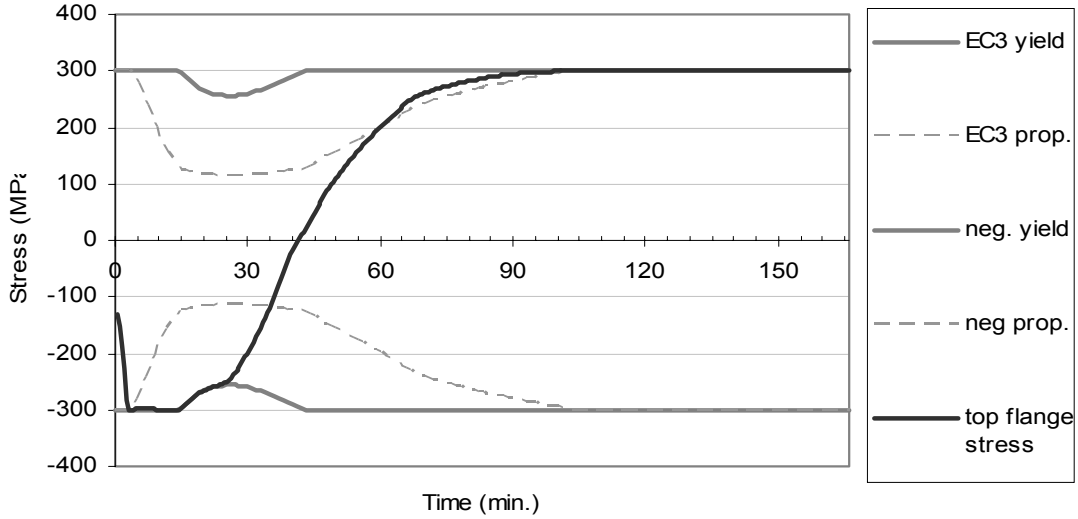

Figure 7-6 Top flange stress sin pin-pin connected steel beam under 8 minutes of the ISO fire with a decay phase

7.2.1.2 Summary of the pin-pin steel beam

Without the presence of the concrete slab to provide composite action, the top flange yielded earlier than the bottom flange in the steel beam case. However, it lasted longer in the ISO fire than the composite beam case and the failure occurred at 40 minutes. Although the beam did not fail under any of the tested fires with a decay phase, the centreline stress distribution diagram shows that the entire steel section at the midspan yielded. When the fire was large, the bottom flange yielded in compression and the upper portion of the beam in tension; when the fire was small, the whole section yielded in tension.

The behaviour found in the midspan vertical displacement was similar to what of the composite beam case, that the displacement became larger when the fire was large. However, without the presence of the concrete slab, the permanent vertical displacement was much larger than of the composite case when being exposed to the same fire.

7.2.2 Fix-fix steel beam

Figure 7-7 shows the axial force and midspan vertical displacement of the single span fix-fix connected steel beam exposed to various durations of the ISO fire followed by a decay phase. The beam exposed to the ISO834 standard fire failed in 22 minutes. Four fires, following 8 to 20 minutes of the ISO fire with a decay phase, were used for comparison. In the case where the beam was exposed to 20 minutes of the ISO fire, the beam failed at 105.5 minutes. No other cases reached failure before the end of the simulation.

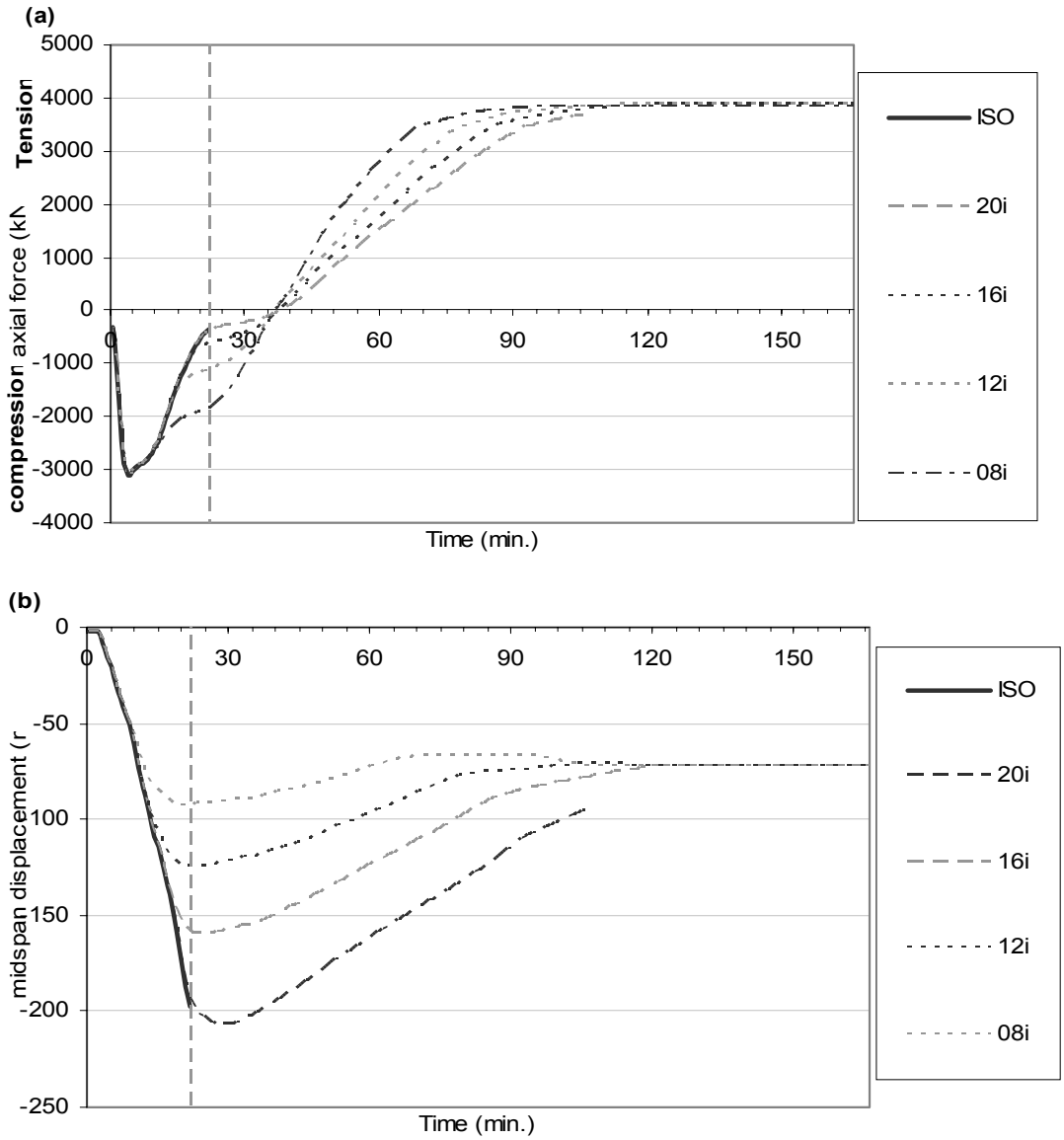

Figure 7-7 Simulation results of single span fix-fix connected steel beam: (a) axial force (b) midspan displacement

7.2.2.1 Comparison with the fix-fix composite beam case

The axial force diagram in Figure 7-7(a) was similar to Figure 5-15(a), the diagram for the fix-fix composite beam. At the end of the simulation, the induced tensile force was at its maximum. The axial force could only increase up to 3900kN because of the yield strength and the cross sectional area of the beam, therefore after the tensile axial force reached this level the beam would start to fail under tension.

The maximum compressive axial force occurred at almost the same time as in the composite beam, but the compressive force decreased faster afterwards. The axial force returned to zero at around 37 minutes in all cases other than the case exposed to the ISO834 standard fire

The vertical displacement in Figure 7-7(b) showed a different behaviour to the composite case shown in Figure 5-15(b). At the end of the simulation, the midspan displacement was around 75mm in all the cases that had not failed. This indicates that the permanent displacement was independent to the fire temperature after the beam started to yield under tension, which was different to the composite case. The graph also shows that the beam exposed to 20 minutes of the ISO fire had a larger maximum vertical displacement than the beam that failed under the ISO834 standard fire, which indicates that the great deflection at the midspan did not cause the beam to fail..

7.2.2.2 Structural behaviour of the beam exposed to the ISO834 standard fire

Figure 7-8 shows the centreline stress distribution at 22 minutes at midspan as well as near the connection, in the case exposed to the ISO834 standard fire. Near the connection, the bottom flange and a major portion of the web were at the temperature reduced compressive yield limit; and the top flange was in tension. At the midspan, the lower part of the beam was under tension; the top part of the beam was under compression; and the top flange reached the compressive yield limit induced by the axial restraints at the end.

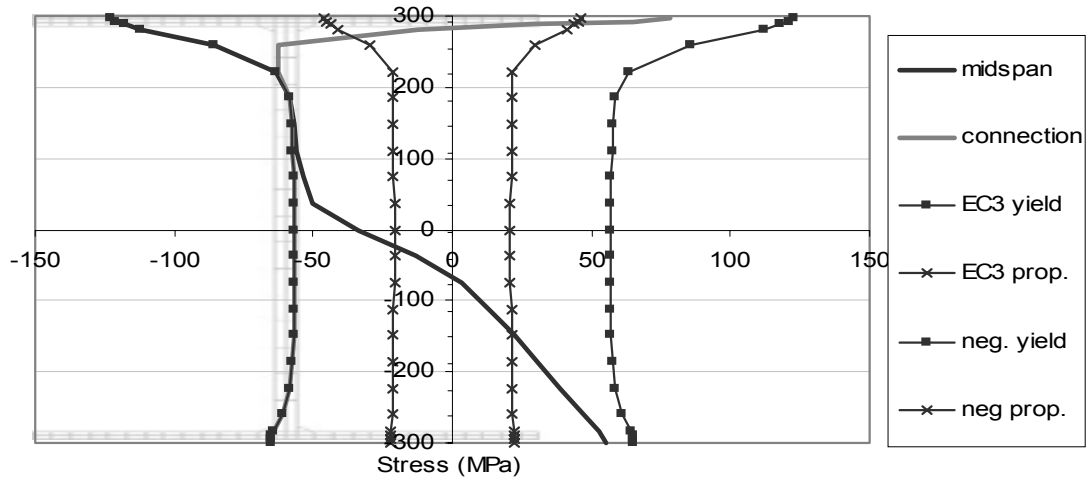

Figure 7-8 Centreline stress distribution at 22 minutes for fix-fix connected steel beam exposed to the ISO834 standard fire

Figure 7-9 compares the centreline stress at 22 minutes for both the ISO fire case and the 20 minutes of the ISO fire case. The darker lines are for the ISO834 standard fire case, and the lighter lines are for the beam exposed to 20 minutes of the ISO fire and a decay phase. At this time, the temperature of the 20 minutes of the ISO fire case was slightly lower than of the ISO834 standard fire case as the yield limit was larger. This may explain why the beam did not fail so early in the 20 minutes of the ISO fire case.

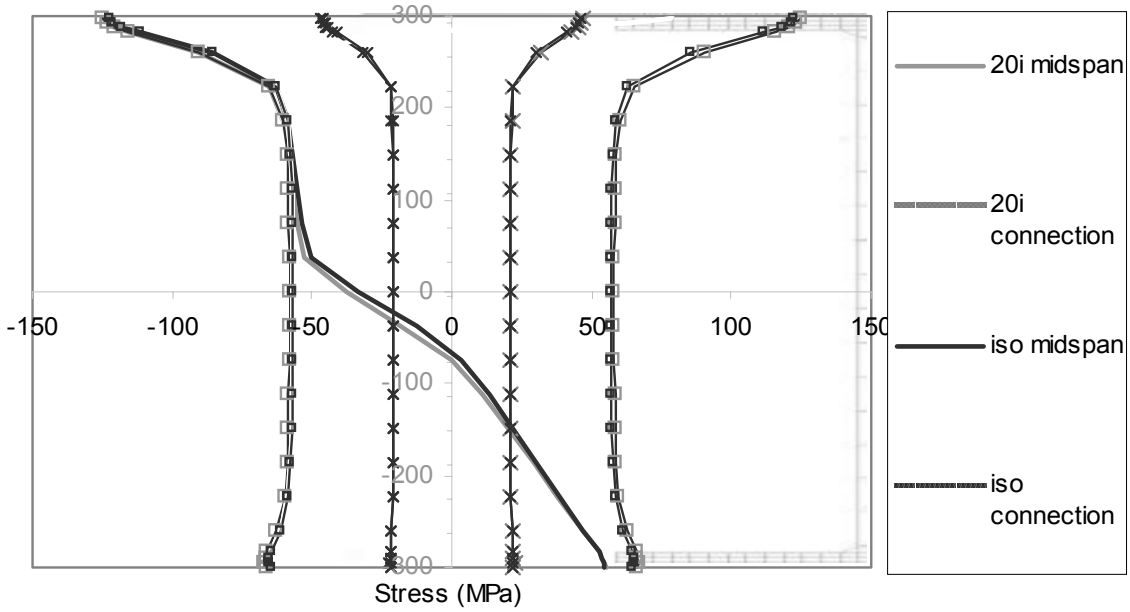

Figure 7-9 Centreline stress distribution of single span fix-fix connected steel beam at 22 minutes exposed to the ISO834 standard fire and 20 minutes of the ISO fire with a decay phase

Figure 7-10 and Figure 7-11 show the bottom and top flange stresses for the beam exposed to the ISO fire. They demonstrate that when the beam reached failure, both the bottom and the top flange stresses at the midspan reached the yield limits; and near the connection, the bottom flange stress reached the compressive yield limit, and the top flange stress reached the tensile proportional limit. However, Figure 7-8 suggested that it is very likely the whole section near the connection yielded in compression except for the top of the top flange. Three plastic hinges need to be formed to complete the failure mechanism for a fix-fix structure, therefore, the beam might fail because the entire steel section near the connections as well as the upper half of the beam at the midspan had yielded in compression, meanwhile, the lower half of the beam at the midspan had yielded in tension.

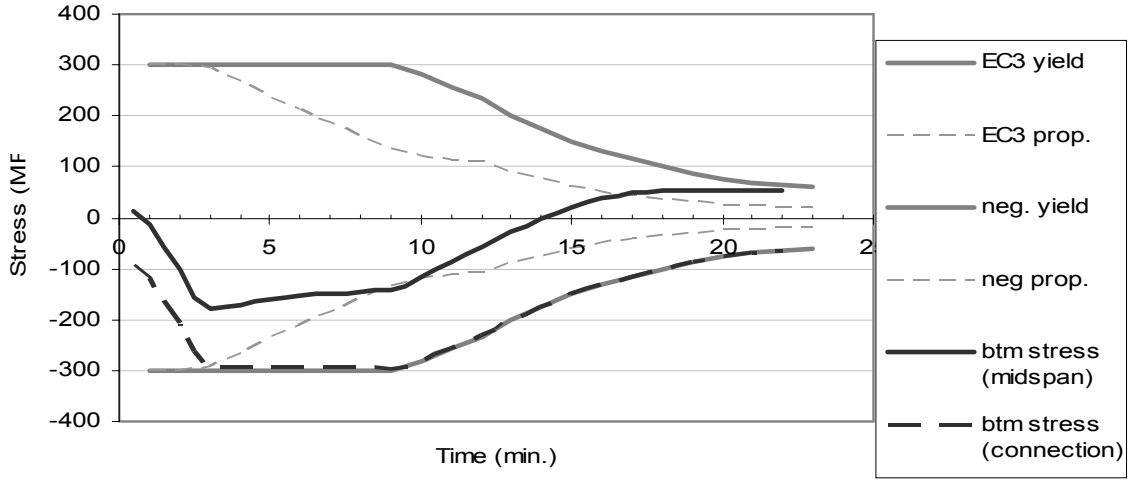

Figure 7-10 Bottom flange stress in single span fix-fix connected steel beam exposed to the ISO fire

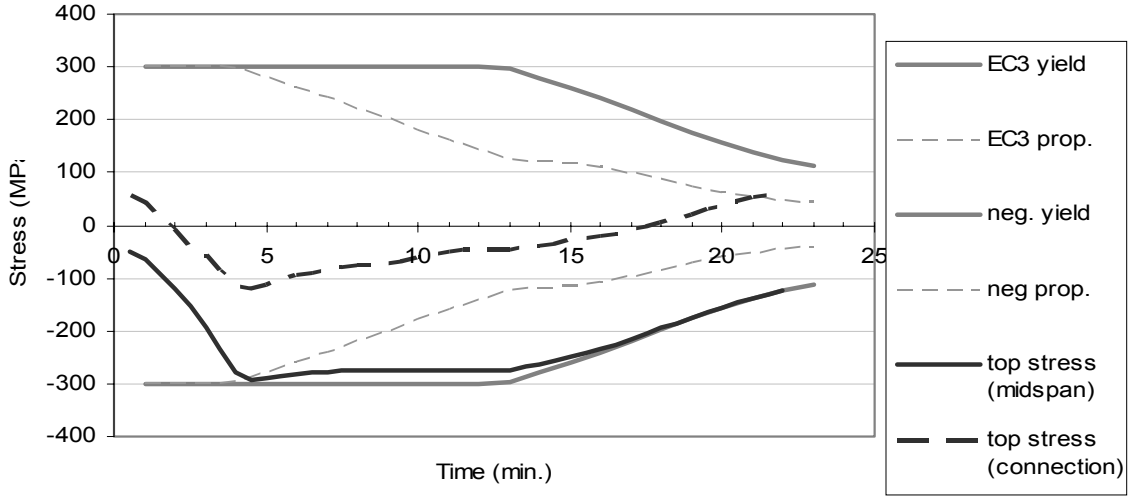

Figure 7-11 Top flange stress in single span fix-fix connected steel beam exposed to the ISO fire

7.2.2.3 Summary of the fix-fix steel beam

The beam exposed to the ISO834 standard fire reached failure after 22 minutes. Four other fires were chosen for comparison, only the fire followed 20 minutes of the ISO fire with a decay phase caused failure at 105.5 minutes. The structure did not reach failure under the other fires within the simulation time.

The axial force was similar to the force of the composite beam case, except the compressive force did not remain at the maximum for such a length of time. However, the relationship of the vertical displacement with time was different to the composite beam as Figure 7-7(b) showed that the permanent displacement was independent of the size of the fire.

Figure 7-8, Figure 7-10 and Figure 7-11 explained the behaviour of the beam when structural failure was reached under the ISO834 standard fire. They showed that the beam near the connections as well as the upper part of the beam at the midspan yielded in compression, meanwhile, the lower part at the midspan yielded in tension. Hence, three plastic hinges were formed and the failure mechanism was completed.

7.2.3 Pin-Roller Steel Beam

Figure 7-12 shows the vertical displacement at the midspan and the horizontal displacement at the roller end. When the beam was exposed to the ISO fire, it failed after 24 minutes. Four other fires, ranging from 8 minutes to 20 minutes of the ISO fire with a decay phase, were used for comparison.

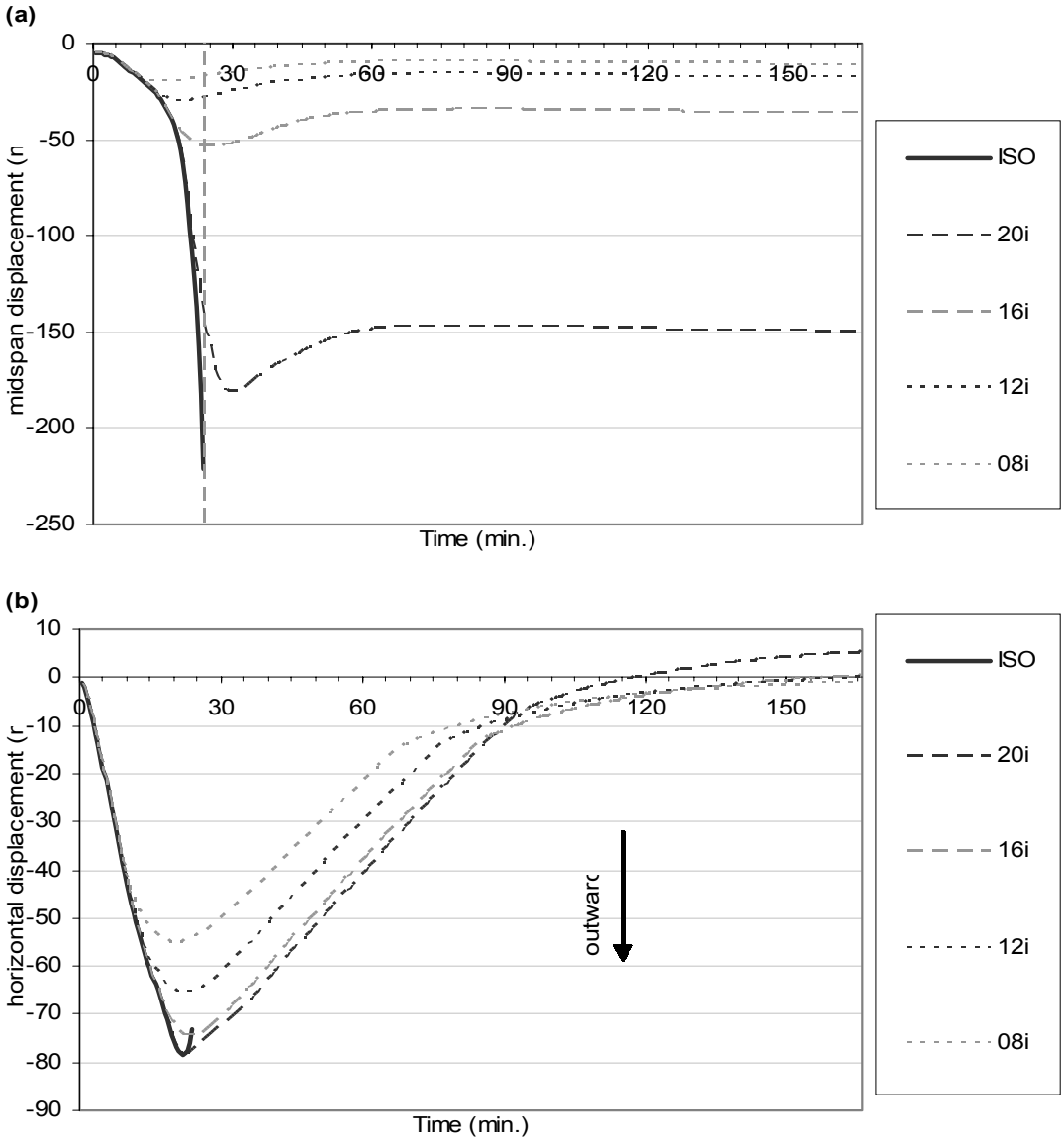

Figure 7-12 simulation results of single span pin-roller connected steel beam: (a) midspan vertical displacement (b) horizontal displacement at the roller end

7.2.3.1 Comparison with the pin-roller composite case

The difference between the steel case and the composite case can be found by comparing Figure 7-12 with Figure 5-23. The vertical displacement graphs in these cases are similar; on the other hand, the amount of displacement was substantially less than in the composite case. This was possibly because the thermal bowing behaviour without the composite action was less significant, so less curvature was at the midspan of the beam.

The horizontal displacement graph shows the movement of the roller end was dominated by the thermal expansion of the beam. Because the midspan vertical displacement was small, the roller end was not pulled inwards like in the composite beam case. Besides, there was no composite reaction between the steel beam and the concrete slab, so without the concrete slab limiting the expansion, the beam could move outward more freely and caused a larger horizontal displacement than in the composite beam case.

Figure 7-13 and Figure 7-14 show the bottom and top flange stresses of the beam exposed to the ISO fire. Comparing these graphs with the ones for the composite beam shown in Figure 5-24 and Figure 5-25, it shows that a lack of the composite action caused a difference in stress distributions. In this case, the bottom flange stress remained almost constant, and yielding of the beam was due to the yield limit being reduced by the temperature of the beam. The top flange went into tension until the bottom flange reached the proportional limit, and then it returned to compression and approximated the compressive yield limit at the time of failure. This behaviour was very different to the composite beam.

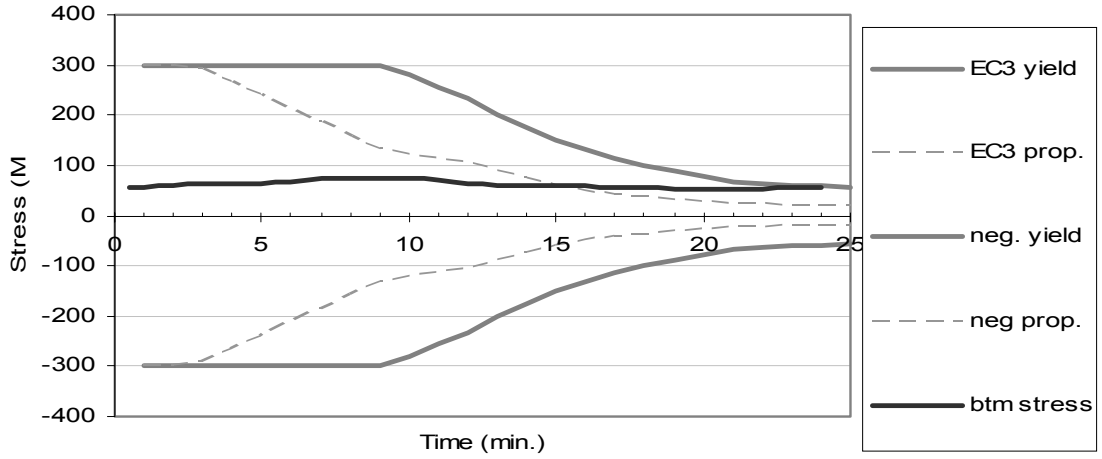

Figure 7-13 Bottom flange stress in pin-roller connected steel beam exposed to the ISO fire

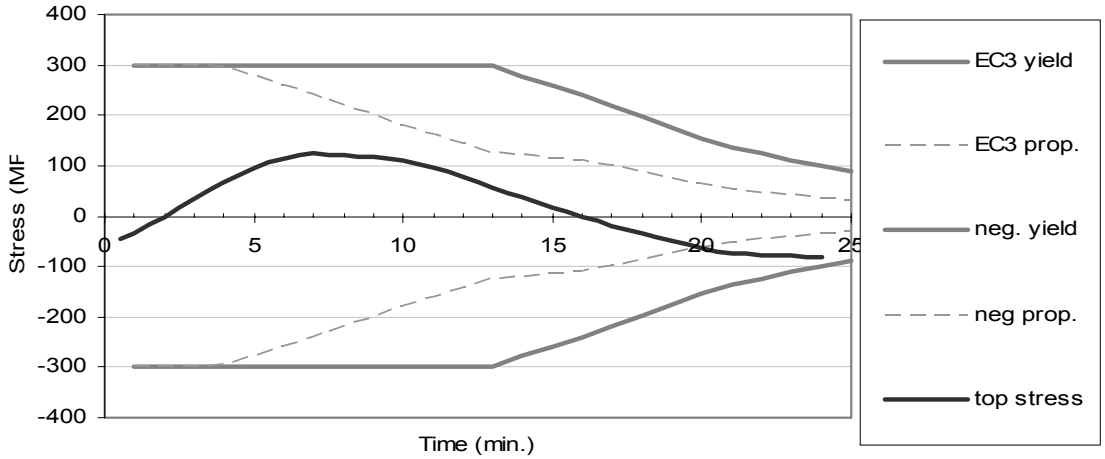

Figure 7-14 Top flange stress in pin-roller connected steel beam exposed to the ISO fire

7.2.3.2 Failure of the beam exposed to the ISO834 standard fire

The midspan vertical displacement graph showed that the displacement increased very rapidly right before the time of failure, which suggests that the failure might be caused by SAFIR not being able to handle the sudden change in deflection at the midspan. Figure 7-15 confirms the idea by showing that not the entire beam section at the midspan yielded at the time of failure.

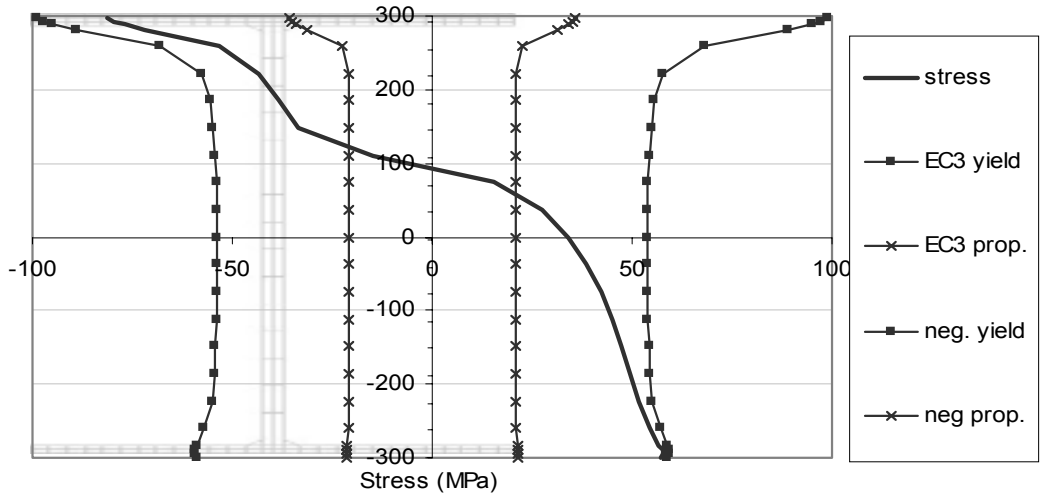

Figure 7-15 Centreline stress distribution at the midspan of the pin-roller connected beam at 24 minutes exposed to the ISO fire

7.2.3.3 Summary of the pin-roller steel beam

The existence of composite action is important in the single span pin-roller beam. When the beam does not have composite action, the vertical displacement is smaller as the steel beam has less thermal bowing than a composite beam. Because the midspan displacement is not large, the thermal expansion dominates the horizontal displacement at the roller end and increases the outwards horizontal displacement.

Because the model did not consider the concrete slab on top of the beam and assumed there was no composite action, the top flange of the steel had to take all the compressive stress induced during the heating phase. Therefore, the failure of the beam was reached when the top flange yielded in compression and the bottom flange in tension. This was different to the pin-roller supported composite beam case, where both the top and bottom flange of the steel beam section yielded in tension and the concrete slab resisted the compressive stress.

7.2.4 Fix-Slide Steel Beam

Figure 7-16 shows the vertical displacement at the midspan and the horizontal displacement at the slide end of the beam. The simply supported fix-slide steel beam exposed to the ISO834 standard fire reached failure at 29 minutes. Five other fires, ranging from 8 to 25 minutes of the ISO fire followed by a decay phase, were used for comparison. None of these fires caused failure of the beam before the end of the simulation.

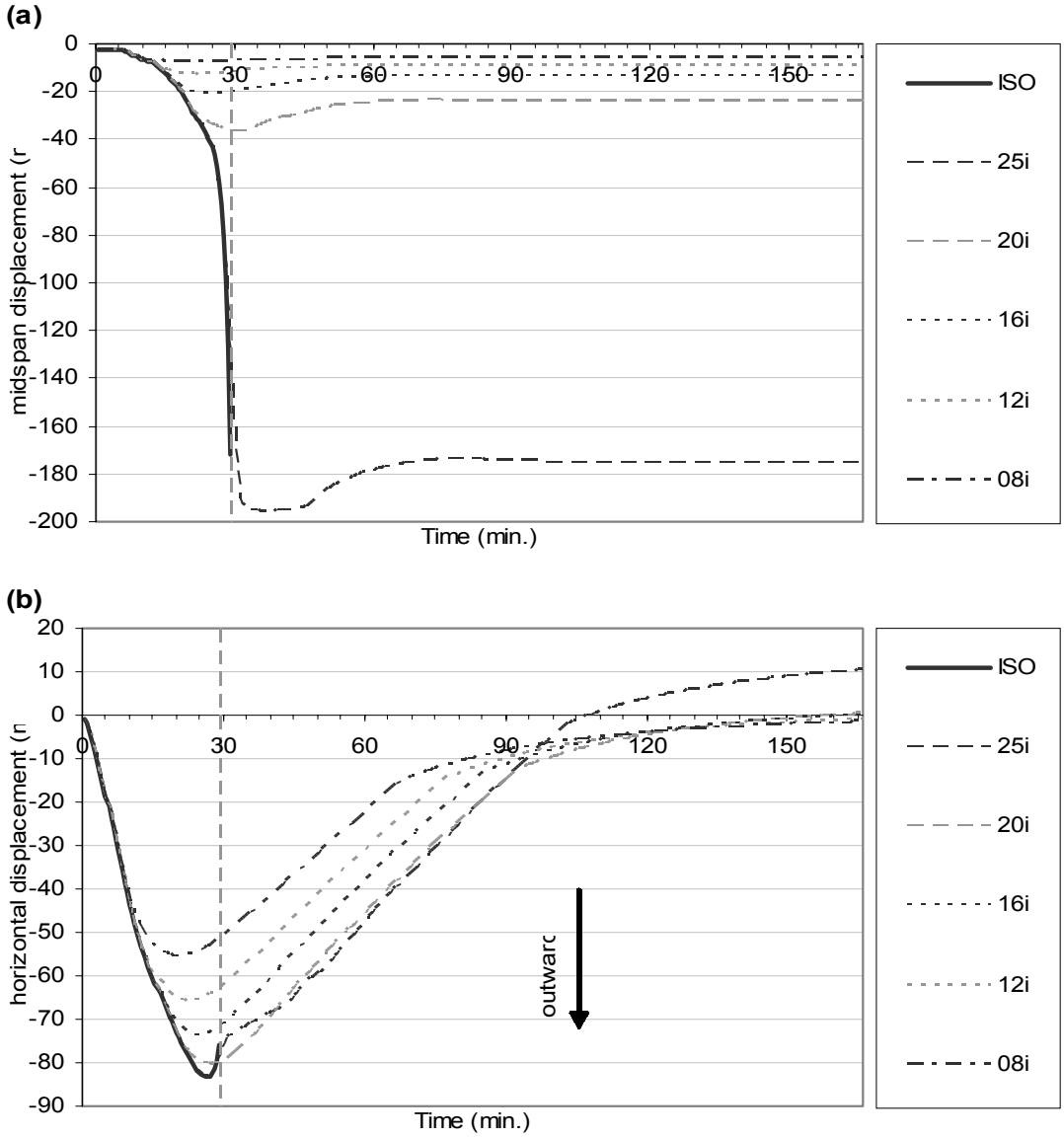

Figure 7-16 simulation results of single span fix-slide connected steel beam: (a) midspan vertical displacement (b) horizontal displacement at the slide end

7.2.4.1 Comparison with the fix-slide composite case

Figure 7-16 could be compared with Figure 5-31 to show the difference caused by the composite slab. The vertical displacement graphs of these two cases were similar especially the curves of the beam exposed to the ISO834 standard fire and to the fires which followed less than 20 minutes of the ISO fire. The magnitude of the vertical displacement was similar as well. When the beam exposed to the ISO fire reached failure, in both the composite and steel cases the vertical displacement approximated 170mm.

The horizontal displacement graph shown in Figure 7-16(b) showed that other than the case exposed to the 25 minutes of the ISO fire, the roller end returned to the original location at the end of the simulation. Comparing Figure 7-16(b) with Figure 5-31(b), it showed that the fix-slide connected beams with or without composite action were similar, but it also indicated that the displacement in the steel beam was approximately 10mm larger than in the composite beam.

7.2.4.2 Failure of the beam exposed to the ISO834 standard fire

Figure 7-16(a) suggests that the failure of the beam exposed to the ISO fire was not caused by the excessive vertical displacement. Figure 7-17 and Figure 7-18 show the bottom and top flange stresses at the midspan as well as near the connection in the beam exposed to the ISO834 standard fire. When the beam reached failure at 29 minutes, both the top and bottom flange at the midspan as well as near the connection had reached the yield limit, therefore three plastic hinges were formed and the failure mechanism of the fix-slide supported structure was completed.

The midspan vertical displacement graph showed the beam exposed to 25 minutes of the ISO fire followed the behaviour of the beam exposed to the ISO fire closely without reaching failure before the end of the simulation. Figure 7-19 and Figure 7-20 show the bottom and top flange stresses of the beam exposed to 25 minutes of the ISO fire. These two graphs indicate that although the bottom and top flange yielded during the simulation, the yielding at the midspan happened later than near the connection. When the midspan of the beam was yielding, the stress at the connection reduced

below the yield limit. Therefore, the beam could not fail in the case with 25 minutes of the ISO fire because the failure mechanism was not completed.

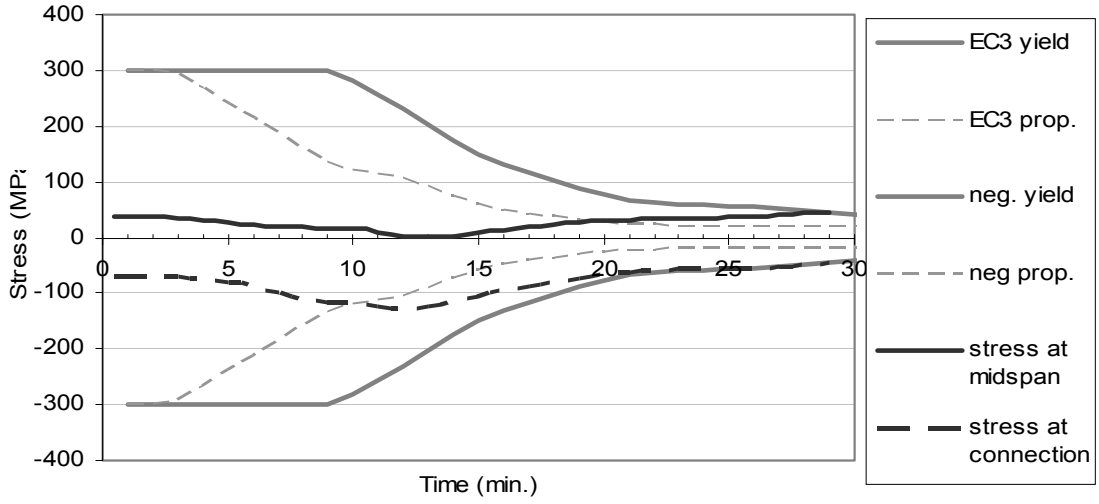

Figure 7-17 Bottom flange stress of the fix-slide steel beam exposed to the ISO834 standard fire

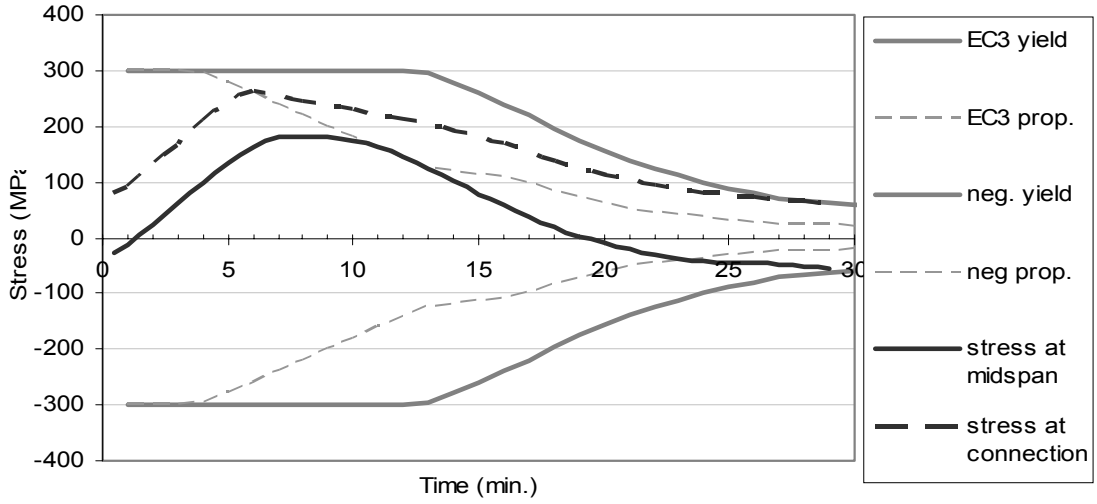

Figure 7-18 Top flange stress of fix-slide steel beam exposed to the ISO834 standard fire

Because Figure 7-19 and Figure 7-20 indicate that the beam exposed to 25 minutes of the ISO fire yielded near the connection earlier than at the midspan, the behaviour of the beam during the time the plastic hinges were formed at the connection should be close to the catenary behaviour of a pin-roller connected beam. The plastic hinges also explain the large vertical displacement at the midspan that happened at around 30 minutes.

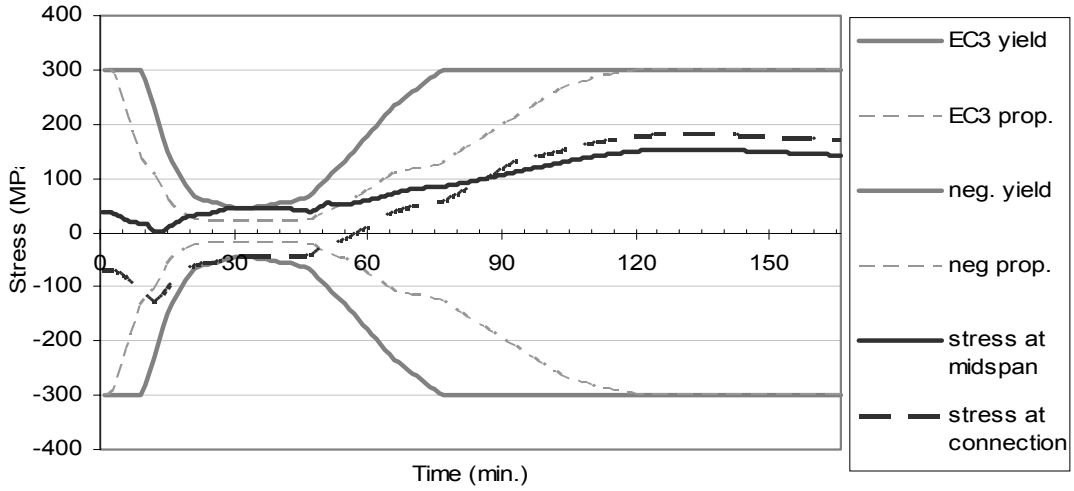

Figure 7-19 Bottom flange stress of fix-slide steel beam exposed to 25 minutes of the ISO fire with a decay phase

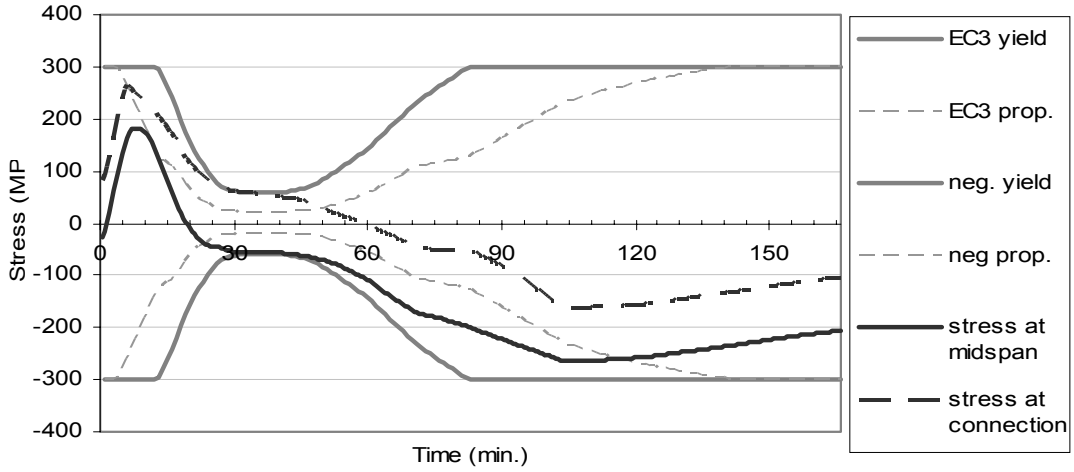

Figure 7-20 Top flange stress of fix-slide steel beam exposed to 25 minutes of the ISO fire with a decay phase

7.2.4.3 Summary of fix-slide connected steel beam

The fix-slide connected steel beam exhibited a similar behaviour to the composite beam. Both the vertical displacement at the midspan and the horizontal displacement at the slide end in these two cases were very similar.

The beam exposed to the ISO834 standard fire reached failure at 29 minutes because three plastic hinges were formed to complete the failure mechanism of this type of structure: one at the midspan, and two at the connections. The beam exposed to 25 minutes of the ISO fire formed plastic hinges at the connections so the beam had catenary behaviour like in a pin-roller supported structure. This is proved by observing the large displacement induced at the midspan.

7.3 Summary of the simulation results of steel beams

Table 7-1 shows the summary of the results for single span steel beams. The simulation results show that the entire beam is likely to yield under tension when the axial restraints at the ends are provided.

This table can be compared with the one for composite beams shown in Table 5-5. From the results it seems that the steel beams last longer than the composite beams under the ISO fire; this can be due to the cracking of the concrete slab under the catenary behaviour causing some difficulties in the calculation.

Table 7-1 Analysis results of the single span steel beams exposed to various durations of the ISO fire

Connection type		**Pin-pin**	**Fix-fix**	**Pin-Roller**	**Fix-Slide**
Time to fail in the ISO fire without a decay phase	Min.	40	22	24	29
Steel temperature at failure (at the bottom flange)	^{o}C	872	724	735	776
Maximum compressive axial force	kN	2410	3000	--	--
Maximum tensile axial force	kN	3860	3900	--	--

This section discussed the difference that may be caused by the lack of composite action in the beam. One of the features was that the vertical displacement in all cases became larger because the composite beams had a larger stiffness. Besides, without the concrete slab bearing the compressive force while heating, the top portion of the steel beam could yield under compression.

8 Simulation results of steel frames exposed to the ISO fire with a decay phase

Two types of beam-column connections were used in the steel frame model: pin-pin and fix-fix. The temperatures of the beams used in the structural analysis were the same as in the single span beams; the columns of the frame were assumed to be fully insulated and at 20^{o}C, the ambient temperature, throughout the simulation.

8.1 Structural analysis results of steel frames

This section discusses the steel frame structural analysis results. In the initial setting, the beam had the same strength and stiffness as the columns.

8.1.1 Frames with pin-pin connected steel beam

The frame exposed to the ISO834 standard fire reached failure after 37.5 minutes. Six other fires, ranging from 8 to 30 minutes of the ISO fire followed by a decay phase, were used for comparison. Figure 8-1 shows the axial force, the vertical displacement at the midspan and the horizontal displacement at one connection.

8.1.1.1 Comparison with the single span cases

The pin-pin connected beam in a frame had a mixed behaviour from the single span pin-pin and pin-roller cases, which are shown in Figure 7-3 and Figure 7-12. The failure time of the beam under the ISO fire was between the two single span cases. The vertical displacement had a similar trend and magnitude to the single span pin-roller case, especially after 90 minutes when the column yielded under larger fires. The horizontal displacement and the axial force were smaller before the column yielded, which indicates that the columns in the frame provide some amount of horizontal restraint to the beam. This situation was discussed before in the composite case.

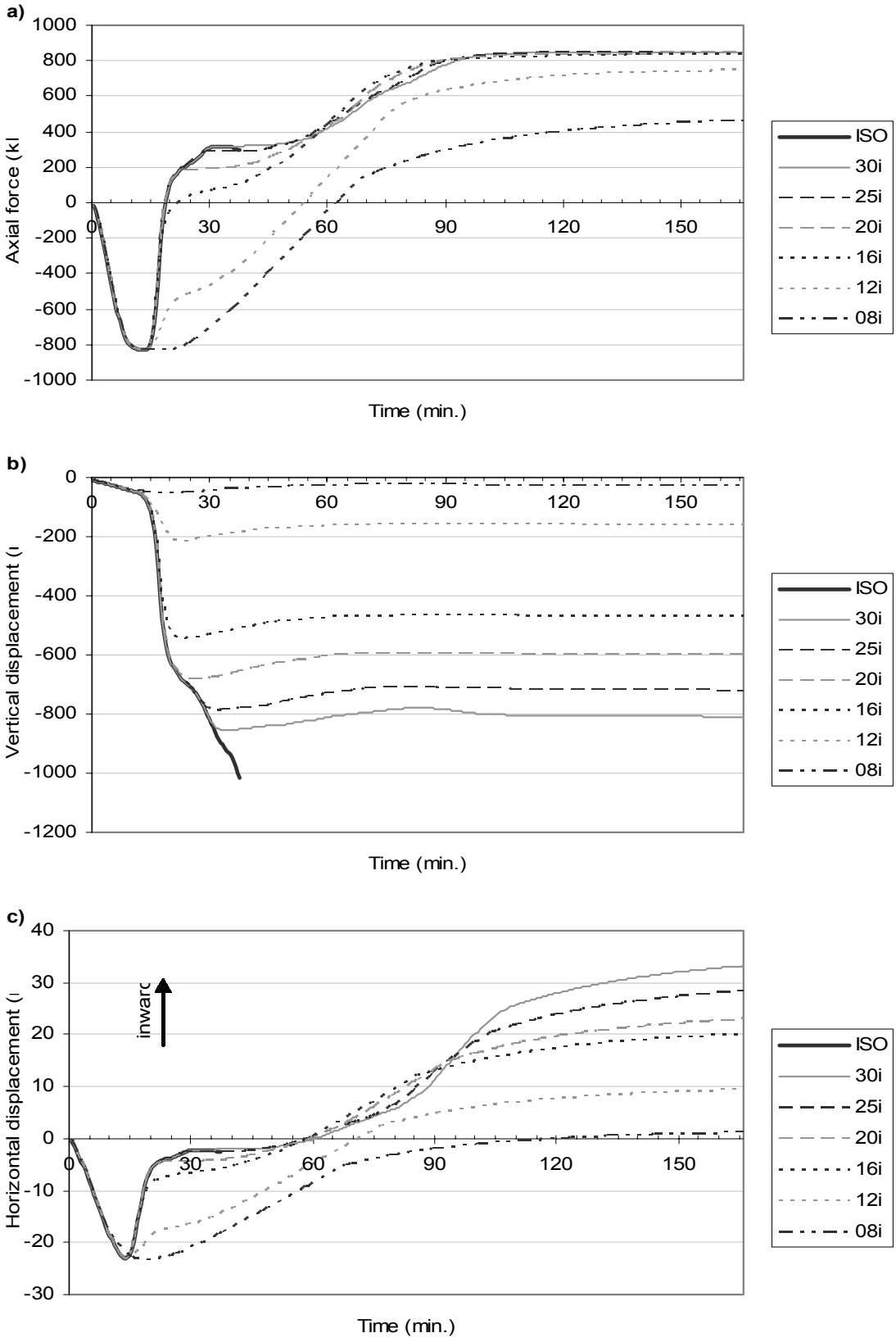

Figure 8-1 Simulation results of frames with pin-pin connected steel beam: a) axial force; b) vertical displacement; c) horizontal displacement

8.1.1.2 Comparison with the pin-pin composite frame

Comparing Figure 8-1 with Figure 6-1 shows that the axial forces in these two cases were similar. However, without the presence of the composite action, the midspan displacement was approximately 100mm larger and the horizontal displacement was larger in both directions.

Figure 8-1(a) shows that the axial force had an envelope which was approximately 850kN. The shape of the plots was similar to the pin-pin connected composite frame with different column stiffness shown in Figure 6-13. One can conclude that the column yielded after the axial force reached its maximum value. This was similar to the composite frames with 100% column stiffness shown in Figure 6-1(a); except in a steel frame, the axial force reached the envelope under a smaller fire.

Figure 8-1(b) shows that before the rapid increase in the midspan vertical displacement occurred, the rate of increase of the displacement was mild compared to the composite frame shown in Figure 6-1(b). Under the larger fires, the midspan of the beam remained at the maximum displacement after the columns had yielded.

Figure 8-1(c) shows that the increase in inward horizontal displacement at the connection was much larger than in the composite frame. This figure indicated that the columns yielded during the simulation as the horizontal displacement was still increasing while both the axial force and midspan vertical displacement were constant. Figure 8-2, the diagram of the stresses in the outer and inner flange of the columns near the beam-column connection, proves the column yielded at around 90 minutes and the connections moved towards each other. This situation was also observed in the cases of composite frames with weak columns.

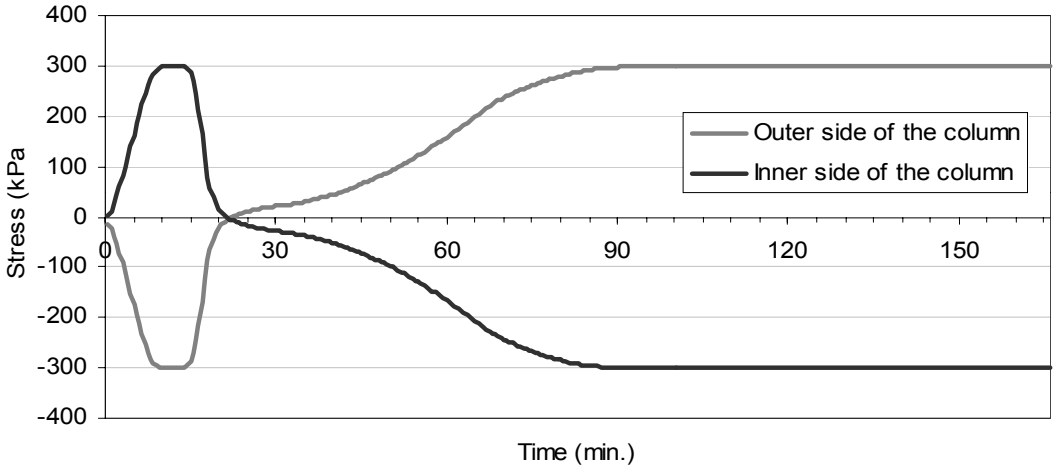

Figure 8-2 Column stresses at the beam-column connection

8.1.2 Frames with fix-fix connected steel beam

The frame exposed to the ISO834 standard fire reached failure after 20.5 minutes. Five parametric fires, following 8 to 18 minutes of the ISO fire with a decay phase, were used for simulation. Figure 8-3 shows the axial force and the displacements from the simulations.

Although the axial force did not reach the magnitude of the force envelope found in the previous section, the column stress shown in Figure 8-4 indicates that in the case with 18 minutes of the ISO fire, the columns yielded at the beam-column connection after 5 minutes due to the high compressive beam axial force. The columns yielded again in the opposite direction at 65 minutes caused by the high tensile beam axial force while cooling.

The figure of horizontal displacement at the beam-column connection agrees with the figure of axial forces during the heating phase and early stage of the cooling phase. However, because the column yielded when the beam was exposed to a larger fire, the horizontal displacement in these cases became larger and was not proportional to the axial force before the end of the simulation.

8.1.2.1 Comparison with the single span cases

The structural behaviour of the steel frame with a fix-fix connected beam lay between those of the single span fix-fix beam and fix-slide beam. The axial force shown in Figure 8-3 grew differently to the force in Figure 7-7. In the steel frame, the rate of change of the axial force from compression to tension while cooling was not affected by the size of the fire, but in the single span fix-fix beam case this change was more rapid if the fire was large. The tensile axial force in the single span beam case reached its maximum when the temperature in the steel beam became stable. Unlike the single span beam case, the maximum tensile force in the frame case depended on the fire size.

The trend and the magnitude of the midspan displacement shown in Figure 8-3 are similar to the single span fix-fix case during the heating phase. However, the beam behaved like in a single span fix-slide beam while cooling and reached the permanent displacement before the steel temperature became stable.

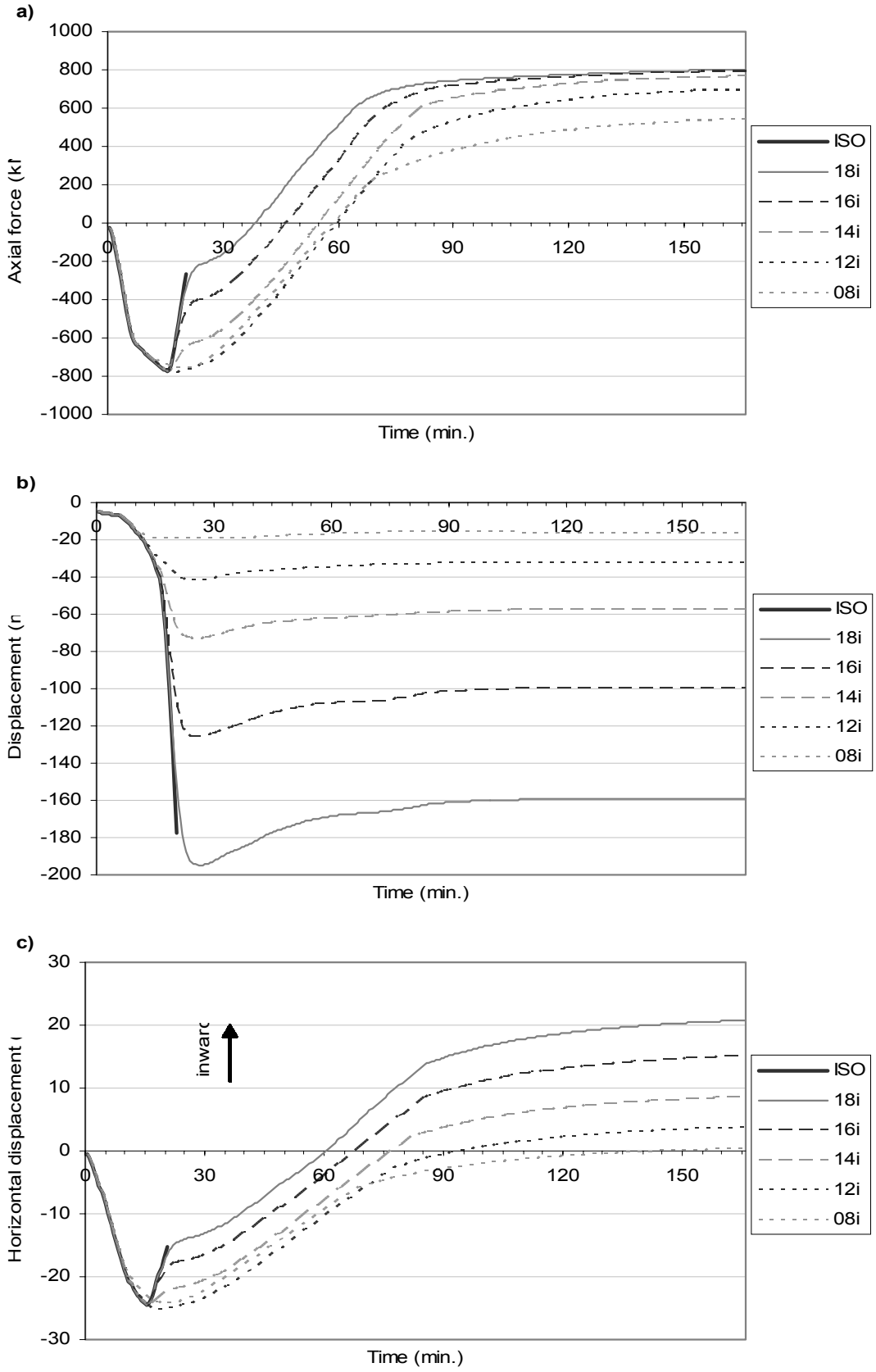

Figure 8-3 Simulation results of frames with fix-fix connected steel beam: a) axial force; b) vertical displacement; c) horizontal displacement

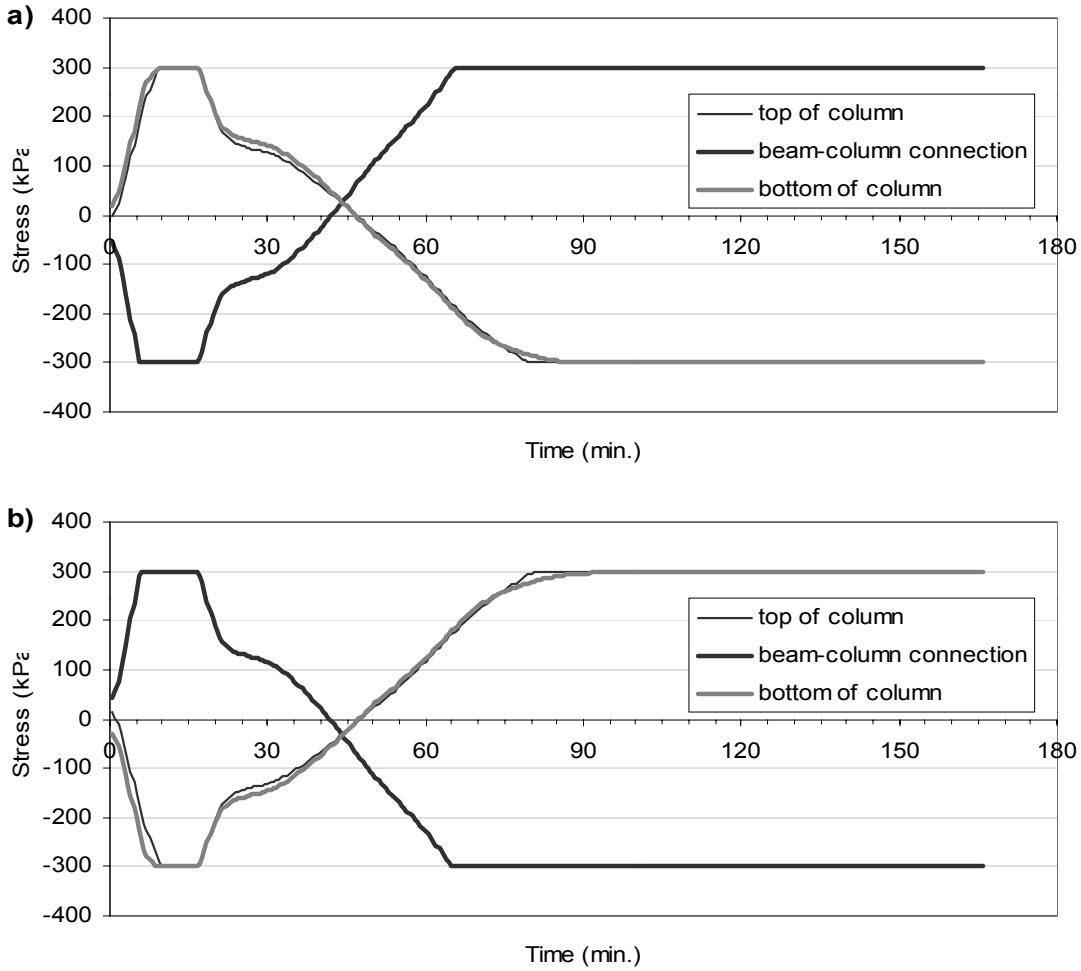

Figure 8-4 Column stress in the fix-fix steel frame exposed to 18 minutes of the ISO fire: a) at outer-side; b) at inner-side

8.1.2.2 Comparison with the fix-fix composite frame

By comparing Figure 8-3 with the fix-fix composite frame case shown in Figure 6-6, it can be seen that the axial force was more dependent on the fire size for a steel frame. Besides, the increase of midspan displacement was milder during the early stage of the heating phase; and the recovery of midspan vertical displacement while cooling was less. The axial force, the vertical displacement at midspan and the horizontal displacement at the connections were all larger in the steel frame than in the composite frame. Similar observations were made in Section 8.1.1.2, and all of these differences were caused by the lack of composite action, which the concrete slab could bear the compressive stress during the heating phase and subsequently protect the upper part of the steel beam.

8.2 Variation in column strengths and stiffness

In this section, the column strength and stiffness in the steel frame are changed. The test method was similar to which was in Section 6.3, 'Variation in column strength and stiffness in a composite frame': only the column stiffness was changed to 50%, 500% and 1000% of its original value initially, then both the column stiffness and strength were varied.

8.2.1 Changed strengths and stiffness in pin-pin steel frame

The first scenario discussed here is a pin-pin connected steel beam in a frame with only the column stiffness was changed. This case simulated a bolted connection where the strength of the bolts limits the axial force that can be transferred between beam and column. Figure 8-5 shows the axial force of the pin-pin connected steel frame with different column stiffness. A larger fire caused a higher tensile axial force at the end of the simulation. The axial force envelope of 850kN was observed in all three graphs of the high column stiffness cases, which indicates that when the column stiffness was high, such as 1000% of its original value, the columns developed plastic hinges that limited the beam axial force in compression during the heating phase and in tension while cooling.

Figure 8-6 shows the midspan vertical displacement of the beam in the steel frame. A larger fire caused a larger displacement, and a stiffer column reduced the midspan vertical displacement. These are the same findings as of the composite frame discussed in Section 6.3.1.1. Initially the vertical displacement was independent of the column stiffness until the sudden increase in the displacement occurred. After the column yielded, which is when the axial force reached its maximum value, the vertical displacement became constant as observed in the previous sections. This was also observed before and described in the previous chapters.

The yielding of the column is best observed from the graph of the horizontal displacement at the beam-column connections which is shown in Figure 8-7. When the fire was small, the horizontal displacements of different column stiffness were similar, however, the horizontal displacement of the 500% and 1000% column

stiffness case under all three fires were still increasing after the axial force became steady. This indicates that the column had yielded during the simulation.

The results for 500% of column stiffness followed those for 1000% in Figure 8-5, Figure 8-6 and Figure 8-7. Hence only three curves can be seen on the graphs.

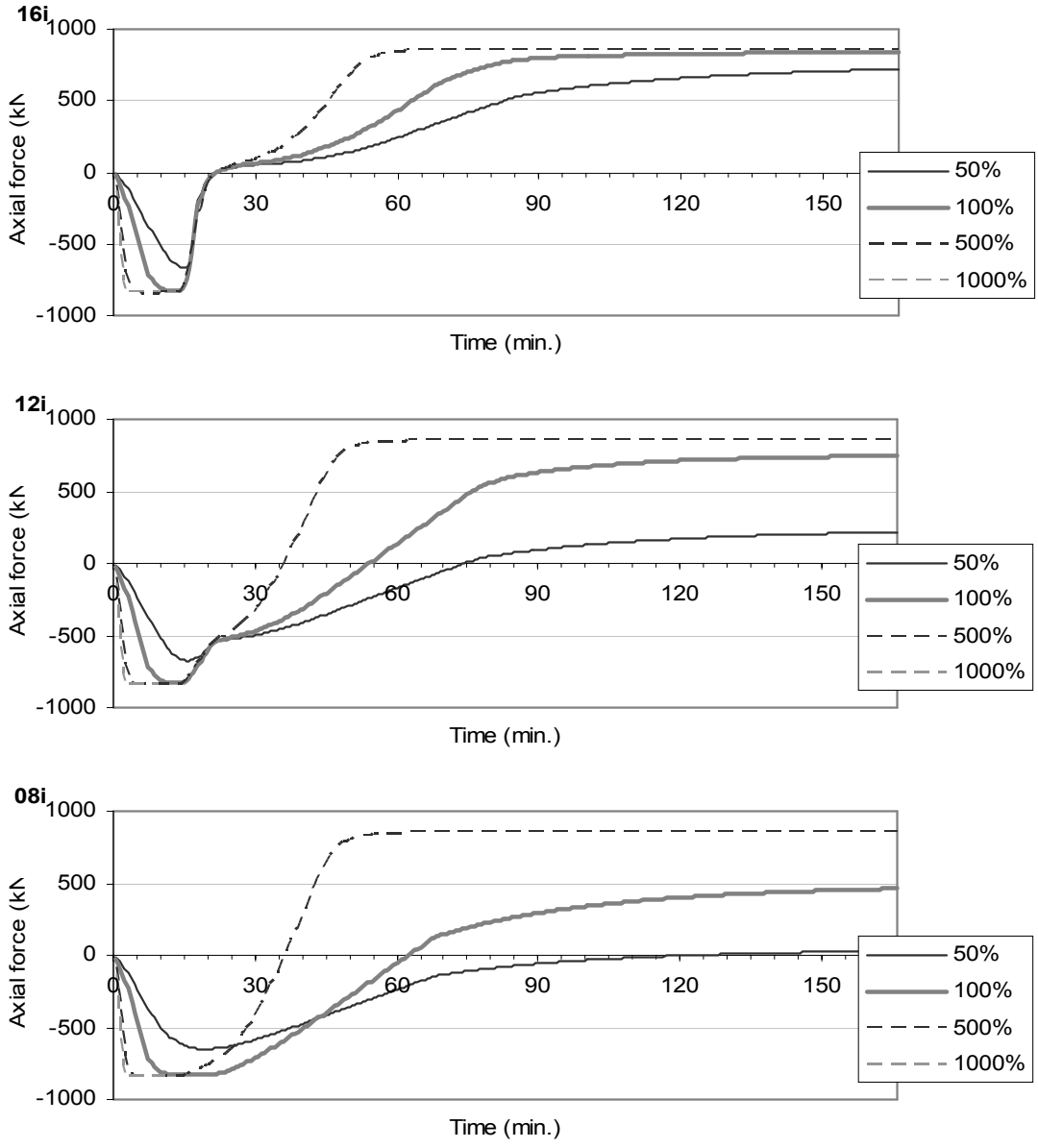

Figure 8-5 Axial force in a pin-pin connected steel beam in a frame with different column stiffness exposed to 16, 12 and 8 minutes of the ISO fire before the decay phase

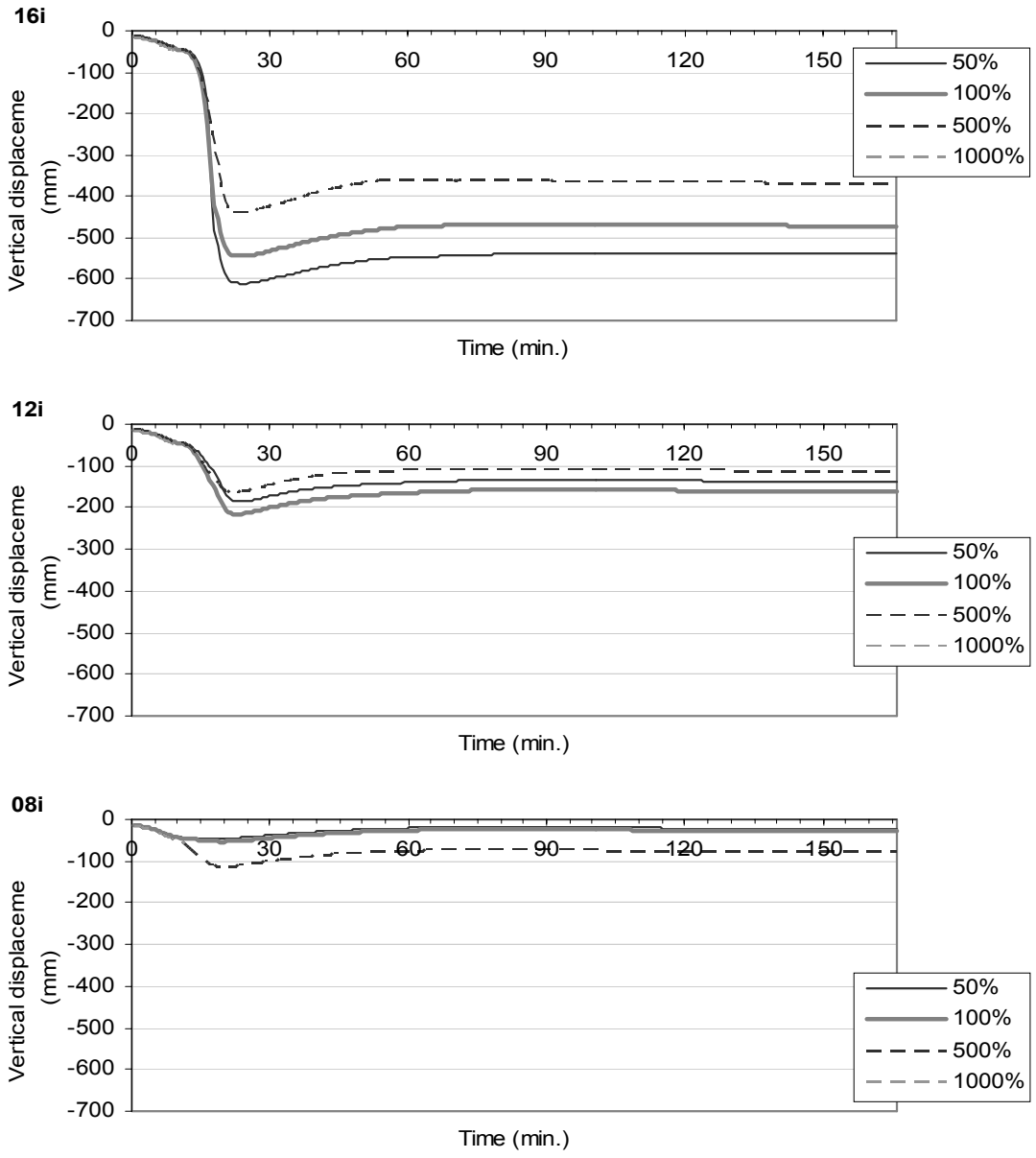

Figure 8-6 Vertical displacement in a pin-pin connected steel beam in a frame with different column stiffness exposed to 16, 12 and 8 minutes of the ISO fire before the decay phase

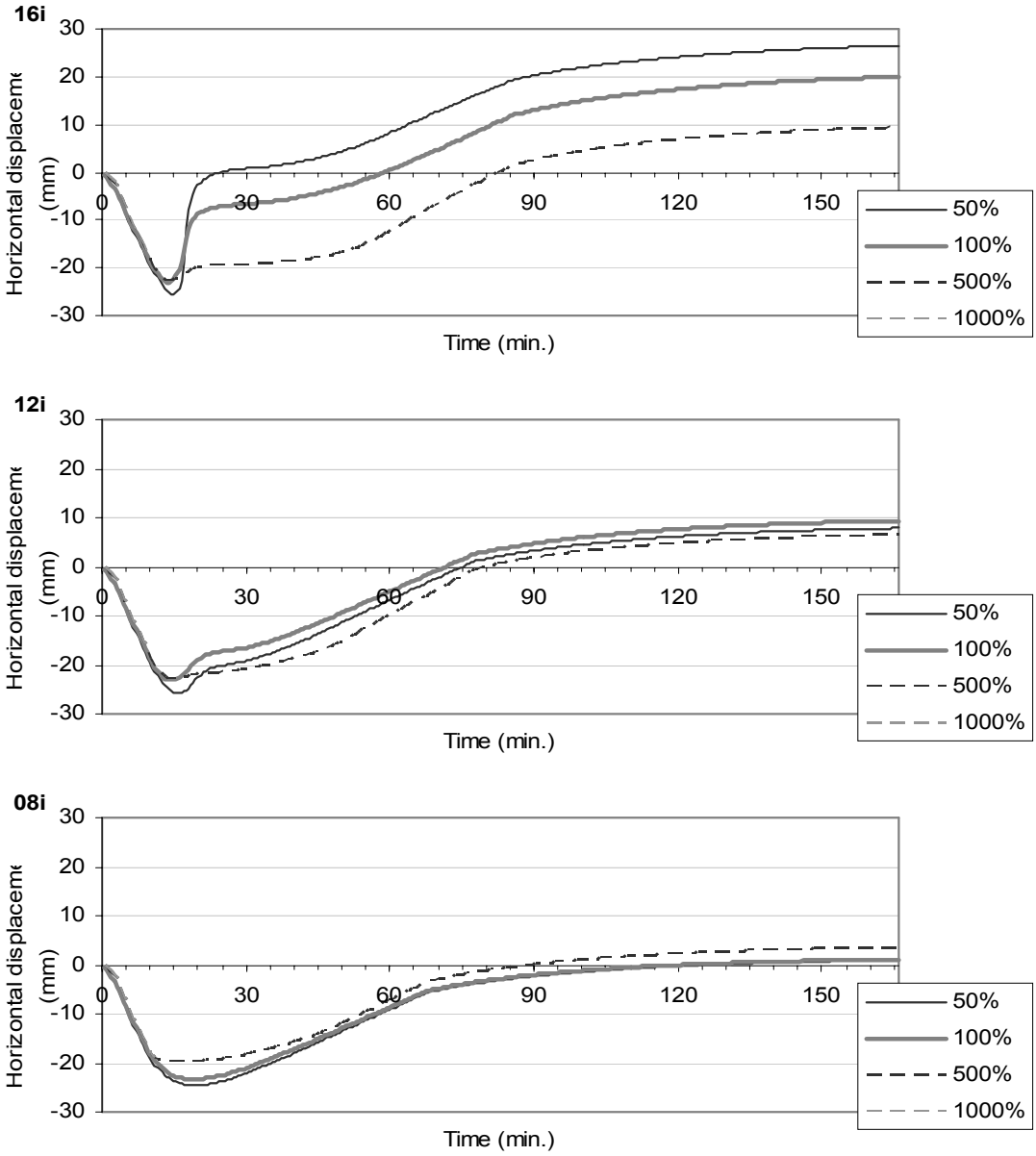

Figure 8-7 Horizontal displacement in a pin-pin connected steel beam in a frame with different column stiffness exposed to 16, 12 and 8 minutes of the ISO fire before the decay phase

In order to prevent the columns yielding, especially when the column stiffness was high, the column strength was changed as well in another set of analyses. Figure 8-8 shows the beam axial force in the steel frame exposed to different durations of the ISO fire. The results can be classified in two parts: the frames with stronger columns, and the frames with weaker columns. In the frames with stronger columns, the tensile axial force at the end of the simulation was very high with a magnitude similar to which of the single span pin-pin steel beam case. Figure 8-8 also showed that a smaller fire caused a higher tensile axial force while cooling. The axial force for the 500% and 1000% column strengths and stiffness were almost the same through out the simulation. In the frames with weaker columns, a larger fire caused a larger axial force, but the difference in the axial force between the 50% and 100% column strength was small.

Figure 8-9 shows the midspan displacements of the frames. A larger fire caused a larger displacement, and this observation is valid despite the difference in the column strengths. The vertical displacement became steady after the early stages of the decay phase. This was possibly because the thermal gradient in a steel beam was smaller than for the composite beam, therefore, less thermal bowing occurred during the heating stage as well as the cooling phase in the steel frame.

Figure 8-10 shows the horizontal displacement at the beam-column connection. The horizontal displacement can also be discussed in two parts. In the stronger column cases, because the beam axial force was larger under a smaller fire, the horizontal displacement also became larger. Also, because the compressive axial force during the heating phase was not as large as the tensile force at the end of the simulation, the outward displacement was less than inward. In the weaker column cases, a larger fire caused a larger axial force, which consequently caused a larger horizontal displacement both inwards and outwards.

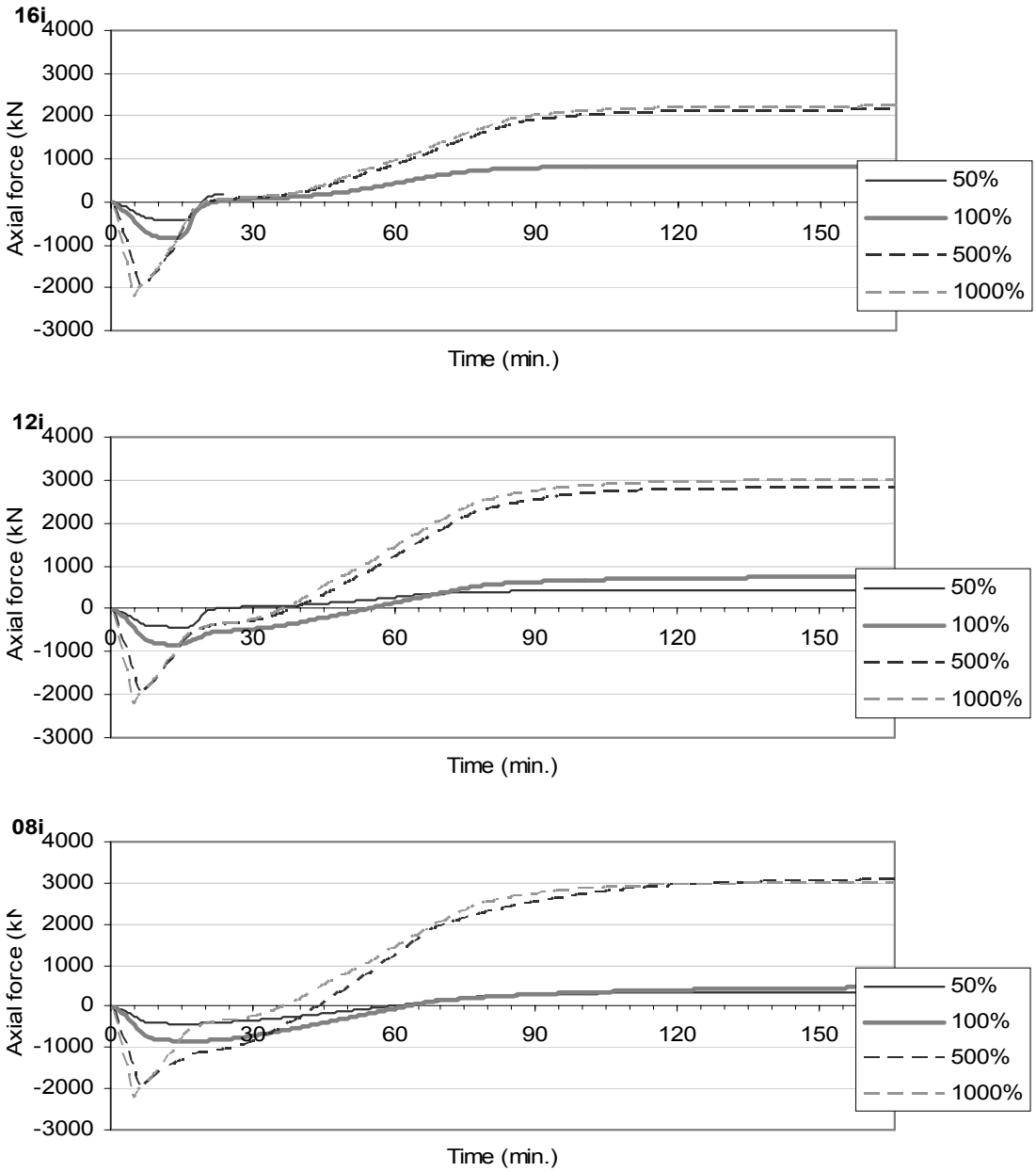

Figure 8-8 Axial force in a pin-pin connected steel beam in a frame with different column strengths and stiffness exposed to 16, 12 and 8 minutes of the ISO fire before the decay phase

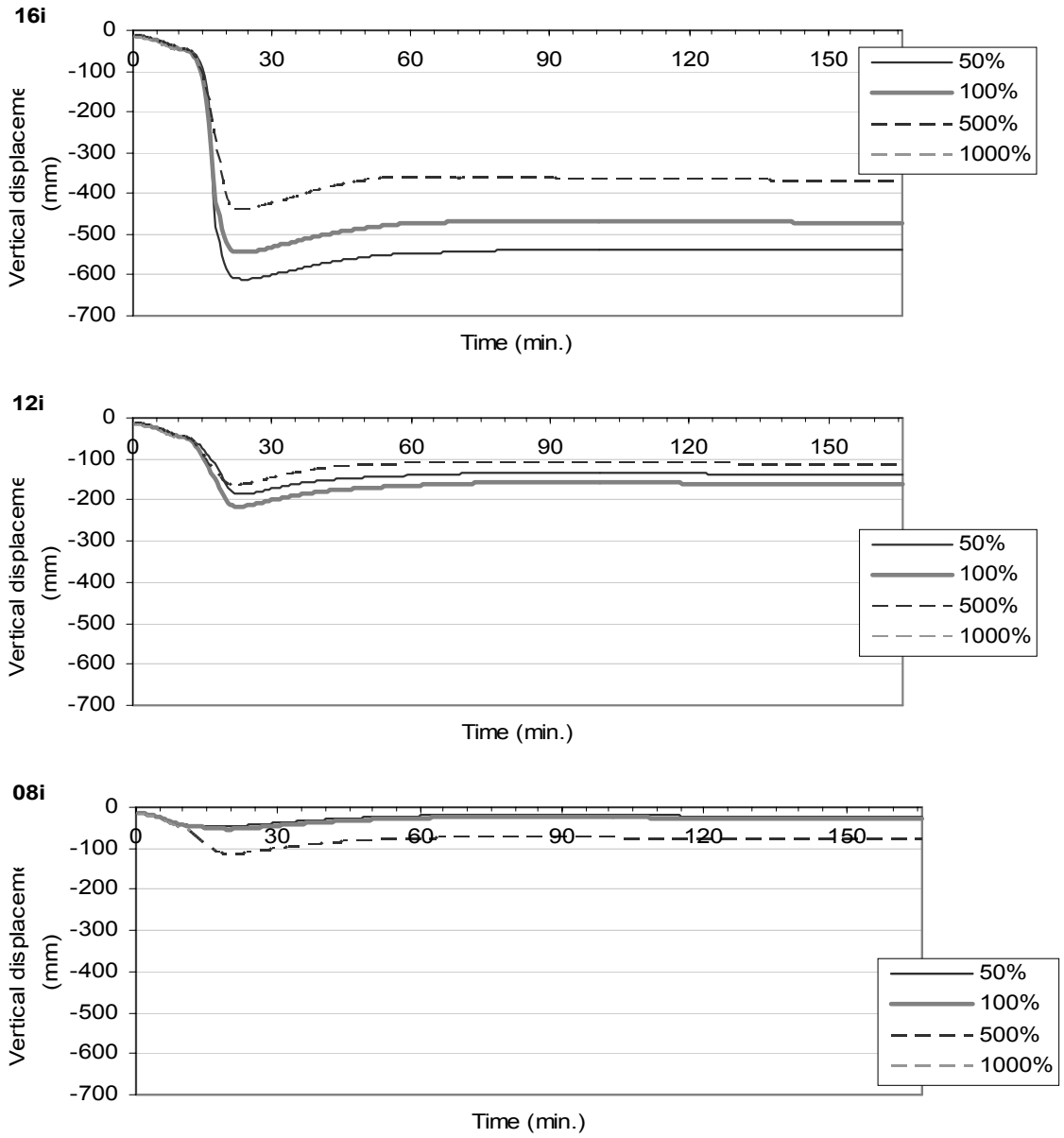

Figure 8-9 Midspan vertical displacement in a pin-pin connected steel beam in a frame with different column strengths and stiffness exposed to 16, 12 and 8 minutes of the ISO fire before the decay phase

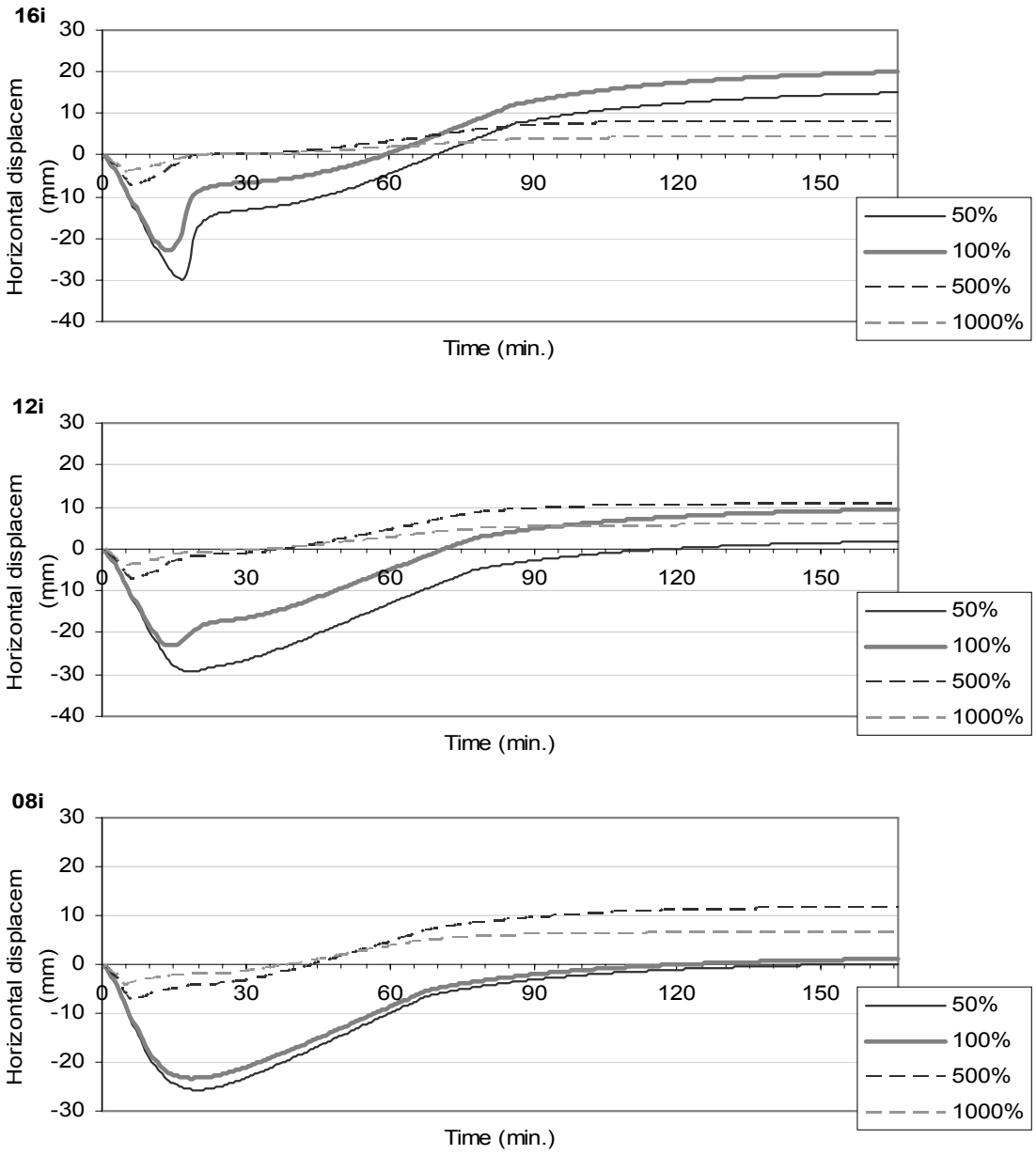

Figure 8-10 Horizontal displacement at the beam-column connection in a frame with pin-pin connected steel beam and different column strengths and stiffness exposed to 16, 12 and 8 minutes of the ISO fire before the decay phase

8.2.2 Changed strengths and stiffness in fix-fix steel frame

This section also starts with a review of the simulation results of a frame with changed column stiffness only. Figure 8-11 shows the beam axial force of the fix-fix connected steel frame with different column stiffness. The figure shows the compressive axial force did not reach the force envelope, i.e. the threshold for the column to yield, as in the pin-pin steel frame case shown in Figure 8-8, but the tensile force reached the force envelope in both the 500% and 1000% column stiffness cases. The graphs also indicate that before the columns yielded, a larger fire caused a larger axial force. This is different to the pin-pin steel frame case.

Figure 8-12 shows the midspan vertical displacement of the fix-fix connected beam in frames with different column stiffness. After the column yielded the midspan vertical displacement stopped changing.

Figure 8-13 shows the horizontal displacement at the beam-column connection. Because a larger fire triggered a larger axial force, the horizontal displacement would also increase with the fire size. The figure further shows that under a larger fire, the horizontal displacement was more influenced by the column stiffness; this was because the axial force became larger when the column was stiffer. In summary, the results from the fix-fix steel frames with changed column stiffness were as expected and most of the behaviour has been discussed in the previous sections.

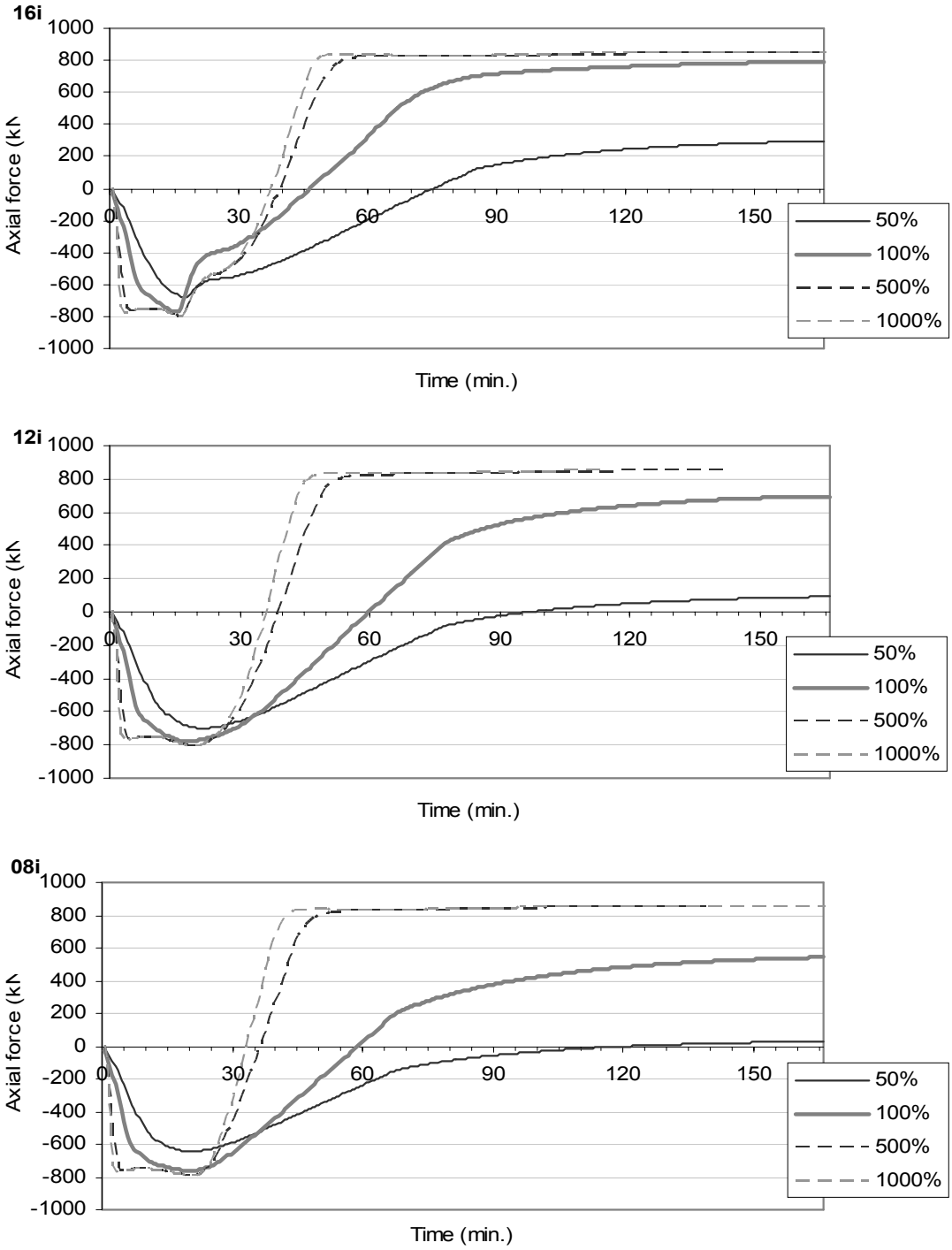

Figure 8-11 Axial force in fix-fix connected steel beam in a frame with different column stiffness exposed to 16, 12 and 8 minutes of the ISO fire before the decay phase

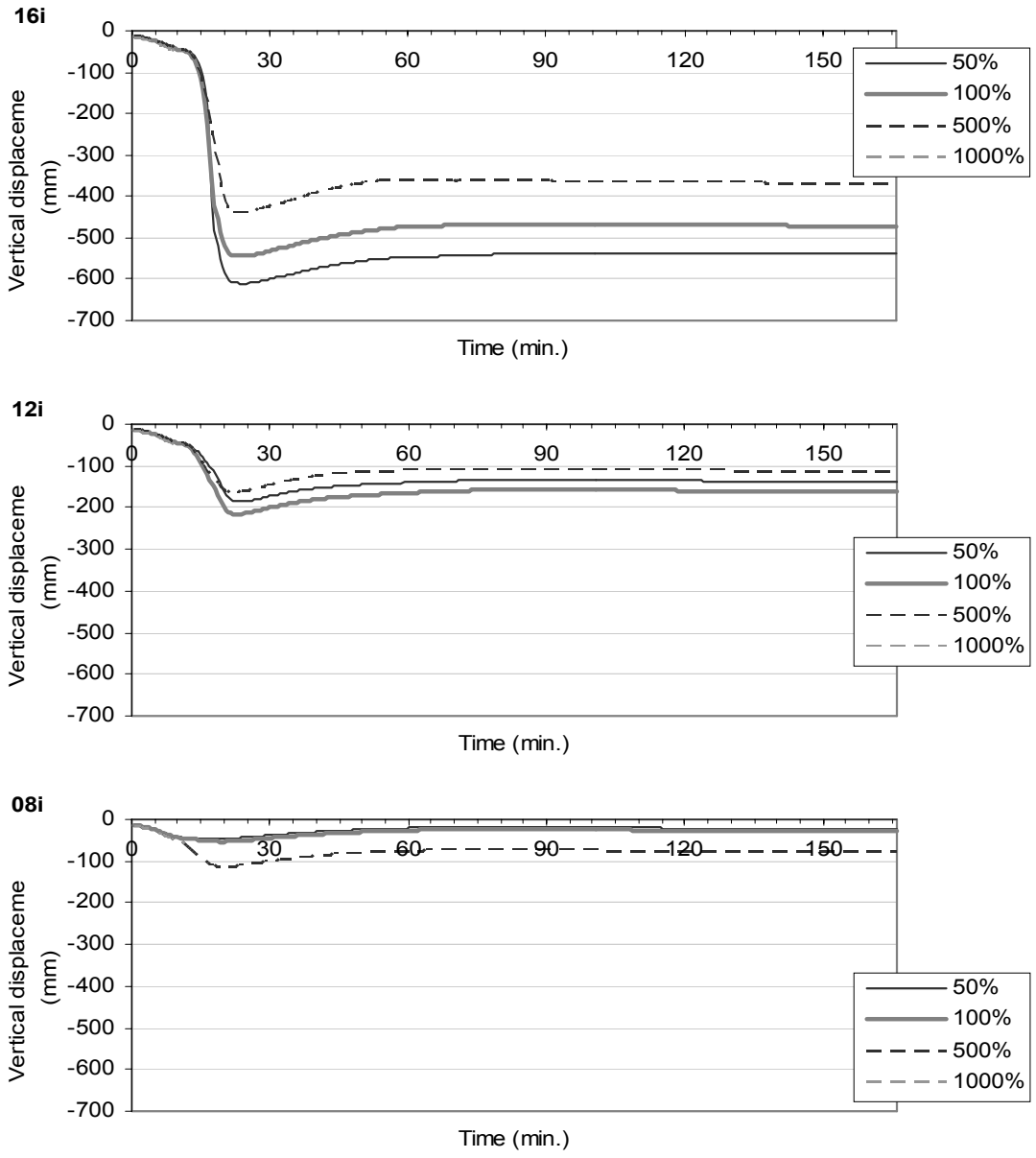

Figure 8-12 Midspan vertical displacement in fix-fix connected steel beam with different column stiffness exposed to 16, 12 and 8 minutes of the ISO fire before the decay phase

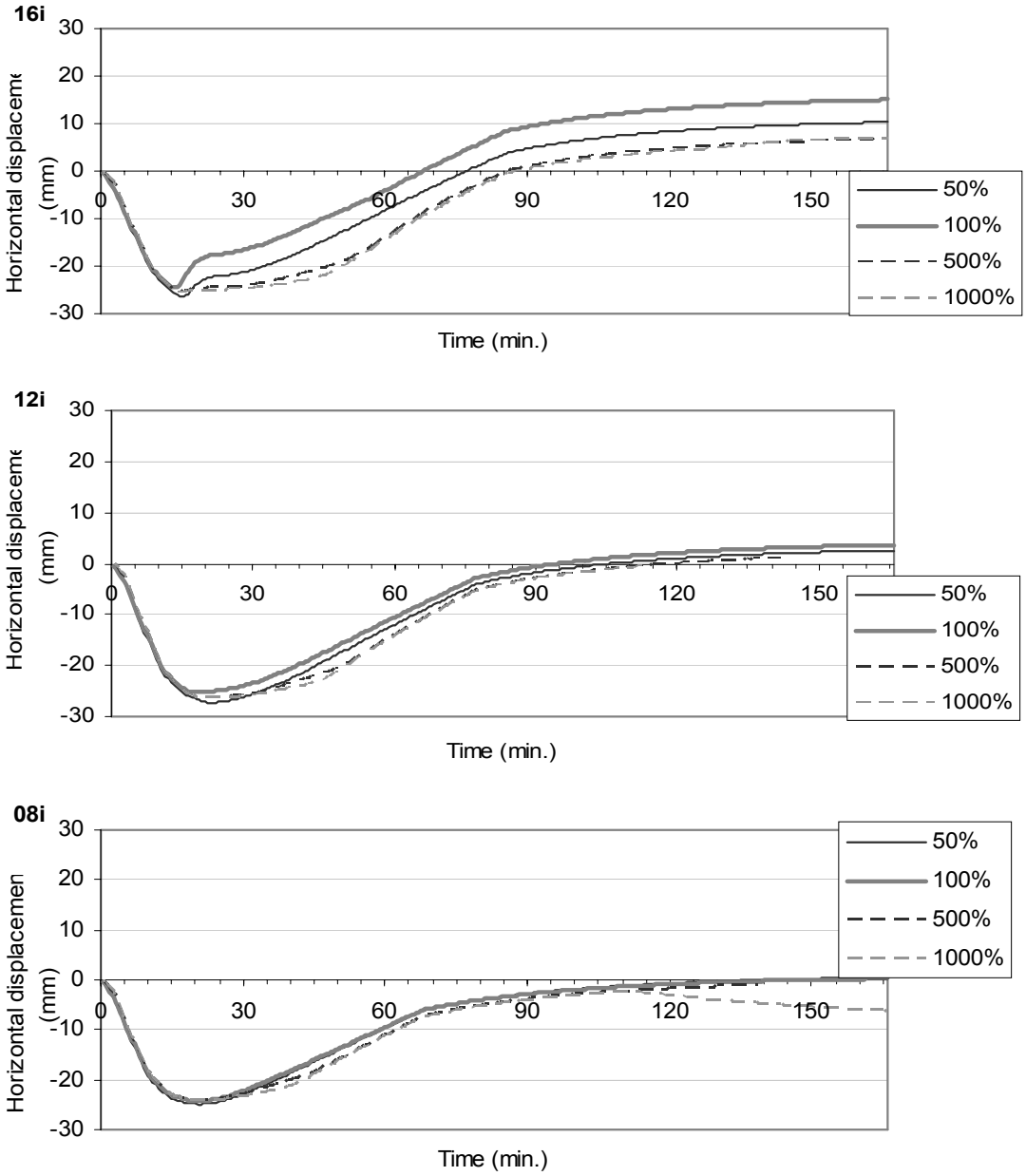

Figure 8-13 Horizontal displacement at the beam-column connection in a frame with a fix-fix connected steel beam and different column stiffness exposed to 16, 12 and 8 minutes of the ISO fire before the decay phase

The last part of this section discusses the behaviour of steel frames with changed both the column strength and stiffness and a fix-fix connected steel beam exposed to three different durations of fire. Figure 8-14 shows the axial force in the steel beam. All the graphs can be discussed in two parts like in the pin-pin steel frame cases: the frames with strong columns, and the frames without. Because the strengths of the columns were also changed, the column could take a much higher axial force before it yields, therefore the axial force of the 500% and 1000% column strength and stiffness cases shown in the graphs are much larger than in Figure 8-11 of the changed stiffness scenario.

One would expect the axial forces in Figure 8-11 and Figure 8-14 to show no significant difference if the columns did not yield. This applies to the 50% and 100% column strengths and stiffness cases. In the scenario with changed column stiffness only, the compressive force of the 500% and 1000% column stiffness case did not reach the axial force envelope, which was 850kN found in the previous section. However, in this scenario, the compressive force increased to around 2500kN. This confirms that the high stiffness columns already started yielding during the heating phase in the changed stiffness only scenario.

The axial force capacity of the beam was 3900kN based on the yield stress and the cross-sectional area of the beam. The beam would start to yield after the axial force reached the force capacity. This has been observed in the single span fix-fix connected steel beam cases in Section 7.2.2. In the strong columns cases in this scenario, the tensile beam axial force would reach 3900kN under a large fire and cause the beam to fail.

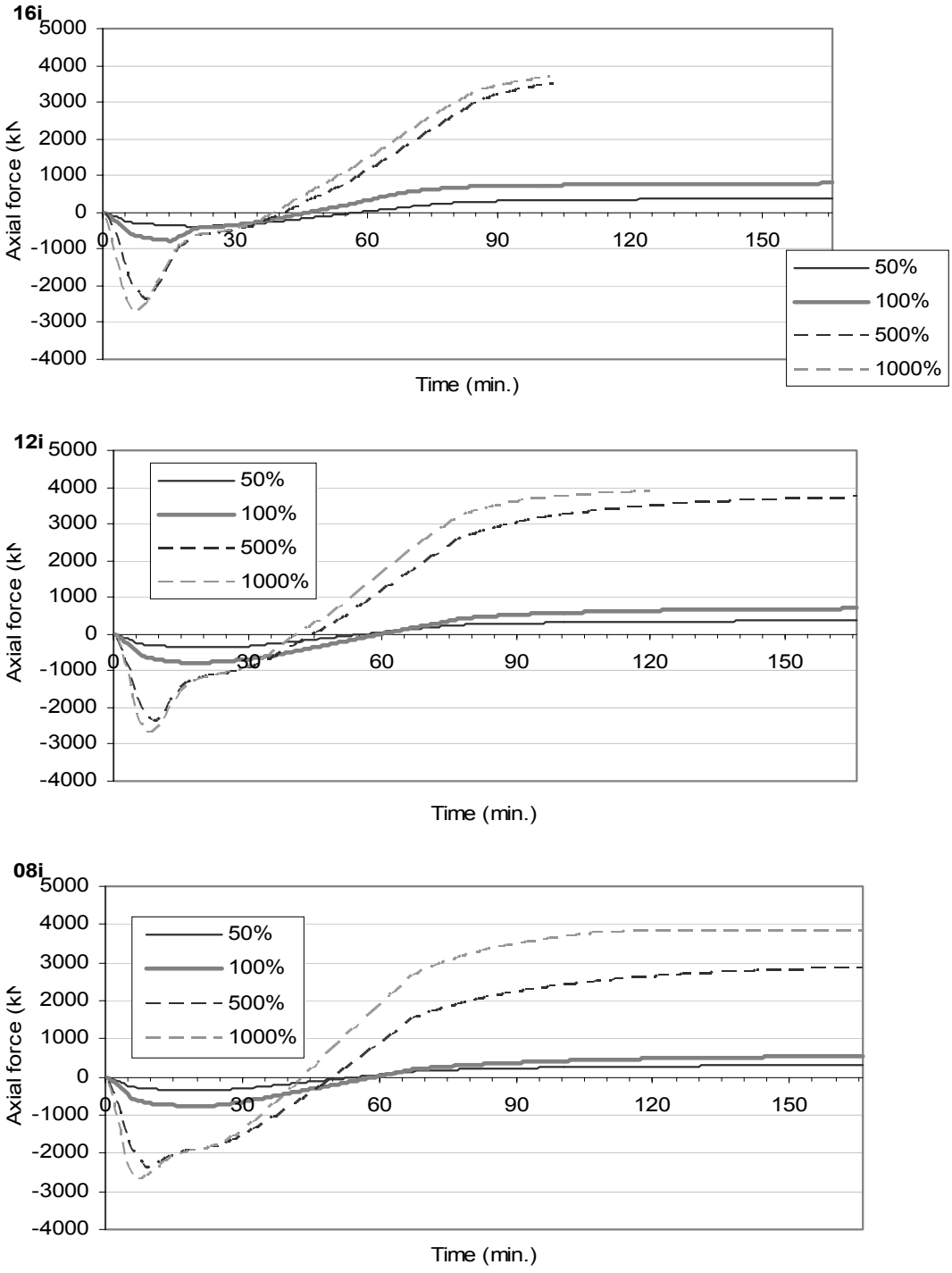

Figure 8-14 Axial force in fix-fix connected steel beam in a frame with different column strengths and stiffness exposed to 16, 12 and 8 minutes of the ISO fire before the decay phase

The graphs of the midspan vertical displacement shown in Figure 8-15 indicate that the stronger beam caused a larger vertical displacement; this was possibly caused by the formation of plastic hinges near the connections in the beam during the heating phase.

Figure 8-15 also shows that under a large fire, because of the plastic hinges developed near the connections, the midspan vertical deflection at the 100% column strength and stiffness case was similar to the frames with strong columns. Under a smaller fire, because the plastic hinges were not formed, the midspan vertical deflection of the 100% column strengths and stiffness case was closer to the 50% case with a small vertical displacement.

Figure 8-16 shows the horizontal displacement at the beam-column connections. In the strong column cases, because the tensile axial force while cooling was higher than the compressive force induced in the heating phase, the inward horizontal displacement was larger. However, because the columns were strong, the overall horizontal displacement at the connections was not as large as in the 100% or 50% column strength and stiffness case.

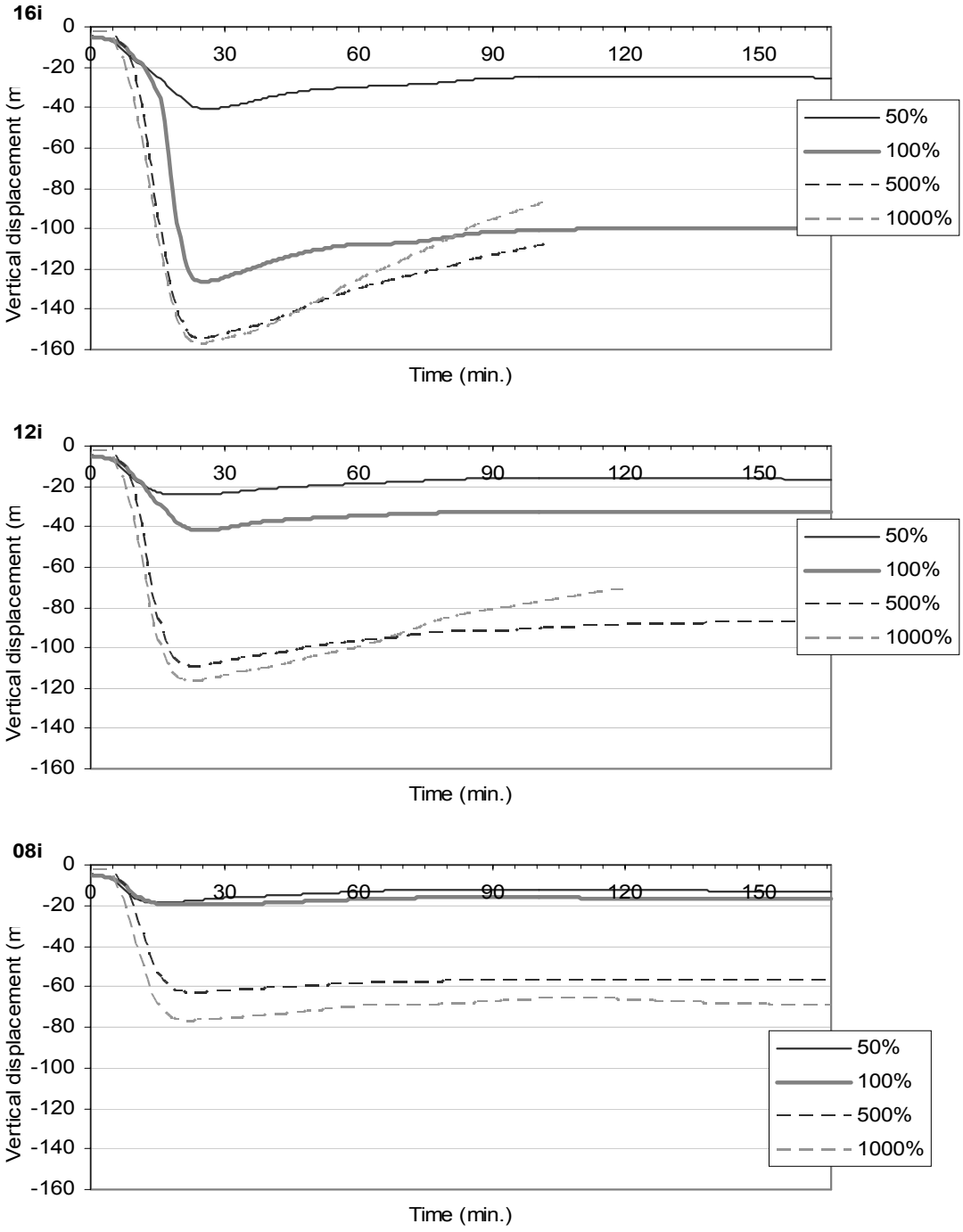

Figure 8-15 Midspan vertical displacement of a fix-fix connected steel beam in a frame with various column strengths and stiffness exposed to 16, 12 and 8 minutes of the ISO fire before the decay phase

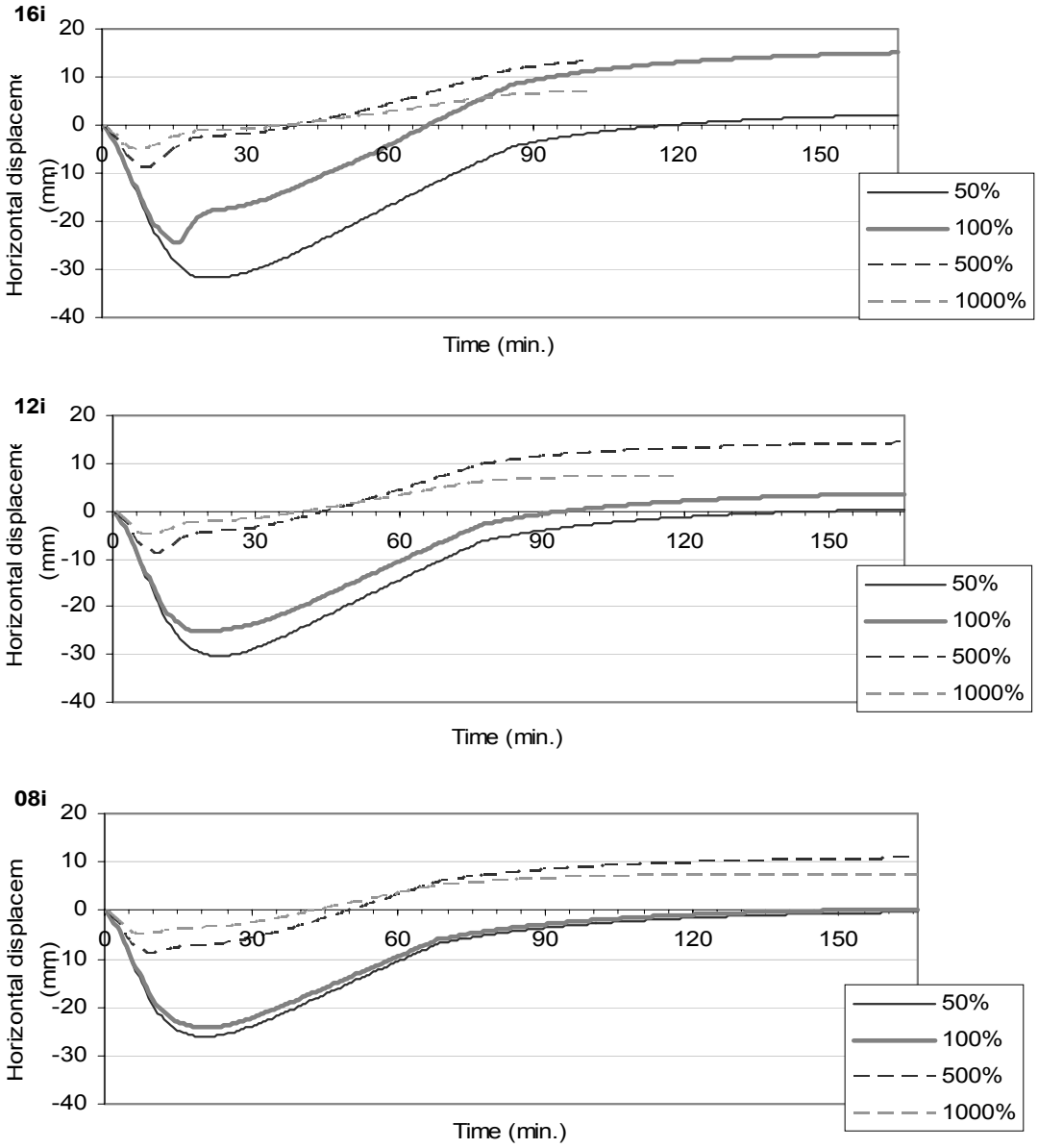

Figure 8-16 Horizontal displacement at the beam-column connection of a frame with fix-fix connected steel beam and various column strengths and stiffness exposed to 16, 12 and 8 minutes of the ISO fire before the decay phase

8.3 Summary of the simulation results of steel frames

This chapter reviewed the simulation results of frames with pin-pin and fix-fix connected steel beams. The structural behaviour observed in this section shows a similar behaviour to the composite frames discussed in Chapter 6. This section also discussed the effect of changing the stiffness and strength of the columns, which can influence the axial force induced in the beam.

One can conclude from the simulation results that whether the column yielded during the heating phase significantly affects the recovery of vertical displacement during the cooling period. The yielding of the columns also determined whether the horizontal displacement would continue progressing as the steel temperature reduced to the ambient. This behaviour was also found in the simulation results of composite beams.

In the initial set-up where the column has 100% strength and stiffness compared to the beams, the beam axial force reached 800kN and the columns yielded in a large fire. When only the column stiffness was changed, the higher stiffness columns induced a higher beam axial force which caused the columns to yield earlier in the fire. When both the column strength and stiffness were changed, the analyses show the beam axial force could grow up to 3900kN with strong columns.

With a very strong columns, when the axial force went up to 3900kN, which was the force capacity of the steel beam, the beam yielded under tension and failed shortly afterwards. To prevent the beam itself failing under its high axial force, one can utilise the composite action between the beam and the concrete slab, which can increase the duration of the frame structure under fire.

9 Simulation results of composite frames exposed to parametric fire

The discussions in the previous chapters showed the behaviour of composite beams and frames under the ISO fire with or without a decay phase. However, it is not practical to assume every room fire develops like the standard fire. The prior discussions also showed that other than the temperature in the elements, the heating time could also be a factor to affect the stability of the structure. This section discusses the behaviour of a composite frame structure exposed to the fires with different rate of growth to the standard fire. Two parametric fires were chosen for simulation: one with a faster growth rate than the ISO fire, which was named P1; the other one with a slower growth rate, which was named P2.

9.1 Selection of the parametric fires

The equation for the ISO834 standard fire temperature is shown in Equation 9-1, where T is the fire temperature (^oC), t is time (min.), and T_0 is the temperature before heating, which was assumed to be 20^oC. If Γ in Equation 9-3 is equal to 1.0, Equation 9-1 is almost the same as the Eurocode equation shown in Equation 9-2.

$$T = 345\log_{10}(8t+1) + T_0 \qquad \textbf{Equation 9-1}$$

$$T = 1325(1 - 0.324e^{-0.2t^*} - 0.204e^{-1.7t^*} - 0.472e^{-19t^*}) \qquad \textbf{Equation 9-2}$$

where t* is a fictitious time in hours given by

$$t^* = \Gamma t \qquad \textbf{Equation 9-3}$$

where t is time in hours and

$$\Gamma = \frac{(F_v / 0.04)^2}{(b/1160)^2} \qquad \textbf{Equation 9-4}$$

where b is $\sqrt{\text{thermal inertia}} = \sqrt{k\rho c_p}$ ($\text{Ws}^{0.5}/\text{m}^2\text{K}$), F_v is the ventilation factor given by

$$F_v = A_v\sqrt{H_v} / A_t \qquad \textbf{Equation 9-5}$$

where A_v is the vertical opening area in m^2, H_v is the height of the vertical opening in metres, and A_t is the total opening area.

For a room with dimensions shown in Figure 9-1, Γ is equal to 1.0 if F_v is 0.04 and b is 1160. The opening for the room was assumed to be 2.1m wide by 2.1m high to achieve the ISO fire temperature. While the height of the opening was assumed to remain the same, for the slower fire, the width was reduced to 1.6m to let F_v be 0.03; and for the faster fire, the width was increased to 3.2m to let F_v be 0.06. Figure 9-2 shows the temperature growth rate of different parametric fires, and Figure 9-3 shows the relationship between the fuel loads in the room and the burning period.

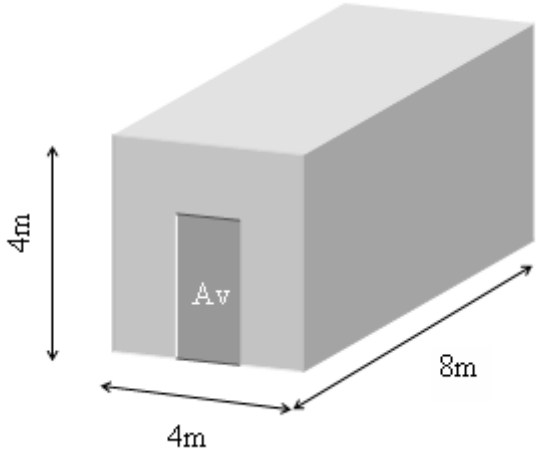

Figure 9-1 Room geometry

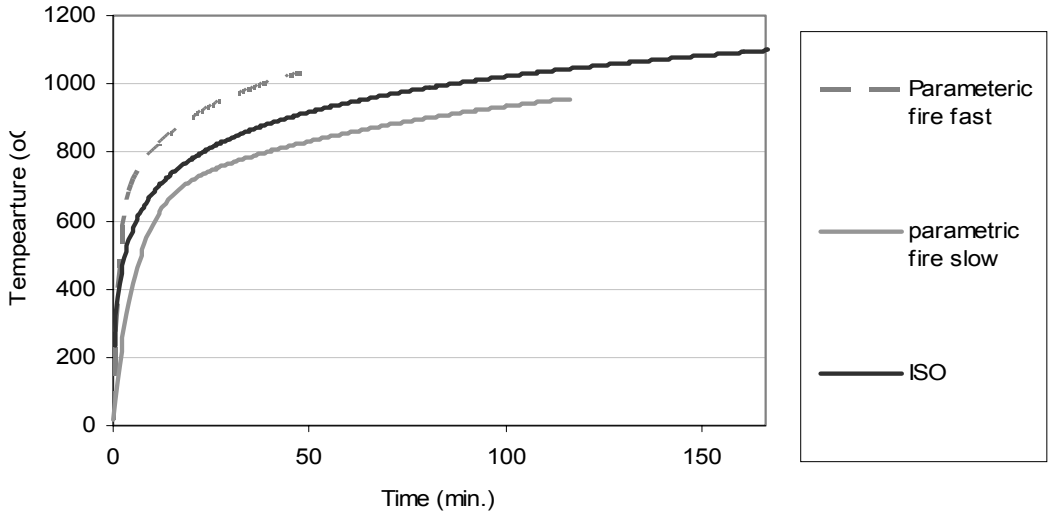

Figure 9-2 Fire temperature of different fires

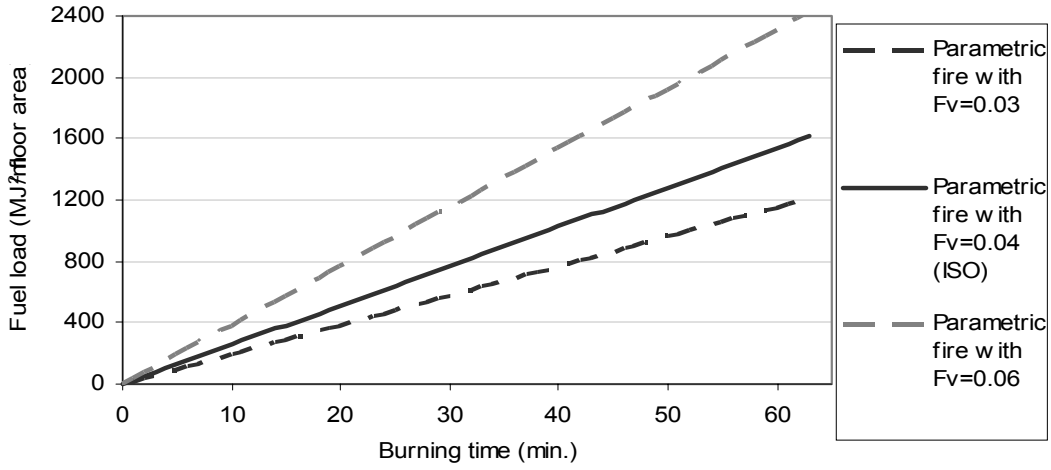

Figure 9-3 Relationship between the burning time and the fuel load

After the burning period, the fire went into the decay phase. The decay rate of temperature in this phase was the same as suggested in the Eurocode, as in Section 5.

9.2 Thermal Analysis Results

Chapter 6 has shown that a pin-pin composite beam in a frame lasts longer than a fix-fix connected beam. The pin-pin connected composite frame reached failure in 23.5 minutes under the faster fire. Seven fires of 2 to 20 minutes of P1 fire before going to the decay phase were chosen for the thermal analysis. Figure 9-4 shows the temperatures of the composite beam at different positions.

Under the slower fire, the pin-pin connected composite frame reached failure after 60 minutes. Five other fires following 10 to 55 minutes of P2 fire before the decay phase were used for comparison. Figure 9-5 shows the composite beam temperature from the SAFIR thermal analysis.

The temperature curve for the composite beam exposed to the parametric fires without a decay phase can be compared to the temperature curve for the beam exposed to the ISO fire shown in Figure 5-2. Based on the maximum temperature reached in the beam, the time under the parametric fire was converted using Excel into the duration under the ISO fire to obtain the equivalent time, as shown in Table 9-1.

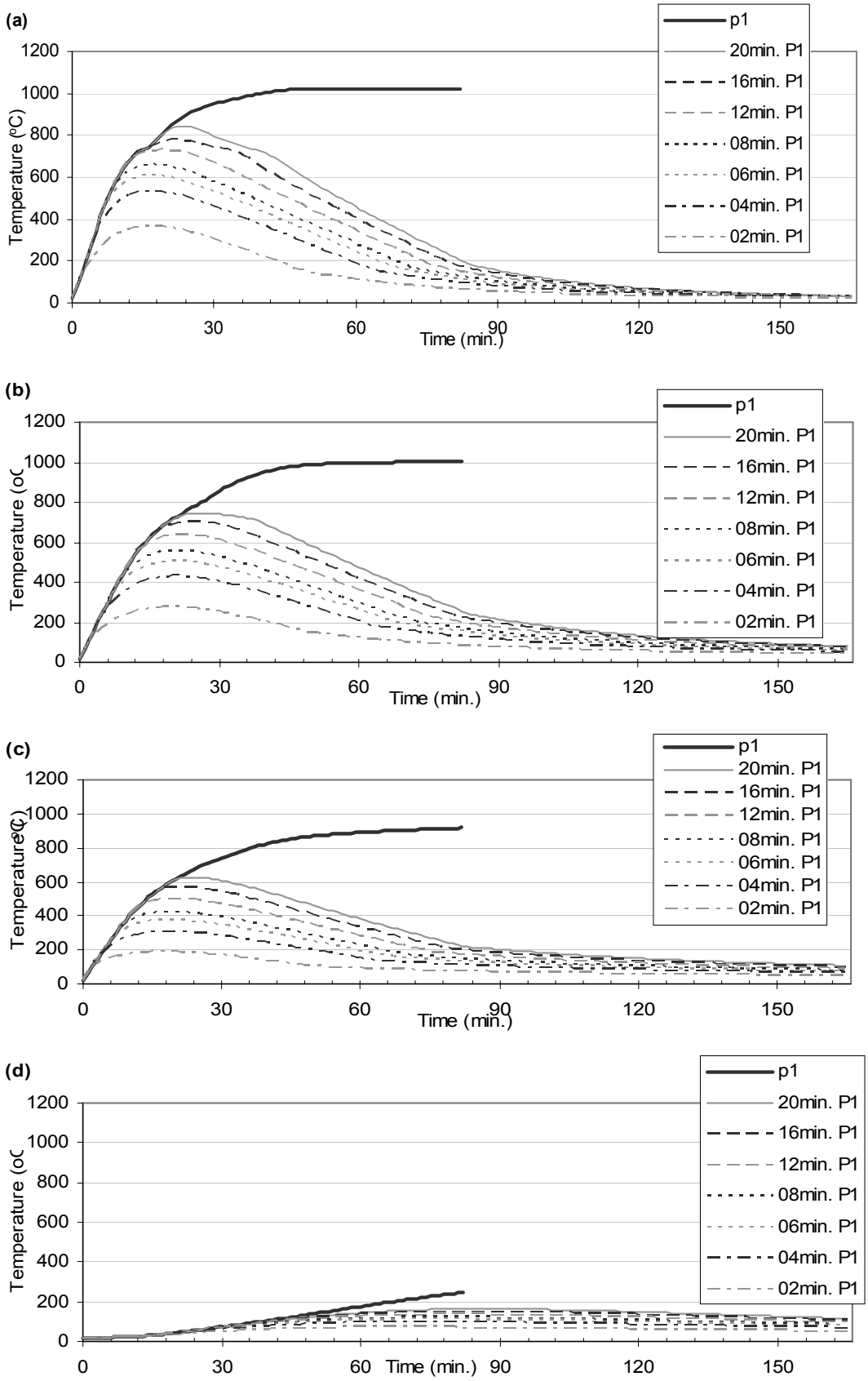

Figure 9-4 Thermal analysis results for composite beam exposed to faster parametric fire: (a) bottom of the steel beam; (b) top of the steel beam; (c) bottom of the concrete slab; (d) top of the concrete slab

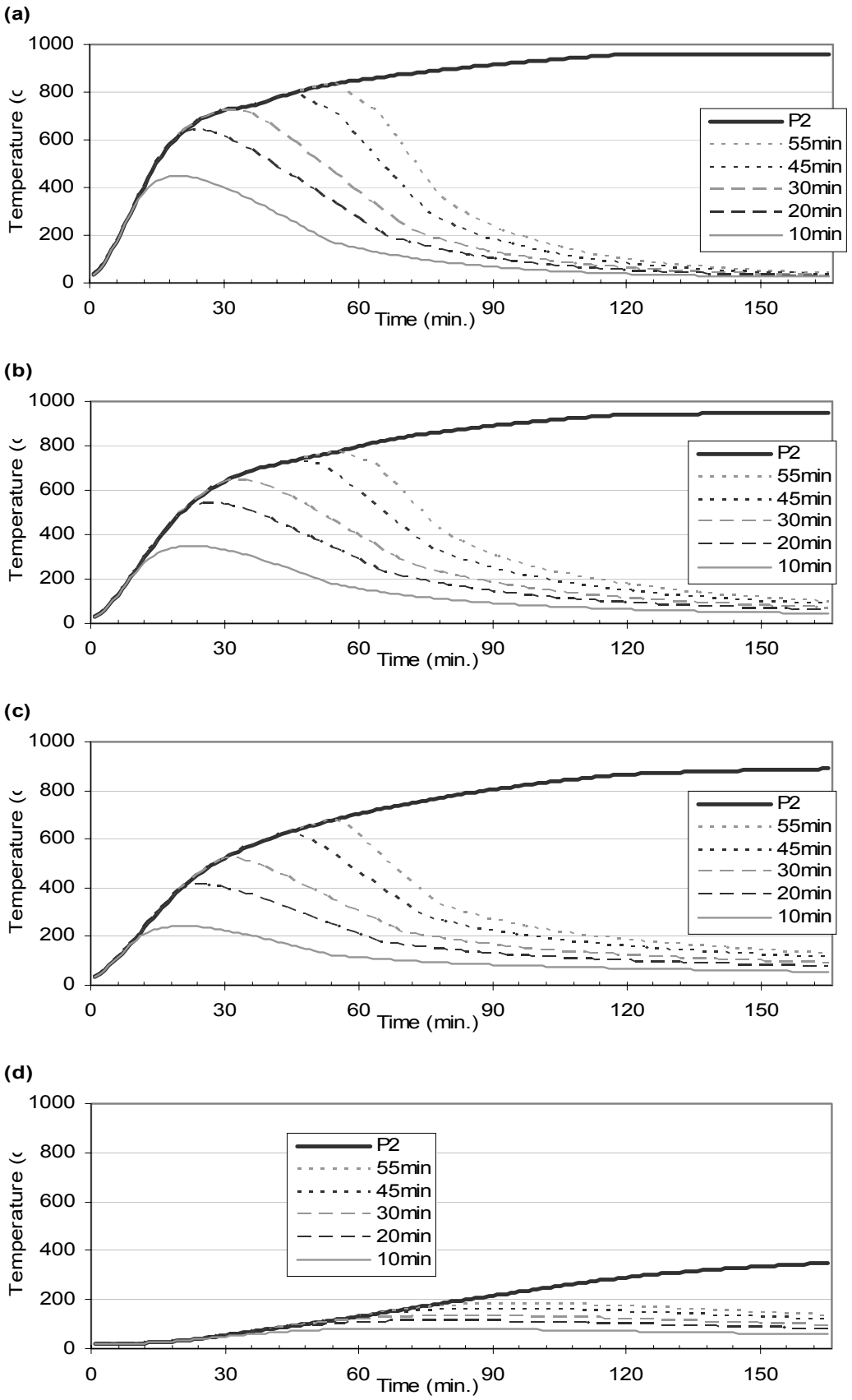

Figure 9-5 Thermal analysis results for composite beam exposed to the slower parametric fire: (a) bottom of the steel beam; (b) top of the steel beam; (c) bottom of the concrete slab; (d) top of the concrete slab

Table 9-1 Equivalent time from the parametric fires

	Time under parametric fire	Equivalent time for faster fire	Equivalent time for slower fire
Symbol	t_d	t_e(P1)	t_e(P2)
Unit	Min.	Min.	Min.
	0	0.0	0.0
	5	6.6	3.8
	10	13.6	7.9
	15	20.7	12.1
	20	27.8	16.2
	25	35.8	20.3
	30	44.1	24.3
	35	52.8	28.0
	40	62.0	31.6
	45	71.8	35.2
	50	82.0	38.6
	55	92.8	41.5
	60	104.1	44.9

(Example: The beam exposed to 50 minutes of the faster fire has the same temperature as being exposed to 82.0 minutes of the ISO fire; the beam exposed to 50 minutes of the slower fire has the same temperature as being exposed to 38.6 minutes of the ISO fire)

9.3 Frame structural behaviour under parametric fires

This section discusses the pin-pin and fix-fix connected composite and steel beams in frames. The dimensions, loadings, and layout of the structure were the same as in the previous chapters, only the fires were changed from different durations of the ISO834 standard fire to the parametric fire.

9.3.1 Pin-pin connected composite frame

Figure 9-6 and Figure 9-7 show the simulation results of exposing pin-pin connected composite frames to the parametric fire with decay phase. The shapes of the curves are similar to the curves in a frame exposed to the ISO fire shown in Figure 6-1. In the cases where the frame was exposed to 20 minutes of the fast fire or 45 minutes of the slow fire, the beam temperature is the same as being exposed to around 30 minutes of the ISO fire, and the columns yielded under the tensile forces in the beams while the frame was cooling. This agrees with the finding in Section 6.2.1 that the columns would yield when the frame is exposed to 30 minutes of the ISO fire.

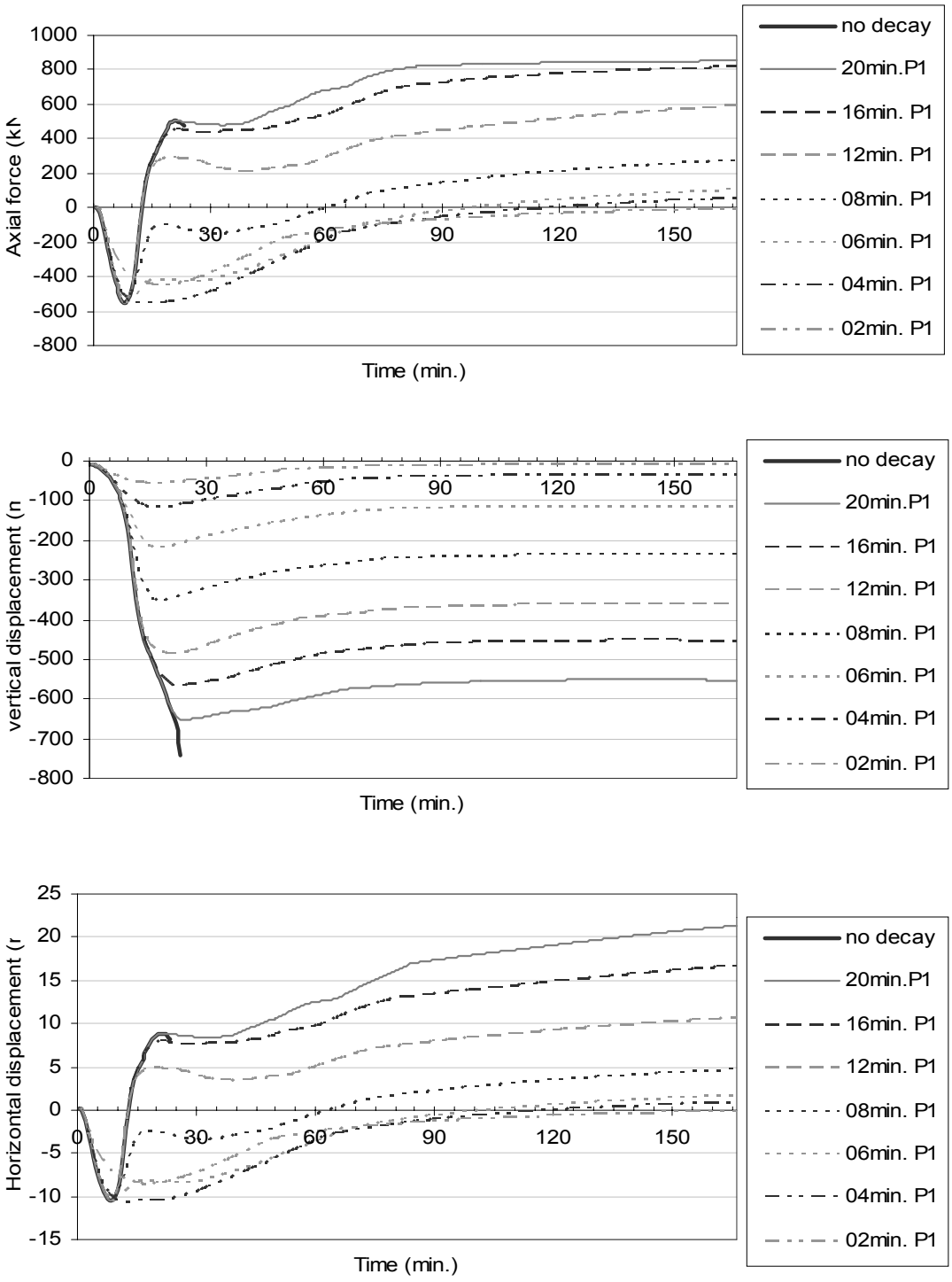

Figure 9-6 Simulation results of a pin-pin connected composite frame exposed to various durations of the faster parametric fire (P1): (from the top) Beam axial force; Midspan vertical displacement; Horizontal displacement at the beam-column connections

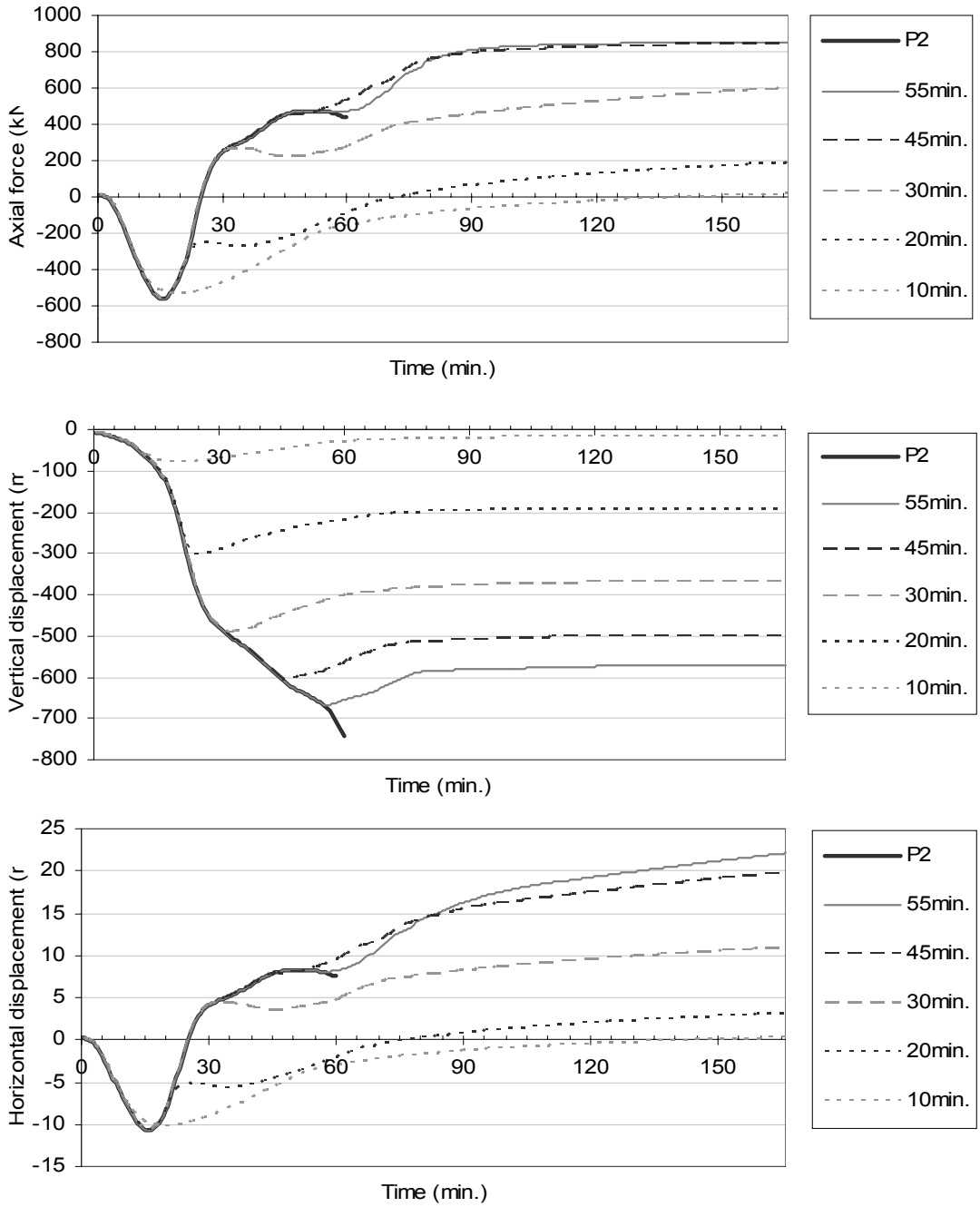

Figure 9-7 Simulation results of a pin-pin connected composite frame exposed to various durations of the slower parametric fire (P2): (from the top) Beam axial force; Midspan vertical displacement; Horizontal displacement at the beam-column connections

The time scale in both Figure 9-6 and Figure 9-7 can be changed to the equivalent time calculated before to allow comparison with the ISO fire case. Figure 9-8 shows the axial force graph of the frame exposed to the parametric fires plotted in the equivalent time scale. The graphs are similar to the axial force plots in Figure 6-1, but the rate of growth of the axial force under a slower fire was slower.

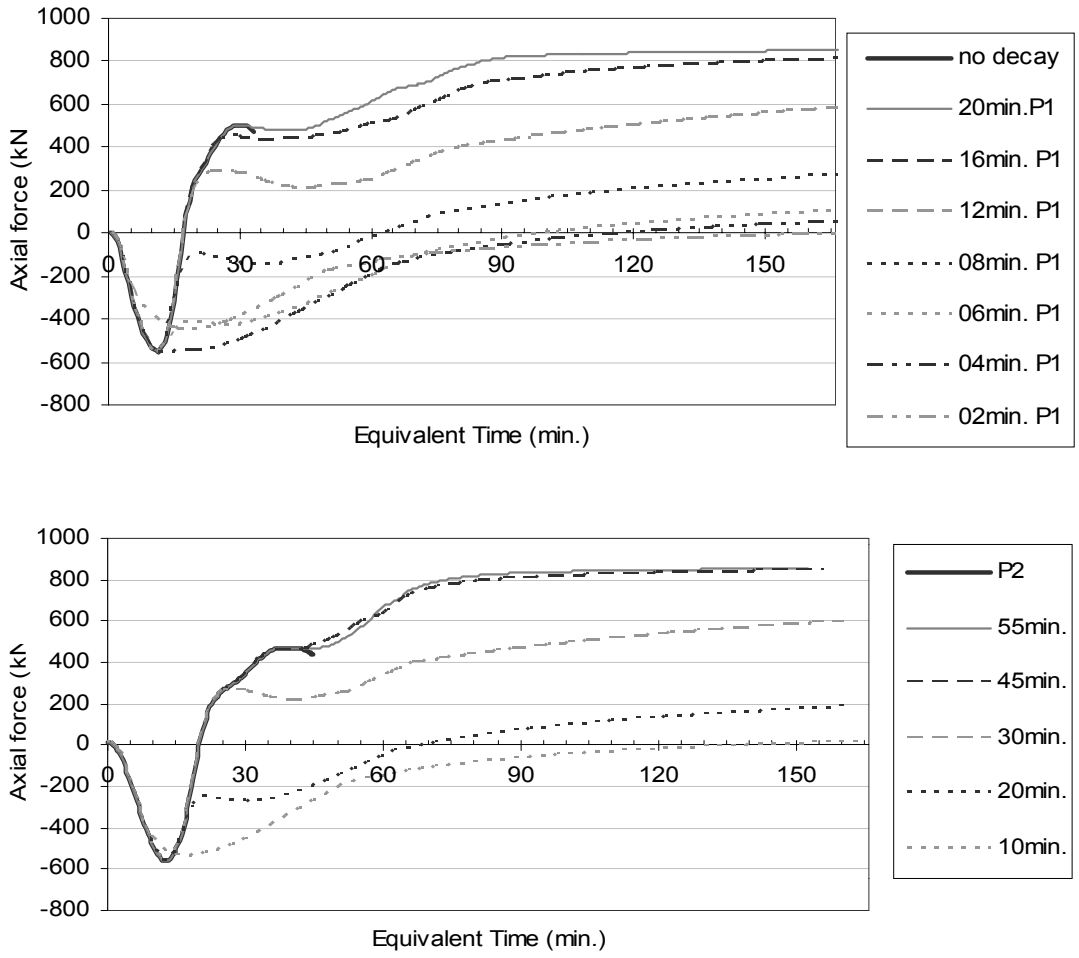

Figure 9-8 Axial force of the pin-pin composite frame exposed to the faster and slower fire (P1 and P2 respectively) plotted in the equivalent time scale

Figure 9-9 shows the axial force in the pin-pin composite frame under the parametric fires as well as the ISO fire without the decay phase plotted in the equivalent time scale. It shows that the maximum axial force has little dependence on the rate of growth of the fire temperature. However, for the faster parametric fire case, the rate of growth in both tension and compression was larger than for the ISO fire case or the slower parametric fire case, and the equivalent failure time was around 5 minutes earlier. However, this difference could be caused by the error in converting the temperature into the equivalent time scale.

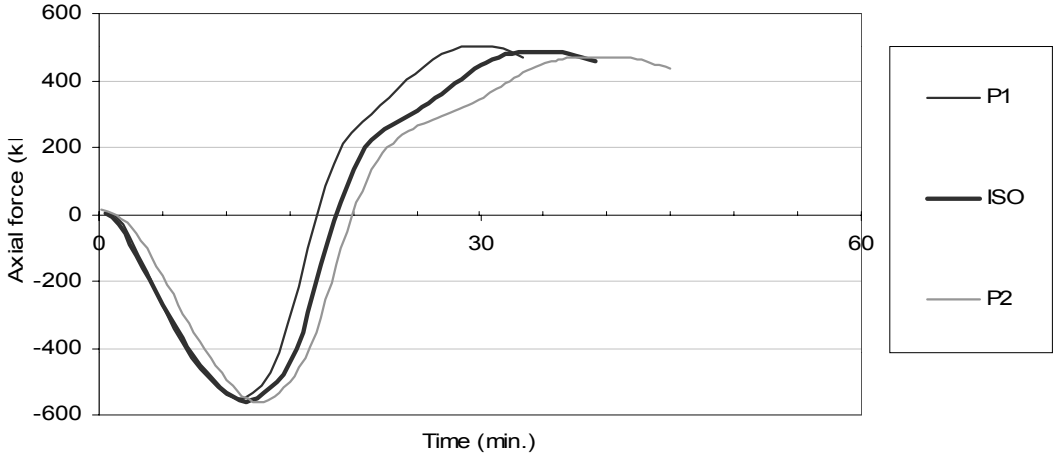

Figure 9-9 Comparison of the axial force in the pin-pin composite frame exposed to the parametric fires and the ISO fire (without decay phase)

9.3.2 Fix-fix connected composite frame

Figure 9-10 and Figure 9-11 show the simulation results of exposing fix-fix connected composite frames to the fires with growth rates different to the ISO fire. The results can be compared with the ISO fire case shown in Figure 6-6, which shows the behaviour of the beam is only slightly different from the ISO fire case. In all cases the maximum tensile force exceeded 400kN, and the maximum compressive force was around 700kN, the maximum horizontal translation of the beam connections was around 23mm outwards, and the vertical displacement at the midspan was generally small unless the fire was large enough to form plastic hinges near the beam connections.

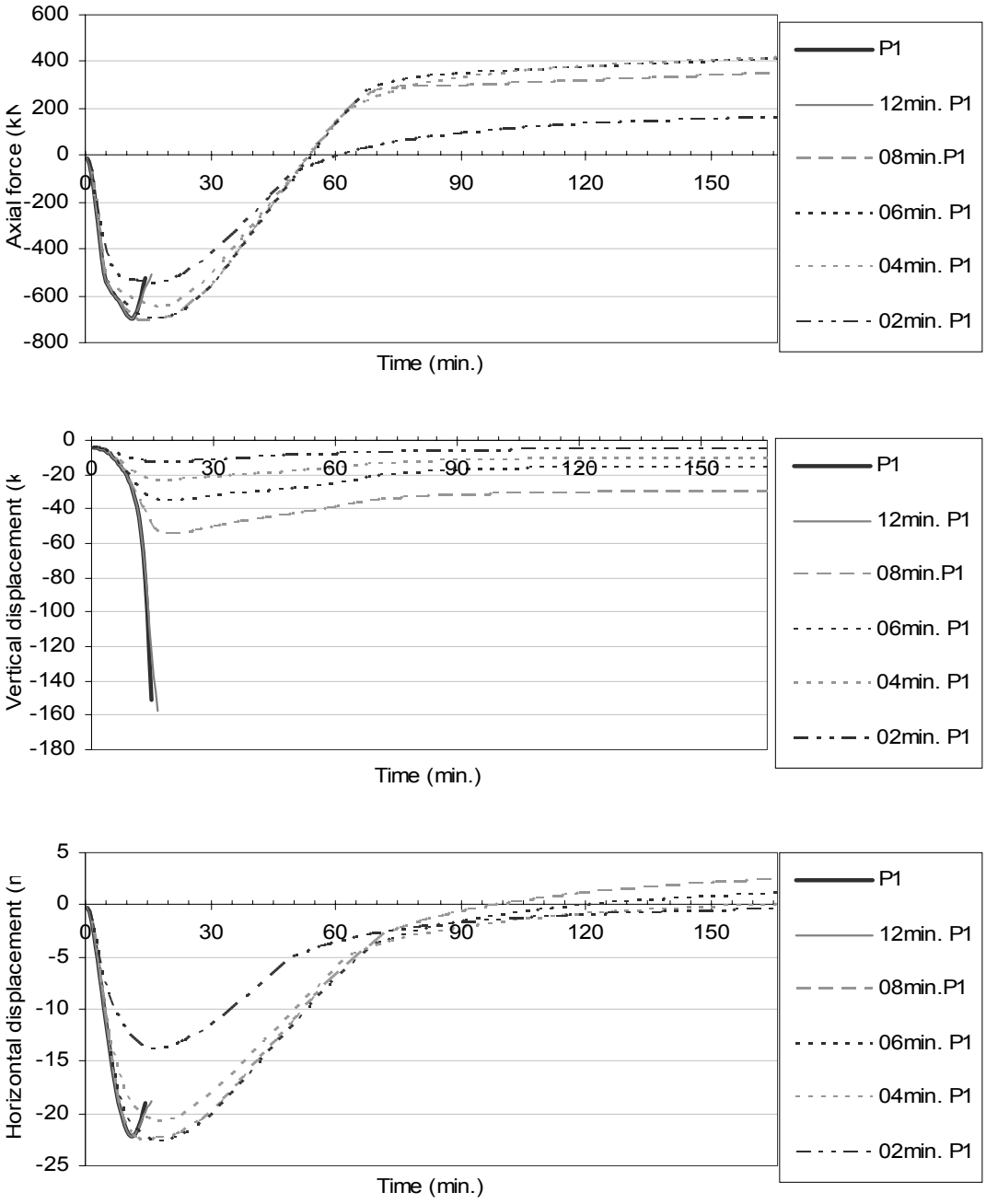

Figure 9-10 Simulation results of a fix-fix connected composite frame exposed to various durations of the faster parametric fire (P1): (from the top) Beam axial force; Midspan vertical displacement; Horizontal displacement at the beam-column connections

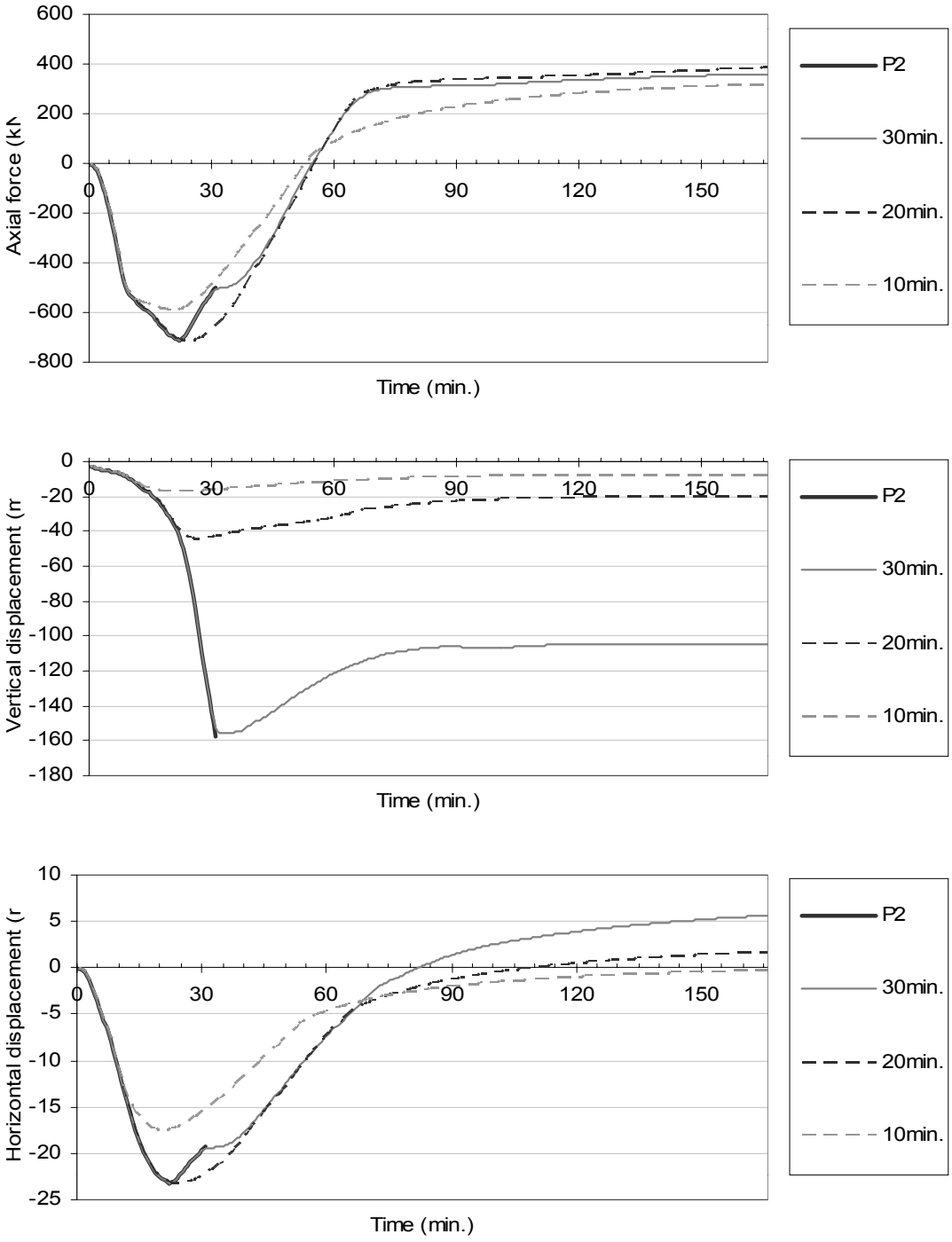

Figure 9-11 Simulation results of a fix-fix connected composite frame exposed to various durations of the slower parametric fire (P2): (from the top) Beam axial force; Midspan vertical displacement; Horizontal displacement at the beam-column connections

Figure 9-12 shows the beam axial force plotted in the equivalent time scale. The graph shows that although the compressive axial force grew much slower under the slower parametric fire, while cooling it went into tension faster than under the fast parametric fire.

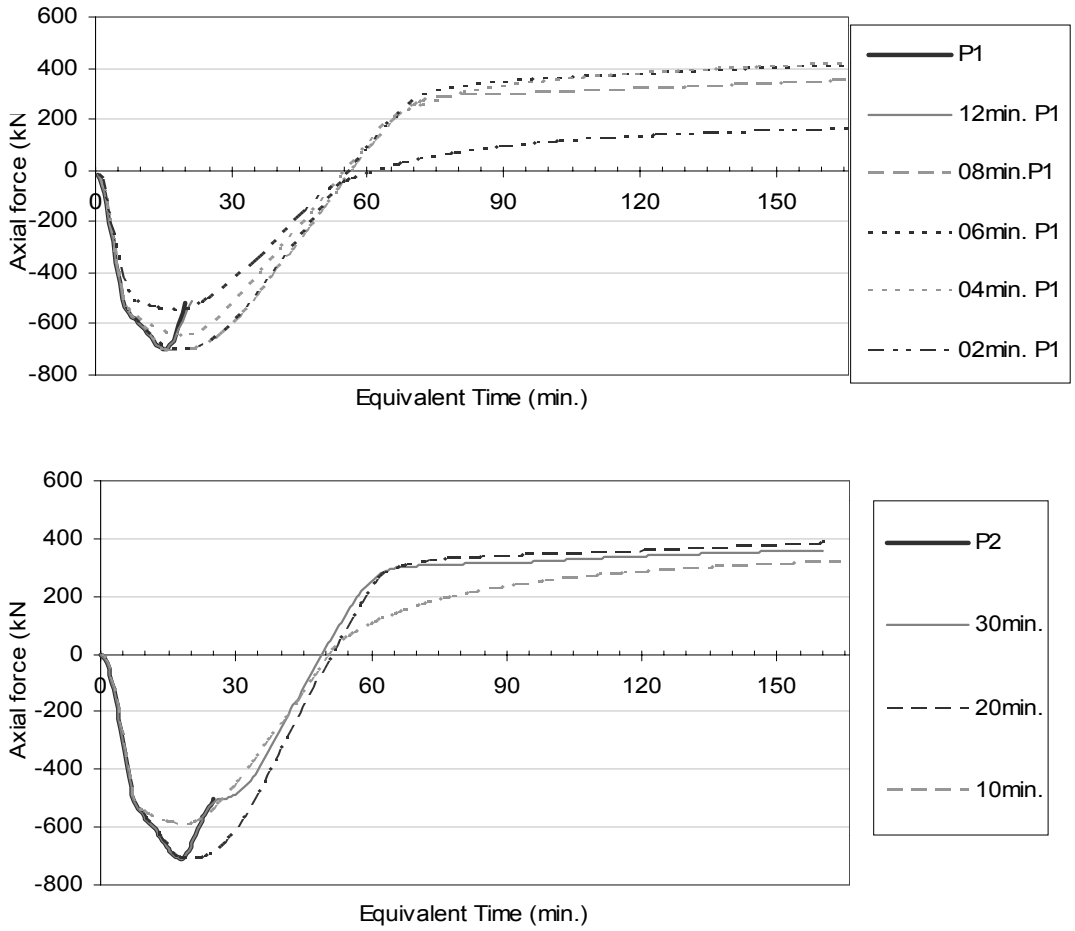

Figure 9-12 Axial force of the fix-fix composite frame exposed to the faster and slower fire (P1 and P2 respectively) plotted in the equivalent time scale

Figure 9-13 shows the beam axial force in the fix-fix composite frame under the parametric fires and the ISO fire without the decay phase plotted in equivalent time scale. It shows the same finding as in the previous section, that the maximum axial force is almost independent from the rate of growth of the fire temperature, and that a slower fire causes a slower rate of growth in axial force during the heating phase even under the equivalent time scale.

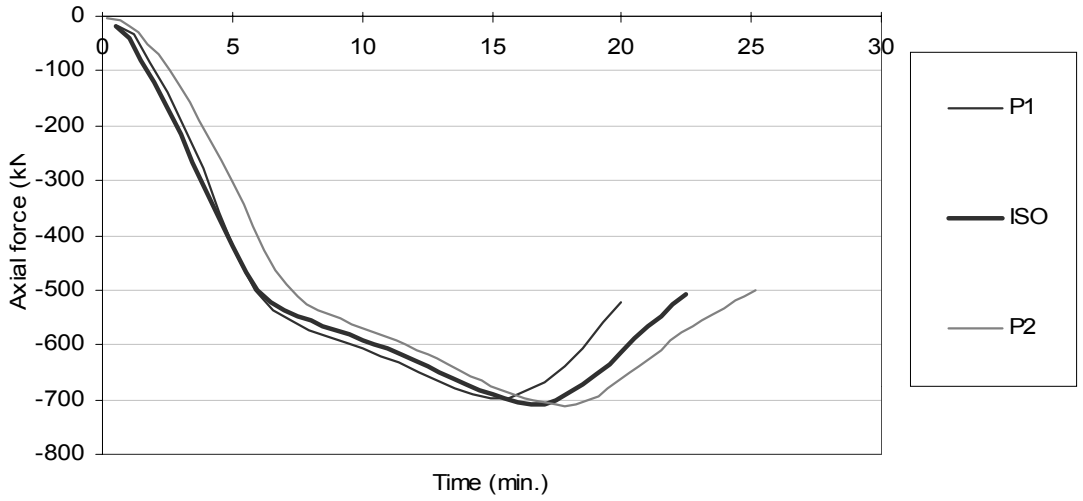

Figure 9-13 Comparison of the axial force in the fix-fix composite frame exposed to the parametric fires and the ISO fire (without decay phase)

9.4 Summary of the simulation results of composite frame exposed to parametric fires

The simulation results discussed in this section showed that that the temperature dominates the structural behaviour, with failure of the structures tending to occur at certain critical temperatures. They also indicated that most of the important characteristics one needs to know in the structural behaviour, i.e. the maximum tensile and compressive force, the midspan vertical displacement and the horizontal displacement at the beam connections, do not vary much with the rate of growth of the fire temperature. However, the failure time was shortened during the simulation under a faster growth fire and lengthened under a slower growth fire in both pin-pin and fix-fix connected composite frames.

10 Simulation results of insulated truss structures exposed to the ISO fire with a decay phase

This section discusses the simulation results of a truss structure exposed to the ISO834 standard fire and to various durations of the ISO fires with a decay phase. The decay rate of the fire temperature is as explained in Chapter 5. The truss structure used in the model refers to the main floor truss in the World Trade Centers 1 and 2. According to the description in FEMA (2002), all the structural members in the World Trade Center towers were insulated, and so were the members in the simulated model. The thickness of insulation was 20mm as described in Section 2.4.1.

10.1 Load ratio

The load capacity of the simulated truss was calculated based on the description in Section 2.4.1, which was about the truss elements, and the material properties in Table 4-1. Figure 2-8 and Figure 2-10 showed the elevation and point load distribution of the truss. The truss is assumed to be pin-roller supported as in the truss designs, so the top chord is in compression, and the bottom chord is in tension, and the axial forces in these members balance each other. Because the concrete slab has a very high compressive strength, the load capacity relies on the tensile strength of the bottom chord angles. Table 10-1 shows the calculation of the load capacity.

Table 10-1 Load capacity calculation of the truss

Item	Calculation	Value	Unit
Bottom chord force capacity (2 of 76 x 51 x 9mm)			
Total area	2 (76 x 9 + 51 x 9 – 9^2)	2124	mm2
Force capacity	248MPa x 2124mm^2	527	kN
Bending moment capacity			
Distance between the top and bottom chords	831-65.1-13.6*	752	mm
Bending moment capacity	527kN x 0.752 m	396	kNm
Load capacity			
Span of truss		18.3	m
Load capacity (in UDL)	396 x 8 / 18.3^2	9.5	kN/m
Distance between point loads		2	m
Load capacity (as point load)	9.5 x 2	19	kN

*: the centre of the top chord is 65.1mm from the top, and the centre of the bottom chord is 13.6mm from the bottom.

The load ratio, r_{load}, is calculated using the following equation:

$$r_{load}=U^*_{fire}/R_{cold} \qquad \textbf{Equation 10-1}$$

where R_{cold} is the load capacity under the cold state, which is calculated to be19kN as point loads. U*fire is the expected loads on the structure during a fire, which Table 2-5 shows is 9kN as point loads. Therefore, r_{load} is calculated to be 9/19 = 0.47.

Buchanan (2001) states that the buildings designed to resist extreme events would have a load ratio much less than 0.5. Although the calculated value was close to 0.5, one should bear in mind that due to the difficulty in modelling using a two dimensional model, this report does not consider the redundancy provided by the secondary floor trusses, hence the actual load ratio in the World Trade Center towers would be smaller than the value calculated here because of the grillage system. Besides, the grillage system would result in longer time to failure than predicted in this thesis.

10.2 Thermal analysis results

In the structural analysis, the pin-pin connected truss reached failure after two hours under the ISO834 standard fire. Five durations of the ISO fire, ranging from 12 to 60 minutes with a decay phase, were used to observe the behaviour of the truss while cooling. Figure 10-1 shows the temperatures of the bottom chord, truss web, top chord and concrete of an insulated truss exposed to various length of the ISO fire.

The time scales of the graphs in this chapter extend beyond 180 minutes because the temperature of insulated steel drops very slowly.

bottom chord temperature in protected truss

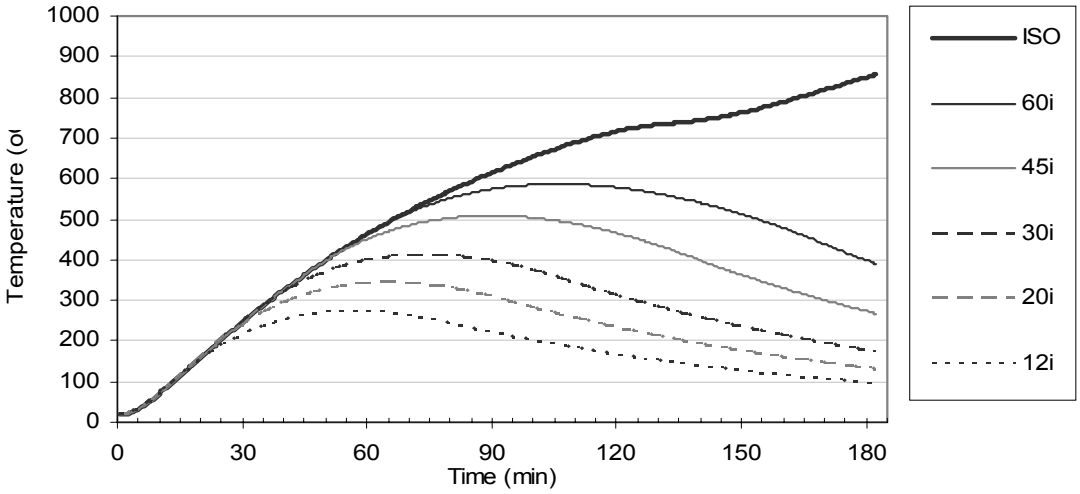

web temperature in protected truss

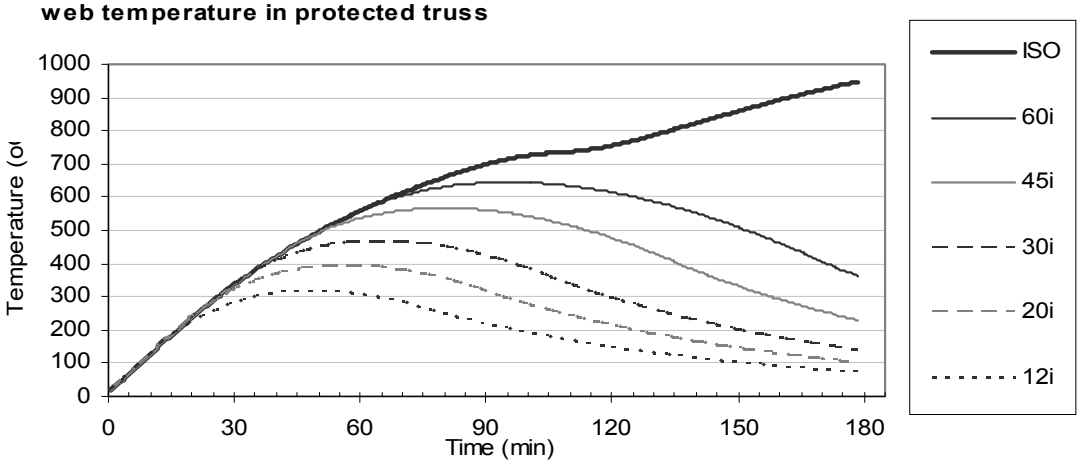

top chord temperature in protected truss

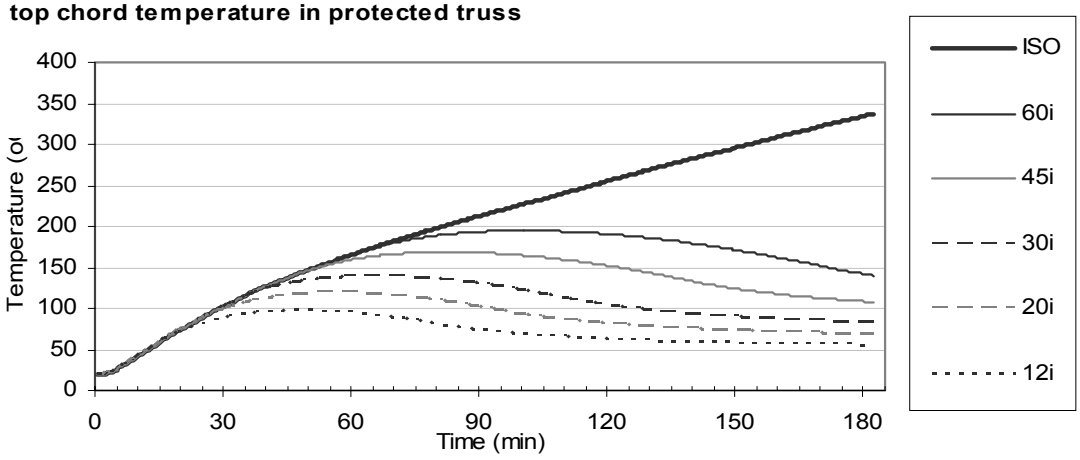

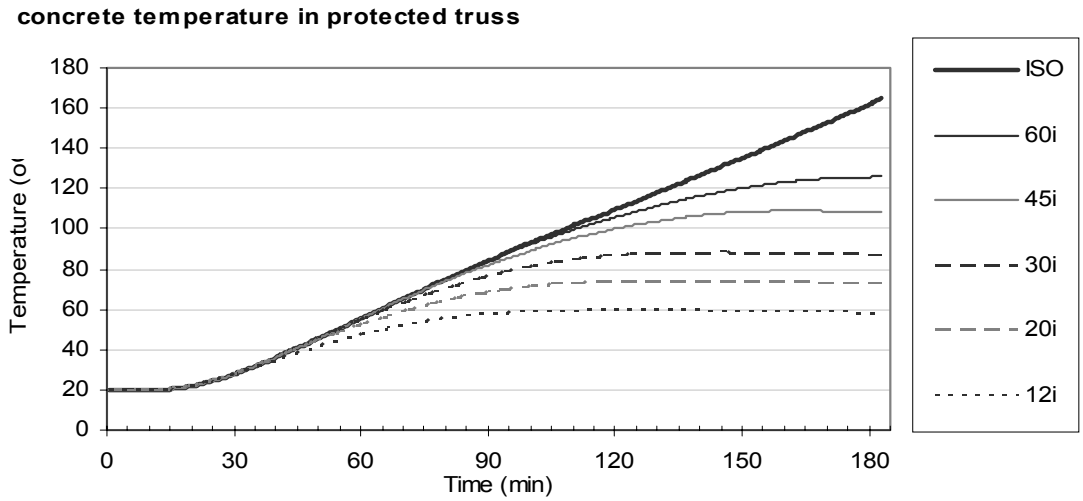

Figure 10-1 Thermal analysis outputs for protected truss exposed to various durations of the ISO fire

10.3 Structural analysis results

10.3.1 Pin-roller connected truss

The pin-roller connected truss reached failure after 74 minutes under the ISO fire. The other five fires shown in the thermal analysis were also used in this model. The truss exposed to 60 minutes of the ISO fire and a decay phase had a failure time of 78 minutes, and the other fires did not cause structural failure.

Figure 10-2 shows the axial force in the top chord and the web near the pinned connection. The dimensions shown in Figure 2-8 indicate that 90% of the web axial force went to the horizontal direction before the truss deforms, so the force from the top chord and the web near connection shown in Figure 10-2 do balance each other, and no horizontal reaction force existed at the ends.

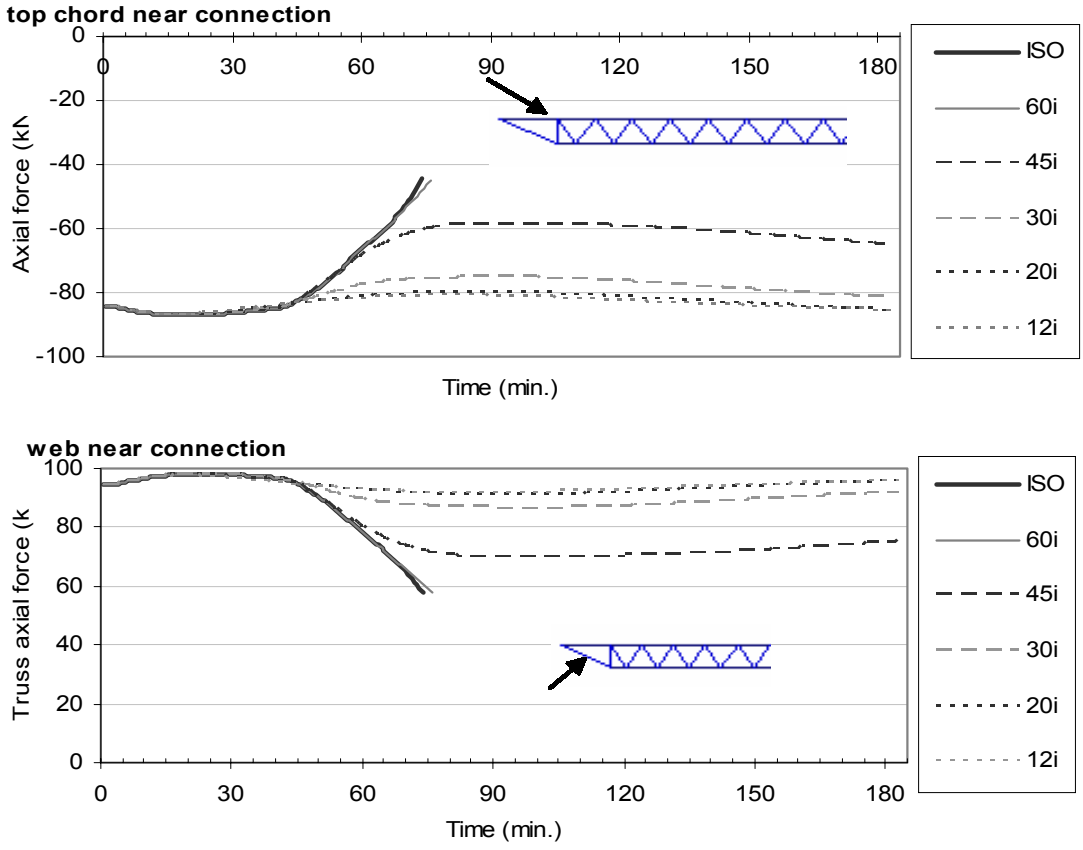

Figure 10-2 Axial force in insulated pin-roller truss near the pinned end

Figure 10-3 shows the axial force at the top and bottom chord at the midspan of the truss. Because the structure is pin-roller supported, the axial force at the top chord should equal the force at the bottom chord. The figure also shows that the size of fire did not influence the forces much because of the insulation.

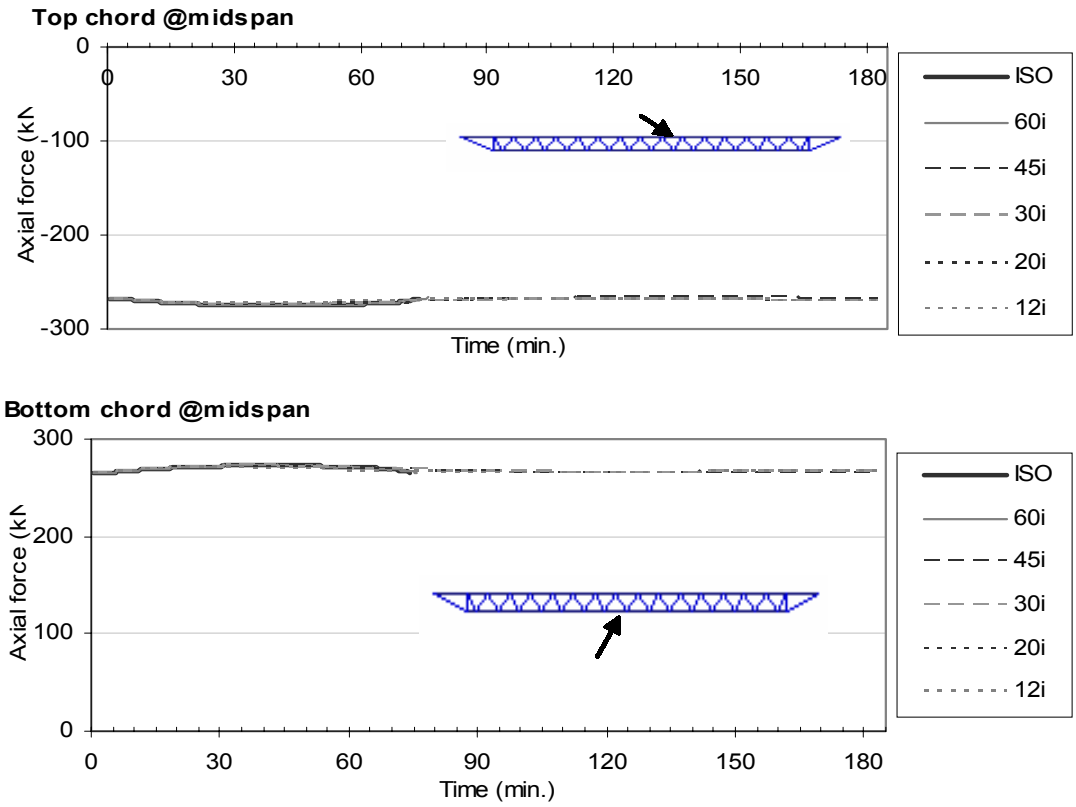

Figure 10-3 Axial force of the top and bottom chord and the web at the midspan in an insulated pin-roller truss

Figure 10-4 shows the vertical displacement at the midspan of the truss. At the end of the simulation a larger vertical displacement resulted from a larger fire, which was almost half of the maximum vertical displacement undergone by the truss. The graph also indicates that the maximum vertical displacement occurred at around 30 minutes after the fire went into the decay phase because the insulation delayed the increase of steel temperature.

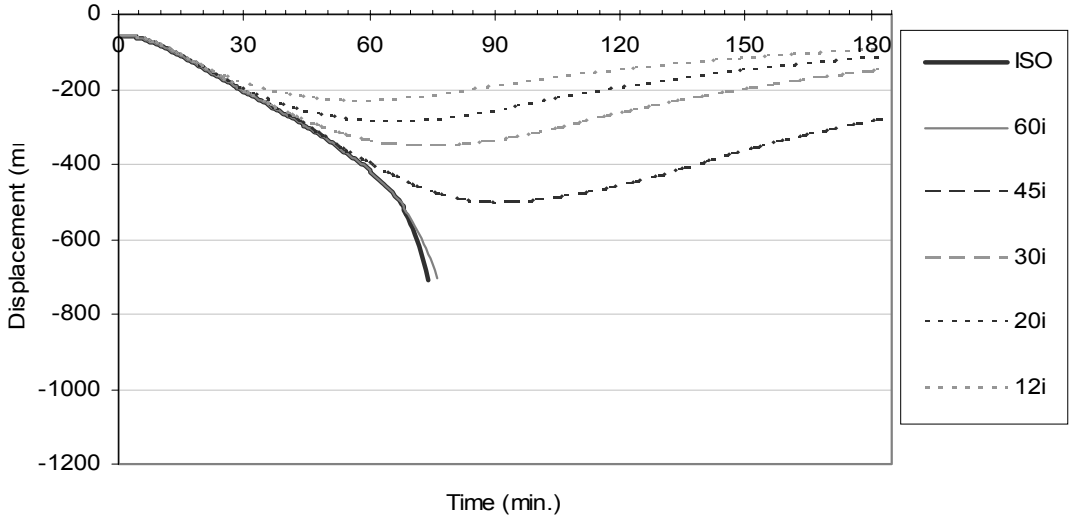

Figure 10-4 Vertical displacement at the midspan of the insulated pin-roller truss

Figure 10-5 shows the horizontal displacement at the roller end of the structure. Other than the two cases where the structure failed, the horizontal displacement almost returned to zero at the end of the simulation. In the cases where the structure was exposed to fires involving less than 30 minutes of the ISO fire, the variation in the horizontal displacement was negligible.

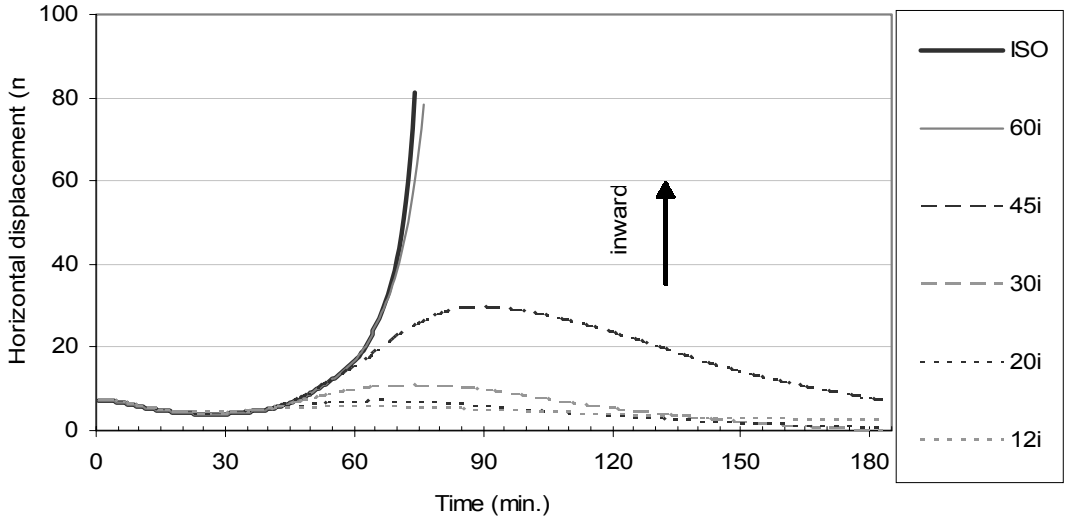

Figure 10-5 Horizontal displacement at the roller end of the insulated pin-roller truss

10.3.2 Pin-pin connected truss

For the truss with pin-pin connections, a horizontal reaction force developed at the connection because of the presence of the horizontal restraints. Figure 10-6 shows the axial force diagram of the truss under ambient temperature. The entire bottom chord was in tension, and the top chord was in compression except the parts near the connection. Therefore, a tensile reaction force was needed to maintain equilibrium.

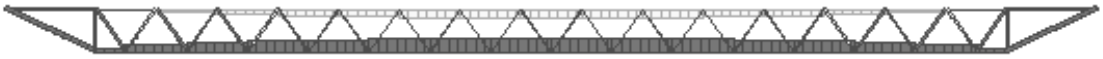

Figure 10-6 Axial force diagram of the truss at the cold state (dark grey: tension; light grey compression)

The pin-pin connected truss reached failure after 122 minutes in the ISO fire, but all the other five fires did not cause failure of the structure. Figure 10-7 shows the axial force at the top chord and at the web near the connection. The changes in the web axial force was much less than those in the top chord axial force because the horizontal restraints provide a reaction force which balanced the increase in tensile force during the decay phase rather than allow an increase of the compressive force in the web.

Figure 10-8 shows the horizontal reaction force at the connection. Before heating the horizontal reaction force was in tension as shown in Figure 10-6. This tensile force reduced while heating following the trend of the top chord axial force shown in Figure 10-7. The maximum tensile reaction force was less than 150kN and occurred around 100 minutes, which is almost one hour after the fire went into the decay phase. However, the horizontal reaction force only became compressive at the end of the simulation.

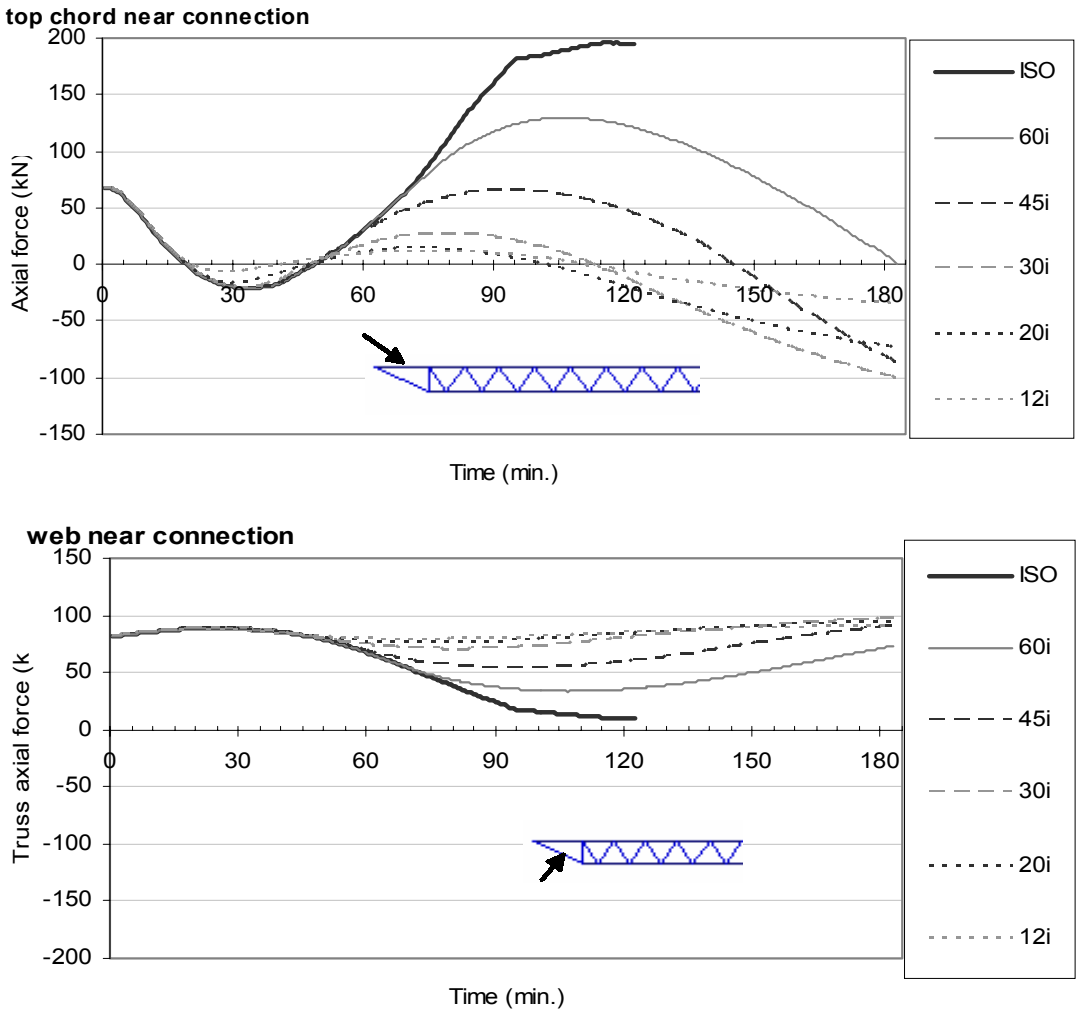

Figure 10-7 Axial force in insulated pin-pin truss near one connection

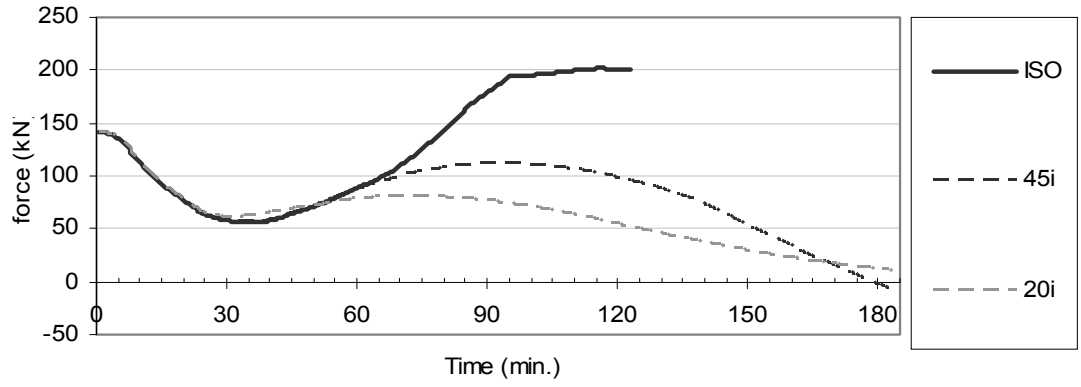

Figure 10-8 Horizontal reaction force at the connection of insulated pin-pin truss

Figure 10-9 shows the axial force in the top and bottom chord at the midspan of the truss. The figure shows that the bottom chord was always in tension, and the top chord was always in compression if the beam did not fail. The sum of the forces at these two members along with the web axial force generated a net tensile force, which is equal to the horizontal reaction forces at the ends. The trend of the curves in the top and bottom chord axial forces at the midspan is almost the same as near the connection shown in Figure 10-7.

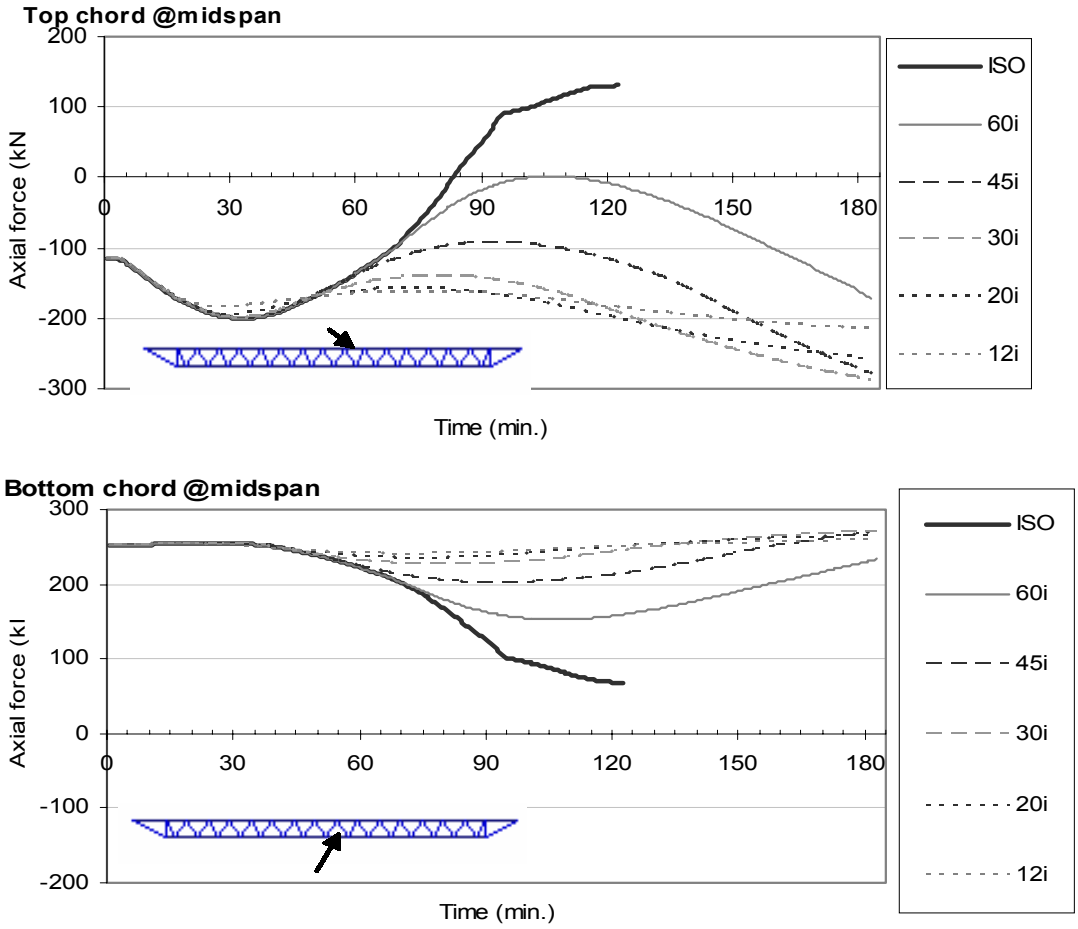

Figure 10-9 Axial forces of the members at the midspan of the insulated pin-pin truss (note: positive is tension, negative is compression)

Figure 10-10 shows the vertical displacements at the midspan of the truss. A larger fire caused a larger deflection at the end of the simulation. The variation in the vertical displacement was slightly smaller than in the pin-roller case shown in Figure 10-4 because of the horizontal restraints.

Figure 10-10 can be explained using Figure 10-9. The situation that top chord never went into tension indicates that a catenary behaviour was not achieved, and therefore the deflection incurred in fire could be recovered.

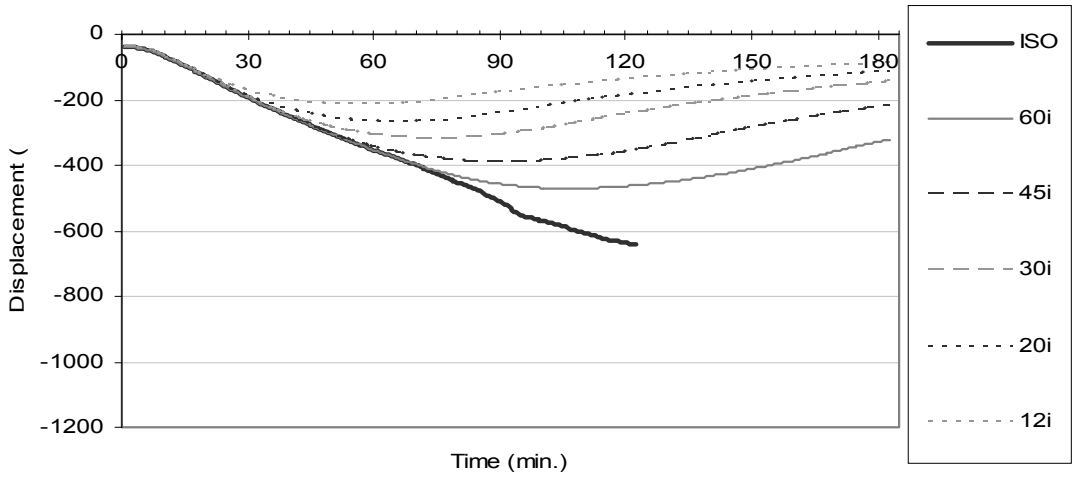

Figure 10-10 Midspan vertical displacements in the insulated pin-pin truss exposed to various durations of the ISO fire

10.3.3 Pin-spring connections

Both pin-pin and pin-roller connections are generally not realistic in real construction, the performance of connections used in the truss structure in the aspect of providing restraints against the horizontal translation lies between the pin-pin and pin-roller connections. To model this behaviour, an unheated axial spring was attached to the structure with a cross section the same as one top chord angle. Based on the description in Section 4.1 and 2.4.2, this spring would yield at 209kN under ambient temperatures, and it represents the limiting strength of a possible connection.

The structure did not fail under the ISO834 standard fire before the end of the simulation; and neither the other five less severe fires caused the failure of the structure. Figure 10-11 shows the axial force at the top chord and the web near the pinned connection. This figure shows the structural behaviour of the pin-spring connected truss is in between the pin-roller and pin-pin connected truss shown in Figure 10-2 and Figure 10-7 respectively

Figure 10-12 shows the horizontal reaction force at the spring end, which equals the horizontal component of the axial forces shown in Figure 10-11. Because the horizontal reaction force never reached 209kN, the spring did not yield during the simulation.

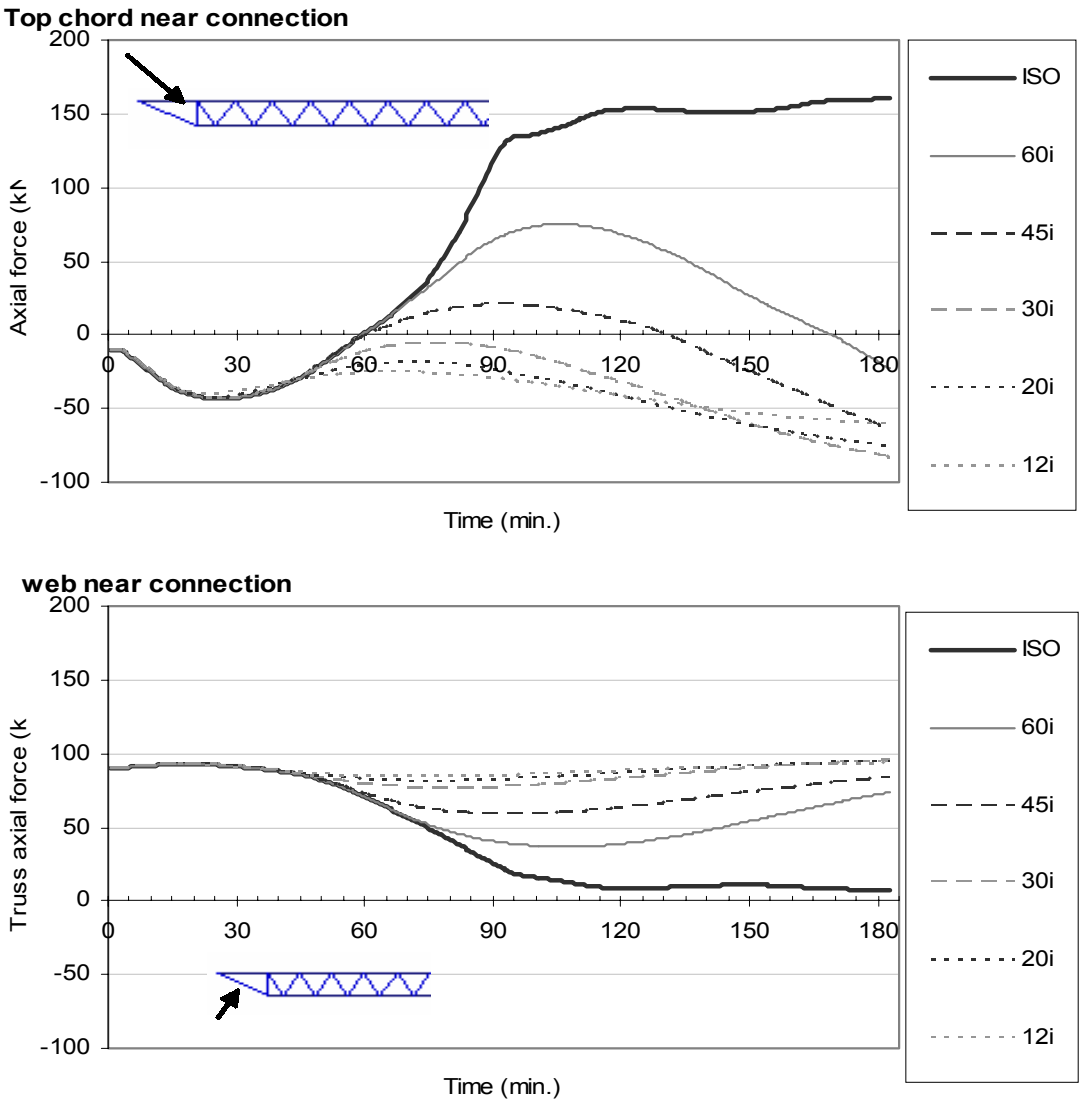

Figure 10-11 Axial force in insulated pin-spring truss near the pinned end

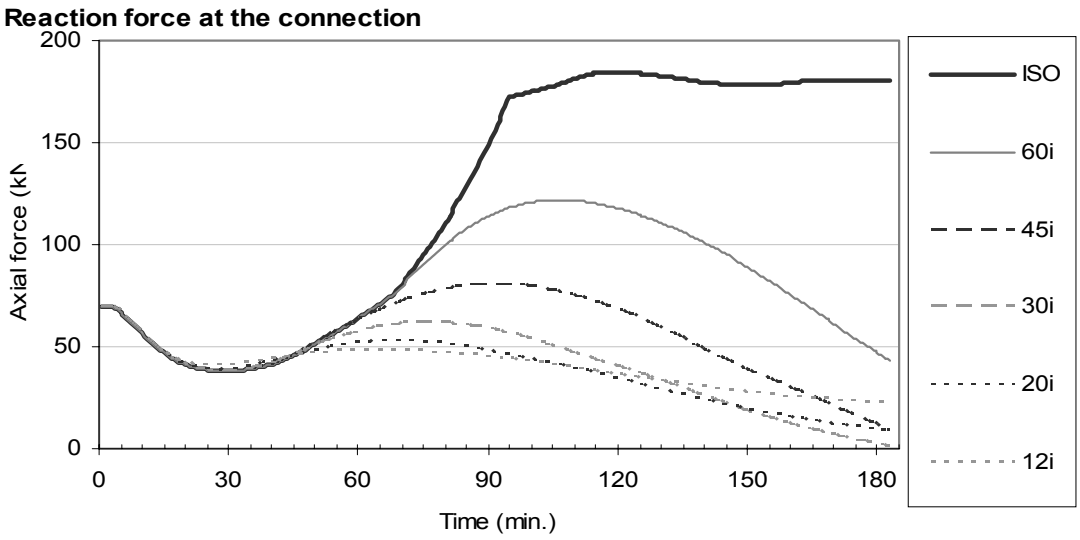

Figure 10-12 Horizontal reaction force in insulated pin-spring truss near the spring end

Figure 10-13 shows the midspan vertical displacement of a pin-spring connected truss. The figure has a similar shape to the vertical displacement graph of the pin-pin connected truss shown in Figure 10-10. This figure is also quite similar to the pin-roller case shown in Figure 10-4, except the curve for the ISO fire without a decay phase did not show a sudden drop during the simulation.

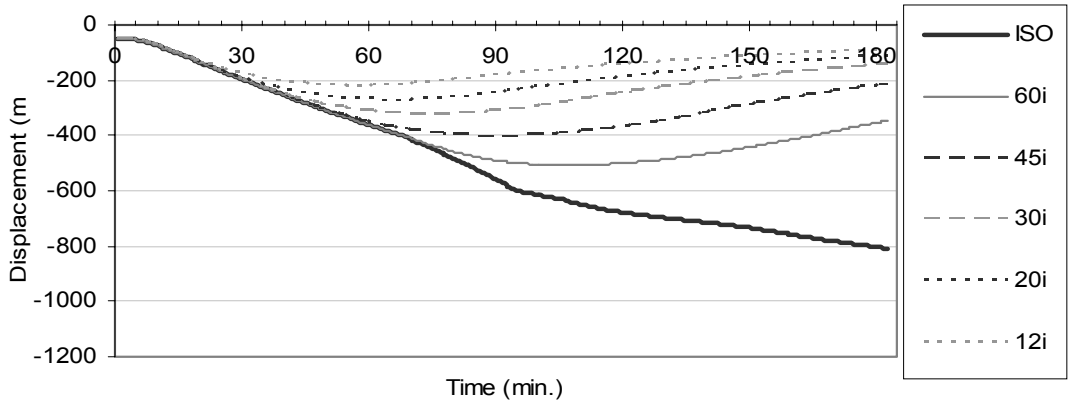

Figure 10-13 Vertical displacement at the midspan of the insulated pin-spring truss

Figure 10-14 shows the horizontal displacement at the spring end, where the inward movement is positive. The horizontal displacement stopped increasing when the axial force became constant or reduced, which indicates the spring did not yield during the simulation. The horizontal displacement went further outwards than its original position at the end of the simulation; this situation was also observed in the pin-roller case shown in Figure 10-5. This increase could have resulted from the thermal bowing arising from the temperature in the steel being lower than in the concrete as the insulation delayed the temperature rise in the steel section.

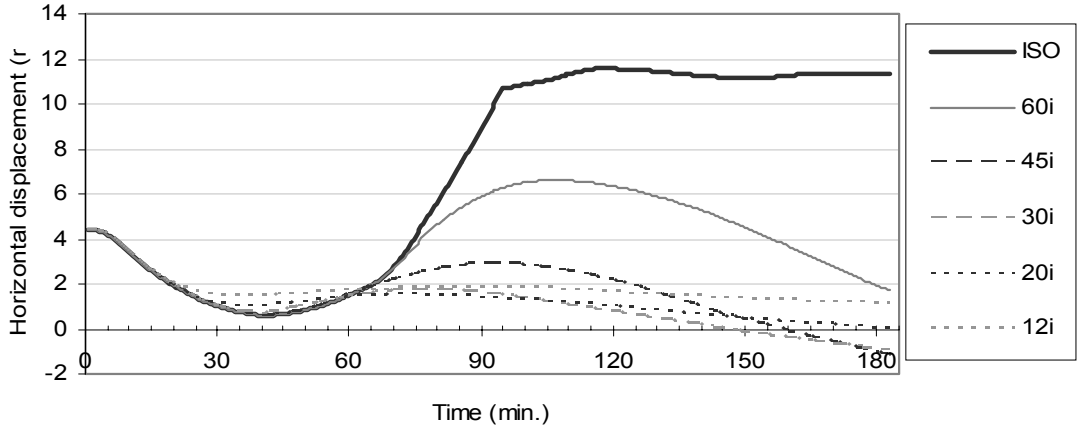

Figure 10-14 Horizontal displacement at the spring end in insulated pin-spring truss

Figure 10-15 compares the behaviour of the insulated pin-spring case with the pin-roller and the pin-pin case exposed to 45 minutes of the ISO fire. The figure shows the behaviour of the pin-spring case lies between the pin-roller and pin-pin case. However, all the graphs also indicate that the structural behaviour in the pin-spring case was more similar to the pin-pin case with the curves having of a similar shape but with a smaller magnitude.

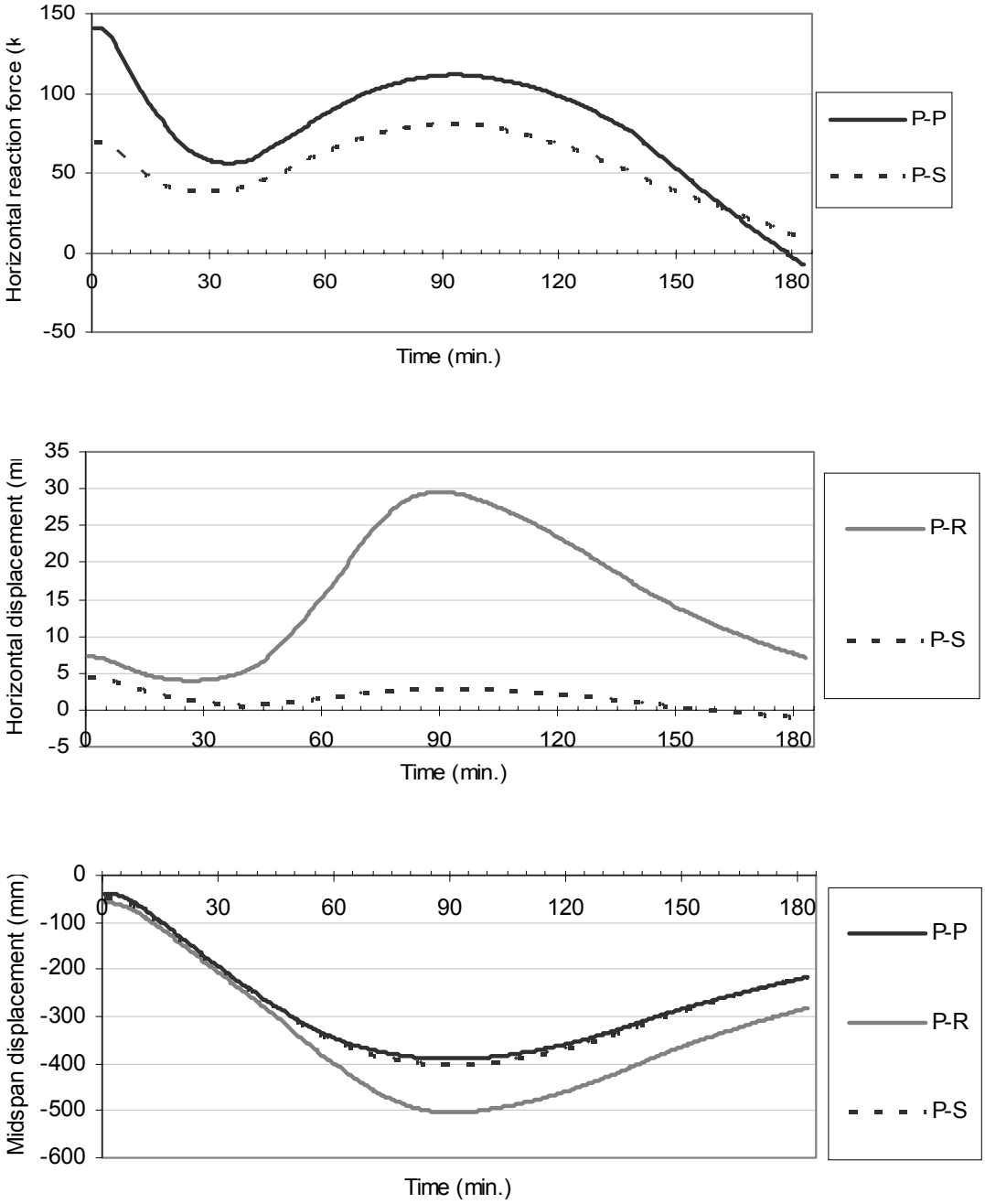

Figure 10-15 Comparison of insulated truss with different connections exposed to 45 minutes of the ISO fire with a decay phase: (from the top) horizontal reaction force at the spring; horizontal displacement at the end if permitted; vertical displacement at the midspan of the truss

10.4 Summary of the simulation results of insulated truss structures

This chapter discussed the behaviour of an insulated truss with three types of supporting conditions exposed to the ISO fire: pin-roller, pin-pin and pin-spring. The pin-roller connected truss lasted 74 minutes and pin-pin 122 minutes under the ISO fire, and the pin-spring connected truss could last longer than 3 hours under the ISO fire.

The deflection and the axial force of the pin-spring structure were found to lie between the pin-pin and pin-roller connected truss. The spring can represent connections that are able to yield when the beam axial force is large. The finding in this chapter shows that allowing a certain amount of horizontal translation at the supports can increase the fire resistance.

11 Simulation results of non-insulated truss structures exposed to the ISO fire with a decay phase

Non-insulated trusses are not used for fire design. However, to understand the behaviour of the floor truss of the World Trade Center towers under fire if the insulation was lost, a non-insulated truss structure was simulated with dimensions and layout the same as the models in Chapter 10. This chapter discusses the simulation results of the non-insulated structure exposed to the ISO834 standard fire and to various durations of the ISO fires with a decay phase. The decay rate of the fire temperature is as explained in Section 5.

11.1 Thermal analysis results

In the structural analysis, the pin-pin connected truss reached a structural failure after 22 minutes under the ISO834 standard fire. Five durations of the ISO fire with a decay phase, ranging from 6 to 16 minutes of the ISO fire, were used to observe the behaviour of the truss while cooling. Figure 11-1 shows the temperatures of the bottom chord, truss web, top chord and concrete of a non-insulated truss exposed to various length of the ISO fire. The temperature of the top and the bottom chord and the web were almost the same and similar to the fire temperature, as expected in an unprotected structure.

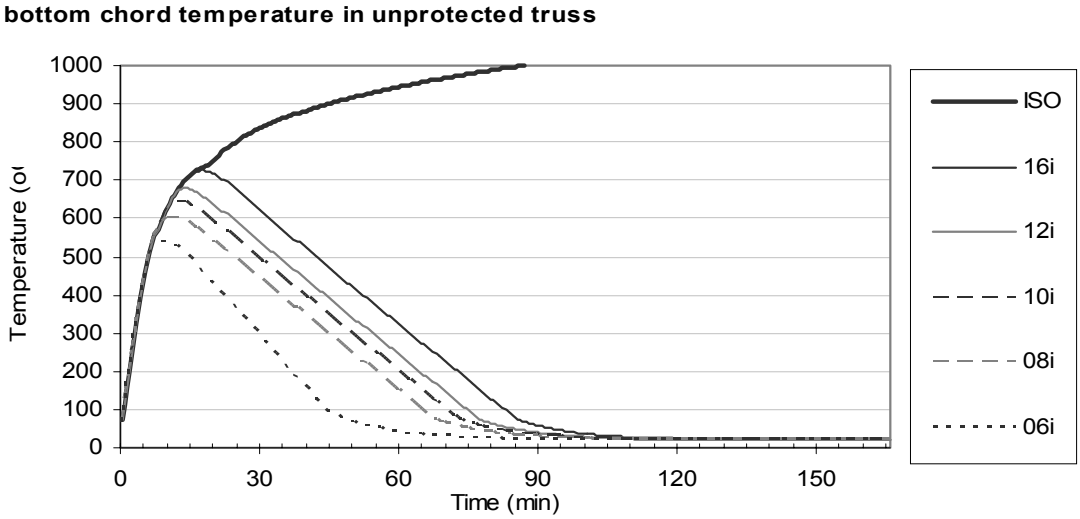

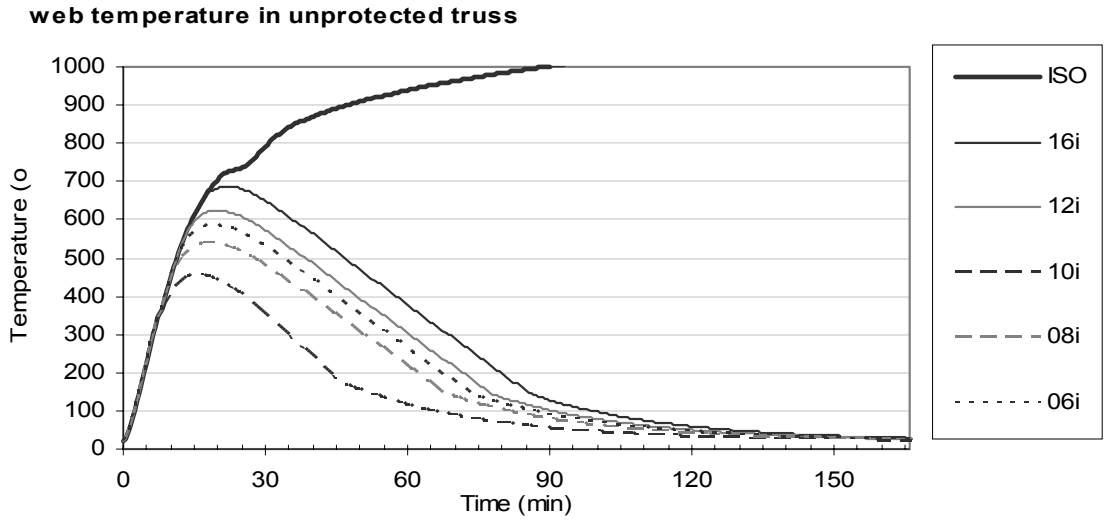

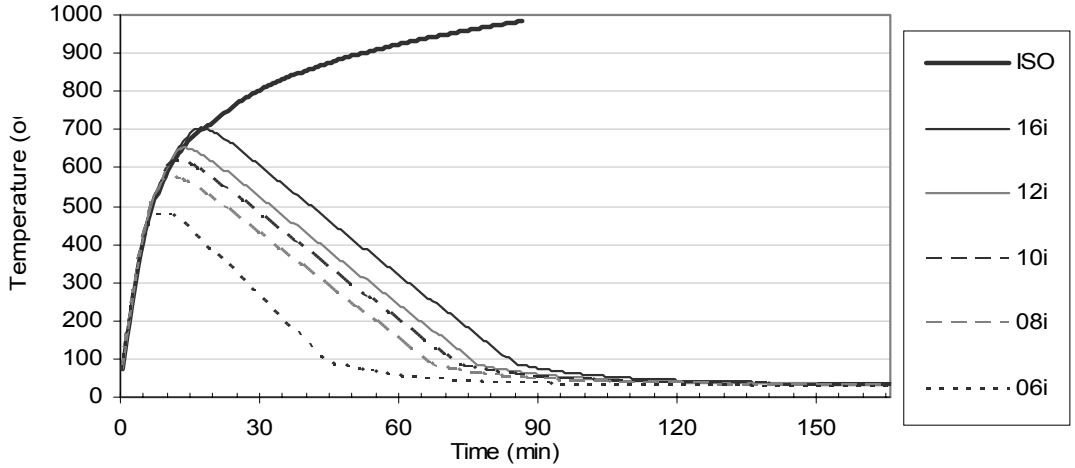

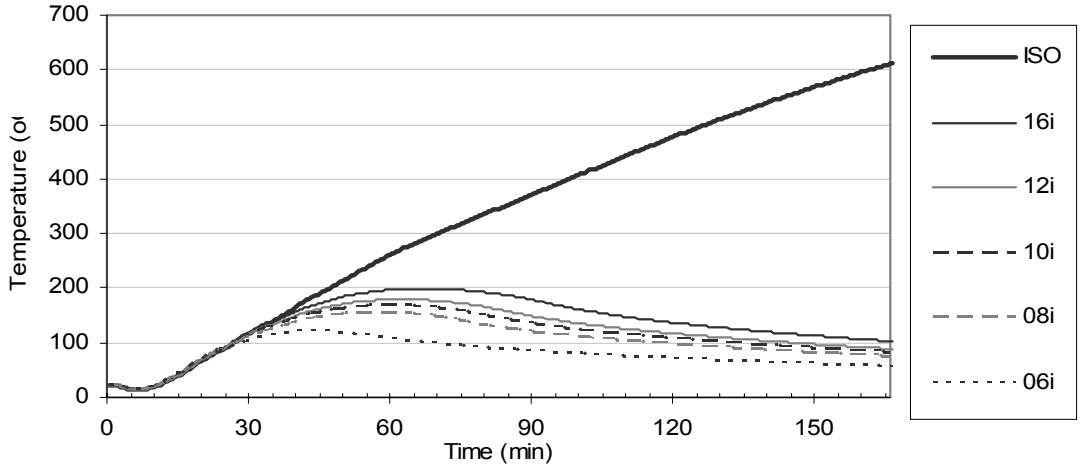

Figure 11-1 Thermal analysis outputs for non-insulated truss exposed to various durations of the ISO fire

11.2 Structural analysis results

The three connection types discussed in the previous chapter were also modelled in the insulated truss: pin-roller, pin-pin and pin-spring connections. Each is discussed separately in the following sections.

11.2.1 Pin-roller connected truss

The pin-roller truss exposed to the ISO834 standard fire had a run-away failure after 10 minutes. Two other fires with eight and six minutes of the ISO fire before the decay phase were used to observe the behaviour of the structure while cooling.

Figure 11-2 shows the axial force of the members near the connection. The figure shows that a larger fire induced a larger axial force. The horizontal reaction force at the connection is zero in a pin-roller structure. Compared to Figure 10-2 for the insulated pin-roller truss, the fluctuation in the axial force of the top chord and the webs was larger. This was due to the insulation reducing and delaying the change of steel temperatures.

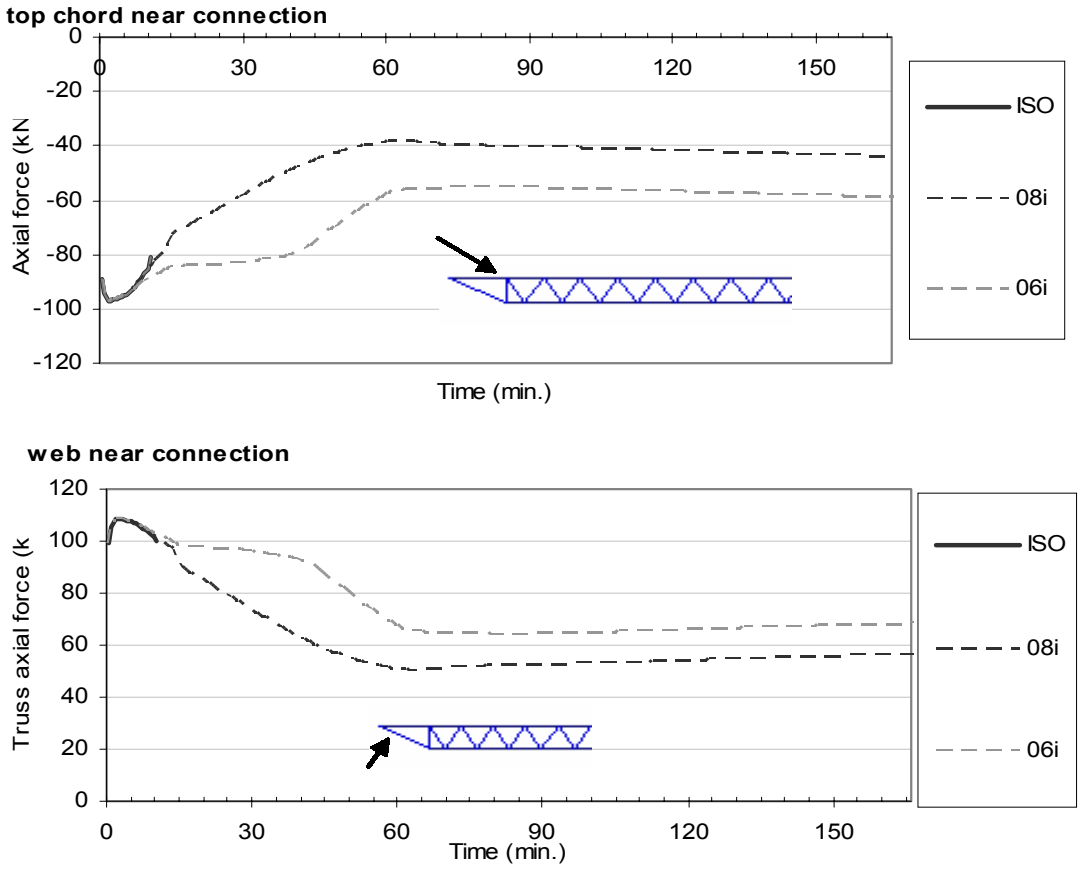

Figure 11-2 Axial force in non-insulated pin-roller truss near the pinned end

Figure 11-3 shows the vertical displacement at the midspan of the truss. During the decay phase the displacement became constant under both fires. The findings from this figure are similar to the vertical displacement plots of pin-roller connected composite or steel beams, Figure 5-23(a) and Figure 7-12(a), that a larger fire caused a larger displacement, and the maximum displacement occurred when the temperature in the structure was at its highest. In this truss structure, since the size of the fires with a decay phase was not large, the midspan remained at the position of its permanent displacement shortly after the decay phase of the fire.

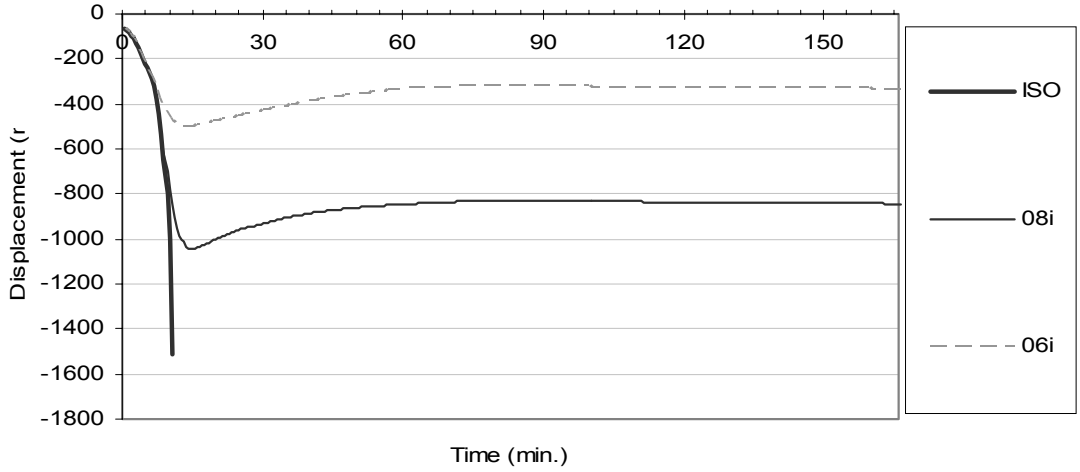

Figure 11-3 Vertical displacement at the midspan of the non-insulated pin-roller truss

Figure 11-4 shows the horizontal displacement at the roller end of the truss. This figure looks similar to Figure 5-23(b), the horizontal displacement of the pin-roller composite beam. Both figures suggest that a larger fire triggers a larger inwards movement. The roller end had an inward displacement at the end of the simulation, and the displacement increased gradually while cooling without reaching a steady state.

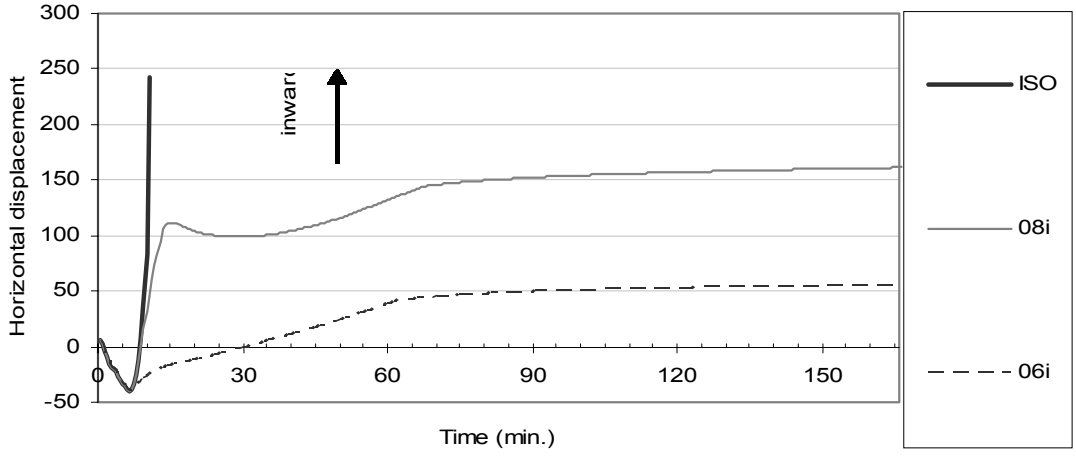

Figure 11-4 Horizontal displacement at the roller end in non-insulated pin-roller truss

11.2.2 Pin-pin connected truss

The truss with pin-pin connections reached failure after 22 minutes under the ISO fire due to the large tensile axial forces in the chords. Six fires following six to 20 minutes of the ISO fire before the decay phase were also used in the simulation. Figure 11-5 shows the axial force of the top chord and the web near the end connection. Before heating, the lack of insulation does not affect the structural behaviour, and both members were in tension as shown in Figure 10-6. When the truss was heated, the top chord immediately went into compression. The trend of the axial forces in the top and bottom chords are similar to the top and bottom flange stresses in the composite beam shown in Figure 5-8 and Figure 5-9. At the end of the simulation, the tensile force in the top chord was much larger than the force in the web, which indicates that the connections had a large horizontal reaction force. The changes of the axial force in the web were much less than in the top chord which has been observed before in the insulated pin-pin truss.

Figure 11-5 indicates that the force at the top chord was not in equilibrium with the force at the bottom chord at the end of the simulation, so the overall structure was in tension. Figure 11-6 shows the horizontal reaction forces at the connection under three of the six fires. The trend is similar to that for the axial force in pin-pin connected composite or steel beams with the maximum tensile axial force occurring at the end of the simulation. The magnitude of the maximum tensile reaction force in this case was larger than the maximum compressive force. The maximum tensile reaction force exceeded 300kN, and the maximum compressive reaction force was larger than 100kN. Both values are larger than the horizontal reaction forces in the insulated truss shown in Figure 10-8. In summary, a very high tensile horizontal reaction force was induced even when the truss was exposed to a small fire.

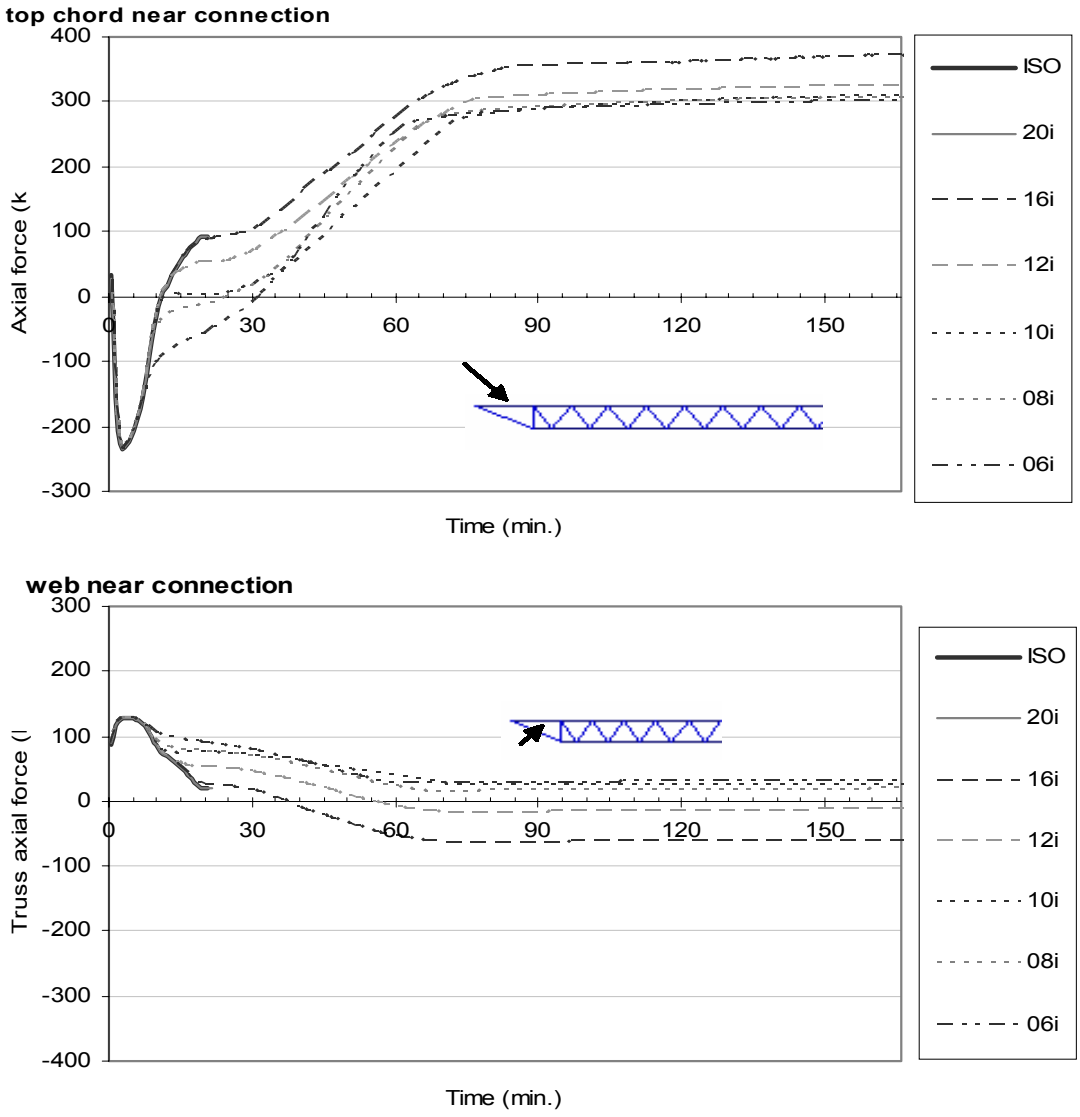

Figure 11-5 Axial force in non-insulated pin-pin truss near one connection

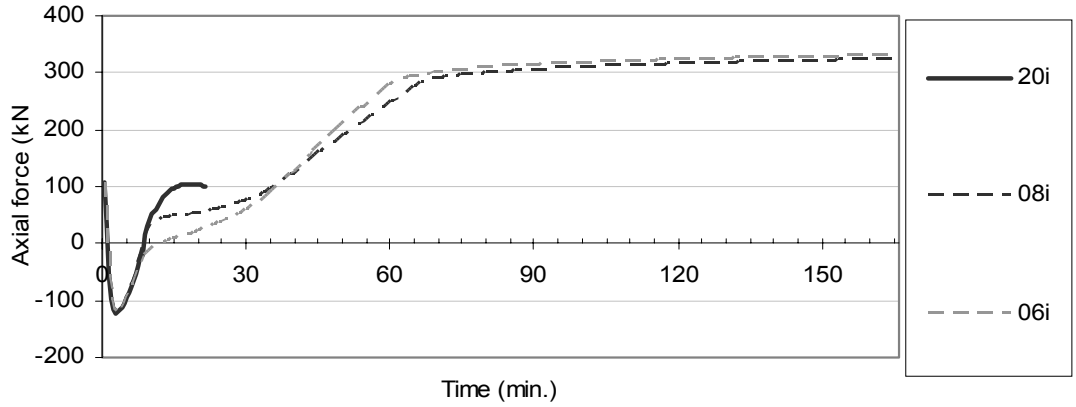

Figure 11-6 Horizontal reaction force at the connection

Figure 11-7 shows the vertical displacement at the midspan of the truss. The increase in the rate of displacement was smaller than in the pin-roller case shown in Figure 11-3. The maximum displacements under different fires in this case were smaller than in the pin-roller truss case, but the rate of reduction in the displacements while cooling was larger. One can also find that both the magnitude and the rate of change of the vertical displacement were larger than for the insulated truss shown in Figure 10-10.

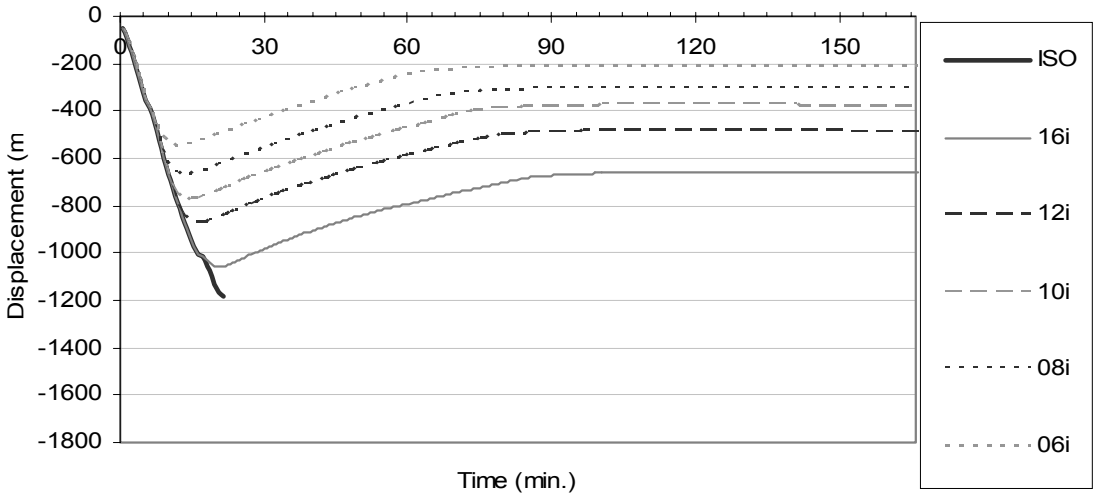

Figure 11-7 Vertical displacement at the midspan of the non-insulated pin-pin truss

11.2.3 Pin-spring connections

The pin-spring connections were simulated in the non-insulated truss for the same reason as in the insulated truss. The spring was the same as in the insulated truss models with an axial force capacity of 209kN.

The structure failed after 24 minutes under the ISO834 standard fire, four other fires having less than 24 minutes of the ISO fire were used for comparison. Figure 11-8 shows the axial force at the top chord and the web near the pinned connection. This figure shows the structural behaviour of the pin-spring connected truss lies across Figure 11-2 and Figure 11-5 for the pin-roller and pin-pin connected truss cases. The sum of the horizontal components in this figure equals the horizontal reaction force shown in Figure 11-9. Figure 11-9 indicates that in a fire with a decay phase, the horizontal reaction force reached 209kN in 60 minutes for all different sizes of fire, at which point the spring reached yield.

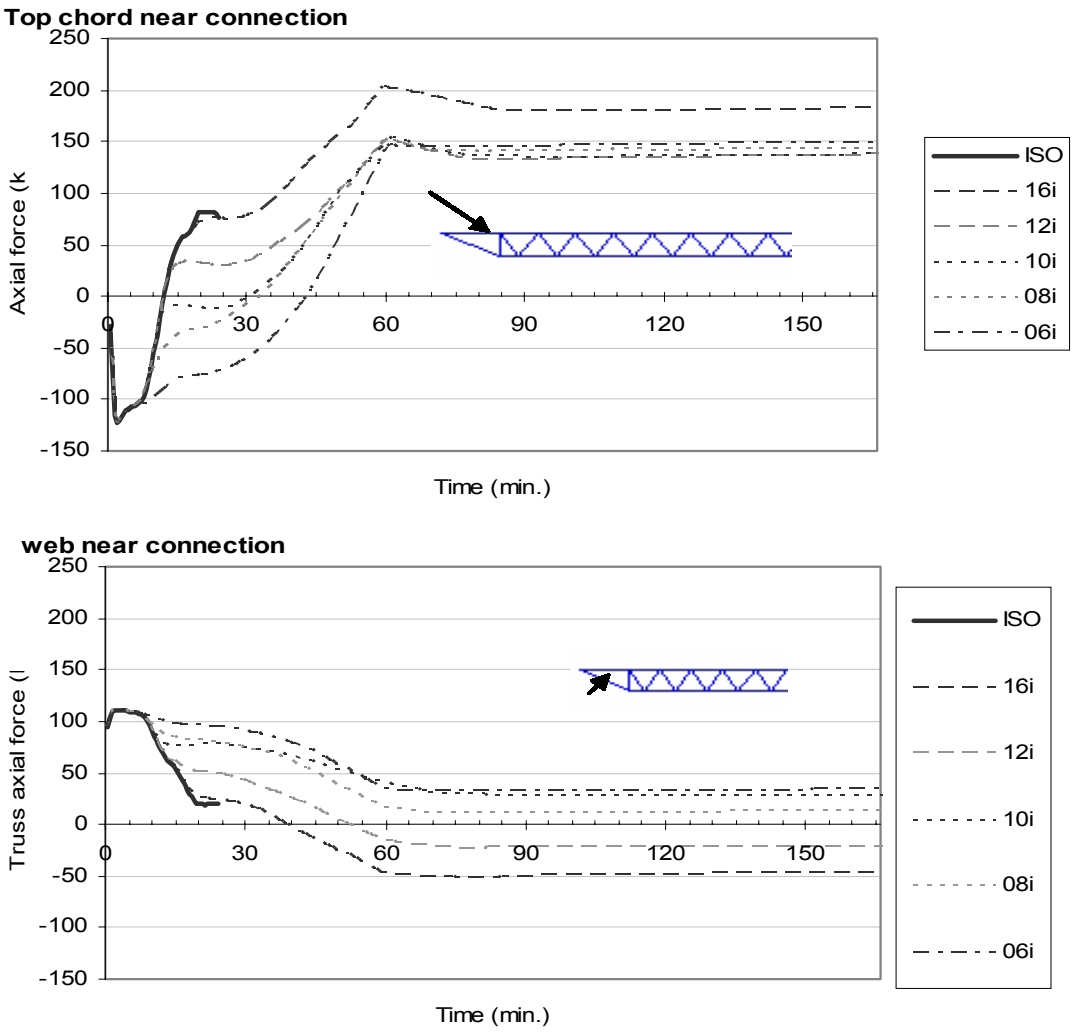

Figure 11-8 Axial force in non-insulated pin-spring truss near the pinned end

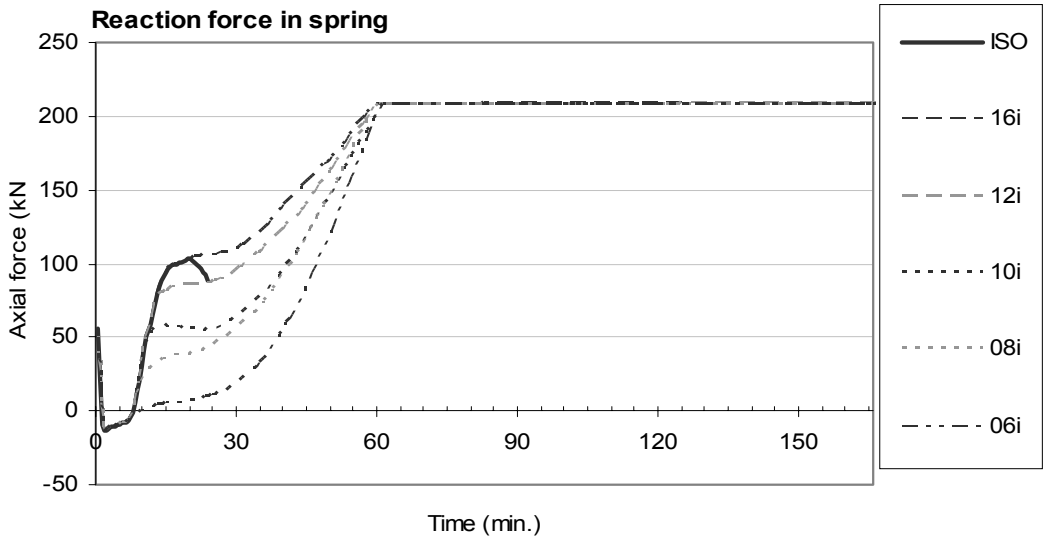

Figure 11-9 Horizontal reaction force in non-insulated pin-spring truss near the spring end

Figure 11-10 shows the axial forces of the truss elements at the midspan. The shape of the midspan top chord axial force plots is not similar to the plots near the pinned connection but more like a mirror image of the midspan bottom chord plots. The forces became constant after 60 minutes because the horizontal reaction force reached its maximum, which is the force capacity of the spring.

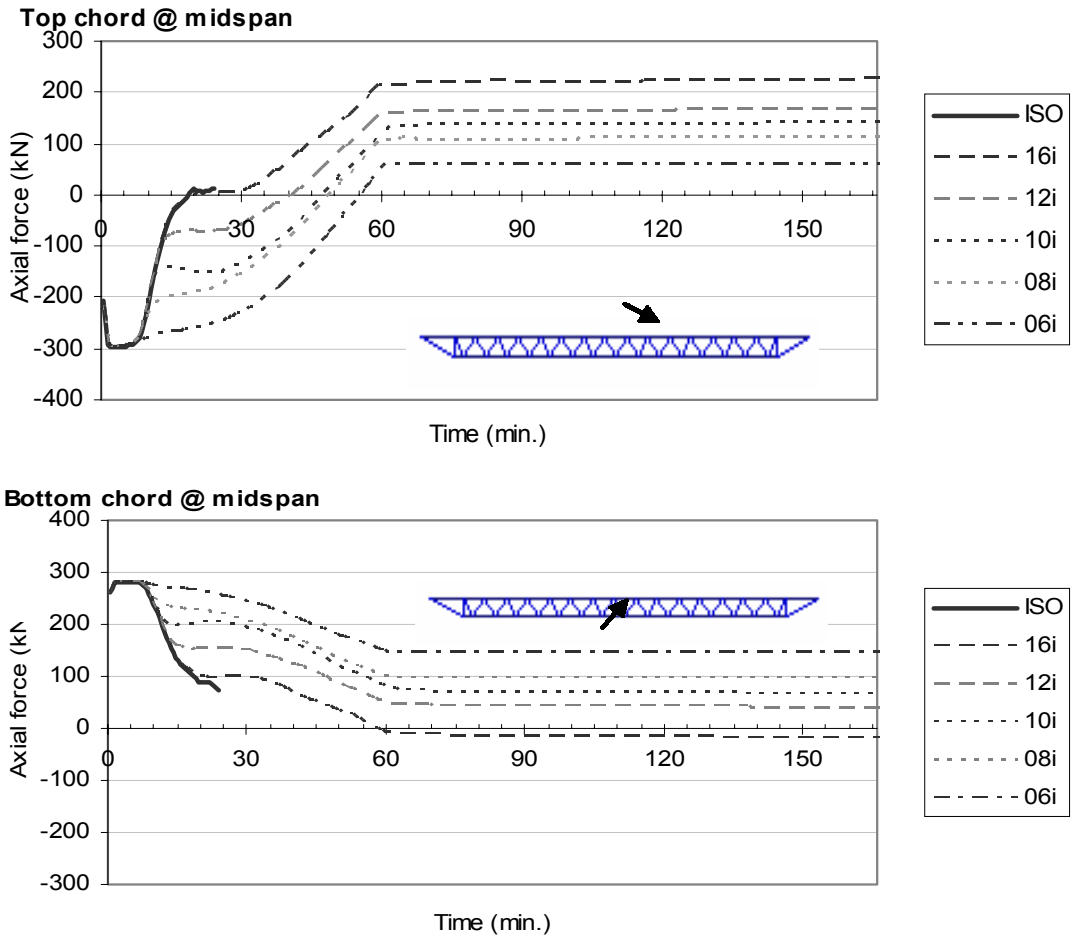

Figure 11-10 Axial force of the top and bottom chord at the midspan in non-insulated pin-spring truss

Figure 11-11 shows the midspan vertical displacement of a pin-spring connected truss. The figure has a similar shape to Figure 11-7, the vertical displacement graph of a pin-pin connected truss. However, the permanent displacement in this case was larger because a limited amount of horizontal translation was allowed at one end, and all the curves went into a steady state at 60 minutes. This was different to the pin-pin connected truss where the time of reaching the permanent displacement was influenced by the size of the fire.

The yielding of the spring is best observed from the horizontal translation plots at the spring end as shown in Figure 11-12. The displacement was relatively small and steady before 60 minutes. During 60 to 80 minutes, the horizontal translation rapidly increased by almost 50mm. After 90 minutes, the displacement increased slowly but steadily. This confirms that the spring started yielding at 60 minutes. The yielding of the spring is also the main reason for the difference between this figure and Figure 10-13 of the insulated case, where the horizontal translations returned to their original position at the end of the simulation.

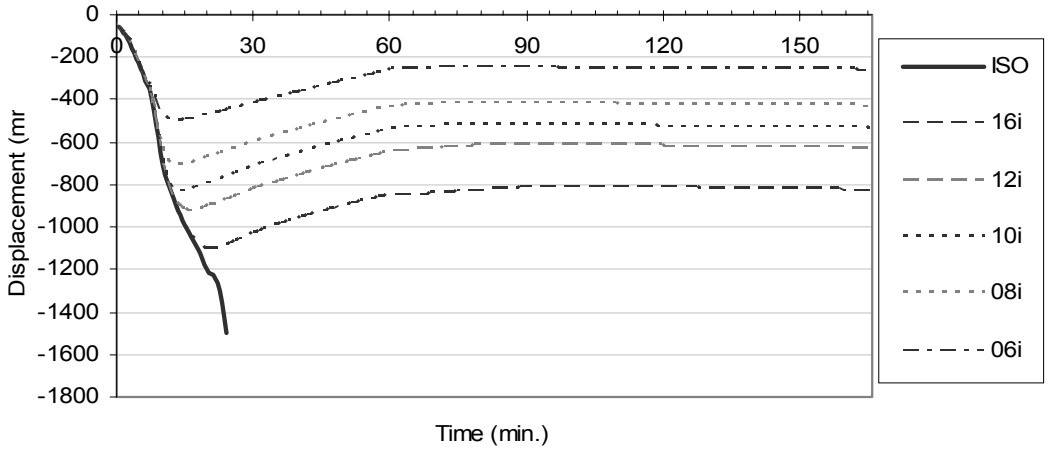

Figure 11-11 Vertical displacement at the midspan of the non-insulated pin-spring truss

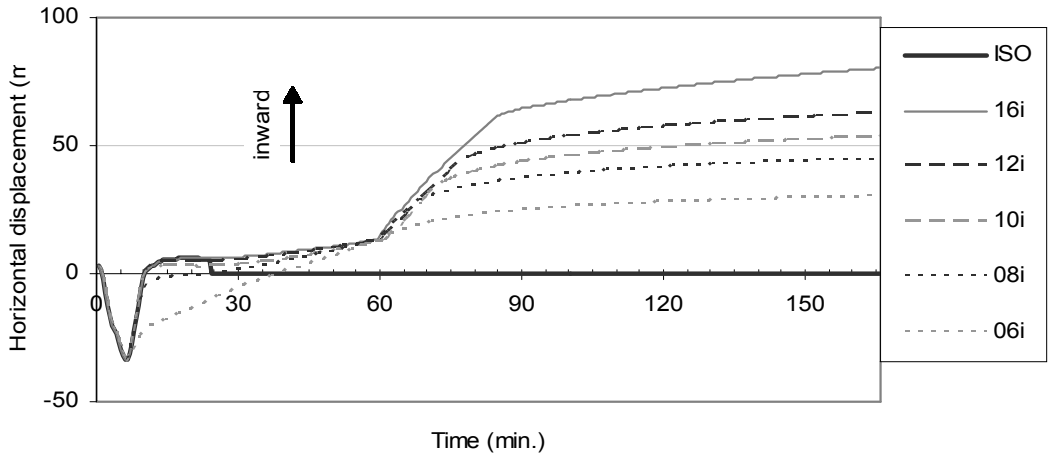

Figure 11-12 Horizontal displacement at the spring end in non-insulated pin-spring truss

Figure 11-13 shows the comparison of an unprotected truss with different supporting conditions exposed to 8 minutes of the ISO fire before the decay phase. All the plots can be divided into two segments: prior to and after the spring yields at 60 minutes. During the first 60 minutes, the force and displacement curves of the pin-spring truss were closer to the pin-pin truss. However, the limiting amount of freedom in horizontal translation at the end reduced the forces and increased the midspan vertical displacement as observed in the previous chapters. After 60 minutes, the curves of the pin-spring connected truss started to follow the trend from the pin-roller connected truss, especially the plots for the horizontal displacement, which had a sudden increase after 60 minutes and followed the shape of the pin-roller connected truss curve afterwards.

Figure 11-13 shows that behaviour of the pin-spring connected structure lies between the pin-pin and pin-roller connected structure. However, because the failure mechanisms for these two structures were different, with the pin-roller structure having a run-away failure, and the pin-pin structure yielding as a result of high temperatures and stresses, the simulation results show that the pin-spring truss lasts longer than the other two structures.

The major difference between the insulated case and this case is the yielding of the spring. Both cases demonstrated that without the yielding of the spring, the pin-spring behaves like a pin-pin connected truss; after the yielding of the spring, the pin-spring connected truss would behave more like a pin-roller connected truss.

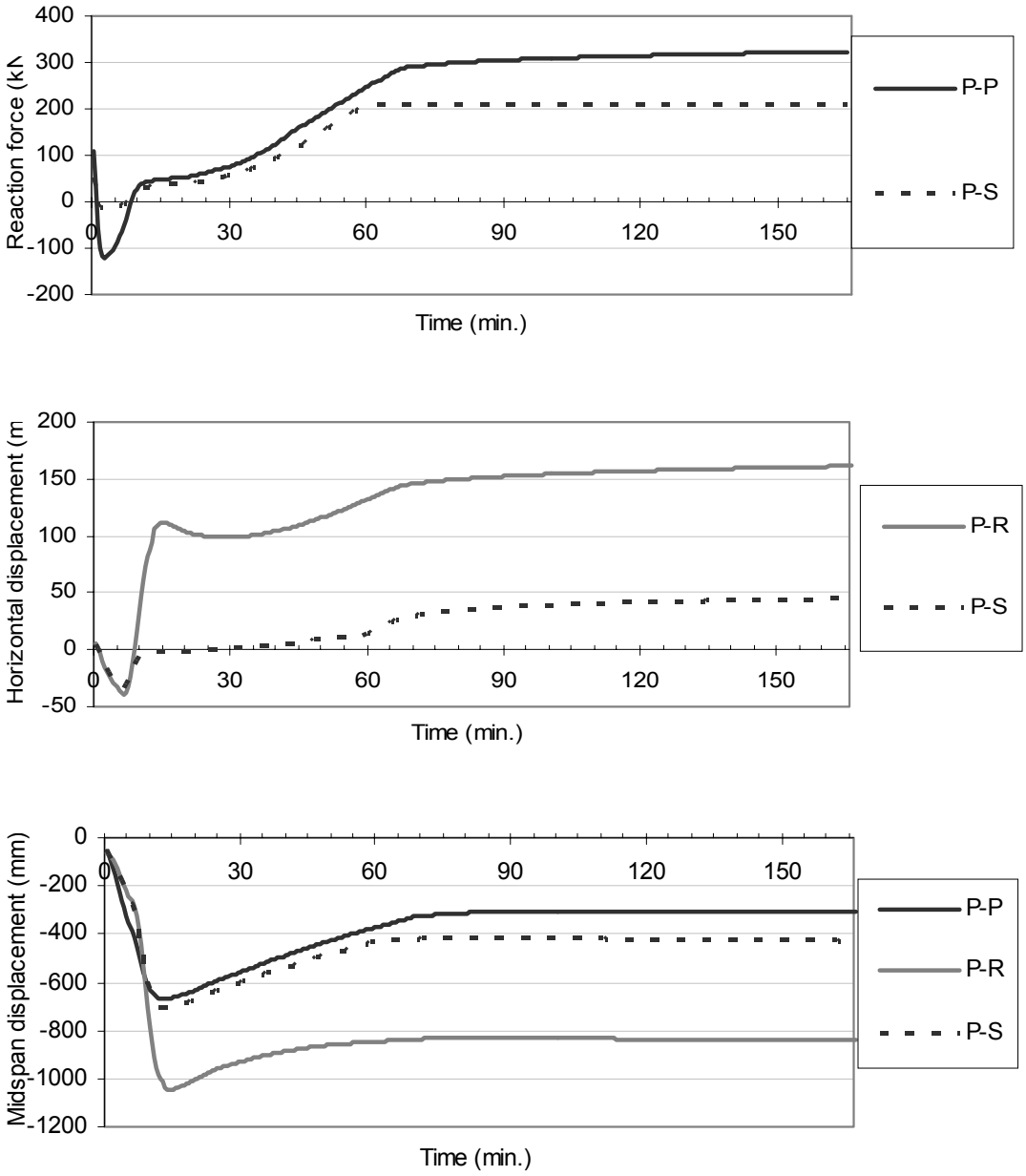

Figure 11-13 Comparison of truss with different connections exposed to 8 minutes of the ISO fire with a decay phase: (from top) reaction force at the spring; horizontal displacement at the end if permitted; vertical displacement at the midspan of the truss

11.3 Simulation results of non-insulated truss structure exposed to non-standard fire

The fire temperature in this section is higher than the ones chosen before; this may provide a different result than what were observed previously. This section studies the pin-spring connected truss model only.

11.3.1 Selection of the non-standard fire

FEMA (2002) calculated that the fire caused by the explosion in the two World Trade Center towers in 2001 developed to 1000^{o}C in 20 seconds. The estimated fuel load may have let the fire last for 8 minutes. However, no fire curves were shown in the report. It was assumed in this report that the fire developed linearly from 20^{o}C to 1000^{o}C in 20 seconds. It was also assumed the fire died quickly after the burning period to simulate a rapid consumption of the fuel. Figure 11-14 shows the temperature of the super-fast fire.

11.3.2 Thermal analysis results

Figure 11-15 shows the temperature of the top and the bottom chord and the web in the truss exposed to the non-standard fire. Three fires chosen for study in this case went into the decay phase after eight, three or two minutes after the fire started. The bottom chord had a slightly higher temperature than the upper chord, and the temperatures in these members were higher than in the web. One of the possible explanations is that the small cross section of the web allowed the heat to dissipate much more easily than the other members; therefore the temperature in the web was more sensitive to the change of the fire temperature and decreased much earlier than the other members were.

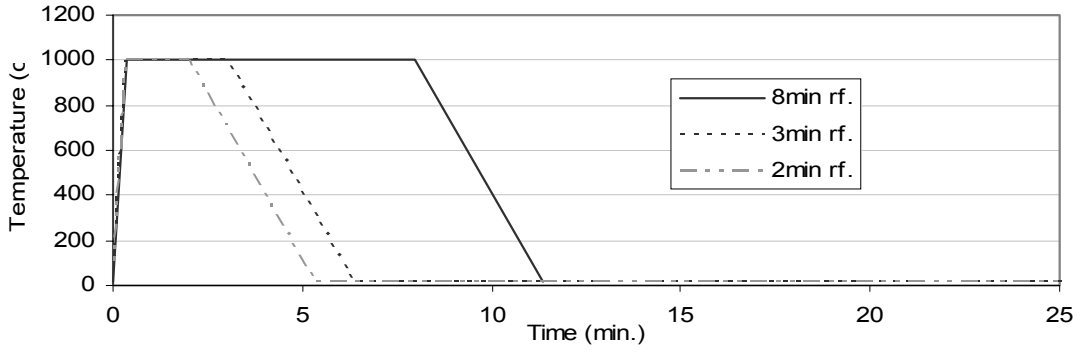

Figure 11-14 Temperature of the super-fast fire (notice the time scale is different)

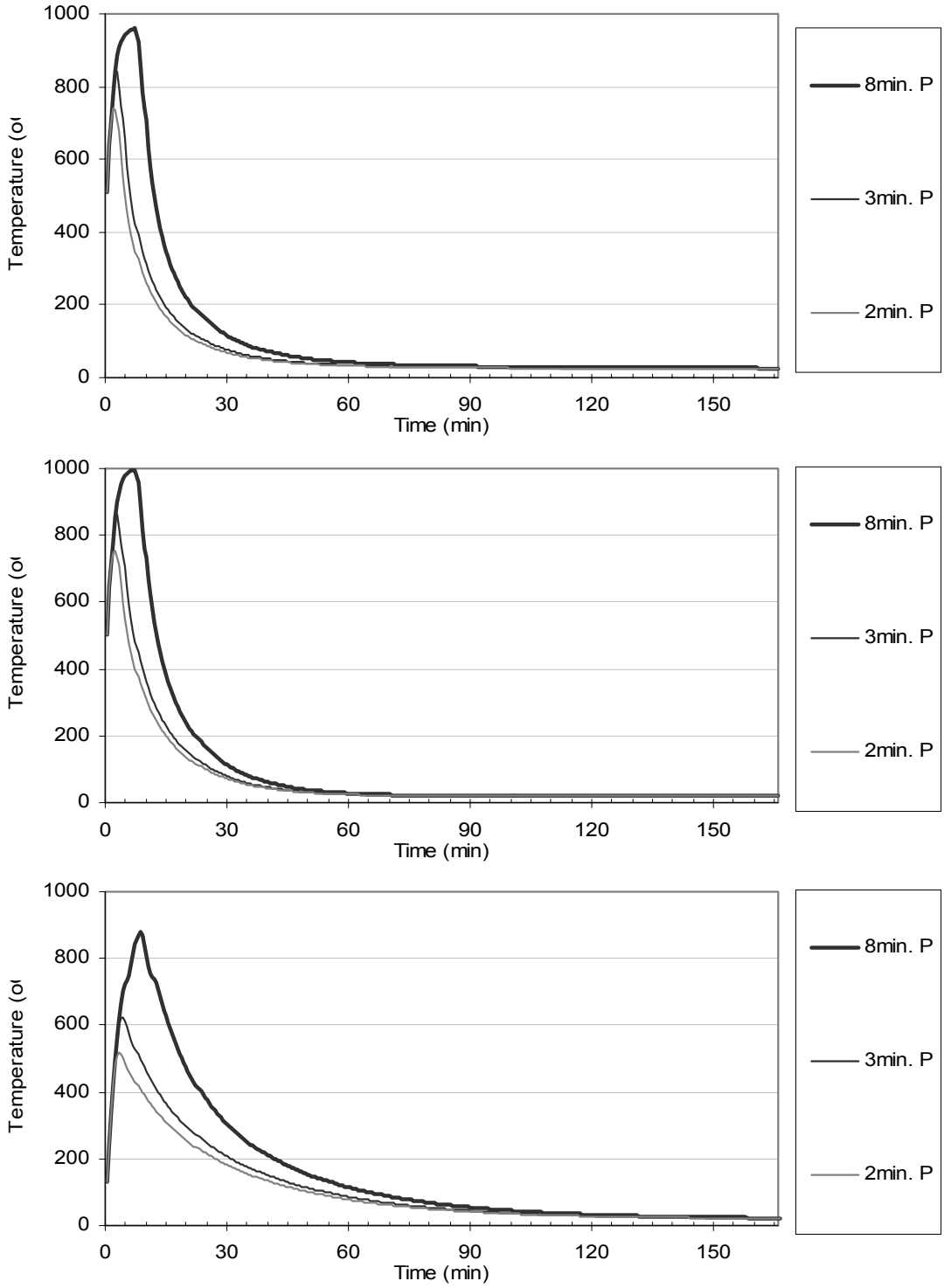

Figure 11-15 Temperatures of the truss members under a non-standard fire: (from the top to the bottom) at the angles of the top flange, at the angles of the bottom flange, at the web

11.3.3 Structural analysis results

In the structural analysis, only the pin-spring connected truss was simulated because this arrangement can represent the yielding of the connection as found in the Section 11.2.3. Figure 11-16 shows the axial force at the top chord and the web near the pinned connection. This can be read in conjunction with the plots for the pin-spring connected truss exposed to the ISO fire shown in Figure 11-8. The magnitude of the maximum axial force in the top chord was similar, but the time for the truss to reach this maximum was 50 minutes earlier. The force at the web was slightly smaller than under the ISO fire.

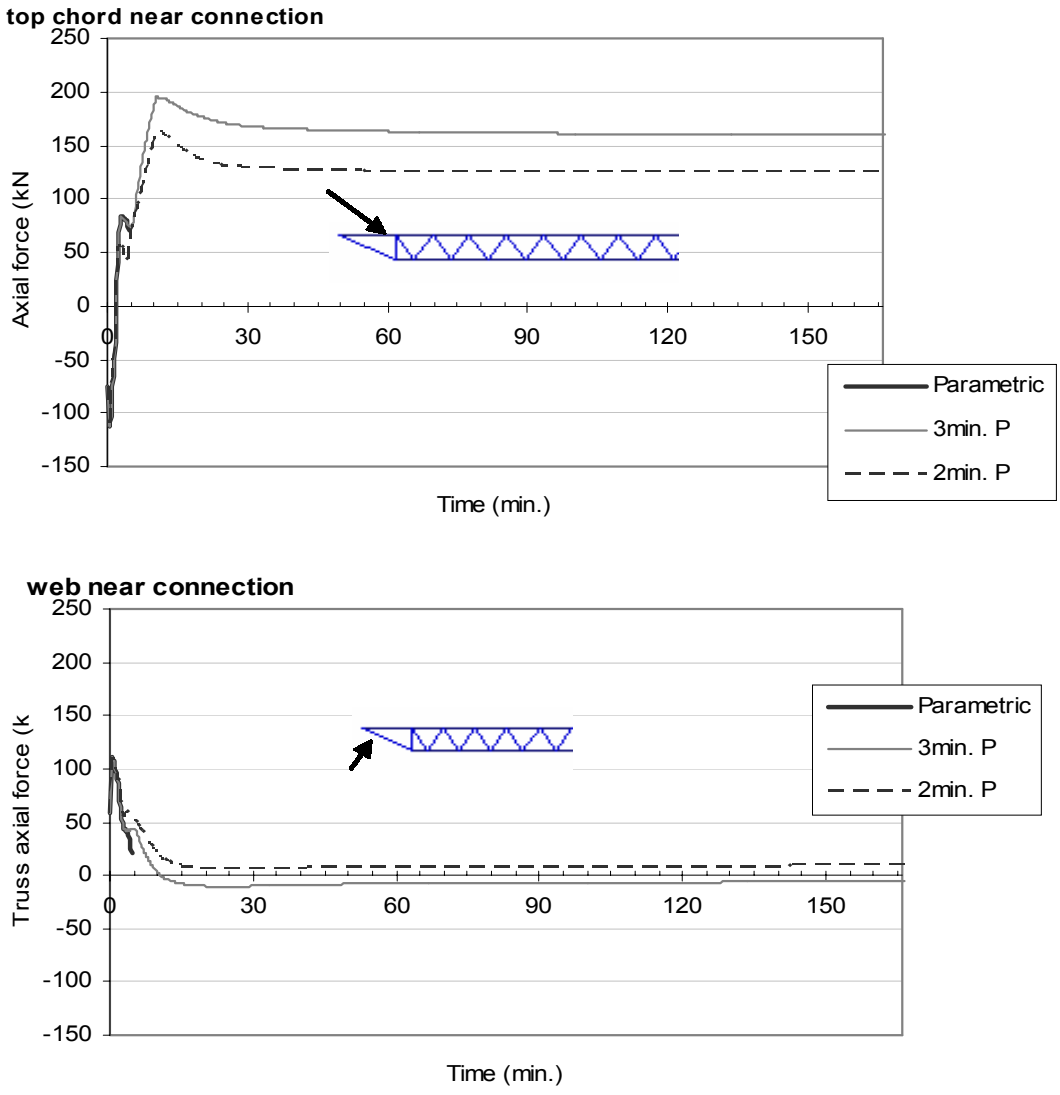

Figure 11-16 Axial force at the members near one connection

Figure 11-17 shows the horizontal reaction force at the connection. This is crucial for connection design. Comparing this figure with the one for the truss exposed to the ISO fire, Figure 11-9, it indicates that all the events that might occur before the spring yield were condensed into the first ten minutes. At 5 minutes, the vertical deflection at the midspan was recovering as shown in Figure 11-18, so the horizontal reaction force reduced slightly until the recovering of the midspan vertical displacement stopped. The axial spring yielded 50 minutes earlier than in the truss under the ISO fire, which shows a good agreement with the finding from the top chord axial force graph near the connection.

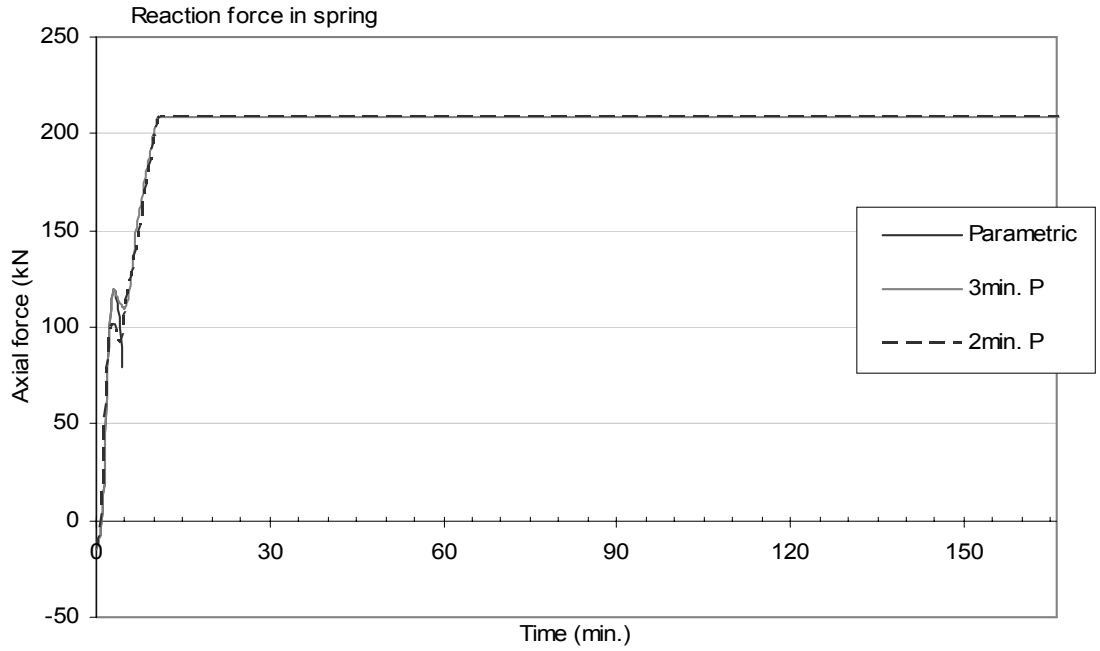

Figure 11-17 Reaction force at the connection

Figure 11-18 shows the midspan vertical displacement in the truss exposed to the non-standard fire. Compared to the vertical displacement under the ISO fire shown in Figure 11-12, the deflection was much larger before the beam failed in the case without the decay phase. However, in the other cases where the duration of fire is shorter, the vertical displacement generated a behaviour similar to that under the ISO fire with the extent of the maximum vertical displacement as well as the recovery during the decay phase.

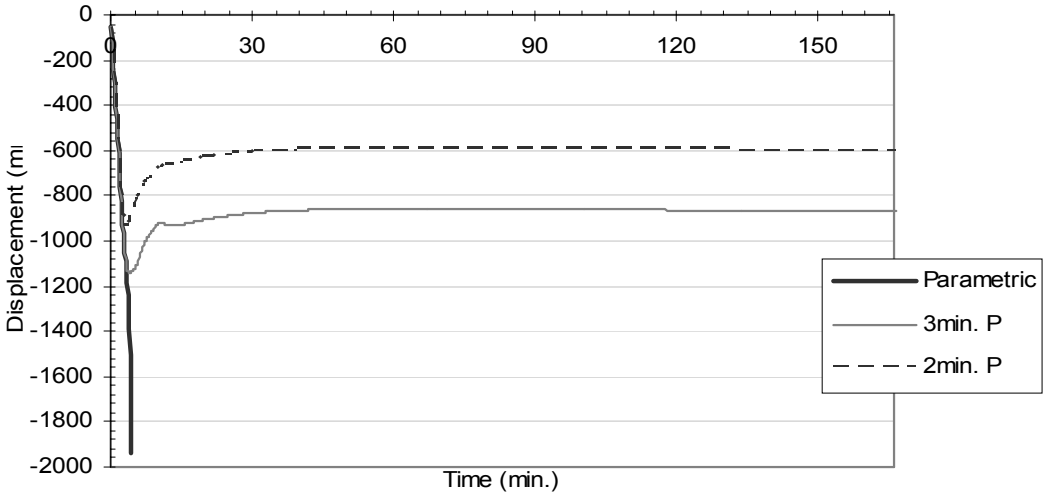

Figure 11-18 Vertical displacement at the midspan of the truss

Figure 11-19 shows the horizontal displacement at the spring end of the truss exposed to the non-standard fire. Comparing this with the case exposed to the ISO fire shown in Figure 11-12, the outward horizontal displacement during the heating phase was smaller. However, this could be due to the time-step of extracting the data not being fine enough. Nevertheless, the inward movement during the decay phase of these cases were similar. It is known from the vertical displacement graph that the thermal expansion of the beam only dominated the horizontal displacement very briefly before the vertical deflection at the midspan started to affect it significantly.

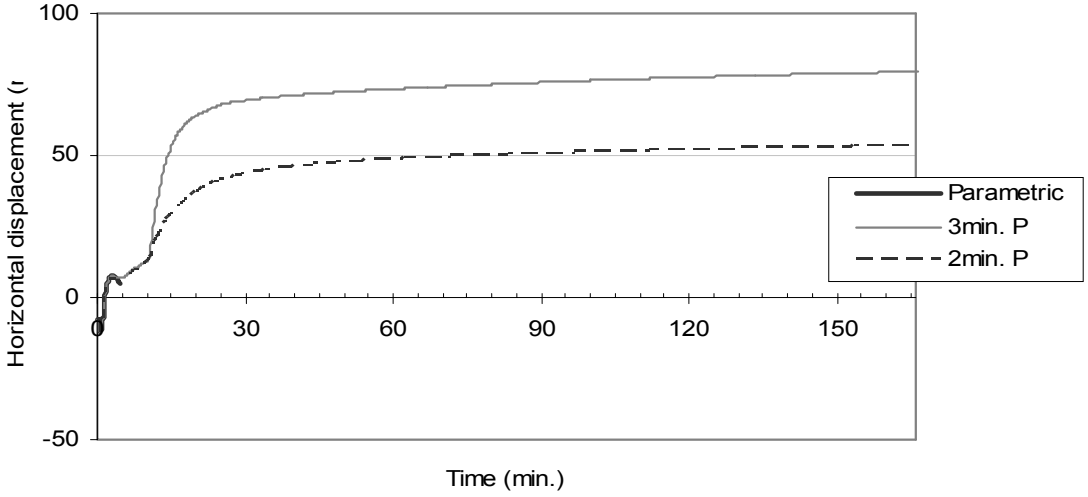

Figure 11-19 Horizontal displacement at the spring end in the truss

11.3.4 Alternative super-fast fire

A similar analysis was carried out with a fire that grew like the super-fast fire, remained at the peak temperature for 1 minute, and decayed following the decay rate from the Eurocode shown in Figure 5-1. The fire temperature is shown in Figure 11-20.

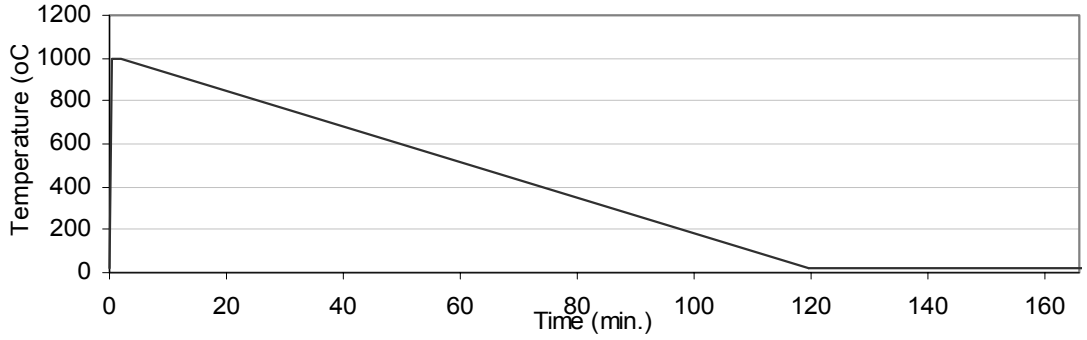

Figure 11-20 Alternative super-fast fire temperature

Because this alternative super-fast fire induced temperatures in the structural elements similar to those from the 8 minutes of super-fast fire discussed previously as shown in Section 14.2.1 in Appendix 2, the structural behaviour was similar as well, and the beam failed in around 4 minutes after the fire started, which is shown in Section 14.2.2 in Appendix 2. This confirmed the finding in the Chapter 9 that the temperatures of the element dominate the structural behaviour instead of the heating time.

11.4 Summary and further discussion of the simulation results of non-insulated truss structures

11.4.1 Summary of results

This chapter discussed the behaviour of a non-insulated truss also with three types of supporting conditions exposed to the ISO fire, as in the previous chapter, i.e. pin-roller, pin-pin and pin-spring. It also looked into the behaviour of a pin-spring connected truss exposed to a fire with very rapid growth and decay rate.

Without a layer of insulation, the pin-roller connected truss lasted 10 minutes, pin-pin 22 minutes, and pin-spring 24 minutes under the ISO fire. The pin-pin and pin-roller connected trusses have a behaviour very similar to the single span composite beam, with the top and bottom chord axial force being similar to the top and bottom flange stresses plotted in Chapter 5. In the pin-spring connected truss, the axial spring has a force capacity of 209kN, and all the fires used in this section caused the spring to yield in tension during the decay phase. During the heating phase the pin-spring truss did not exhibit a run-away failure as in a pin-roller truss, and the yielding spring limited the axial force so the pin-spring truss was able to last longer than the other two cases under the ISO fire.

The last part of this chapter reviewed the simulation results of exposing a pin-spring connected truss to a very rapid fire. The horizontal reaction force and the axial force diagrams all indicate that the magnitude of the force was the same as under the ISO fire limited by the capacity of the spring. However, all the events that would occur in the truss before failure happened much faster and were condensed into the first 10 minutes. When the fire burned for longer than 4 minutes, the structure would fail. The result shows that the actual failing time will be very different to the failure time in the ISO fire, reducing from 24 minutes to 4 minutes.

11.4.2 Comparison with the insulated truss

The results in this chapter can be read in conjunction with the results in Chapter 10 of insulated truss structures and show that the insulation increased the durability of structures under fire. In the pin-spring truss, a layer of insulation limited the horizontal reaction force so that the spring did not yield throughout the time of simulation unlike the behaviour shown in this chapter. Although the insulation brings a lot of benefit to the structure, one must ensure that the insulation is intact when the fire happens, otherwise the durability of the structure can be seriously compromised.

11.4.3 Further discussion about World Trade Center trusses

Quintiere (2002) used a temperature based calculation method to predict the failure time of the structure which matches the actual scenario quite well. Instead of presuming the connections had a shear failure as suggested in FEMA (2002), Quintiere proposed that the reason for the structural failure was the webs buckled under its compressive axial force.

This report acknowledges that if the webs have compressive axial forces, they are very likely to buckle. The case with largest compressive axial force in the web was used as the example, which is the truss exposed to 16 minutes of the ISO fire before the decay phase. Figure 11-21 compares the axial force of the web with its yield limit based on the thermal properties of the steel section from the Eurocode (EC3:1995). The web stress is represented by the solid black line. The graph shows that although the web stress exceeded the proportional limit, it did not yield throughout the simulation.

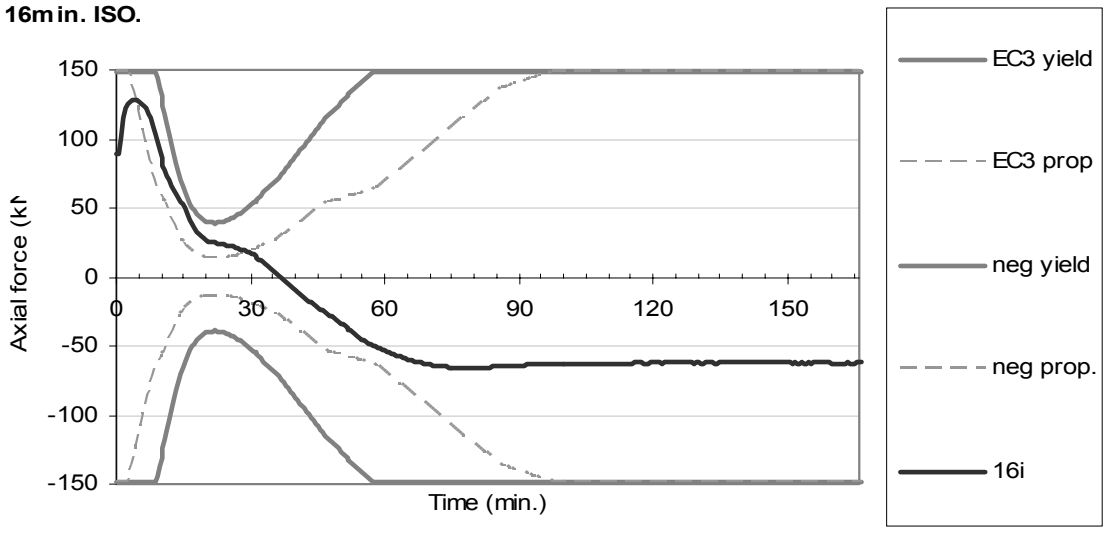

Figure 11-21 Axial force limit for the web near the connection yielding

In Quintiere's calculation, the rod was assumed to have pinned connections at both ends. The critical buckling load of the rod, P, was calculated as:

$$P = \frac{\pi^2 E}{L^2}\left(\frac{\pi^4 D^4}{64}\right) \qquad \textbf{Equation 11-1}$$

where E is the elastic modulus equal to 200,000MPa, L is the length of the rod and equals 1.69m, and D is the diameter of the rod which was 27.7mm. The critical buckling force was 20kN before heating. When the web temperature increases, the elastic modulus reduces and so does the critical buckling force. Figure 11-22 compares the axial force with the critical buckling force. The axial force almost immediately exceeded the critical buckling force limit when it went into compression and Figure 11-5 shows that the horizontal reaction force at the connection at this time was still low. Hence, according to this calculation, the rod would buckle before the connection failed.

However, based on the building description in FEMA, it seems that the web members have rotation fixation at the ends, and the calculation of the critical buckling load should use the following equation:

$$P = \frac{4\pi^2 E}{L^2}\left(\frac{\pi^4 D^4}{64}\right) \qquad \textbf{Equation 11-2}$$

The critical buckling force is 80kN before heating. Figure 11-23 shows the comparison between the modified critical buckling force with the web axial force. It also shows that the web would buckle while cooling, but the time to buckle is 10 minutes later than using the original assumption.

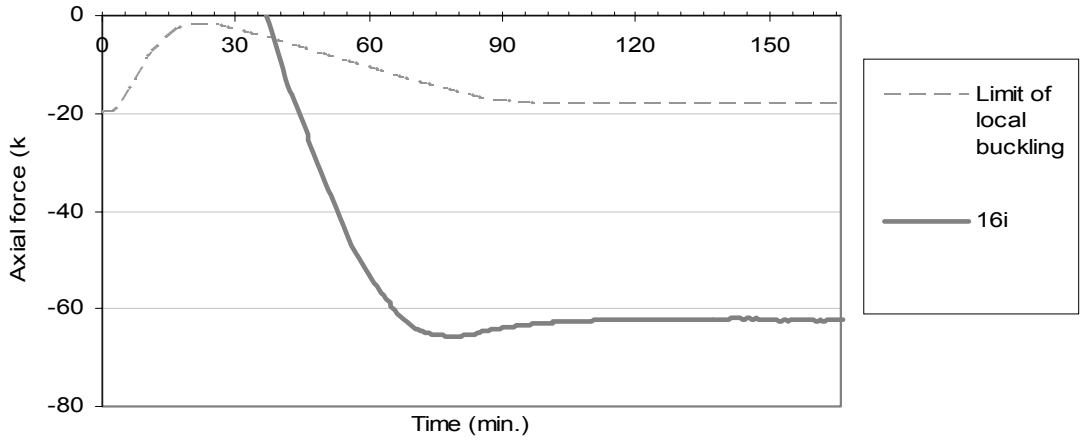

Figure 11-22 Axial force limit for web near the connection buckling (web has pinned connections)

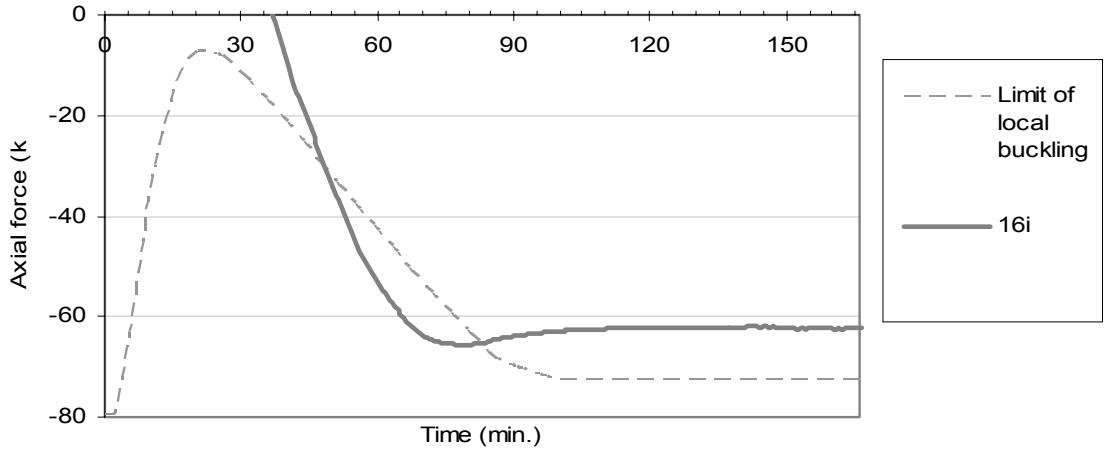

Figure 11-23 Axial force limit for web near the connection buckling (web has fixed connections)

Despite the previous example, the findings in this report favour the FEMA viewpoint, because among the scenarios discussed before, only the non-insulated pin-pin supported case exhibited a compressive axial force in the webs; and even in such scenario only the webs near the connections could buckle because of their length. In the other cases the webs were in tension while the horizontal reaction force at the connection became very large. Since the pin-spring connected truss is more similar to the actual structure, the finding in this report favours the idea that the connection failure was the main reason of the collapse of the floor slabs of the World Trade Center towers.

12 Conclusions

Several topics have been discussed in this report. The investigated beam and frame structures exposed to the ISO834 standard fire in this report were also modelled previously by Seputro (2001), Wastney (2002) and Welsh (2001). However, introducing a decay phase after the heating phase added a new variable into the analyses, and the simulation results show that large tensile forces can develop during the cooling period. The results of the beam or frame models suggest that a truss structure may have a similar behaviour with large tensile force while cooling, so a truss structure was also modelled.

Knowing the behaviour of a structure exposed to a length of the ISO fire with a decay phase, one can compare the structural behaviour under fires with different rates of fire growth to it under the ISO fire by adjusting the time scale based on the maximum temperatures of the members.

The most important and useful outcome from this report is the effect of the decay phase on the connection design. This topic, along with the other findings, is discussed separately below.

12.1 Connections for composite frames

For a composite beam with axial restraints exposed to the ISO fire, Wastney (2002) and Welsh (2001) showed that large compressive axial forces can be caused by thermal expansion before the stress at the bottom flange reaches the proportional limit. This study shows that the large tensile axial forces can be generated while cooling.

The results for the fix-fix connected composite beam show that the maximum tensile axial force approximates half of the value of the maximum compressive force. In a frame with a pin-pin connected composite beam, the maximum tensile force can be 1.5 times the value of the maximum compressive force; therefore, the tensile force would cause greater concern in pinned connection designs.

It is more likely that a steel structure will have bolted connections rather than welded connections. One shall be cautious about the strength as well as the location of the

bolts in connection designs. Even if the combined strength of the bolts is sufficient to resist the tensile axial force induced during the decay phase, the upper portion of the beam will be subjected to a larger tensile stress than the lower portion, so the bolts in that region are more likely to fail and need to be stronger.

12.2 Connections for steel frames

The following comments about the steel beams and frames exposed to fires can be found in this report as well as in Seputro (2001) and Wastney (2002). The steel frame fails earlier than the composite frame and has larger displacements for the same load because of a lack of composite action.

The beam axial force in the steel frame case is generally larger than in the composite frame case; however, this depends on the stiffness and strength of the horizontal restraint at the ends. In a layout with very strong columns, the beam experiences a very large axial force that will cause the entire beam to yield in tension during the decay phase. This is especially so in fix-fix connected beams. For design purposes, it is more desirable to allow for some degree of horizontal displacement than design for a very strong connection.

12.3 Effects of changing stiffness and strength of columns

The frame structures modelled in this report do not only represent a frame structure with insulated columns but also show the behaviour of beams with the end supports as strong as the columns in the model.

In both the composite and steel frames, it was observed that a large axial force in the beam is induced if the columns are stiff. The results also show that increasing the column strength and stiffness causes the beam to behave similar to a single span beam with axial restraints; this finding is the same as in Wastney (2002).

Large beam axial forces are induced if the columns are stiff. This resultant force eventually can cause the columns to yield. The behaviour of the beams in frames with yielded columns would be the same as if the connections yield. While being exposed to the ISO fire, the beams in frames with stiff columns would initially follow the behaviour of a single span beam with axial restraints until the columns yield, and then

their behaviour would be closer to the behaviour of a single span beam without axial restraints.

12.4 Connections for steel trusses

The truss modelled here has the same dimensions as the floor truss in World Trade Centers 1 and 2. The results show that the top chords of the truss have a similar behaviour to the top flange in a composite beam, and the bottom chord is similar to the bottom flange: while heating, the tensile axial force in the lower chords increases, and the axial force in the upper chords shifts from tension to compression until the lower chords yield in tension.

In the pin-spring connected structure which allows for yielding at one connection, the structure exhibits a behaviour between those of pin-pin and pin-roller connected trusses, but the failure time is longer. This is because the intermediate level of axial restraint is sufficient to prevent a run-away failure which would occur with a pin-roller connected truss, and the stress in each member is not sufficient to cause yielding which would occur in a pin-pin connected truss.

12.5 Effects of insulation on steel trusses

Having insulation allows the structural members to absorb heat slowly, which significantly benefits the structural behaviour during the fire as shown in Chapter 10. The results show that pin-roller and pin-pin connected insulated trusses resisted 74 and 122 minutes of the ISO fire respectively, and the pin-spring connected insulated truss can withstand at least 3 hours of the ISO fire. Without the insulation, the pin-spring connected truss could only last for 24 minutes under the ISO fire, and 4 minutes under the super-fast fire. One can notice that the insulated structure can sustain a much larger fire than the non-insulated truss, and the midspan of the truss is able to return to its original height after the temperature returns to ambient.

Because of such a difference with and without insulation cases for the truss structure, it is important to keep the insulation intact or the stability of the structure under elevated temperatures would be drastically compromised, and failure of the truss can contribute to the overall structural failure.

12.6 Effects of changing rate of heating and cooling

Chapter 9 discussed the structural behaviour of a composite beam exposed to the fires with different growth rate to the ISO fire. The results show that the axial force and the vertical deflection are dominated by the maximum temperature of the structural members reached during the fire, and are independent of the fire duration. Modelling with the ISO fire will allow the critical temperature to be estimated, but will not predict the time to failure.

12.7 Recommendations for further research

It is important to understand that this study has been limited in scope an duration. It is recommended that future research should consider the following:

- A studied relationship between the connection stiffness and strength under elevated temperatures as an input for the computer program
- A more sophisticated computer program which allows for change in stiffness and strength of connections as part of the input.
- A three-dimensional model for the SAFIR program to analyse the local buckling and torsional behaviour in the beams and columns
- Analysis of frames with columns exposed to the fire
- The effect of continuity of the beam if the concrete slab can continue past the columns
- Experimental verification of analytical results

13 References

Buchanan, A.H. (2001). *Structural Design for Fire Safety*, John Wiley & Sons Ltd., Chichester, England

EC2 (1993). *Eurocode 2: Design of Concrete Structures. ENV1992-1-2: General Rules - Structural Fire Design*. European Committee for Standardisation, Brussels.

EC3 (1995). *Eurocode 3: Design of Steel Structures. ENV 1993-1-2: General Rules - Structural Fire Design*. European Committee for Standardisation, Brussels

ECCS (1995). 'Fire resistance of steel structures". *ECCS Technical Note No.89.* Technical Committee 3. European Commission for Constructional Streelwork, Brussels, Belgium.

El-Rimawi, J.A., Burgess, I.W & Plank, R.J (1997), 'The influence of connection stiffness on the behaviour of steel beams in fire', *Journal of Constructional Steel Research*, Vol.43, pp. 1-15, Elsevier Science Ltd., Great Britain

FEMA (2002), *World Trade Centre Building Performance Study: Data Collection, Preliminary Observations, and Recommendations*, FEMA, Washington, DC

Franssen, J.M. Kodur V.K.R. Mason J. (2000) *User's Manual for SAFIR2002 - A Computer Program for Analysis of Structures Submitted to the Fire*, Department Structures du Génie Civil, Service Ponts et Charpentes, University of Liège, Belgium.

Gorenc. B.E. (1996), *Steel Designer's Handbook*, UNSW Press, Kensington, NSW

Liu, T.C.H (1999), 'Fire resistance of unprotected steel beams with moment connections', *Journal of Constructional Steel Research*, Vol. 51, pp.61-77, Elsevier Science Ltd, Great Britain

Martin, D.M. & Moore, D.B. (1997), "Introduction and background to the research programme and major fire tests at BRE Cardington", *Proceedings of the National Steel Construction Conference*, London, UK

Nethercot, D.A. (1985). "Steel Beam to Column Connections - A Review of Test Data", *CIRIA Project Record 338*, UK

Seputro, J. (2001). *Effect of Support Conditions on Steel Beams Exposed to Fire*, Fire Engineering Research Report 01/06, School of Engineering, University of Canterbury, Christchurch, NZ

Trahair, N.S. & Bradford, M.A (1998). *The Behaviour and Design of Steel Structures to AS 4100*, E & FN Spon, London

Wang, Y.C (2002). *Steel and Composite Structures: Behaviour and Design For Fire Safety*, Spon Press, London

Wastney, C. (2002), *Performance of unprotected Steel and Composite Steel Frames Exposed to Fire*, Fire Engineering Reseasrch Report 02/11, School of Engineering, Unversity of Canterbury, Christchurch, NZ

Welsh, R.D (2001). *2-D Analysis of Composite Steel-Concrete Beams in Fire*, Fire Engineering Research Report 01/08, School of Engineering, University of Canterbury, Christchurch, NZ

Quintiere, J.G, di Marzo, M., Becker, R. (2002), "*A suggested cause of the fire-induced collapse of the World Trade Towers*", Fire Safety Journal, vol. 37, p.707-716, Elsevier Science Ltd, Great Britain

14 Appendix

14.1 Appendix 1: Properties of steel and concrete at elevated temperatures from EC3 (1995) and EC2 (1993)

14.1.1 EC3 (1995) grade S 355 steel

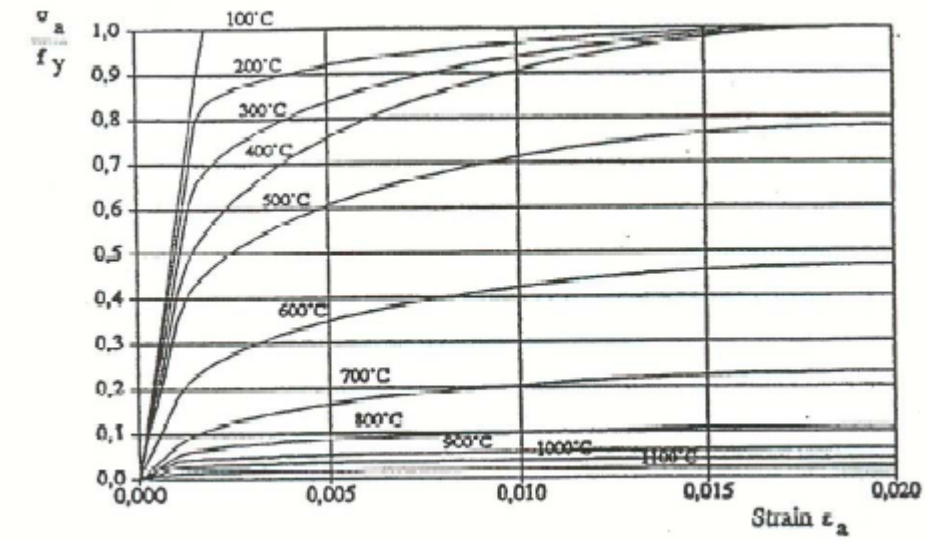

Figure 14-1 EC3 (1995) variation of stress-strain relationship with temperature for grade S 355 steel (Strain hardening not included)

Table 14-1 EC3 (1995) reduction factors for stress-strain relationship of steel at elevated temperatures

Steel Temperature θ_a	Reduction factor at temperature θ_a relative to the value of f_y or E_a at 20°C		
	Reduction factor for effective yield strength	Reduction factor for proportional limit	Reduction factor for the elastic modulus.
20°C	1.000	1.000	1.000
100°C	1.000	1.000	1.000
200°C	1.000	0.807	0.900
300°C	1.000	0.613	0.800
400°C	1.000	0.420	0.700
500°C	0.780	0.360	0.600
600°C	0.470	0.180	0.310
700°C	0.230	0.075	0.130
800°C	0.110	0.050	0.090
900°C	0.060	0.0375	0.0675
1000°C	0.040	0.0250	0.0450
1100°C	0.020	0.0125	0.0225
1200°C	0.000	0.0000	0.0000

14.1.2 EC2 (1993) hot rolled reinforcing steels

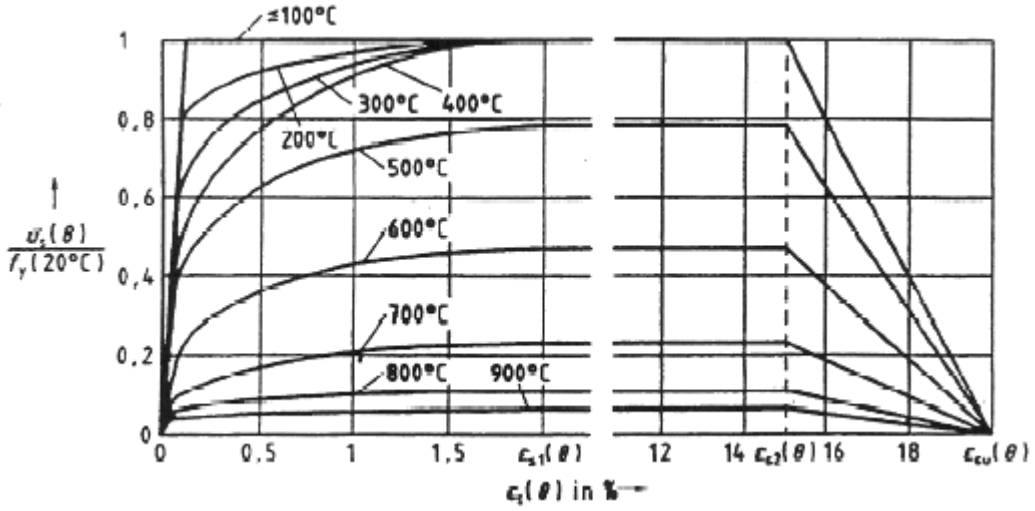

Figure 14-2 EC2 (1993) variation of stress-strain relationship with temperature of hot rolled reinforcing steels at elevated temperatures

Table 14-2 EC2 (1993) reduction factors for stress-strain relationship of hot rolled reinforcing steels at elevated temperatures

Steel Temperature θ_a	Reduction factor at temperature θ_a relative to the value of f_y or E_a at 20°C		
	Reduction factor for effective yield strength	Reduction factor for proportional limit	Reduction factor for the elastic modulus.
20°C	1.000	1.000	1.000
100°C	1.000	0.960	1.000
200°C	1.000	0.920	0.870
300°C	1.000	0.810	0.720
400°C	0.940	0.630	0.560
500°C	0.670	0.440	0.400
600°C	0.400	0.260	0.240
700°C	0.120	0.080	0.080
800°C	0.110	0.060	0.060
900°C	0.080	0.050	0.050
1000°C	0.050	0.030	0.030
1100°C	0.030	0.020	0.020
1200°C	0.000	0.000	0.000

14.1.3 EC2 (1993) siliceous concrete

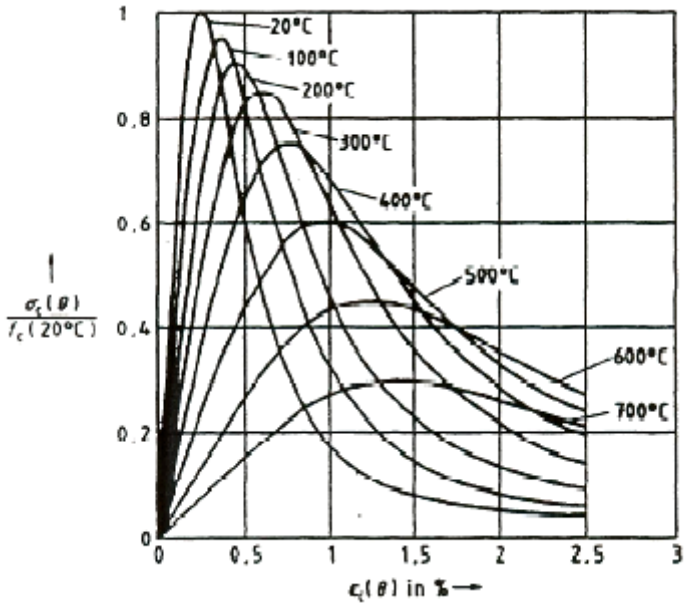

Figure 14-3 EC2 (1993) stress-strain relationships of siliceous concrete under uniaxial compression at elevated temperatures

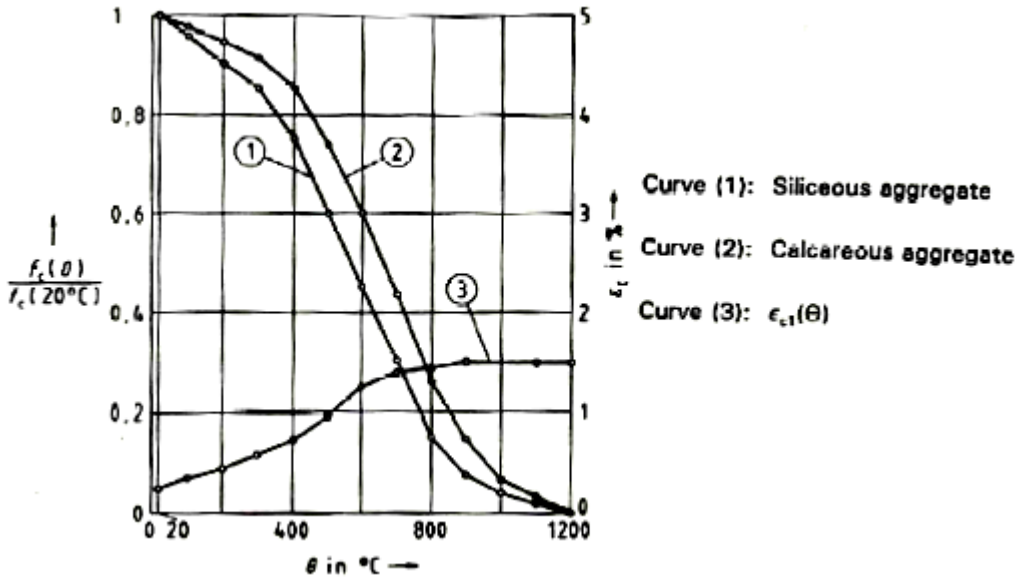

Figure 14-4 EC2 (1993) parameters for stress-strain relationships of concrete at elevated temperatures

Table 14-3 EC2 (1993) reduction factors for stress-strain relationship in compression of concrete at elevated temperatures

Concrete Temperature (^oC)	$f(\theta)/f_c(20^oC)$		$\varepsilon_c(\theta) \times 10^3$
	siliceous	calcareous	
20	1.00	1.00	2.5
100	0.95	0.97	3.5
200	0.90	0.94	4.5
300	0.85	0.91	8.0
400	0.75	0.85	7.5
500	0.60	0.74	9.5
600	0.45	0.60	12.5
700	0.30	0.43	14.0
800	0.15	0.27	14.5
900	0.08	0.15	15.0
1000	0.04	0.05	15.0
1100	0.01	0.02	15.0
1200	0.00	0.00	-

14.2 Appendix 2: Alternative super-fast fire outputs

14.2.1 Thermal analysis

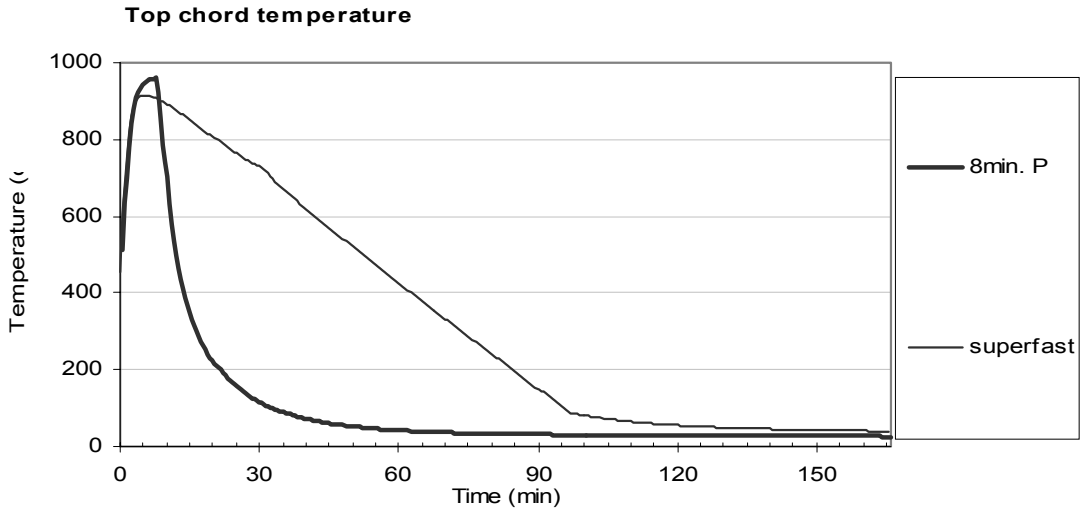

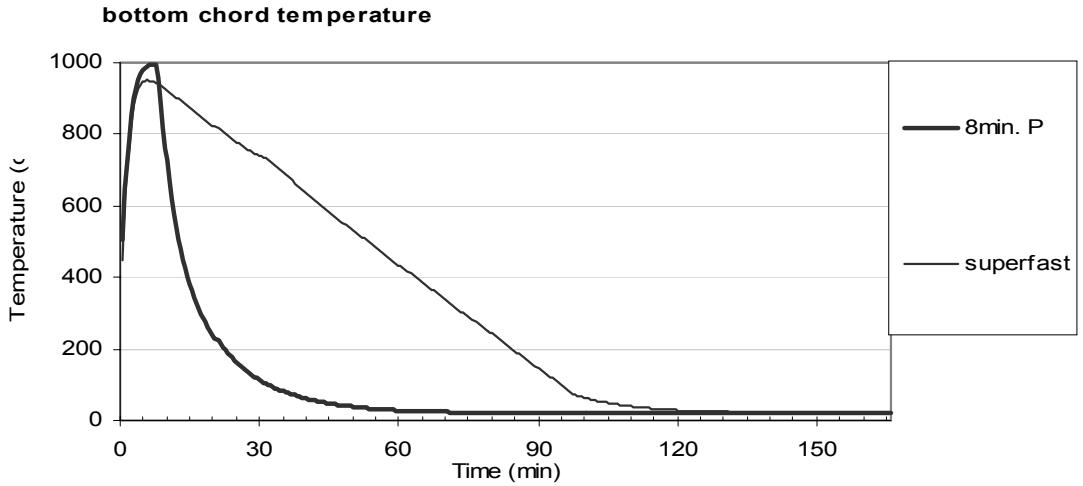

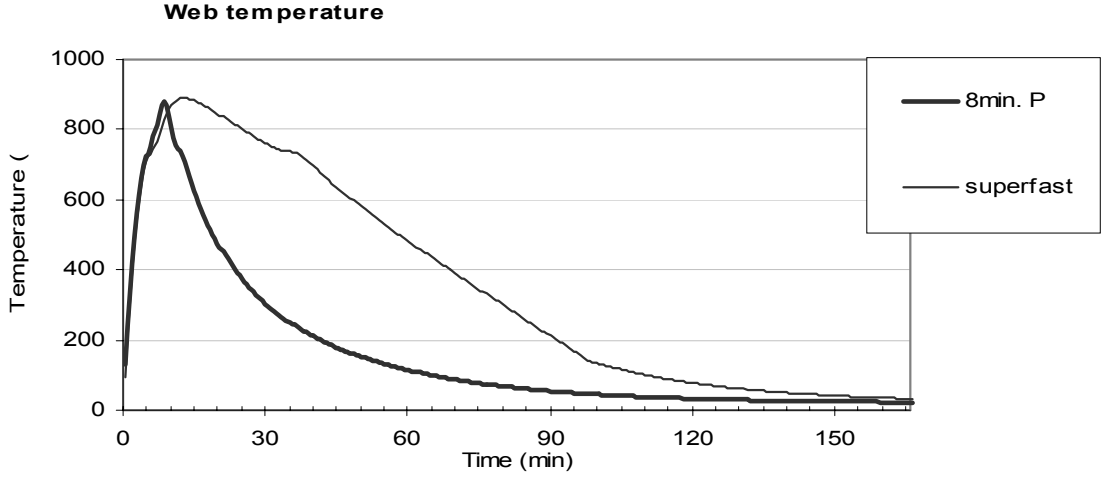

14.2.2 Structural analysis

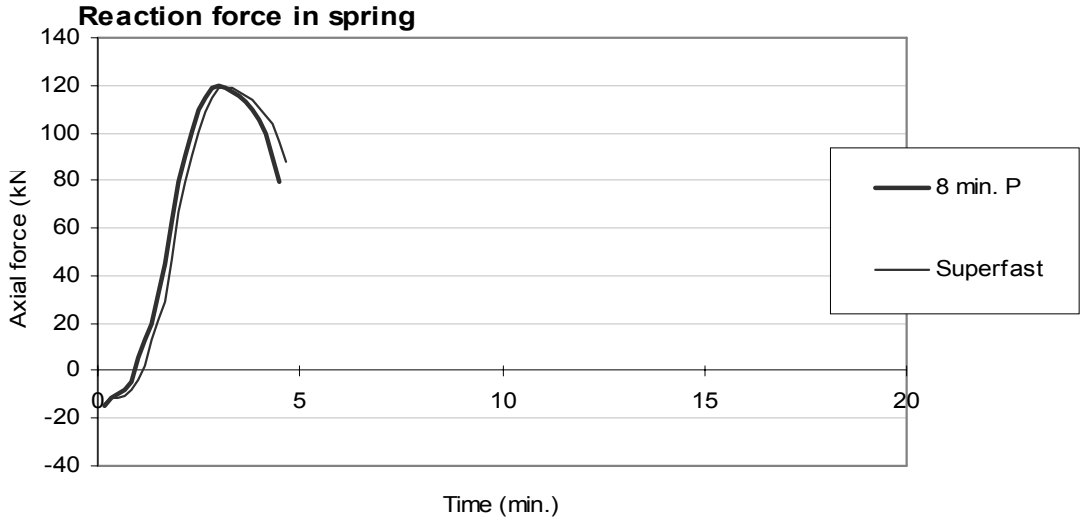

Figure 14-5 Horizontal spring reaction force

14.3 Appendix 3: Thermal analysis input files

14.3.1 Composite beam

```
    NPTTOT       2
   NNODE 1507
    NDIM   2
NDIMMATER   1
 NDDLMAX   1
    FROM   1   TO 1507 STEP    1 NDDL    1
 END_NDDL
 TEMPERAT
    TETA     0.90
 TINITIAL       20
 MAKE.TEM
LARGEUR11     50000
LARGEUR12      1000
  NORENUM
finishedslab.TEM
    NMAT   3
 ELEMENTS
   SOLID 1349
     NG   2
   NVOID   0
 END_ELEM
   NODES
NODE      1          0          0
NODE      2          -0.0125    0
NODE      3          -0.025     0
NODE      4          -0.02943   0
NODE      5          -0.04129   0
NODE      6          -0.05315   0
NODE      7          -0.065     0
NODE      8          -0.07417   0
NODE      9          -0.08334   0
NODE      10         -0.09251   0
NODE      11         -0.10168   0
NODE      12         -0.11085   0
NODE      13         -0.12      0
NODE      14         -0.12075   0
.
.
.
NODE      1493       -0.72275   0
NODE      1494       -0.72275   0.0053
NODE      1495       -0.72275   0.0132
NODE      1496       -0.72275   0.0216
NODE      1497       -0.72275   0.03
NODE      1498       -0.72275   0.0384
NODE      1499       -0.72275   0.0468
NODE      1500       -0.72275   0.0552
NODE      1501       -0.72275   0.0636
NODE      1502       -0.72275   0.072
NODE      1503       -0.72275   0.0804
NODE      1504       -0.72275   0.0888
NODE      1505       -0.72275   0.0972
NODE      1506       -0.72275   0.1056
NODE      1507       -0.72275   0.114
 NODELINE       -0.120       0
   YC_ZC          0       0
 FIXATIONS
  END_FIX
NODOFSOLID
ELEM      1          2          16         15         1          3          0
ELEM      2          3          17         16         2          3          0
ELEM      3          4          18         17         3          3          0
ELEM      4          5          19         18         4          3          0
ELEM      5          6          20         19         5          3          0
ELEM      6          7          21         20         6          3          0
ELEM      7          8          22         21         7          3          0
ELEM      8          9          23         22         8          3          0
ELEM      9          10         24         23         9          3          0
```

```
ELEM    10      11      25      24      10      3       0
ELEM    11      12      26      25      11      3       0
ELEM    12      13      27      26      12      3       0
ELEM    13      14      28      27      13      1       0
ELEM    14      16      30      29      15      3       0
ELEM    15      17      31      30      16      3       0
ELEM    16      18      32      31      17      3       0
ELEM    17      19      33      32      18      3       0
ELEM    18      20      34      33      19      3       0
ELEM    19      21      35      34      20      3       0
ELEM    20      22      36      35      21      3       0
ELEM    21      23      37      36      22      3       0
ELEM    22      24      38      37      23      3       0
ELEM    23      25      39      38      24      3       0
.
.
.
ELEM    1344    1501    1502    1487    1486    1       0
ELEM    1345    1502    1503    1488    1487    1       0
ELEM    1346    1503    1504    1489    1488    1       0
ELEM    1347    1504    1505    1490    1489    1       0
ELEM    1348    1505    1506    1491    1490    1       0
ELEM    1349    1506    1507    1492    1491    1       0

 FRONTIER
F       1       NO      NO      F20     NO
F       14      NO      NO      F20     NO
F       27      NO      NO      F20     NO
F       40      NO      NO      F20     NO
F       53      NO      NO      F20     NO
F       66      NO      NO      F20     NO
F       79      NO      NO      F20     NO
F       92      NO      NO      F20     NO
F       105     NO      NO      F20     NO
F       118     NO      NO      F20     NO
.
.
.
F       1258    NO      NO      FISO    NO
F       1259    NO      NO      FISO    NO
F       1260    NO      NO      FISO    NO
 END_FRONT
 SYMMETRY
   YSYM
  ENDSYM
 PRECISION    0.001
 MATERIALS
  STEELEC3
25 9 0.5
  STEELEC2
25 9 0.5
SILCONCEC2
92 25 9 0.5
    TIME
          1.     10.
         10.   3600.
         15.   7200.
  END_TIME
IMPRESSION
 TIMEPRINT     60.
```

14.3.2 Non-insulated Upper chord (Truss structure)

```
   NPTTOT       2
    NNODE 239
     NDIM    2
 NDIMMATER    1
  NDDLMAX    1
     FROM    1   TO 239 STEP    1 NDDL    1
 END_NDDL
 TEMPERAT
    TETA     0.90
 TINITIAL      20
 MAKE.TEM
LARGEUR11    4665
LARGEUR12    1
  NORENUM
wtcupiso.TEM
    NMAT    3
 ELEMENTS
   SOLID 206
      NG    2
    NVOID    0
 END_ELEM
   NODES
NODE      1          0          0
NODE      2          -0.00635   0
NODE      3          -0.0127    0
NODE      4          -0.01905   0
NODE      5          -0.0254    0
NODE      6          -0.03175   0
NODE      7          -0.0381    0
NODE      8          -0.04445   0
NODE      9          -0.0508    0
NODE      10         -0.05715   0
NODE      11         -0.0635    0
.
.
.

NODE      223        -0.06985   0.06579
NODE      224        -0.0762    0.06579
NODE      225        -0.08255   0.06579
NODE      226        -0.0889    0.06579
NODE      227        -0.09525   0.06579
NODE      228        -0.1016    0.06579
NODE      229        -0.06985   0.07214
NODE      230        -0.0762    0.07214
NODE      231        -0.08255   0.07214
NODE      232        -0.0889    0.07214
NODE      233        -0.09525   0.07214
NODE      234        -0.1016    0.07214
NODE      235        -0.06985   0.07849
NODE      236        -0.06985   0.08484
NODE      237        -0.06985   0.09119
NODE      238        -0.06985   0.09754
NODE      239        -0.06985   0.10389
 NODELINE            -0.0635    0.0519
   YC_ZC             0          0.0519
 FIXATIONS
  END_FIX
NODOFSOLID
ELEM      1          2          13         12         1          2          0
ELEM      2          3          14         13         2          2          0
ELEM      3          4          15         14         3          2          0
ELEM      4          5          16         15         4          2          0
ELEM      5          6          17         16         5          2          0
ELEM      6          7          18         17         6          2          0
ELEM      7          8          19         18         7          2          0
ELEM      8          9          20         19         8          2          0
ELEM      9          10         21         20         9          2          0
ELEM      10         11         22         21         10         2          0
ELEM      11         13         24         23         12         2          0
ELEM      12         14         25         24         13         2          0
ELEM      13         15         26         25         14         2          0
```

```
ELEM    14      16      27      26      15      2       0
ELEM    15      17      28      27      16      2       0
ELEM    16      18      29      28      17      2       0
ELEM    17      19      30      29      18      2       0
.
.
.
ELEM    196     223     229     132     121     1       0
ELEM    197     224     230     229     223     1       0
ELEM    198     225     231     230     224     1       0
ELEM    199     226     232     231     225     1       0
ELEM    200     227     233     232     226     1       0
ELEM    201     228     234     233     227     1       0
ELEM    202     229     235     143     132     1       0
ELEM    203     235     236     154     143     1       0
ELEM    204     236     237     165     154     1       0
ELEM    205     237     238     176     165     1       0
ELEM    206     238     239     187     176     1       0

 FRONTIER
F       70      FISO    NO      NO      NO
F       80      FISO    NO      NO      NO
F       90      FISO    NO      NO      NO
F       100     FISO    NO      NO      NO
F       161     FISO    NO      NO      NO
F       162     FISO    NO      NO      NO
F       163     FISO    NO      NO      NO
F       164     FISO    NO      NO      NO
F       165     FISO    NO      NO      NO
F       166     NO      FISO    NO      NO
F       167     NO      FISO    NO      FISO
F       168     NO      FISO    NO      FISO
F       169     NO      FISO    NO      FISO
F       170     NO      FISO    NO      FISO
F       171     FISO    FISO    NO      FISO
.
.
.
F       198     NO      FISO    NO      FISO
F       199     NO      FISO    NO      FISO
F       200     NO      FISO    NO      FISO
F       201     FISO    FISO    NO      FISO
F       202     FISO    NO      NO      NO
F       203     FISO    NO      NO      NO
F       204     FISO    NO      NO      NO
F       205     FISO    NO      NO      NO
F       206     FISO    NO      NO      NO

 END_FRONT
 SYMMETRY
 ENDSYM
 PRECISION    1.e-4
 MATERIALS
  STEELEC3
25 9 0.5
SILCONCEC2
92 25 9 0.5
  STEELEC3
25 9 0.5
TIME
          1.     10.
         10.   3600.
         15.  10000.
  END_TIME
IMPRESSION
 TIMEPRINT     30.
```

14.4 Appendix 4: Structural analysis input files

14.4.1 Pin-pin connected composite frame

```
Composite-Steel frame

   NPTTOT    70440
    NNODE  123
     NDIM   2
 NDIMMATER   1
  NDDLMAX   3
     FROM   1          TO  41    STEP   2 NDDL   3
     FROM   2          TO  40    STEP   2 NDDL   1
     FROM  42          TO  82    STEP   2 NDDL   3
     FROM  43          TO  81    STEP   2 NDDL   1
     FROM  83          TO 123    STEP   2 NDDL   3
     FROM  84          TO 122    STEP   2 NDDL   1
 END_NDDL
   STATIC
    NLOAD   1
  OBLIQUE   0
 COMEBACK  0.000001
NARCLENGTH     0.05
 LARGEUR11     1902
 LARGEUR12       50
  NORENUM
     NMAT   4
 ELEMENTS
     BEAM  60   2
       NG   2
   NFIBER 1349
 END_ELEM
    NODES
     NODE   1         -4.00000   0.00000    0.00000
    GNODE  41         4.00000    0.00000    0.00000
     NODE  42         -4.00000   4.00000    0.00000
    GNODE  82         -4.00000   -4.00000   0.00000
     NODE  83         4.00000    4.00000    0.00000
    GNODE 123         4.00000    -4.00000   0.00000
 FIXATIONS
    BLOCK  42          F0      F0      F0
    BLOCK  82          F0      F0      F0
    BLOCK  83          F0      F0      F0
    BLOCK 123          F0      F0      F0
     SAME   1  62      YES     YES     NO
     SAME  41 103      YES     YES     NO
  END_FIX
 NODOFBEAM
Column1.tem
 TRANSLATE   1   1
 END_TRANS
finishedslab.tem
 TRANSLATE   1   2
 TRANSLATE   2   3
 TRANSLATE   3   4
 END_TRANS
     ELEM   1          1          2          3          2
    GELEM  20         39         40         41          2          2
     ELEM  21         42         43         44          1
    GELEM  40         80         81         82          1          2
     ELEM  41         83         84         85          1
    GELEM  60        121        122        123          1          2
 PRECISION    1.e-4
    LOADS
 FUNCTION    FLOAD
 DISTRBEAM         1          0.   -50.E3
 GDISTRBEAM       20          0.   -50.E3   1
 END_LOAD
 MATERIALS
 STEELEC3
 210.0E+9 0.3 300.0E+6
```

```
 STEELEC3
210.0E+9 0.3 300.0E+6
 STEELEC2
210.0E+9 0.3 430.0E+6
SILCONCEC2
0.2 30.0E+6 0 0
    TIME
              5.            600.
             10.            7200.
  ENDTIME
LARGEDISPL
   EPSTH
IMPRESSION
 TIMEPRINT      30.
PRINTREACT
  PRINTMN
PRNSIGMABM   1   1
```

14.4.2 Pin-spring connected truss

World Trade Center 1 truss WITH ANGLE

```
   NPTTOT    100000
    NNODE   70
     NDIM    2
 NDIMMATER    1
  NDDLMAX    3
EVERY_NODE 3
FROM      2          TO        34        STEP      2          NDDL      1
FROM      37         TO        67        STEP      2          NDDL      1
FROM      69         TO        69        STEP      1          NDDL      1
 END_NDDL
  STATIC
   NLOAD    1
  OBLIQUE    0
 COMEBACK     0.000001
 ARCLENGTH     0.05
 LARGEUR11     5000
 LARGEUR12      8
  NORENUM
    NMAT    4
 ELEMENTS
    BEAM   34    3
     NG    3
  NFIBER 5000
  TRUSS 34 1
 END_ELEM
   NODES
NODE      1          0         0         0
NODE      2          0.508     0         0
NODE      3          1.524     0         0
NODE      4          2.032     0         0
NODE      5          2.54      0         0
NODE      6          3.048     0         0
NODE      7          3.556     0         0
NODE      8          4.064     0         0
NODE      9          4.572     0         0
NODE      10         5.08      0         0
NODE      11         5.588     0         0
NODE      12         6.096     0         0
NODE      13         6.604     0         0
NODE      14         7.112     0         0
NODE      15         7.62      0         0
NODE      16         8.128     0         0
NODE      17         8.636     0         0
NODE      18         9.144     0         0
NODE      19         9.652     0         0
NODE      20         10.16     0         0
NODE      21         10.668    0         0
NODE      22         11.176    0         0
NODE      23         11.684    0         0
NODE      24         12.192    0         0
NODE      25         12.7      0         0
NODE      26         13.208    0         0
NODE      27         13.716    0         0
NODE      28         14.224    0         0
NODE      29         14.732    0         0
NODE      30         15.24     0         0
NODE      31         15.748    0         0
NODE      32         16.256    0         0
NODE      33         16.764    0         0
NODE      34         17.272    0         0
NODE      35         18.288    0         0
NODE      36         1.524     -0.736    0
NODE      37         1.778     -0.736    0
NODE      38         2.032     -0.736    0
NODE      39         2.54      -0.736    0
NODE      40         3.048     -0.736    0
NODE      41         3.556     -0.736    0
NODE      42         4.064     -0.736    0
NODE      43         4.572     -0.736    0
```

```
NODE    44      5.08    -0.736  0
NODE    45      5.588   -0.736  0
NODE    46      6.096   -0.736  0
NODE    47      6.604   -0.736  0
NODE    48      7.112   -0.736  0
NODE    49      7.62    -0.736  0
NODE    50      8.128   -0.736  0
NODE    51      8.636   -0.736  0
NODE    52      9.144   -0.736  0
NODE    53      9.652   -0.736  0
NODE    54      10.16   -0.736  0
NODE    55      10.668  -0.736  0
NODE    56      11.176  -0.736  0
NODE    57      11.684  -0.736  0
NODE    58      12.192  -0.736  0
NODE    59      12.7    -0.736  0
NODE    60      13.208  -0.736  0
NODE    61      13.716  -0.736  0
NODE    62      14.224  -0.736  0
NODE    63      14.732  -0.736  0
NODE    64      15.24   -0.736  0
NODE    65      15.748  -0.736  0
NODE    66      16.256  -0.736  0
NODE    67      16.51   -0.736  0
NODE    68      16.764  -0.736  0
NODE    69      17.764  0       0
NODE    70      18.764  0       0

 FIXATIONS
        BLOCK   1       F0      F0      NO
        BLOCK   35      NO      F0      NO
        BLOCK   70      F0      F0      NO
        BLOCK   69      NO      F0      NO
END_FIX
 NODOFBEAM
UPiso.TEM
 TRANSLATE   1   1
 TRANSLATE   2   2
 TRANSLATE   3   4
END_TRANS
wtcLOWiso.TEM
 TRANSLATE   1   1
 TRANSLATE   2   4
END_TRANS
ANGLENiso.TEM
 TRANSLATE   1   1
END_TRANS
    ELEM   1   1   2   3   1
   GELEM  17  33  34  35   1   2
    ELEM  18  36  37  38   2
   GELEM  33  66  67  68   2   2
    ELEM  34      35  69  70   3

 NODOFTRUSS
wtcRODiso.FCT 0.602212E-3 0 3
ELEM    1       1       36      1
ELEM    2       36      3       1
ELEM    3       3       38      1
ELEM    4       38      5       1
ELEM    5       5       40      1
ELEM    6       40      7       1
ELEM    7       7       42      1
ELEM    8       42      9       1
ELEM    9       9       44      1
ELEM    10      44      11      1
ELEM    11      11      46      1
ELEM    12      46      13      1
ELEM    13      13      48      1
ELEM    14      48      15      1
ELEM    15      15      50      1
ELEM    16      50      17      1
ELEM    17      17      52      1
ELEM    18      52      19      1
ELEM    19      19      54      1
ELEM    20      54      21      1
```

```
ELEM      21          21          56          1
ELEM      22          56          23          1
ELEM      23          23          58          1
ELEM      24          58          25          1
ELEM      25          25          60          1
ELEM      26          60          27          1
ELEM      27          27          62          1
ELEM      28          62          29          1
ELEM      29          29          64          1
ELEM      30          64          31          1
ELEM      31          31          66          1
ELEM      32          66          33          1
ELEM      33          33          68          1
ELEM      34          68          35          1

 PRECISION     1.e-4
    LOADS
  FUNCTION     FLOAD
NODELOAD          36          0          -9.00E+03 0
NODELOAD          40          0          -9.00E+03 0
NODELOAD          44          0          -9.00E+03 0
NODELOAD          48          0          -9.00E+03 0
NODELOAD          52          0          -9.00E+03 0
NODELOAD          56          0          -9.00E+03 0
NODELOAD          60          0          -9.00E+03 0
NODELOAD          64          0          -9.00E+03 0
NODELOAD          68          0          -9.00E+03 0
  END_LOAD
 MATERIALS
  STEELEC3
 200.0E+9 0.3 248.2E+6
SILCONCEC2
 0.2 30.0E+6 0 1
   STEELEC2
 200.0E+9 0.3 248.2E+6
  STEELEC3
 10  0.3   430.0E+6

TIME
              1.      10.
              5.     600.
             10.     900.
                        10.            10000.
   ENDTIME
LARGEDISPL
    EPSTH
IMPRESSION
 TIMEPRINT      30.
PRINTREACT
   PRINTMN
PRNSIGMABM   1   1
```